Universidad Complutense de Madrid
Facultad de CC. Físicas
Departamento de Física de la Tierra, Astronomía y Astrofísica II
(ASTROFÍSICA Y CC. DE LA ATMÓSFERA)

CARMENES science preparation: characterisation of M dwarfs with low-resolution spectroscopy and search for low-mass wide companions to young stars

Preparación científica de CARMENES: caracterización de enanas M con espectroscopia de baja resolución y búsqueda de compañeros separados poco masivos de estrellas jóvenes

Dirigido por
Prof. Dr. David Montes Gutiérrez
Dr. José A. Caballero Hernández

Memoria que presenta
D. Francisco Javier Alonso Floriano
para aspirar al grado de
Doctor en Astrofísica
Madrid, septiembre de 2015

Some of the figures and material included in this document have already been published in *Astronomy and Astrophysics*.

A mi familia,
a mi madre

Agradecimientos

"Si he logrado ver más lejos, ha sido porque he subido a hombros de gigantes."
— Sir Isaac Newton (1676)

Esta tesis doctoral no habría sido posible de no ser por mis directores, Prof. David Montes y Dr. José Antonio Caballero. Gracias por darme la oportunidad de realizar esta tesis y por enseñarme lo que es la investigación científica. También quiero agradecer al consorcio de CARMENES por permitirme realizar mi tesis dentro de un proyecto tan extraordinario. De entre los miembros del consorcio quiero agradecer especialmente al Prof. Ansgar Reiners y al Insitut für Astrophysik Göttingen, por acogerme durante mi estancia en Alemania, la cual fue una gran experiencia profesional y personal. Quiero mostrar también mi gratitud al Dr. Alexis Klutsch por su inestimable ayuda en la realización de esta tesis. Extiendo este agradecimiento a los profesores y compañeros del departamento por ayudarme con sus consejos siempre que les he consultado, especialmente al Prof. Manuel Rego, Profa. María José Fernández, Profa. Elisa De Castro y Prof. Manuel Cornide. Por supuesto estos años no hubieran sido lo mismo sin mis compañeros de despacho, Miguel, Miriam, Hugo y Víctor, con los que he compartido día a día las alegrías y penas de este oficio.

También quiero reconocer el increíble apoyo de familiares y amigos durante todos estos años. En especial gracias a mi padre, al que tengo que agradecer muchas más cosas de las que pudiera escribir en estas líneas, y a mi abuela, la cual siempre me ha escuchado y dado buenos consejos. Me gustara dar las gracias a mi novia que ha sido mi mayor apoyo y mi puerto seguro en los últimos meses antes de acabar. Quiero extender este agradecimiento a sus padres por haberse preocupado por mí y esta tesis como si fueran los míos. Gracias a mis amigos, especialmente a Fátima, Adrián, Julio y todos mis amigos de la universidad, por soportarme y hacerme reír incluso en los días más difíciles.

No podía faltar en estos agradecimientos una mención especial a quien ha sido una de las personas mas importantes de mi vida, mi madre. Ella siempre me apoyó en todo lo que decidí hacer y se preocupó porque lo consiguiera, incluso en sus últimos días. Por eso, este trabajo se lo dedico a ella.

Finalmente, quería agradecerte a ti, lector, por el mero hecho de interesarte en este trabajo. Porque el objetivo de esta investigación no es obtener un título, es llegar a tus manos.

En Madrid, a 10 de septiembre de 2015

Acknowledgements

"If I have seen further, it is by standing on the shoulders of giants."
— Sir Isaac Newton (1676)

This Ph.D. thesis would not have been possible were it not for my thesis directors, Prof. Dr. David Montes and Dr. José Antonio Caballero. Thanks for giving me the opportunity to perform this thesis, and teach me what is scientific research. I also thank the CARMENES consortium for allowing to develop my thesis within such an extraordinary project. Among the members of the consortium, I want to especially thank Prof. Dr. Ansgar Reiners and the Institut für Astrophysik Göttingen, for welcoming me during my stay in Germany, which was a great experience both professional and personal. I also express my gratitude to Dr. Alexis Klutsch for their invaluable help in the realization of this thesis. I extend my thanks to the professors and colleagues in the department for helping me with their advice whenever I asked them, especially to Prof. Dr. Manuel Rego, Prof. Dr. María José Fernández, Prof. Dr. Elisa De Castro and Prof. Dr. Manuel Cornide. Of course these years would not have been the same without my officemates, Miguel, Miriam, Hugo and Victor, with whom I shared everyday the joys and sorrows of this profession.

I also want to acknowledge the incredible support of my family and friends over the years. **Special thanks to my father, to who I have to thank many more things that the ones I could write in these lines, and to my grandmother, who has always listened to me and given me good advices.** I also want to thank my girlfriend who has been my biggest supporter, my safe harbour in the months before the end of this work. I want to extend my thanks to her parents for caring about me and this thesis as if they were my parents. Thanks to my friends, especially to Fátima, Adrián, Julio and all the friends from my universitary period, for supporting me and making me laugh even during the hardest days.

I also would like to do a especial mention to who has been one of the most important people in my life, my mother. **She always supported me in everything I chose to do and cared about it**, even in her last days. Therefore, this work is dedicated to her.

Finally, I wanted to thank you, the reader, for the mere fact of showing interest in this work. Because the purpose of this research it is not to get a degree, it is to arrive to your hands.

Madrid, September 10, 2015

Resumen

Contexto

La proporción de masas entre planetas rocosos y enanas de tipo M es mucho menor que entre dichos planetas y estrellas como el Sol. Este hecho las ha convertido en los principales objetivos para la detección de planetas similares a la Tierra en la zona de habitabilidad usando el método Doppler. Sin embargo, las estrellas M presentan más dificultades observacionales que estrellas más calientes. Su máximo de emisión se produce en longitudes de onda infrarroja, lo que provoca un menor brillo superficial en el rango óptico, especialmente para los subtipos menos masivos. Además, las bandas moleculares que llenan sus espectros, y el incremento de actividad y rotación que ocurre a partir de subtipos medios, complican la determinación de sus velocidades radiales. Para la caza exoplanetaria, esto se traduce en un gran consumo de tiempo de telescopio y la construcción de caros espectrógrafos infrarrojos de alta resolución. Para que este esfuerzo merezca la pena, es decir, detectar un número significativo de exoplanetas en la zona de habitabilidad de enanas M, es necesaria una intensa preparación científica que permita seleccionar los mejores candidatos. Sin embargo, la detección de exotierras en la zona de habitabilidad no implica la habitabilidad de las mismas. Recientes estudios nos obligan a plantear la posibilidad de que estos planetas no lleguen a mantener la suficiente agua para albergar vida tal y como la conocemos, o incluso que la actividad estelar haya esterilizado sus superficies. Para resolver estas cuestiones es necesario estudiar la formación y evolución de los planetas, lo cual requiere de la búsqueda de planetas entorno a estrellas M jóvenes.

Este trabajo se centra en el estudio de objetos poco masivos que puedan ser objetivos para la búsqueda de exoplanetas con espectrógrafos sensibles al infrarrojo cercano, y para CARMENES en particular. El consorcio CARMENES está compuesto por 11 instituciones españolas y alemanas que están construyendo un espectrógrafo de alta resolución ($\mathcal{R} = 82{,}000$) con dos canales, visible (0.55–1.05 μm) e infrarrojo (0.95–1.7 μm), para el telescopio de 3.5 m del Observatorio de Calar Alto. Se observará una muestra de 300 enanas M durante 600 noches de tiempo garantizado durante al menos tres años, comenzando en enero de 2016. La muestra final se seleccionará a partir de las $\sim$2200 enanas M contenidas en el catálogo de entrada CARMENCITA. Para estas estrellas hemos obtenido o compilado una gran cantidad de datos: tipos espectrales, velocidades radiales y rotacionales, fotometría en diversas bandas, etc. Parte de los esfuerzos en la ciencia de preparación, los cuales son necesarios para la selección final de objetivos para CARMENES y otros espectrógrafos en el infrarrojo cercano, se han recogido en dos publicaciones presentadas en este trabajo de tesis.

Objetivos y metodología

En el primer artículo, obtuvimos espectroscopia de baja resolución con el espectrógrafo CAFOS en el telescopio 2.2 m de Calar Alto para 753 estrellas. El objetivo principal era la obtención de tipos espectrales precisos, que son un parámetro fundamental para la selección de la muestra. Nosotros

usamos una red de 49 estrellas estándares, de los tipos K3 V a M8 V, junto con una doble técnica de minimización de mínimos cuadrados, y 31 índices espectrales previamente definidos por otros autores. Además, cuantificamos la gravedad superficial, metalicidad y actividad cromosférica de la muestra para detectar estrellas de poca gravedad (gigantes y muy jóvenes), pobres y muy pobres en metales (subenanas), y muy activas.

En la segunda publicación buscamos compañeros de movimiento propio común, especialmente poco masivos, de estrellas pertenecientes al grupo de movimiento joven cercano β Pictoris. Primero, recopilamos una lista de 185 miembros y candidatos de β Pictoris a partir de 35 trabajos representativos en este grupo de movimiento. A continuación, hicimos uso de herramientas de observatorio virtual, Aladin y STILTS, así como del catálogo de movimientos propios PPMXL y el catálogo de estrellas dobles "Washington double star". Los objetos que presentaron movimientos propios similares a las estrellas de la muestra fueron sometidos a un estudio astro-fotométrico. Los 36 compañeros de movimiento propio común obtenidos finalmente fueron objeto de un estudio de energías de ligadura para determinar su unión física.

Resultados y conclusiones

En el primer trabajo, obtuvimos tipos espectrales, con un error típico de 0.5 subtipos, para 753 estrellas, de los cuales, 305 fueron determinados por primera vez y 448 fueron revisados. Medimos pseudoanchuras equivalentes de Hα para todos los objetos y concluimos que nuestros tipos espectrales no se ven afectados por la actividad de las estrellas de la muestra. Pudimos distinguir dos estrellas candidatas a subenanas, tres T Tauri, 25 gigantes, 44 enanas K y 679 enanas M. Además, la muestra contenía 261 estrellas con tipos espectrales M4–8.0 V, muchas de las cuales se encuentran entre las estrellas más brillantes conocidas de sus subtipos. Por último, comparamos nuestros tipos espectrales con los obtenidos por otros catálogos usados en la base de datos CARMENCITA, demostrando la homogeneidad de los tipos espectrales usados en el catálogo de entrada de CARMENES.

En la segunda publicación, presentamos un compendio de 185 estrellas miembros o candidatos de la asociación β Pictoris. Medimos movimientos propios precisos para 184 objetos. Descartamos cinco compañeros previamente conocidos e identificamos 36 compañeros de movimiento propio común. De ellos, ocho eran nuevos sistemas, y tres tenían secundarias en o por debajo del límite de fusión del hidrógeno. Además, 16 estrellas fueron propuestas por primera vez como candidatos a la asociación. Finalmente, de los 36 sistemas, 14 eran triples o cuádruples, una cantidad mayor de la esperada. Esto podría sugerir un sesgo en la muestra hacia estrellas binarias cercanas o un incremento de la fracción de sistemas de alto orden de multiplicidad para sistemas muy separados.

Los resultados expuestos anteriormente, no solo son importantes para búsquedas de exoplanetas por velocidad radial como la de CARMENES, si no que pueden ayudar a ampliar los estudios en otros campos relacionados con los objetos poco masivos en la vecindad solar.

Abstract

Context

The mass ratio between rocky planets and M-type dwarfs is much lower than between rocky planets and stars like the Sun. This fact has made them prime targets for the detection of Earth-like planets in the habitable zone using the Doppler method. However, M stars show more observational difficulties than hotter stars. Their maximum emission occurs at infrared wavelengths, which causes a low surface brightness in the optical range, especially for the lowest-mass subtypes. In addition, the molecular bands that fill their spectra, and the increase on activity and rotation that occurs from mid-subtypes, complicate the radial velocity determinations. For exoplanetary hunting, it translates into a great consumption of telescope time, and the construction of expensive high-resolution infrared spectrographs. To make this effort worthwhile, that is, to find a significant amount of exoplanets in the habitable zone of M dwarfs, an intense scientific preparation is needed to enable the selection of the best candidates. However, the detection of exo-Earths in the habitable zone does not imply the habitability of such planets. Recent investigations force us to raise the possibility that these planets do not maintain enough water to harbour life as we know it, or even that stellar activity sterilizes their surfaces. To solve these issues, it is necessary to investigate the planet formation and evolution, which requires planet searches around young M stars.

This work is focused on the study of low-mass objects that can be targets of exoplanet searches with near-infrared spectrographs in general and CARMENES in particular. The CARMENES consortium comprises 11 institutions from Germany and Spain that are building a high-resolution spectrograph ($\mathcal{R} = 82{,}000$) with two channels, visible (0.55–1.05 μm) and infrared (0.95–1.7 μm), for the 3.5 m Calar Alto telescope. It will observe a sample of 300 M dwarfs in 600 nights of guaranteed time during at least three years, starting in January 2016. The final sample will be chosen from the $\sim$2200 M dwarfs included in the CARMENCITA input catalogue. For these stars, we have obtained and collected a large amount of data: spectral types, radial and rotational velocities, photometry in several bands, etc. Part of the effort of the science preparation necessary for the final selection of targets for CARMENES and other near-infrared spectrographs has been collected in two publications, which are presented in this PhD thesis.

Aims and methodology

In the first publication, we obtained low-resolution spectra for 753 stars using the CAFOS spectrograph at the 2.2 m Calar Alto telescope. The main goal was to derive accurate spectral types, which are fundamental parameters for the sample selection. We used a grid of 49 standard stars, from spectral types K3 V to M8 V, together with a double least-square minimisation technique and 31 spectral indices previously defined by other authors. In addition, we quantified the surface gravity, metallicity and chromospheric activity of the sample, in order to detect low-gravity stars (giants and

very young), metal-poor and very metal-poor stars (subdwarfs), and very active stars.

In the second publication, we searched for common proper motion companions, especially of low mass, to members of the near young β Pictoris moving group. First, we compiled a list of 185 members and candidate members to β Pictoris from 35 representatives studies on this moving group. Next, we used the Aladin and STILTS virtual observatory tools, as well as the PPMXL proper motion and Washington double stars catalogues. The objects that showed similar proper motions to those stars of the sample were targets of an astro-photometric follow-up. The 36 common proper motion companion eventually obtained were subjects of a study of binding energies to determine their physical ligation.

Results and conclusions

In the first paper, we obtained spectral types, with a typical error of 0.5 subtypes for 753 stars, of which 305 were obtained for the first time and 448 were revised. We measured pseudo-equivalent widths of Hα for all the objects and concluded that the activity of the sample stars does not affect our spectral types. We were able to distinguish two subdwarf candidates, three T Tauri stars, 25 giants, 44 K dwarfs and 679 M dwarfs. In addition, the sample contained 261 stars of spectral types M4–M8 V, many of which are among the brightest stars known of their subtypes. Finally, we compared our spectral types with those of catalogues used by CARMENCITA, proving the homogeneity of the spectral types used in the input catalogue of CARMENES.

In the second publication, we showed a compilation of 185 members or candidate members to β Pictoris. We measured a accurate proper motions for 184 objects. We discarded five known companions and identified 36 common proper motion companions. Of them, eight were new systems, and three presented companions at or below the hydrogen burning limit. In addition, 16 star were proposed for the first time as candidates to the association. Finally, of the 36 systems, 14 were triples or quadruples, which is a larger number than expected. This concern might suggest a biased sample towards close companions or an increment of the high-order-multiple fraction for very wide systems.

The results previously exposed are not only important for radial velocity exoplanetary surveys like CARMENES, but can also help to inform the researches in other fields related with the low-mas objects of the solar neighbourhood.

Contents

1

Introduction

"We are all very ignorant, but not all ignorant of the same things"
— Albert Einstein

The discovery of the first extrasolar planet orbiting a main sequence star, 51 Peg b, by Mayor & Queloz (1995), exposed to the world that our Solar System was not unique and fuelled old dreams of finding habitable worlds. After 20 years of exoplanetary science, we know that the so called "planetary zoo" is composed by a larger variety of objects than we could imagine. For example there are unexpected hot-Jupiter planets, which are Jupiter-mass objects orbiting so close to their host stars that they are swollen as balloons; or "Tatooine" planets, which are circumbinary extrasolar planets with two or more host stars, only seen before in fantasy movies. However, life as we know it would not exist in most of these planets. We know that life might not need the same conditions that our planet provides, but it is reasonable to look for planets that provide similar conditions, such as liquid water. On the way to the discovery of the first habitable planet, the detection of Earth-like planets in the habitable zone (HZ, i.e., the region around the star within which a planet can support liquid water –Kasting 1993; Joshi et al. 1997; Lammer et al. 2007; Tarter et al. 2007; Scalo et al. 2007) is a fundamental step. We are still years away to develop the technology necessary for the detection and confirmation of an Earth-like planet orbiting a twin of the Sun, but it is currently possible to find them in the HZ of smaller stars than the Sun.

The difference of masses between Earth-like planets and solar-like stars is too large to detect them by Doppler effect, because radial velocity measurements are currently not accurate enough. The lower mass ratio between rocky planets and M-type dwarfs made these stars to be the main targets of habitable exo-Earth searches. The identification of a rocky planet in the HZ of a M-type dwarf is an important point about its possible habitability. However, the habitability of planets does not only depend on the possibility of finding liquid water, but on several factors, such as some stellar processes that occur in the young host star during the planetary formation. Nowadays, several radial velocities surveys –and transit ones– are turning their gaze to these faint objects. As outlined below, the peculiarities of these faint objects cause the need of an intense science preparation to obtain a target sample properly characterised. In this work, we characterise a number of low-mass star candidates as part of the science preparation of the CARMENES project (*Calar Alto high-Resolution search for M dwarfs with Exo-earths with Near-infrared and optical Échelle Spec-*

trographs; see Quirrenbach et al. 2014), and compiled a sample of young low-mass stars, which is interesting for studying the formation, evolution and habitability of exoplanets detected around M dwarfs.

This first chapter aims to outline some of the main characteristics of the M-type dwarfs, the state of the art of exoplanetary searches around M dwarfs and young low-mass objects, as well as the instrumentation used in the radial velocity surveys, with special dedication to the CARMENES project. The chapter also aims to provide with an integrative introduction of the two publications that form the main part of this PhD thesis work.

1.1 M dwarfs

M dwarfs are the most common stars in the Galaxy and are among the coolest and smallest stars, preceded only by some old early L-type stars. They were first described in the 19th century by Father Angelo Secchi (Secchi 1866). The main feature of this spectral type is the prevalence of molecular bands at optical wavelengths, especially the ones produced by the titanium oxide molecule (TiO). For feature identifications refer to Fig. 1.1. They have been used to establish subtypes since Morgan (1938) described the M0, M1 and M2 subtypes, followed by the studies of Kuiper (1942) and Joy (1947), who expanded the classification to mid- and late-M dwarfs based on the strength of the TiO molecular bands. However, it was not until Boeshaar (1976) when the first standard classification of M subtypes from M0 to M6.5 was established over the optical wavelength region (4400–6800 Å), which was further extended to M7, M8 and M9 subtypes in a later publication (Boeshaar & Tyson 1985). This standard classification was based on the appearance of TiO bands for early M dwarfs, and on the ratio between the molecular bands of VO at 5736 Å and TiO at 5759 Å, together with the strength of the CaOH molecular band at 5530 Å for later M subtypes. However, longer wavelengths become more important for the spectral classification according to the advance of the spectral types sequence towards cooler subtypes, showing other easily recognisable molecular bands, such as other VO and CaOH molecular features. The strength of TiO bands are distinguishable from mid-K to M6, after which the VO bands and the sharper slope of the pseudocontinium stand out (e.g., VO band at 7300 Å; see Fig. 1.1). It was Kirkpatrick et al. (1991) who reanalysed the entire M-dwarf sequence using longer wavelengths, until the optical red (6300 to 9000 Å), to provide a standard spectral type classification in agreement with those of Boeshaar (1976) and Boeshaar & Tyson (1985). The spectral types sequence from K3 V to M8.0 V is showed in Chapter 2, Fig. 2.

The spectral typing is a very important task, because each spectral subtype is also related with some parameters, namely effective temperature ($T_{\rm eff}$), radius (R), mass ($\mathcal{M}$), luminosity (L) and surface gravity (g). The variation of these parameters as a function of spectral type is shown in Table 1.1. These fundamental parameters are, as the name indicate, crucial to understand the physical processes that take place in each star and are commonly obtained for stars with solar metallicity. In hotter stars, the variations of these parameters caused by different metallicity values are commonly neglected, unless the metallicity measurements are very different from the solar values. Unfortunately, the metallicity measurements on M dwarfs are inaccurate and the inference of other fundamental parameters are more complicated than in hotter stars due to the complex spectra exhibited by these low-mass objects. A few recent investigations try to solve this problem using different approaches to the determination of these parameters, especially for metallicity measurements: high resolution spectra and PHOENIX models (Rojas-Ayala et al. 2013; Mann at al. 2013b,2015; Passegger et al. 2014), ratios of spectral features on high-resolution spectra (Maldonado et al. 2015),

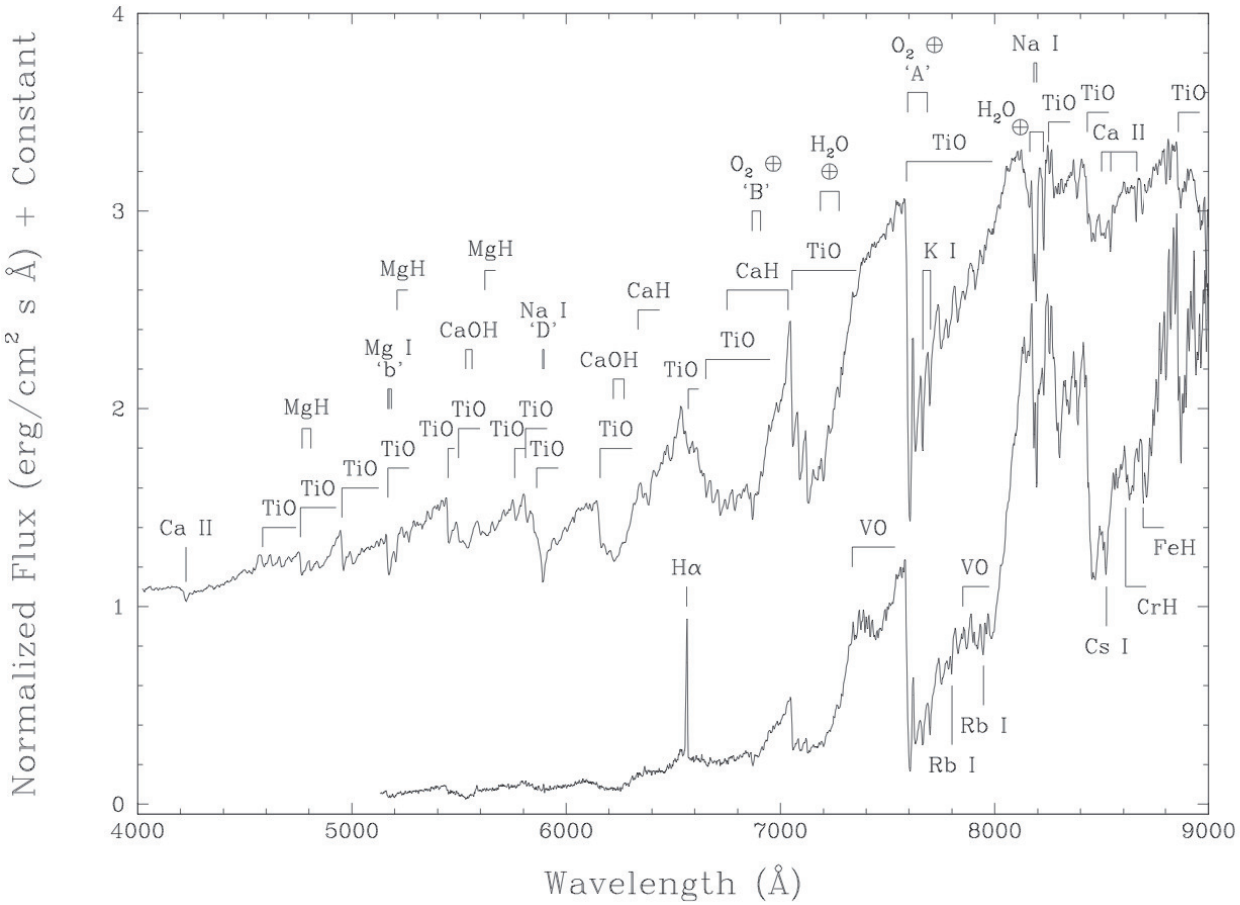

FIGURE 1.1— Optical spectra of the M4.5 dwarf ν And B (Lowrance et al. 2002) and the M9 dwarfs LHS 2065 (Kirkpatrick et al. 1997). The main features of M dwarfs are marked in the upper spectrum, including telluric absorption lines not subtracted ($\oplus$). Additional bands that become relevant in later spectral types are marked on the bottom spectrum. Fluxes are normalized to unity at 7500 Å and the M4.5 spectrum has been offset by one unit. Figure from Gray & Corbally (2009).

photometric calibrations (Hejazi et al. 2015), interferometric observations (Boyajian et al. 2011, 2012, 2014), and extrapolations of the metallicity values of F-, G-, K-primary stars in M companions with the goal of developing metallicity calibration grid based on photometric or spectral features of M-dwarfs (Mann et al. 2013a, 2014).

Beyond the prevalence of M-type stars in the Milky Way, the physical relevance of these low-mass objects lies in that they are the bridge between the helium and hydrogen burning stars (O, B, A, F, G and K) and substellar objects (depending on the age, the transition could be at M or L spectral types –Burrows et al. 1997; Baraffe et al. 1998; Chabrier et al. 2000; Zapatero Osorio et al. 2006). Objects of spectral type M6.5 or later can either be young brown dwarfs, or dwarf stars at ages of several Ga[1] (Reiners & Basri 2008). Likewise, there are old stars above the hydrogen burning limit with spectral types as late as L3–5 (Kirkpatrick et al 2011). Young brown dwarfs are

[1]In this thesis we followed the recommendation of the IAU, SI, DIN and NIST to use 'annus' (symbol 'a') for astronomical applications. It is one Julian year of 365.25 days. The unit 'a' can be supplemented with prefixes k ($\times 10^3$), M ($\times 10^6$) and G ($\times 10^9$) to designate thousand, million and thousand million years, respectively.

TABLE 1.1— Fundamental properties of M dwarfs (Reid & Hawley 2005).

Spectral type	$T_{\rm eff}$ [K]	R [$R_\odot$]	$\mathcal{M}$ [$M_\odot$]	L [$10^{-2}\,L_\odot$]	$\log g$ [c.g.s.]
M0	3800	0.62	0.60	7.2	4.65
M1	3600	0.49	0.49	3.5	4.75
M2	3400	0.44	0.44	2.3	4.8
M3	3250	0.39	0.36	1.5	4.8
M4	3100	0.36	0.20	0.55	4.9
M5	2800	0.20	0.14	0.22	5.0
M6	2600	0.15	0.10	0.09	5.1
M7	2500	0.12	∼0.09	0.05	5.2
M8	2400	0.11	∼0.08	0.03	5.2
M9	2300	0.08	∼0.075	0.015	5.4

still cooling down and contracting and, therefore, show different surface gravity and stellar radius values than dwarf stars of the same spectral type (i.e., brown dwarfs are larger and less massive than dwarfs of the same effective temperatures). The spectra of M brown dwarfs and dwarf stars show variations in the features sensitive to gravity at optical wavelengths, similar to those variations on M-giant spectra, but less pronounced. In this case, alkaline atomic lines and doublets, such as K I ($\lambda\lambda$7665,7699 Å) and Na I ($\lambda\lambda$8183,8195 Å), are good gravity indicators (see Kirkpatrick et al. 1991; Kirkpatrick 2005; Gray & Corbally 2009). These variations are easier to detect at longer wavelengths because the maximum continuum radiation of these stars occurs at these wavelengths (see Fig. 1.1).

Furthermore, there are major changes in some stellar physical processes while the sequence of M dwarfs moves to cooler subtypes. The Hα atomic line at λ6563 Å –widely used to study stellar chromospheric activity– is in emission for active M dwarfs. In general, mid- and late-M dwarfs tend to show this feature in emission more often than earlier-type stars (e.g., Hawley et al 1996; West et al. 2004; Reiners et al. 2013; and Chapter 2). **Mohanty & Basri (2003) proposed a rotation-activity connection for M-type stars down to spectral type M8.5 (i.e., cooler M-type stars are faster rotators and more active than earlier dwarfs with slower rotation, see also Reiners et al. 2014). The fact of being fully convective may be the cause of the difference in rotational braking between early- and mid-M stars (Reiners & Basri 2008). It is commonly accepted that the transition between partially and fully convective stars occur at M3.5–M4 V for main-sequence stars (see Chabrier & Baraffe 1997; Reiners & Basri 2009; Stassun et al. 2011; Shulyak et al. 2014). Stars with masses less than ∼0.5 $M_\odot$ (M0) are fully convective throughout their pre-main-sequence evolution, while stars with masses less than 0.25 $M_\odot$ (M4.5) are fully convective for their entire lifetimes (Sills et al. 2000; Reiners 2008; see Fig. 1.2). Early-M stars show the same relation between rotation and magnetic activity that solar-type stars (Pizzolato et al. 2003; Reiners 2007). In this relation, those stars with faster rotation present higher activity levels. This rotation-activity connection is explained by an $\alpha\Omega$ dynamo (rotation-convection), which is probably only operating in the presence of a radiative core and not in fully convective stars (Durney et al. 1993). However, mid- and late-type stars also show the rotation-activity relation, and therefore, it should be explained by other models that take into account other stellar processes (e.g., α^2 dynamo; see**

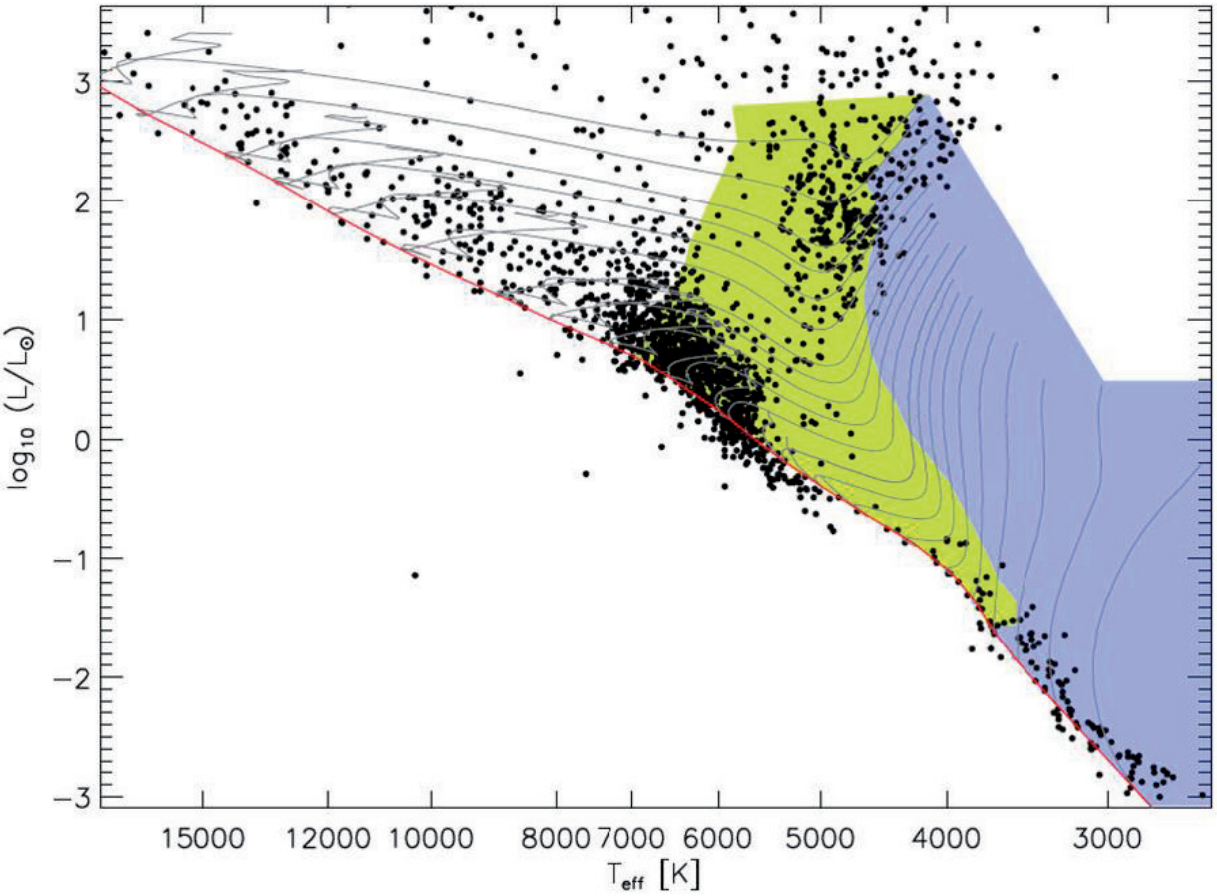

FIGURE 1.2— Hertzsprung-Russell diagram showing the regions where partial convection (green) and full convection (blue) is presented in the interior of stars (Reiners & Basri 2008). Evolutionary tracks (grey lines) are from Siess et al. (2000). Plot from Reiners (2008).

Chabrier & Küker 2006).

The grain formation is another process that adds complexity to the study of the M-dwarf spectra. Dust is formed in the atmospheres of late-M dwarfs ($T_{\rm eff} < 2800\,{\rm K}$ –Tsuji et al. 1996; Tsuji 2002; Helling et al. 2008) and causes higher effective temperature and weakening of molecular features in comparison with stellar atmospheres without dust.

Most of the physical processes outlined above are still a matter of discussion, making the study of M dwarfs very relevant for key questions in astrophysics. Furthermore, the study of M-type stars becomes even more relevant because the technology is already evolved enough to detect the small variations that Earth-like planets produce on the radial velocity of low-mass stars (see below).

1.2 Planets orbiting M dwarfs

M dwarfs are nowadays the preferred targets to detect Earth-like planets in the HZ, mainly because they are suitable targets for radial velocity and transit surveys. **These techniques are responsible of almost all the exoplanet detections, but they both present the disadvantage**

of not being sensitive to exoplanets with face-on orbits. The main advantages of the transit method are the number of detections (hundreds a year) and the possibility of measuring the planets radii. However, these detections present a high number of false positive (Santerne et al. 2012) and radial velocity follow-up measurements are needed to confirm most of the transiting exoplanets. In addition, the full potential of this technique can be only obtained with space telescopes ($Corot, Kepler, TESS, PLATO$) that avoid the photometric perturbations introduced by the atmosphere. On the contrary, the Doppler technique can develop its full potential from ground telescopes, but requires of high precision radial velocity measurements, which can be only obtained in a few high-stabilized high-resolution spectrographs. This technique also detects false positives, mainly caused by the stellar activity. The main advantage of this method is the possibility of measure the minimum masses of the planets ($M_p \sin i$), together with some of their orbital parameters.

However, there are other methods that can be used for exoplanetary detections in low-mass stars, such as microlensing and direct imaging. Both methods share in common the disadvantage of not being really profitable in the number of exoplanet detections in comparison with the radial velocity or the transit methods. Their main advantage is that they can detect planets with face-on orbits. The microlensing method is sensitive to Earth-sized planets but the phenomena is very rare and cannot be observed again. In contrast, the direct imaging is sensitive to several time Jupiter-mass objects orbiting far from the host star, which can be observed continuously.

The beginning of this section pointed the relevance of radial velocity method among the exoplanetary hunting techniques. Most of the exoplanets orbiting M dwarfs have been discovered or confirmed by this technique. The lower the mass of a host star, the higher the radial-velocity amplitude induced by a planet:

$$K_{\rm star} \propto M_{\rm planet}\ a^{-1/2}\ (M_{\rm star} + M_{\rm planet})^{-1/2} \approx (a\ M_{\rm star})^{-1/2} \tag{1.1}$$

when $M_{\rm star} \gg M_{\rm planet}$. As it was described in the previous section, dwarf stars of M spectral type have effective temperatures between 2300 and 3900 K (Kirkpatrick 2005; Rajpurohit et al. 2013). For stars with ages greater than that of the Hyades, of about 0.6 Ga (see Sect. 1.7), these effective temperatures translate in the main sequence into a mass interval from 0.07 to 0.60 $M_\odot$, approximately (Chabrier et al. 2000; Allard et al. 2011; Baraffe et al. 2015). In addition, the lower luminosity of an M dwarf with respect to a star of earlier spectral type causes its HZ to be located very close to the host star, which makes detecting possible habitable planets around M dwarfs (at $\sim$0.1 au) easier than around solar-like stars (at $\sim$1 au).

For M-dwarf stars, some radial-velocity studies have already been carried out (ESO CES, UVES and HARPS by Zechmeister et al. 2009, 2013; CRIRES by Bean et al. 2010; HARPS by Bonfils et al. 2013a) and yielded results similar to Sun-like stars, but still with poor statistical significance (i.e., only some tens of planets have been confirmed around M dwarfs; see Table 1.2). In particular, the abundance of planets as a function of mass and orbital distance to their M-dwarf hosts is very loosely constrained, and the much-sought value of $\eta_\oplus$, that is, the relative abundance of Earth-type planets in the HZ is as yet only poorly constrained from radial-velocity data (e.g., $\eta_\oplus = 0.41^{+0.54}_{-0.13}$ from HARPS estimations; Bonfils et al. 2013a). On the other hand, from *Kepler* data, Swift et al. (2013) calculated an occurrence rate of 1.0 ± 0.1 planets per M dwarf, regardless of

the planet mass. However, Dressing & Charbonneau (2013) and Kopparapu (2013) investigated the occurrence rate of planets with masses in the 0.5–1.4 and 1.4–4 $M_\oplus$ intervals around cool stars ($T_{\rm eff} < 4000$ K in their sample). With the new conservative HZ estimations from Kopparapu et al. (2013), the terrestrial planet frequency around M dwarfs becomes $\eta_\oplus = 0.48^{+0.12}_{-0.24}$, in agreement with the HARPS radial-velocity estimation. These values are certainly favourable for the detection of Earth-like planets around M-dwarf stars. Indeed, according to Dressing & Charbonneau (2013) and with 95 % confidence, the nearest non-transiting Earth-size planet in the HZ of a cool star is just within 5 pc (21 pc for the nearest transiting Earth-size planet). See also other estimations of one or more bound planets per Milky Way star from microlensing observations (e.g., Cassan et al. 2012).

Table 1.2: M dwarfs with confirmed exoplanets discovered by transit or radial velocity methods.

Host star & Planet		Sp. type	P [d]	a [au]	$\mathcal{M}$ [$M_{\rm Jup}$]	Reference
GX And	b	M2V	11.4433 ± 0.0016	0.0717 ± 0.003	0.017 ± 0.002	How14
CD–44 170	b	M0.5V	$15.82^{+0.05}_{-0.03}$	$0.101^{+0.009}_{-0.013}$	$0.041^{+0.013}_{-0.020}$	Tuo14
CD–23 1056	b	M0V	57.44 ± 0.04	0.13	0.4	Bry09; For11a
BD–21 784	b	M0V	$5.235^{+0.003}_{-0.006}$	$0.053^{+0.004}_{-0.007}$	$0.032^{+0.020}_{-0.019}$	Tuo14
L 229–91	b	M3.5	8.6330 ± 0.0016	0.0607 ± 0.0001	0.0334 ± 0.0019	Bon13b
	c		25.64 ± 0.02	0.1254 ± 0.0001	0.023 ± 0.003	Bon13b
	d		601 ± 7	1.027 ± 0.009	0.069 ± 0.009	Bon13b
L 591–6	b	M2.5	30.60 ± 0.02	0.14	0.081 ± 0.005	Ast15
	d		124.0 ± 0.4	0.364	0.070 ± 0.005	Ast15
BD+18 683	b	M2.5V	8.784 ± 0.005	0.066	0.03	End08; For09
Wolf 1539	b	M3.5	2290 ± 60	2.41 ± 0.04	0.82 ± 0.07	How10
L 736–30	b	M2V	$17.380^{+0.018}_{-0.020}$	$0.103^{+0.006}_{-0.014}$	$0.026^{+0.011}_{-0.017}$	Tuo14
	c		$24.33^{+0.05}_{-0.07}$	$0.129^{+0.007}_{-0.017}$	$0.020^{+0.012}_{-0.013}$	Tuo14
Kapteyn's	b	M1	48.62 ± 0.04	0.168 ± 0.008	0.015 ± 0.003	Ang14
	c		121.5 ± 0.3	$0.311^{+0.014}_{-0.040}$	0.022 ± 0.004	Ang14
L 521–2	b	M2.5	14.207 ± 0.007	0.089	0.357 ± 0.005	Ast15
BD–21 1377	b	M1/M2V	471^{+20}_{-12}	$0.97^{+0.12}_{-0.09}$	0.10 ± 0.05	Tuo14
GJ 3470	b	M1.5	3.33671 ± 0.00005	0.0356 ± 0.0010	0.044 ± 0.005	Bon12; Lop14
L 675–81	b	M3.5	692 ± 5	1.15 ± 0.05	1.80 ± 0.05	Joh07; Ang12a
	c		10000	30 ± 10	2	Joh07; Ang12a
GJ 3634	b	M2.5	2.6456 ± 0.0007	0.0287 ± 0.0011	0.022 ± 0.004	Bon11
HD 304043	b	M3.5V	$26.16^{+0.08}_{-0.10}$	$0.119^{+0.014}_{-0.011}$	$0.031^{+0.018}_{-0.012}$	Tuo14
CD–31 9113	b	M1.5	$7.370^{+0.003}_{-0.004}$	$0.060^{+0.004}_{-0.008}$	0.017 ± 0.006	Don10; Tuo14
	c		3700 ± 200	3.6	0.14	Del13
Ross 1003	b	M4V	41.397 ± 0.016	0.163506 ± 0.00004	0.30 ± 0.02	Hag10
Ross 905	b	M2.5	2.64394 ± 0.0001	0.0289 ± 0.0010	0.070 ± 0.005	But04; Sou10
HO Lib	b	M2.5V	5.36865 ± 0.00009	0.04	0.05	Bon05; For11b
	c		12.918 ± 0.002	0.07	0.017	Udr07; For11b
	e		3.14945 ± 0.00017	0.03	0.006	May09; For11b
LP 804–27	b	M3V	111.7 ± 0.7	0.36	2	App10
BD+25 3173	b	M1.5	5980 ± 4	1.14 ± 0.04	0.33 ± 0.03	Joh10
	c		4.4762 ± 0.0004	0.0430 ± 0.0010	0.030 ± 0.008	Wit13
GJ 1214	b	M4.5V	$1.58040482 \pm 0.00000018$	0.0141 ± 0.0003	0.020 ± 0.003	Cha09
CD–34 11626C	b	M1.5V	7.2004 ± 0.0017	$0.0505^{+0.004}_{-0.005}$	0.018 ± 0.004	Bry09; Ang13
	c		28.14 ± 0.03	$0.125^{+0.012}_{-0.013}$	$0.01^{+0.05}_{-0.06}$	Bon13a; Ang13
	d		$91.6^{+0.8}_{-0.9}$	$0.276^{+0.02}_{-0.03}$	$0.016^{+0.006}_{-0.005}$	Ang12b; Ang13
	e		62.2 ± 0.6	0.213 ± 0.02	$0.008^{+0.005}_{-0.004}$	Ang13
	f		$39.03^{+0.19}_{-0.20}$	$0.156^{+0.014}_{-0.017}$	0.008 ± 0.004	Ang13
	g		256^{+14}_{-8}	$0.549^{+0.052}_{-0.058}$	$0.014^{+0.008}_{-0.007}$	Ang13
CD–46 11540	b	M2.5	4.6944 ± 0.0018	0.04	0.04	Bon07; Wan11
CD–51 10924A	b	M0V	1050.3 ± 1.2	1.80 ± 0.07	5.0 ± 0.3	For11a; Ang12c
	c		4400.0	5	3	Ang12c
	d		3.6000 ± 0.0008	0.0413 ± 0.0014	0.014 ± 0.002	Ang12c
	e		35.37 ± 0.07	0.187 ± 0.007	0.036 ± 0.005	Ang12c
BD+68 946	b	M3.5V	38.14 ± 0.015	0.16353 ± 0.00004	0.058 ± 0.007	Bur14
CD–44 11909	b	M3.5V	$17.48^{+0.06}_{-0.04}$	$0.08^{+0.014}_{-0.004}$	$0.014^{+0.012}_{-0.008}$	Tuo14
	c		$57.3^{+0.4}_{-0.5}$	$0.176^{+0.030}_{-0.009}$	$0.027^{+0.018}_{-0.014}$	Tuo14

Table 1.2: M dwarfs with confirmed exoplanets discovered by transit or radial velocity methods (cont.).

Host star & Planet		Sp. type	P [d]	a [au]	$\mathcal{M}$ [$M_{\rm Jup}$]	Reference
BD–05 5715	b	M3.5V	1910 ± 30	2.35	0.90 ± 0.05	But06; Mon14
	c		$7000\,^{+2000}_{-6000}$	...	0.8	Mon14
IL Aqr	b	M4 V	61 ± 4	0.20832 ± 0.00002	1.927 ± 0.003	Del98; Riv10
	c		30.23 ± 0.19	0.12959 ± 0.00002	0.637 ± 0.002	Mar01; Riv10
	d		1.94 ± 0.01	0.0208066 ± 0.0000002	0.0170 ± 0.0010	Riv05; Riv10
	e		124.69 ± 90	0.3343 ± 0.0013	0.0390 ± 0.0010	Riv10

Notes. References of the discovery and, if not the same, planet properties. Ang12a: Anglada-Escudé et al. (2012a); Ang12b: Anglada-Escudé et al. (2012b); Ang12c: Anglada-Escudé et al. (2012c); Ang13: Anglada-Escudé et al. (2013); Ang14: Anglada-Escudé et al. (2014); App10: Apps et al. (2010); Ast14: Astudillo-Defru et al. (2015); Bon05: Bonfils et al. (2005); Bon07: Bonfils et al. (2007); Bon11: Bonfils et al. (2011); Bon12: Bonfils et al. (2012); Bon13a: Bonfils et al. (2013a); Bon13b: Bonfils et al. (2013b); Bur14: Burt et al. (2014); But04: Butler et al. (2004); But06: Butler et al. (2006); Bry09: Bryden et al. (2009); Cha09: Charbonneau et al. (2009); Del98: Delfosse et al. (1998); Del13: Delfosse et al. (2013); Don10: Donnison (2010); End08: Endl et al. (2008); For09: Forveille et al. (2009); For11a: Forveille et al. (2011a); For11b: Forveille et al. (2011b); Hag10: Haghighpour et al. (2010); How10: Howards et al. (2010); How14: Howards et al. (2014); Joh07: Johnson et al. (2007); Joh10: Johnson et al. (2010); Lop14: López & Fortney (2014); Mar01: Marcy et al. (200l); May09: Mayor et al. (2009); Mon14: Montet et al. (2014); Riv05: Rivera et al. (2005); Riv10: Rivera et al. (2010); Sou10: Southworth (2010); Tuo14: Tuomi et al. (2014); Udr07: Udry et al. (2007); Wan11: Wang & Ford (2011); Wit13: Wittenmyer et al. (2013)

1.3 Planets orbiting young stars

Although young stars are a hot topic in astrophysics, especially for their implications on the stellar evolution, only some tens of planets orbiting young stars have been discovered (in this thesis we consider the commonly used definition of young stars as those objects younger than the Hyades open cluster, $\sim$600 Ma). Most of them were discovered in direct imaging (e.g., β Pic b, $\sim$20 Ma; GU Psc b, $\lesssim$150 Ma).

Young stars, especially of the latest spectral types (K and M), are good candidates for direct image searches because of the overluminosity of the substellar objects during their first evolutionary stages and the high star-planet contrast (see Bonnefoy & Chauvin 2013). On the other hand, young stars show higher activity levels than those older ones (see Soderblom 2010), which induce significant effects on the determination of the radial velocity of stars and affects the ability to detect terrestrial planets in their HZ, especially at optical wavelengths (Desort et al. 2007; Reiners et al. 2010).

There are controversial planets discovered by radial velocity that have been argued as false positives because of the radial velocity jitter induced by large starspots. For example, TW Hya (10 Ma) was claimed to host a massive young planet of 10 $M_{\rm Jup}$ discovered with the Doppler technique (Setiawan et al. 2008), but soon after other studies argued that the periodic variation on the radial velocity measurements was caused by starspots on the surface of the star (e.g., Huélamo et al. 2008; Figueira et al. 2010b). However, Facchini et al. (2014) proposed the existence of a planetary object between 10–14 $M_{\rm Jup}$ responsible of the warp in the disc. Another example is that of BD+20 1790 b (30–80 Ma), a hot-Jupiter proposed by Hernán-Obispo et al. (2010), which was claimed to be a false positive by Figueira et al. (2010c). Recently, Hernán-Obispo et al. (2015) have reanalysed the variations on the radial velocity measurements and concluded that they are produced by an exoplanet.

Even when the activity strongly affects the radial velocity measurements, there are confirmed exoplanets orbiting young stars that were discovered with the Doppler technique. HD 70573 (100 Ma, member of the Local Association or Hercules-Lyra association) hosts a planetary mass object of $\sim$6 $M_{\rm Jup}$ at 1.76 au (Setiawan et al. 2007; Bryden et al. 2009; Soto et al. 2015). Another example

is ι Hor b, an exoplanet of twice the mass of Jupiter orbiting at 1 au of a solar-twin, G0 V, 600 Ma old and member of the Hyades supercluster (Kürster et al. 2000; Laymand & Vauclair 2007; Boisse et al. 2011).

It is expected that the reliability of the detection of exoplanets will improve by the use of high-resolution infrared spectrographs, as the longer wavelengths are less affected by the activity of the star (e.g., Martín et al. 2006; Reiners et al. 2010; Figueira et al. 2010a). However, even when we are able to distinguish a real planet from stellar activity, the mass of the star and the location of the HZ depends on the age of the star. While those M dwarfs older than the Hyades present a range of masses between 0.07–0.60 $M_{\odot}$, for younger stars, such as those belonging to younger associations like β Pictoris (20 Ma; see Chapter 3), this range of masses goes from 0.02 to 0.70 $M_{\odot}$. Since the amplitude of the radial drift produced by an exoplanet depends on the mass of the host star (see Eq. 1.1), the age of the star enables to determine the minimum mass planet detectable by radial velocity measurements. In the case of young M stars of the latest subtypes, their lower mass with respect to older stars of the same subtype made them better candidates to detect Earth-like planets. On the other hand, the HZ of M dwarfs moves inward for up to 1 Ga. The inner edge of the HZ moves in by nearly and order of magnitude after only 10 Ma for the lowest mass objects (Luger & Barnes 2015). In general, the smaller the semi-major axis (a) of a planet, the higher the effect on the radial velocity measurements (see Eq. 1.1). Therefore, old M stars might be better candidates to detect exoplanets in the HZ, but as we will see below, these planets might be uninhabitable.

The detection of an Earth-like planet in the HZ of a star does not imply the habitability of it. Since M stars are the main targets to detect exo-Earths in the HZs, the study of habitability around these objects is mandatory. The habitability of a planet depends on its ability to acquire and retain water (see Ramírez & Kaltenegger 2014), and the activity displayed by young low-mass objects play a major role on this process. M-type stars can take up to 1 Ga to end their contraction (Baraffe et al. 1998, 2015; Reid & Hawley 2005; Dotter et al. 2008). During this time, planets in the HZs may be exposed to intense X-ray and UV fluxes (Sanz-Forcada et al. 2015). Even if a young planet acquires enough water, the large amount of water lost by photoevaporation could cause atmospheres too rich in abiotic O_2 (Luger & Barnes 2015). In addition, the intense flux of high-energetic particles can erode their atmospheres and sterilize the surface (Scalo et al. 2007; Segura et al.2010). These concerns make necessary for the habitability that planets are formed with more water or, once that they are formed, they acquire more water (e.g., accretion of comets) to be habitable (Ramírez & Kalteneger 2014).

It is still not well understood if the planets formed during the pre-main sequence of the star could retain enough water for carbon/water based life. Some authors suggested that rocky planets formed in the HZs of M stars could be small ($\lesssim 0.3\,M_{\oplus}$) and dry, because the planetesimals that assemble to form these planets are deficient in volatiles (Lissauer 2007; Raymond et al. 2007). However, Hansen (2015) took into account the water that might be delivered to these planets and developed *insitu* models that predicted planets in the HZ with similar or even several hundred of times the amount of water contained in the Earth. The work of Tian & Ida (2015) obtained intermediate results in comparison with the above mentioned studies. The authors proposed that the evolution of stellar luminosity mainly leads to two types of Earth-like planets in the HZ of M dwarfs: extremely arid or ocean planets without continents. However, the authors noticed that their model assume that all the water of the planet is located on the surface, discarding the possibility of water reservoirs during the magma ocean phase (i.e., giant impacts produce the fusion of the planet surface and the

water, highly soluble in magma, emerges during the cooling process –Matsui & Abe 1986; Zahnle et al. 1988; Elkins-Tanton 2008, 2011; Lammer 2013; Hamano et al. 2013). Other studies suggest that planets formed farther out could acquire and keep enough water (during the magma ocean phase) and potentially migrate to the HZs (Ida & Lin 2008a,b; Ogihara & Ida 2009; Cossou et al. 2013). The habitability of these planets has to face questions about the ability to lose the thick H/He envelopes accreted from the disc during the migration of planets with masses similar or higher than the Earth (Mizuno et al. 1978; Wuchterl 1993; Ikoma et al. 2000; Rafikov 2006; Lammer et al. 2014). However, Luger et al. (2015) proposed that migrated mini-Neptunes might lose their thick envelopes and become super-Earths in habitable zones of M dwarfs –so called habitable evaporated cores. The authors suggested that this process can be one of the dominant formation mechanisms for volatile-rich Earths around M-dwarfs, instead of *insitu* formation models that likely produce small and dry Earth-mass planets. However, this process of photoevaporation, in which several Earth masses of hydrogen and helium are removed from the planet, is highly dependent on the early X-ray and UV emission evolution of the host star.

More observation of young M dwarfs are needed to shed light on the formation, evolution and habitability of exoplanets. For example, multi-band spectral observation and bulk density measurements can be used to distinguish between Earth-mass planets with Earth-like water from those arid or oceanic planets (Tian & Ida 2015), which might help to constrain the models.

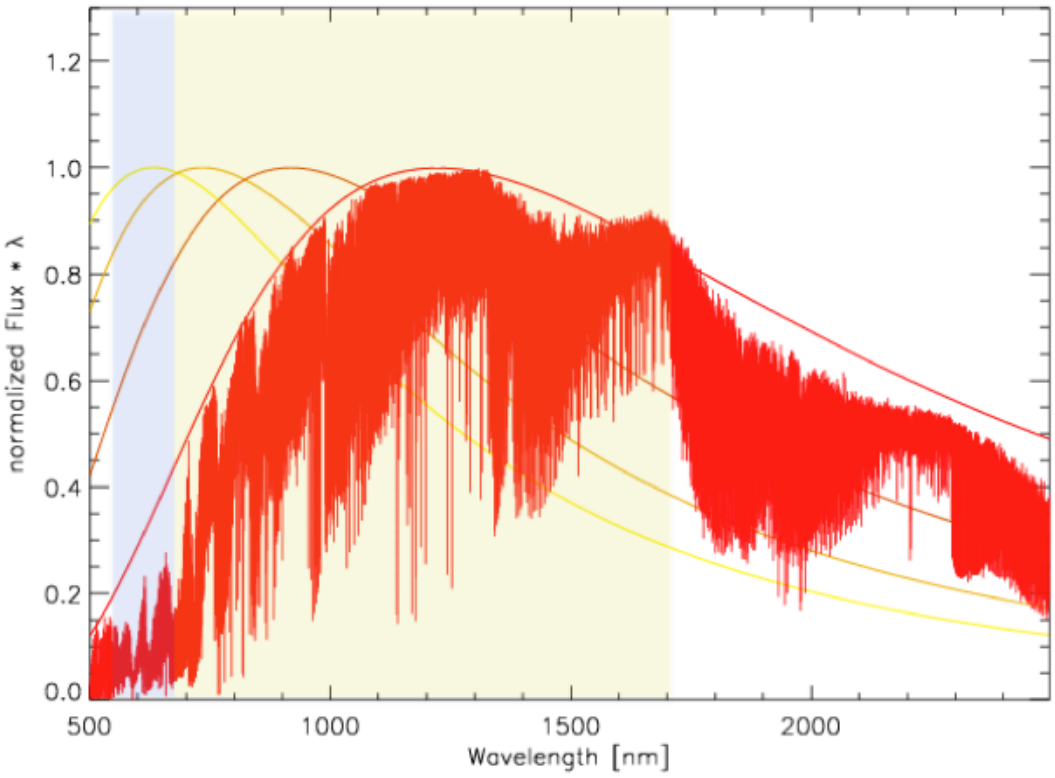

FIGURE 1.3— Synthetic spectrum of an M dwarf. The optic region (blue) is commonly used for exoplanetary surveys using the Doppler method. CARMENES will use the optic and near-infrared region (yellow) to increase the efficiency of the radial velocity measurements. The color lines are black body spectral energy distributions for some M dwarfs effective temperatures.

1.4 High-resolution near-infrared spectrographs

As outlined in detail by Reiners et al. (2010), the most basic idea behind using near-infrared spectrographs instead of optical ones for intensive radial-velocity monitoring of M dwarfs is that the spectral energy distributions of these stars approximately peak at 1.0–1.2 μm **(see Fig. 1.3)**. The optical faintness of these objects is illustrated quantitatively with the V magnitudes of the brightest M dwarfs in the northern hemisphere (HD 79210, HD 79211, and HD 95735) at 7.5–7.7 mag, far from the limit of the naked human eye. Another advantage of using longer-wavelength spectra for M stars is the apparent decline of the effects induced in radial velocity measurements by the stellar activity. Martín et al. (2006) reported a radial velocity signal induced by a starspot on a M9 dwarf ten times smaller at infrared wavelengths than at optical ones. In addition, Reiners et al. (2010) concluded that for temperature differences of a few hundred kelvins between the stellar surface and starspot, the induced radial velocity signal becomes much weaker (up to ten times lower for ΔT ∼200 K). This advantage is highly valuable in the observation of mid- and late-M stars, which tend to be more active than early-M stars. However, going to the near-infrared inherits complications, mainly technological ones, not discussed here (need of cooling/cryogenics, telluric absorption, or behaviour of hybrid CMOS sensors).

Table 1.3— High-resolution near-infrared spectrographs.

Instrument name	Telescope (diameter)	$\Delta\lambda$ (λ coverage) [μm]	R ($\Delta\lambda/\lambda$)	Remark	First light
CSHELL	IRTF (3.0 m)	1.00–5.00 (0.0025)	40,000	To be decommissioned	1993
Phoenix	KPNO (2.1/4.0 m)	1.00–5.00 (0.005)	70,000	Operating	1996
IRCS	Subaru (8.2 m)	0.90–5.60 (∼0.2)	20,000	Polarimetry, AO	1999
NIRSPEC	Keck (10 m)	0.95–5.50 (∼0.1)	25,000	AO	1999
ARIES	MMT (6.5 m)	1.00–2.5	50,000	Operating	2007
GIANO[a]	TNG (3.6 m)	0.95–2.45	50,000	Operating	2012
NAHUAL	GTC (10.4 m)	0.90–2.40	70,000	Cancelled	...
IRET	ARC (3.5 m)	0.80–1.35	22,000	Cancelled	...
PRVS	Gemini (8.1 m)	0.95–1.80	70,000	Cancelled	...
MINERVA-Red	Mt. Hopkins (2×0.7 m)	0.84–0.89	50,000	Cheap	2015
CARMENES	CAHA (3.5 m)	0.50–1.70	82,000	VIS & NIR channels	2015
ISHELL	IRTF (3.0 m)	1.00-5.00 (0.25)	70,000	Gas cell, upgrade	2016
IRD	Subaru (8.2 m)	0.97–1.75	70,000	Laser comb, ceramics, AO	2016
HPF	HET (10 m)	0.84–1.30	50,000	Laser comb	2016
CRIRES+	VLT UT (8.2 m)	1.00–5.00 (0.40)	100,000	Polarimetry, upgrade	2017
SPIRou	CFHT (3.6 m)	0.98–2.35	75,000	Polarimetry	2017
TARdYS	TAO (6.5 m)	0.84–1.11	54,000	Cheap	>2017
HIRES	E-ELT (39 m)	0.31–2.50	100,000	Notional, 2–4 channels	>2020
NIRES	TMT (30 m)	1.00–2.50	100,000	Notional	>2020
GMTNIRS	GMT (25 m)	1.00–5.00	≥60,000	Notional	>2020

Notes. [a]GIARPS (Claudi et al.) is the new common feeding for HARPS-N and GIANO.
`http://www.bo.astro.it/premiale.elt/sesto_2015_talks/Sesto_Carleo.pdf`

The beginning of this century saw the birth and development of some projects aimed at the construction of high-resolution near-infrared spectrographs, which had varying degrees of success (Giano/TNG: Oliva et al. 2012; IR ET/ARC 3.5 m: Zhao et al. 2010; NAHUAL/GTC: Martín et al. 2010; PRVS/Gemini: Jones et al. 2008; CRIRES/VLT: Käufl et al. 2004). Currently, the upcoming "big" instruments with secured funding and that have passed design reviews are SPIRou (Artigau et al. 2014, France-Canada), IRD (Kotani et al. 2014, Japan), HPF (Mahadevan et al.

2014, US), and CARMENES (Quirrenbach et al. 2014, Germany-Spain). In addition to these spectrographs, the CRIRES instrument is in process of renovation to CRIRES+ (Follert et al. 2014), which will increase the wavelength coverage by a factor of ten. It is expected that all of these high-resolution near-infrared spectrographs will have their first light between 2015 and 2017 (see Table 1.3), and that will be demanded at short term not only for radial-velocity surveys of M dwarfs with exo-Earths, but also at mid and long term for the spectroscopic follow-up and confirmation of exoplanet candidates of all masses discovered by *Gaia*, *TESS* and *PLATO*. By the end of the next decade, we may also have infrared spectrographs at very large telescopes: HIRES (Maiolino et al. 2013), NIRES (Skidmore et al. 2015) at the 30 m TMT, and GMTNIRS (Jaffe et al. 2006; Lee et al. 2010) at the 25 m GMT. They fill the gap noticed by the European Telescopes Strategic Review Committee and many other astronomers worldwide, and open the window to the spectroscopic characterisation of exo-Earths. The infrared spectrographs mentioned above, as well as, other representative ones, are outlined in Table 1.3 (see also Crossfield 2014; Caballero et al. 2015).

1.5 CARMENES

1.5.1 The project

The previous sections have contextualized the relevance of M dwarfs in modern astrophysics and the importance of using high-resolution infrared spectrographs to improve the knowledge on these stellar objects. In this regard, it highlights the study of planet formation and its evolution in relation with the stellar host mass, which is poorly constrained at the low-mass regime.

Radial velocity surveys have played an important role in the study of exoplanets and are especially advantageous in the investigation of M-type stars. From January 2016 on, the CARMENES consortium[2] will start a radial velocity survey of 300 well-characterised M dwarfs using a high-resolution spectrograph of the same name with a wavelength coverage from the visible to the near-infrared for the 3.5 m telescope at Calar Alto Observatory. The main goal is to find low-mass planets (i.e, Earth-size planets and several times larger) orbiting mid- to late-M dwarfs, and around moderately active M dwarfs in general. The radial velocity precision and stability that the consortium aims to achieve is $1\,\mathrm{ms}^{-1}$, sufficient to detect in the habitable zone a $2\,M_\oplus$ planet orbiting an M5 V, super-Earths of $5\,M_\oplus$ for stars later than ∼M4, and even Earth-mass planets around stars near the hydrogen-burning limit (see Fig. 1.4).

The consortium has more than 600 clear guaranteed nights until at least 2018 to observe the final CARMENES sample. It is expected that these observations will provide between 50 and 100 low-mass planets, many of them in the HZ (see Sect. 1.2). This will provide enough data to constrain the ratio of Earth-like planets around M dwarfs. As well, it will be possible to assess the overall distribution of planets orbiting M dwarfs with an unprecedented statistical sample.

In addition, the CARMENES consortium will determine fundamental parameters of the observed M dwarfs. The consortium will use the high-resolution spectra obtained, especially the near-infrared wavelengths, to derive effective temperatures, abundances and surface gravities. This will help to characterise planets that might be found orbiting those stars.

[2] `http://carmenes.caha.es/`

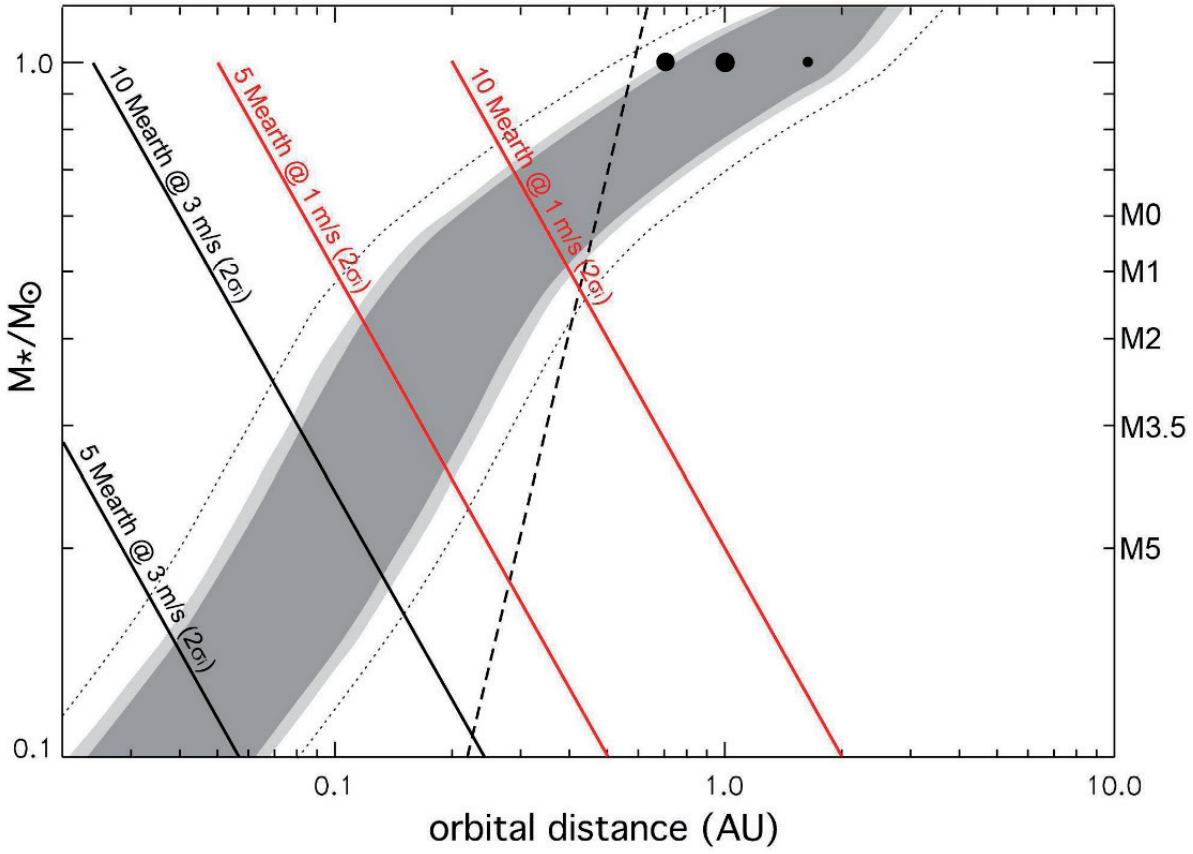

FIGURE 1.4— Habitable zone (shaded area) as a function of stellar mass and orbital separation. Approximate stellar spectral types are indicated in the right y-axis for reference. The dashed line indicates the tidal locking separation. Solid lines illustrate the limits for the detection (at the significance of twice the individual measurement error, σ_i) of super-Earth type planets ($5\,M_\oplus$ and $10\,M_\oplus$) at different radial velocity precisions (1 and 3 ms^{-1}). The accessible regions are to the left of the lines. Figure from Quirrenbach et al. (2010).

However, CARMENES represents the unique possibility to obtain high-resolution spectra at visible and near-infrared wavelengths simultaneously, which will be also of use for other scientific purposes (see Amado et al. 2015):

- Asteroseismology: the search for pulsations in M stars, the study of solar-like oscillations in red giants, and the attempt to perform mode identification in the complicated frequency spectrum of classical pulsators in both the main and pre-main sequence phase, with or without planets, will benefit from high resolution, simultaneous observations with large spectral coverage.
- Stellar magnetic activity: magnetic activity in (ultra) cool dwarfs, exoplanet-induced activity and the effect in radial velocities.
- Stellar fundamental parameters: determination of effective temperature (T_{eff}), surface gravity ($\log g$), rotation velocity ($v \sin i$) and abundances, specially for bright massive stars that present very few lines in their optical spectrum.
- Exoplanetary atmospheres: the observation of molecular bands in the transmission and emission near-infrared spectra of giant planet atmospheres would allow to measure their Doppler displacement and detect specific molecules.

- Follow-up for space missions: confirmation of transiting planets detected by space missions, such as *TESS*, *CHEOPS* and *PLATO* **(see below)**. In addition, *Gaia* could use the visible CARMENES spectroscopy of red targets to calibrate its Ca II infrared triplet observations for metallicity determinations.

- Others: proto-planetary and proto-stellar discs; moving groups and cluster member kinematics; high precision radial velocity of eclipsing binaries (Rossiter-McLaughlin effect); near-infrared spectra of embedded objects; planetary nebulae; Solar System; 'gamma ray bursts'; interstellar and circumstellar medium; etc.

Possible collaborations of space mission with CARMENES were pointed above. However, these exoplanetary surveys have associated radial velocities follow-up measurements, and therefore, it is interesting to compare these space missions and the CARMENES project. The main advantages –leaving budgets out– are the earlier starting of the project, durability and adaptability. The only space telescopes currently in orbit are *Kepler* and *Gaia*, while the other space mission are expected to be launched in between 2017 (*TESS*, *CHEOPS*) and 2024 (*PLATO*). Opposite to *Gaia*, *Kepler* main objective is the detection of exoplanets and can detect exo-Earths in the habitable zone of M dwarfs. However, these detections are not their main duty and are done only for those stars in the *Keppler* field of view (∼0.25 percent of the sky), while CARMENES access to more sky regions and it is optimized for detecting exoplanets in the HZ of M dwarfs. In addition, CARMENES will provide the necessary targets for these space mission, especially for *CHEOPS*, into which measure true planet masses and densities. CARMENES is also a previous technological step before the detection or confirmation of exoplanets in solar like stars by radial velocity measurements, which will be needed by the space transit surveys. The useful life of these space telescopes is commonly 2–4 years, although in some exceptions like *Kepler* –with big issues– can be extended. Finally, possible instrument failures are really complicated to solve for space telescopes (e.g., the *Hubble* myopia). In contrast, the CARMENES instrument presents a useful life of over a decade (e.g., HARPS started in 2004 and still working), during which possible issues can be easier solved or even the instrument can be updated (e.g., CRIRES is being updating to CRIRES+; see Sect. 1.4).

1.5.2 The consortium

The construction of the spectrograph and the development of the project are carried out by 11 institutions divided in five Spanish, five German and the Calar Alto observatory. It also involves more than 13 industrial collaborators and manufactures around the world that provide expertise (e.g., design, system engineering services) or pieces (e.g., detectors; cameras; échelle grating mosaics) that the institutions of the consortium cannot provide. The construction of different parts of the instrument and the science-preparation needed before starting the survey is divided between the 11 institutions approximately as follow:

- Max-Planck-Institut für Astronomie (Heidelberg): near-infrared detector system (including CMOS mosaic, cryostat, electronics and readout software)

- Instituto de Astrofísica de Andalucía (Granada): near-infrared spectrograph (opto-mechanics, electronics, control, final assembly). This is also the institution of the deputy principal investigator.

- Landessternwarte Königstuhl (Heidelberg): visible spectrograph (opto-mechanics, CCD detector system, final assembly) and front-end (opto-mechanics). The principal investigator and the deputy system engineer belong to this institution.
- Institut de Ciències de l'Espai (Barcelona): instrument control system and scheduler, and project scientist.
- Insitut für Astrophysik Göttingen (Göttingen): visible and near-infrared vacuum systems, Fabry-Pérot etalons, pipeline, high-resolution spectroscopy science preparation and deputy project scientist.
- Universidad Complutense de Madrid (Madrid): construction and maintenance of the input catalogue (CARMENCITA, see below), sample characterisation using low-resolution spectroscopy (this thesis) and high-resolution imaging, and numerous science preparation tasks.
- Thüringer Landessternwarte Tautenburg (Tautenburg): near-infrared and visible Calibration units.
- Instituto de Astrofísica de Canarias (Tenerife): construction of key mechanical components of visible and near-infrared channels.
- Hamburger Sternwarte (Hamburg): electronics of the visible spectrograph and front-end, and responsible for the acquisition and guiding system.
- Centro de Astrobiología (Madrid): coordination of management, science preparation and website maintenance. The deputy project manager belongs to this institution.
- Centro Astronómico Hispano-Alemán (Calar Alto): interlocks, coudé room refurbishing, operation of the instrument.

1.5.3 The instrument

CARMENES will observe in optical and infrared wavelengths simultaneously, which will provide highly valuable information to distinguish exoplanets from stellar activity (of high relevance for young and late-M stars). The consortium tests show that the wavelength dependence of activity-induced radial velocity signals will result in at least a factor of 2 to 3 different amplitude in the range 0.55–1.7 μm (Quirrenbach et al. 2010, 2012, 2014). In addition, the instrument covers the spectral region around 1.0 μm, which is the most important region for radial velocity studies of mid- to late-M stars (see Sect. 1.4). The main parts of this instrument are described below and a scheme of them is plotted on Fig. 1.5.

The CARMENES front-end is attached to the Cassegrain focus of the telescope and it is built to allow the use of other instruments (especially PMAS integral-field spectrograph; Roth et al. 2005). Here, the light is compensated from atmospheric dispersion and passes to a dichroic mirror that feeds the optical fibres of the two channels (seven for each spectrograph plus additional ones for the calibration system, see Stürmer et al. 2014). It also includes an optical element that provides light to the guiding camera. The fibres go then to the coudé room, where there are the two high-resolution spectrographs. The internal losses are always smaller than 5 % for both channels.

The CARMENES spectrographs are as similar to each other as possible. Both are based on an échelle design, with a resolution of $R = 82{,}000$, in the wavelength ranges of 0.55–1.05 μm and

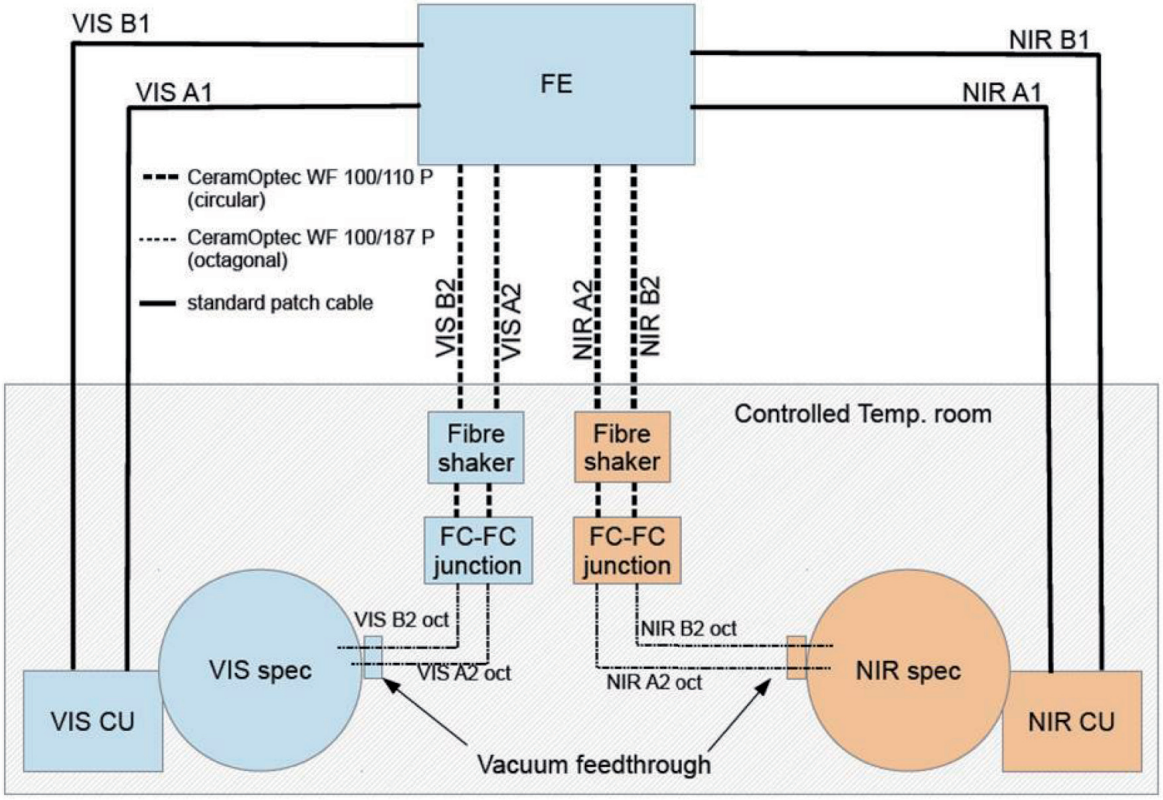

FIGURE 1.5— CARMENES instrument scheme: the front-end (FE) feeds the two spectrographs (VIS and NIR) through fibres. The calibration light from the Calibration Units (CU) is also fed with fibres to the FE and, from there, to the spectrographs in the coudé room of the telescope. Image from Amado et al. (2015).

0.95–1.7 μm. The visible detector is a back-side illuminated 4112×4096 pixel CCD, while the near-infrared detector is a mosaic of two 2048×2048 pixel HAWAii-2RG sensors. The spectrographs are inside of two vacuum tanks, for a better mechanical and thermal control, placed in temperature-stabilized rooms (see Fig. 1.6). The cooling of the visible channel is done by a continuous flow of liquid nitrogen, which avoids the vibrations produced by mechanical coolers and it is similar to a number of European South Observatory instruments. On the other hand, the working temperature needed by the near-infrared detector, 140 K, forces the use of another cooling system provided by a continuous flow of gaseous nitrogen (see Becerril et al. 2012, Mirabet et al. 2014), which ensures a stability within ± 0.01 K over 24 hours.

The calibration system consists on hollow-cathode emission line lamps for spectral calibration (Th-Ne for the visible channel, U-Ne in the near-infrared; Sarmiento et al. 2014). The differential nightly drift of the spectrograph is traced with daily calibration lamps switched on during the observations. These lamps have to be calibrated regularly against "master" lamps used less frequently (only used for providing wavelength solution). The "master" lamps should be calibrated twice a year against a set of "super-master" lamps that are stored in a dedicated tank filled with a low-pressure neon atmosphere. Moreover, the calibration units provide additional input ports for two Fabry-Pérot etalons in order to provide a better tracking of the spectrograph drifts during the night.

All the observation and calibration systems are controlled by the instrument control system

FIGURE 1.6— Visible vacuum tank inside the thermal controlled chamber at the coudé room of the Calar Alto 3.5 m telescope.

(Guàrdia et al. 2012; García-Piquer et al. 2014). The observations are also supported by an operational scheduler that provides an optimized survey plan based on previous known data (e.g., target visibility and magnitude, moon phase and position, sky background) and dynamic changes (e.g., weather and system conditions). When one observation will take place, immediately after, there will be a "science" reduction and radial velocity measurements.

1.5.4 CARMENCITA

As outlined above, CARMENES will observe a final sample of 300 M dwarfs over >600 nights. To obtain the best sample possible, the consortium is building an input catalogue, dubbed CARMENCITA (CARMENES Cool dwarf Information and daTa Archive; see Caballero et al. 2013). This input catalogue contains approximately 2200 M dwarfs and is filled with a number of parameters collected from the literature or measured by the consortium. Among the most important parameters, there are reliable spectral types (see Chapter 2), astrometry and kinematics (α, δ, $\mu_\alpha \cos\delta$, μ_δ, π, V_r, U, V, W), photometric information (22 photometric bands covering from the ultraviolet to the infrared), multiplicity information (close and wide companions, see Chapter 3), activity and age indicators ($pEW(H\alpha)$, X-ray information, rotational velocity) and common used spectral indices (TiO 5, CaH 2; see Chapter 2).

The information summarized above is needed to prepare the CARMENES input catalogue with the most promising targets. The members of the consortium have collected systematically all published M dwarfs in the literature that fulfilled two simple criteria:

- Stars observable from Calar Alto with declinations $\delta > -23$ deg (i.e., zenith distances < 60 deg, air masses at culmination < 2.0).

- Stars selected according to late spectral type and brightness. We only catalogued confirmed dwarf stars with an accurate spectral type determination from spectroscopic data (i.e., not from photometry) between M0.0 V and M9.5 V. Additionally, we only compiled the brightest stars of each spectral type. Our database contains virtually all known M dwarfs that are brighter than the completeness magnitudes shown in Chapter 2, Table 1, and most of them brighter than the limiting magnitudes. No target fainter than $J = 11.5$ mag is in our catalogue.

The initial source of CARMENCITA are the M dwarfs from the Research Consortium on Nearby Stars (RECONS), which catalogues all known stars with measured astrometric parallaxes that place them within 10 pc (e.g., Henry et al. 1994; Kirkpatrick et al. 1995; Riedel et al. 2014; Winters et al. 2015). The RECONS stellar compilation was next completed with the Palomar/Michigan State University survey catalogue of nearby stars (PMSU –Reid et al. 1995, 2002; Hawley et al. 1996; Gizis et al. 2002). Afterwards, we gave special attention to the comprehensive proper-motion catalogues of Lépine et al. (2003, 2009, 2013) and Lépine & Gaidos (2011), and the "Meeting the Cool Neighbors" series of papers (Cruz & Reid 2002; Cruz et al. 2003, 2007; Reid et al. 2003, 2004, 2008). In Chapter 2, Table 2, we provide the sources of our information on M dwarfs. Until the start of the survey at the beginning of 2016, the consortium will still include some new, particularly bright, late, single, M dwarfs.

A precise knowledge of the targets is critical to ensure that most of the CARMENES guaranteed time is spent on the most promising objects. This selection involves not only a comprehensive data compilation from the literature, but also summarises the consortium's observational effort to achieve new low- and high-resolution optical spectroscopy and high-resolution imaging. This thesis includes some of the preparation science used to provide new low-mass objects to the input catalogue and to gather suitable information for selecting the candidates for CARMENES.

1.6 Low-resolution spectroscopy

M dwarfs are the most common stellar objects in the Galaxy, but they are also among the faintest ones at optical wavelengths (see Sect. 1.4). The large amount of observational time that they need and their complex spectra at optical wavelengths have prevented the performance of large radial-velocity surveys using high-resolution spectroscopy, especially for the latest spectral types. At the beginning of this chapter, it was described how M-type stars have been classified over the years mainly using their molecular bands. These classifications have been possible thanks to low-resolution spectra. However, even the surveys of M dwarfs with low-resolution spectra need a considerable amount of observational time (e.g., see exposure times in Table B.1). Therefore, some authors have used large photometric surveys like SUPERBLINK (Lépine et al. 2002; Cruz et al. 2010; Lépine 2011; Lépine & Gaidos 2013), 2MASS and more recently *WISE* (O'Donnell et al. 2013), to find M-type candidates –as well as cooler objects of the last spectral types. We highlight the work of Lépine & Gaidos (2011), who presented spectral types and parallaxes derived from photometry for 8,889 bright M-dwarfs candidates ($J < 10$ mag) based on the SUPERBLINK catalogue (i.e., proper-motion catalogue of stars with $\mu > 40$ mas a^{-1} and $V < 20$ mag, based on a re-analysis of images from the Digitized Sky Surveys) and supported by 2MASS photometry. This work is still ongoing and nowadays the SUPERBLINK catalogue is filled with around 150,000 M-dwarf candidates within 100 pc of the Sun (Lépine & Gaidos 2013). The power of the photometric technique to study M-type stars

is remarkable. However, what is gained in quantity is lost on precision. The spectral typing using photometry can be considered as a very low-resolution spectroscopy and, therefore, it loses relevant information provided by the molecular bands. The comparison of spectral types derived from photometry and spectra, plotted on Chapter 2, Fig. 5 illustrates how much precision can be lost. Lépine et al. (2013) presented accurate spectral types for 1564 bright ($J < 9$ mag) M-dwarf candidates from Lépine & Gaidos (2011), and they found that 1408 of them were late-K and M dwarfs with spectral subtypes K7–M6.

The previous sections presented the purpose of the CARMENES consortium to fill CARMENCITA with well characterised M-type stars. The low-resolution spectroscopy was the natural selection for spectral typing those M-dwarf candidates without accurate spectral types and also to obtain other suitable information like the pseudo-equivalent width of Hα. This was a crucial first step because the selection criteria of CARMENES are based on a combination of magnitudes and spectral types (see, Chapter 2, Table 1). That is why some of the objects studied with low-resolution spectra are not part of the CARMENCITA database. Moreover, this work is basic for the other science preparation tasks, such as high-resolution spectra and imaging. We have based our study on previous spectroscopic surveys, mainly Kirkpatrick et al. (1991) and the Palomar/Michigan State University catalogue (PMSU). It is also comparable to the MILES catalogue (Medium-resolution Isaac Newton Telescope Library of Empirical Spectra; see Sánchez-Blázquez et al. 2006) and the spectroscopic catalogue of the brightest ($J < 9$ mag) M dwarfs in the northern sky by Lépine et al. (2013).

1.6.1 Some investigations that have influenced our survey

The study of Kirkpatrick et al. (1991) introduced a relevant innovation on spectral typing: they did not only use the strength of the molecular bands, but a comparison on the slopes of the spectra using a least square minimisation technique. This method can be understood as the translation to mathematics of the naked eye comparison used on the first spectral typing studies. The technique uses the general spectrum slope, which is mainly related with the effective temperature of the object, to determine the spectral type without a strong influence of metallicity, chromospheric activity or surface gravity. However, it needs the appropriate corrections of the spectra due to observational effects, such as deformations introduced by the sensitivity of the detectors and interstellar reddening for distant objects (our samples are near the Sun and, therefore, this effect can be neglected). As well, other techniques are needed to be sensitive to the luminosity class or the previous mentioned parameters. Therefore, their research made use of the strength of molecular features using the indices technique (i.e., ratios between the flux at a selected "continuum" and the deepest part of the molecular features). The principal advantage of this technique is the sensitivity to other physical properties and the unnecessary spectral correction. On the other hand, a careful selection of the wavelength intervals used to measure the fluxes is needed, which becomes a tricky task due to the emergence of new molecular bands in cooler objects. That is why most of the indices are useful for spectral typing in a short range of spectral types (see Chapter 2). Both techniques have in common the need of a careful selection of a set of standard stars for an appropriate calibration, which also depends on the used instrumental configuration.

Kirkpatrick et al. (1991) provided a homogeneous classification of M-type stars and a set of standard stars. Unfortunately, only 77 spectra, from K5 to M9, were studied in the large wavelength coverage (λ6300 to 9000 Å) and at a quite low-resolution of 18 Å. Later, there were other studies focused on providing a significant number of spectral types. One of the earliest and most relevant surveys of M-type stars was the PMSU series. The research of Reid et al. (1995) made use of the

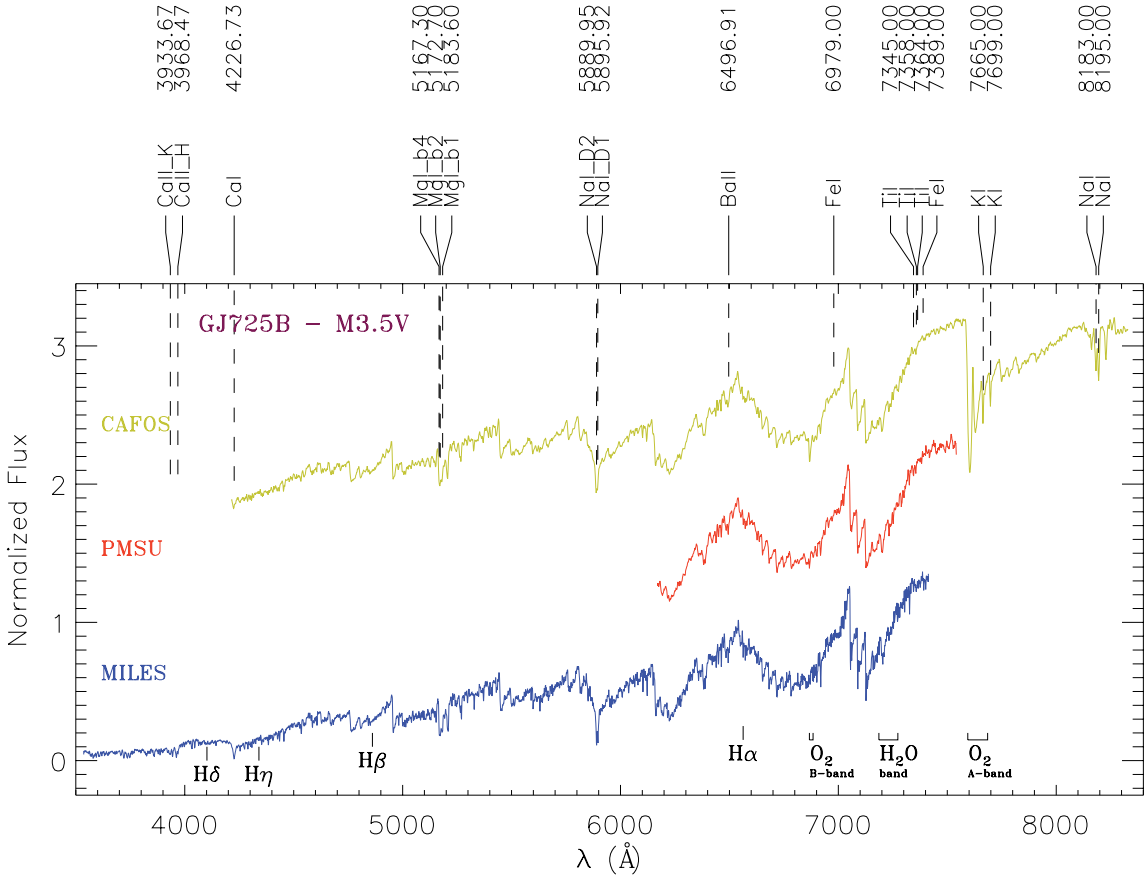

FIGURE 1.7— Comparison of the GJ 725 B (M3.5 V) low-resolution spectra taken at the 2.5 Calar Alto (green), 1.5 m Palomar (red) and 2.5 m Isaac Newton (blue) telescopes with their respective spectrographs. While the resolution differences are hardly distinguishable, the variations on wavelength ranges are important. The most important atomic features are marked. For reference of the molecular bands see Fig.1.1.

Third Catalogue of Nearby Stars (CNS3, Gliese & Jahreiss 1991), and studied 1746 of the 1876 stars that the CNS3 had identified as spectral type M or suspected to be M-type stars –these stars lie north of $\delta = 30°$. They obtained spectra with a relative short wavelength coverage of λ6120 to 7500 Å with a resolution of 1.5 Å. Hawley et al. (1996) added 317 southern stars, using spectra with a similar wavelength coverage, λ6300 to 7200 Å, and a slightly smaller resolution of 3.1 Å. The narrow range of wavelengths selected was enough to study the most useful molecular features of TiO and CaH, as well as the Hα atomic line, but made a feature-by-feature minimisation approach harder. Therefore, they based their classification on the indices technique. Unfortunately, some important features for the latest spectral types, such as VO bands, felt at the limits or outside of the wavelength range covered by this study (see Fig. 1.7).

Other useful study is the MILES catalogue, which provided a stellar library in a wide range of spectral types, including the M-type stars. The wavelength coverage used by MILES, λ3525–7500 Å, is useful to study the variations on the shape of the spectra due to the broad effective temperatures of the targets. This project was aimed to establish a spectral library useful for population-synthesis models, therefore the low-resolution used, 2.3 Å, obeyed this goal. In comparison with PMSU, this investigation improved the wavelength coverage and resolution, but it was not aimed to provide M

dwarfs. In addition, it does not cover important atomic and molecular features for the classification of the latests M dwarfs (see Fig. 1.7).

Our research intended an appropriate characterisation of M dwarfs using the least square minimisation and indices technique. From the studies described above, we understood the need of a wide wavelength coverage combined with an appropriate resolution for the success. Moreover, we took into account the large amount of time needed to observe a large sample mainly composed of faint objects. The availability at the observatory of Calar Alto of an appropriate telescope with a efficient low-resolution spectrograph, and the good predisposition of the Observatory staff and Time Allocation Committee to perform this survey at their installations, made the instrument selection a unique choice. The 2.2 m telescope, at Calar Alto, holds a spectrograph called CAFOS (Calar Alto Faint Object Spectrograph) that allows the observer to take direct imaging, spectroscopy (with grism and longslit or multi-object mask) or polarimetry. We selected the longslit mode because our objects were located around the whole sky and quite separated. The grism selection took into account that the wavelength range had to cover the most relevant features of mid-K to late-M dwarfs, as well as that some of the indices needed resolutions of a few angstroms. There were eight possible grisms to choose: five had not enough resolution (B-400, R-400, B-200, G-200, R-200) and another one (B-100) had a wavelength coverage too blue λ3200–5800 Å. Of the two remaining grisms, the R-100 one had a redder wavelength coverage than the G-100 one, which is appropriate for M dwarfs of the latest spectral types (λ5900–9000 Å), but missed important features to distinguish late-K from early-M stars or M giants from M dwarfs (e.g., the M giants present a typical tooth shape below 5600 Å; see Gray & Corbally 2009). The grism G-100 combined an appropriate resolution of $\sim$4 Å with a suitable wavelength coverage (wider than PMSU and redder than MILES) for the dynamical range of spectral types studied. Therefore, it was a good compromise for the two used methodologies (see Fig.1.7).

Finally, although the research of Lépine et al. (2013) has not had direct influence on our methodology, it is comparable to our study and an indirect scientific collaboration. Among the studies used for our low-resolutions spectroscopy observations (see Chapter 2), a significant amount of objects comes from Lépine & Gaidos (2011). We presented some previous results of our work on spectral typing at several conferences where Prof. Lépine noticed them. After it, the CARMENES consortium and Prof. Lépine started a conversation to achieve a scientific agreement. The main reason was that he was already working on a similar investigation using low-resolution spectroscopy to characterise the objects of Lépine & Gaidos (2011). The agreement allowed us to be the only ones to observe the objects presented by Lépine & Gaidos (2011) that were accessible from Calar Alto and fainter than $J > 9$ mag. These stars were very interesting for the goals of CARMENES because they could include objects of the latest spectral types, but they needed larger exposure times. The main difference between the work of Lépine et al. (2013) and our research is that the spectra of Lépine et al. (2013) were taken using two different spectrographs, which makes the sample heterogeneous. However, it does not affect the accuracy and validity of the derived spectral types. Furthermore, the spectral types derived by us, PMSU and Lépine et al. (2013) were used to fill the spectral type information of CARMENCITA, due to the excellent agreement between the results of the three studies (see Chapter 2, Fig. 5).

1.7 Nearby young M dwarfs

Until the late nineties the typical method to find (very) young stars, from $\sim10^6$ to $\sim10^8$ a, was to find them in classical star forming regions, such as Scorpion-Centaurus ($\sim$130 pc, de Zeeuw et al. 1999),

Taurus-Auriga (∼140 pc, Frink 1999), ρ Oph (∼135 pc, Wilking & Lada 1983) and Orion (∼412 pc, Hillenbrand 1997). Some nearby isolated T Tauri stars were known outside these star forming regions (e.g., de la Reza et al. 1989; Gegorio-Hetem et al. 1992), but it was not demonstrated that they could be part of bigger groups of stars, which would allow to find other young objects around them. However, Kastner et al. (1997) proposed that the TW Hydrae star and other four T Tauri objects were part of the same physical association with similar physical properties (e.g., X-ray emission, Galactic velocities, age), so called TW Hya association (see Table 1.4). This publication opened the window to find close young stars outside the star-formation regions by studying groups of stars with similar kinematics.

TABLE 1.4— Properties of young Local Association subgroups.

Moving group	Age [Ma]	d [pc]	U [km s^{-1}]	V [km s^{-1}]	W [km s^{-1}]	References
TW Hydrae	8–12	40–62	-10.5 ± 0.9	-18.0 ± 1.5	-4.9 ± 0.9	1, 2, 4, 5
β Pictoris	∼20	18–40	-10.1 ± 2.1	-15.9 ± 0.8	-9.2 ± 1.0	1, 2, 3, 4, 5, 6
Tucana-Horologium	20–40	38–55	-9.9 ± 1.5	-20.9 ± 0.8	-1.4 ± 0.9	1, 2, 4, 5, 6
Columba	20–40	50-120	-13.2 ± 1.3	-21.8 ± 0.8	-5.9 ± 1.2	1, 2, 4, 5, 6
Carina	20–40	50–120	-10.2 ± 0.4	-23.0 ± 0.8	-4.4 ± 1.5	1, 2, 4, 5, 6
AB Doradus	70–120	10–60	-6.8 ± 1.3	-27.2 ± 1.2	-13.3 ± 1.6	1, 2, 4, 5, 6
ϵ Chamaeleontis	∼6	99–117	-11.0 ± 1.2	-19.9 ± 1.2	-10.4 ± 1.6	1, 4, 5

Notes. The reference for the U, V, W kinematics comes from Torres et al. 2008 (1). The age and distance are indicative limits based on information taken from: Malo et al. 2013 (2); Binks & Jeffries 2013 (3); Gagné et al. 2014 (4); Elliot et al. 2014 (5); Elliot et al. 2015 (6).

Stellar kinematic groups (SKGs) are kinematically coherent groups of stars that could share a common origin (the evaporation of an open cluster, the remnants of a star formation region, or a juxtaposition of several little star formation bursts at different epochs in adjacent cells of the velocity field; see Montes et al. 2001). The main references of this theory are the studies of Olin Eggen (e.g., Eggen 1958, 1984, 1989, 1994, 1995). He studied the Galactic velocities on the three space directions (U, V, W) to determine groups of stars with similar motions and that maintain a kinematic signature over long periods of time (see Fig. 1.8). Eggen (1994) defined a supercluster as a group of stars gravitationally unbound that share the same kinematics and may occupy extended regions in the Galaxy. In this same paper he stated that a moving group (MG) is the part of the supercluster that enters the solar neighbourhood and can be observed all over the sky. Therefore, he proposed the possibility of determining the memberships of stars in the solar neighbourhood to these groups based on kinematic criteria, so called Eggen's kinematic criteria (see Montes et al. 2001).

However, this theory faces physical processes that act against the persistence of any kinematic signature over long periods of time. For example, the Galactic differential rotation tends to spread the stars, and the disc heating causes an increment of the velocity dispersion of stars of the disc with the age. In addition, the SKGs may also be the result of resonant dynamical structures (e.g., Famaey et al. 2007 determined that the Hyades MG is a mixture of stars evaporated from the Hyades cluster and a group of older stars trapped at a resonance) or the dissolution of larger stellar aggregates, such as stellar complexes or fragments of old spiral arms. Therefore, SKGs have had detractors since its origins (e.g., Griffin 1998; Taylor 2000), but the use of astrometric data from *Hipparcos* (Perryman et al. 1997; van Leeuwen 2007) confirmed the existence of these MGs (e.g., Chereul et al. 1998, 1999; Mülläri et al. 2000; Torra et al. 2000). Nowadays, the SKGs are commonly used to study the solar neighbourhood, especially for the coolest stellar population.

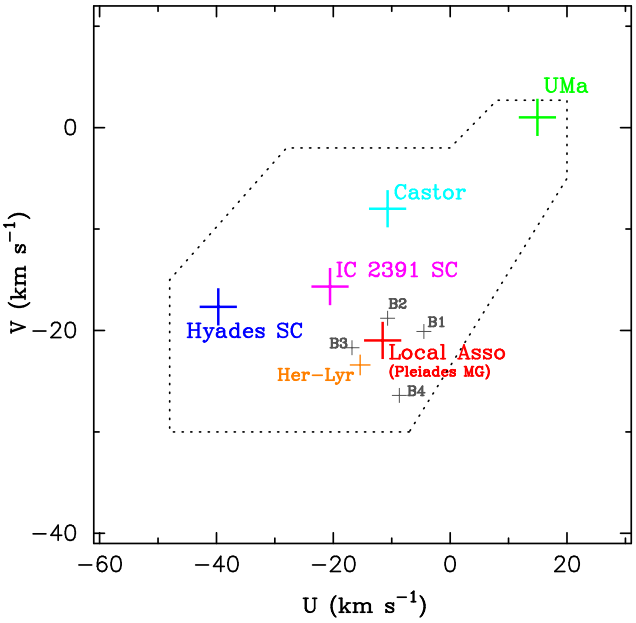

FIGURE 1.8— Space galactocentric velocities V vs. U diagram around the boundaries (dashed line) that determine the young disc population as defined by Eggen (1984, 1989; see Montes et al. 2001). Colour crosses are centred on the classical moving groups (Local Association, Hyades Supercluster, Ursa Major, Castor, IC 2391 and Hercules-Lyra). The smaller black crosses correspond to other four subgroups of the Local Association. Figure from Montes (private communication).

The classical superclusters are the Hyades (600 Ma), Ursa Major (300 Ma), Local Association or Pleiades (20-150 Ma), IC 2391 (35–55 Ma), Castor (200 Ma) and Hercules-Lyra (see Soderblom & Mayor 1993; Montes et al. 2001; López-Santiago et al. 2006; Eisenbeiss et al. 2013; Klutsch et al. 2014, and references therein). More recently, other very young SKGs have been identified with similar kinematics to the Local Association (see Table 1.4) and to other MGs like Argus to IC 2391 and Octans to Castor (e.g., Zuckerman et al. 2001a; Song et al. 2003; Torres et al. 2006; Lépine & Simon 2009; Schlieder et al. 2010, 2012; Shkolnik et al. 2011, 2012; Desidera et al. 2011; Kiss et al. 2011; Rodríguez et al. 2011; Mamajek et al. 2015).

The β Pictoris moving group (Zuckerman et al. 2001b; Ortega et al. 2002; Song et al. 2003) stands out among these young identified subgroups. It has been studied by a good number of the authors cited in this section (see Chapter 3), due to the combination of proximity and youth shown by this moving group. There are even new associations identified, such as the All Sky Young Association (ASYA, Torres et al. 2015).

These nearby associations are close enough to be observed all over the sky, instead of being located in a region of the sky like the star formation regions (e.g., Orion at 50 pc would cover almost the whole sky; Torres et al. 2008). Therefore, it is needed to cover big areas of the sky to find members of the same association (same age and similar distances), which presents an important observational issue. However, the arrival of large sky surveys provided the necessary data (i.e., proper motions, photometry, parallax, radial velocities, distances) to solve the problem. These surveys (e.g., 2MASS, *WISE*) has made possible to identify young nearby objects as members of these associations. In the first studies (e.g., Zuckerman & Web 2000; Torres et al. 2000; Zuckerman et al. 2001a; Song et al. 2003; Zuckerman & Song 2004; Torres et al. 2006), the main identifications corresponded to

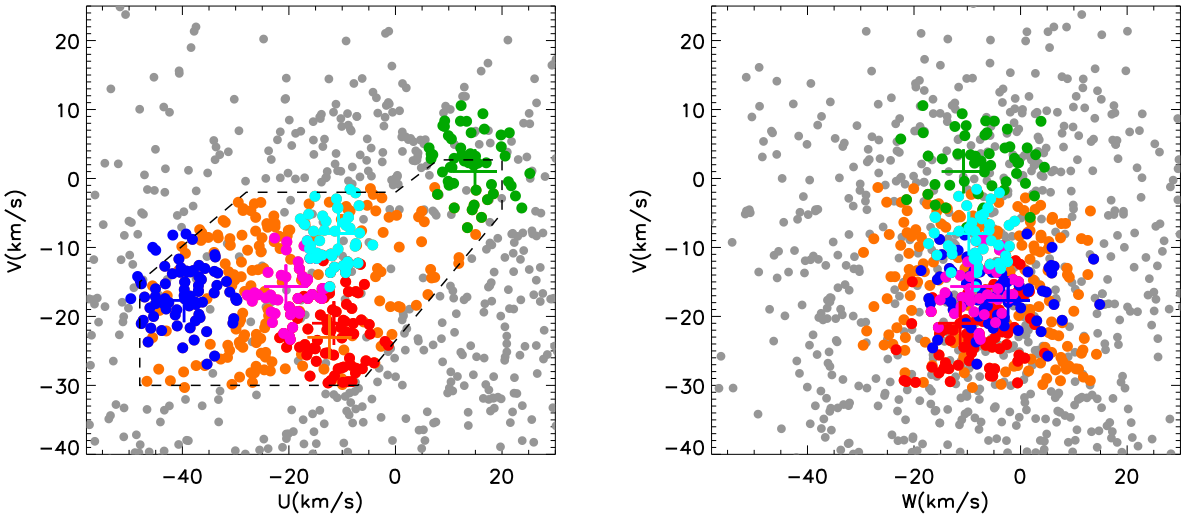

FIGURE 1.9— Böttlinger diagrams (U, V and V, W) zoomed around the young disc population (see Fig.1.8). The dots represent the CARMENCITA sample, the different colours correspond to possible candidates in the six young SKGs represented in Fig.1.8, other young disc stars (orange), and old disc population (grey). Figure from Montes et al. (2015)

relatively early-type stars (A, F, and some G). Nowadays, research projects like BANYAN (Malo et al. 2013; Gagné et al. 2014), SACY (Torres et al. 2008; Elliot et al. 2014) or LACEwING (Riedel 2015) have studied enormous amount of stars, taking into account kinematic and photometric data simultaneously, in order to provide new members and candidate members in the lowest stellar mass regime (see also Lépine & Simon 2009; Schlieder et al. 2010, 2012; Kraus et al. 2014). They have contributed in this way to a better knowledge of the formation and evolution of the solar neighbourhood. In addition, the members of these association are very interesting for exoplanetary surveys due to their proximity, higher brightness, and lack of studies on planets orbiting young, low-mass stars.

Some studies on stellar associations (e.g., Shkolnik et al. 2009, 2012; Caballero 2010a; Malo et al 2013; Riedel et al. 2014) have been useful to gather suitable information for the CARMENES project (e.g., radial and space velocities, close and wide multiplicity, X-ray emission, lithium measurements). Furthermore, the stars contained in CARMENCITA with enough information (astromery, radial velocity and parallax) can be plotted in a Böttlinger diagram such as the one of Fig. 1.9 to study their possible membership to SKGs (see Montes et al. 2015).

1.7.1 Common proper-motion companions

Common proper-motion companions are the bridge between unbound members of SKGs and wide binary systems. Large sky surveys with proper motion data, such as *Hipparcos*, Tycho and Tycho-2 (Høg et al. 1997, 2000), SUPERBLINK, USNO-B1 (Monet et al. 2003), PPMXL (Röser et al. 2010) or URAT (Zacharias et al. 2015), have helped to investigate on stars that show similar proper motions. For example, Lépine (2011) used the SUPERBLINK catalogue to find 18,000 co-moving pairs, which are mainly nearby ($d < 100$ pc) low-mass systems with K- or M-dwarf components. However, pairs of stars with similar proper motions might be wide binaries, or stars of a same association or Galaxy stream that for chance are co-moving. Binary systems can be distinguished from co-moving

pairs because the components of bound systems show similar physical parameters (e.g., distances, radial velocities, age) that co-moving stars do not show.

The proper motion technique is useful to discover M-type companions to hotter stars or even low-mass systems highly interesting for testing evolutionary models (see Chapter 3). The search for wide (low-mass) companions around the appropriate targets using the proper motion technique (e.g., members or candidate members of young stellar association) can provide valuable information, such as the age of the system, which can be used in turn to compute the masses of each component. Wide systems (especially the ones with the lowest binding energies) can also help to constrain the upper limit between physical bound systems and co-moving stars of the same association (e.g., Shaya & Oling 2011; Caballero 2010a). In addition, the wide companions of the lowest masses help to improve the knowledge of young associations. For example, they are used to constrain the age of these associations with lithium depletion boundary technique (Jeffries et al. 2006; Binks & Jeffries 2013). The CARMENES consortium has also used investigations on wide systems to gather low-mass candidates and suitable information for the final selection (e.g., Gizis & Reid 1997; Gizis et al. 2000; Lépine 2003, 2009; Scholz et al. 2005; Caballero 2007, 2009, 2012; Cortés-Contreras et al. 2014, 2015; see Chapter 2, Table 2).

However, wide systems can be separated from some arcseconds to several arcmin (or even degrees; see Caballero 2010b). The search of binary systems with the common proper-motion technique requires large searching areas of the sky (several square arcminutes), which involves the processing of large amounts of data. Some authors use their own "scripts" to work with this problem, but nowadays the scientific community has powerful virtual observatory tools developed by the International Virtual Observatory Alliance (IVOA[3]) to access and to work with large astronomical catalogues like the ones mentioned above. Probably the most known virtual observatory tools are the VizieR catalogue access tool (Ochsenbein et al. 2000) and the SIMBAD database (Wenger et al. 2000), but there are more useful virtual observatory tools to analyse and visualise astronomical datasets (images, spectra and photometry). In case of searching for common proper-motion companions the most useful virtual observatory tools might be the Aladin sky atlas (Bonnarel et al. 2000) and the Starlink Tables Infrastructures Tool Set (STILTS, Taylor 2006).

1.8 Objectives and description of the work

The main goal of this PhD thesis focuses on the development of the CARMENES science preparation. The participation into this process is shown in the two papers published in Astronomy & Astrophysics and on several contributions to international conferences included in Appendix A. The two journal publications provide and characterise objects that can be targets of exoplanetary studies (e.g., habitability, formation and evolution of exoplanetary systems, detection of exo-Earths in HZs, etc). However, they both are independent studies and, therefore, each of them presents interesting results for different astrophysical investigations.

The first published paper of the science preparation for CARMENES (Alonso-Floriano et al. 2015a) is presented in Chapter 2. In this paper, we aimed to compile, observe and characterise a big sample of nearby low-mass candidates from which the CARMENES consortium will choose the best candidates to be observed during CARMENES guaranteed time observations or to be followed-up using high-resolution spectra or image. Therefore, we observed with low-resolution spectroscopy

[3] http://www.ivoa.net/

a sample of 753 stars from different sources that cover a wide range of age, activity, multiplicity, metallicity, and dynamical evolution. The main objective achieved was the catalogue of accurate spectral types derived for all the stars in the sample. However, we also measured 31 spectral indices and pseudo-equivalent widths of Hα (λ6562.8 Å), with which we made a study of metallicity, surface gravity and chromospheric activity of our sample.

Chapter 3 presents the study publicated by Alonso-Floriano et al (2015b). In this research, we aimed to study a sample of β Pictoris members to find low-mass objects that increase the number of possible young M-type objects. We compiled a list of 185 β Pictoris members and candidate members from 35 representative investigations in the last 16 years, to which we searched for wide companions using the common proper motion technique. The wide pair candidates obtained were subjects of a astro-photometric study to probe their reliability. In this process, we obtained a catalogue of accurate proper motions for 184 objects (most of them β Pictoris members) and a compilation of unresolved β Pictoris systems. The main results were the 36 pairs and multiple systems obtained, of which we discovered eight. Most of these pairs have at least one low-mass component (three present masses at or below the hydrogen burning limit). In addition, we proposed 16 new stellar candidate members of β Pictoris.

Finally, Chapter 4 presents the conclusions of the thesis as one big project focused on the science preparation of CARMENES and the independent conclusions derived of each publication. In addition, this chapter outlines some of the future work, such as the metallicity calibration of M dwarfs using wide pairs of F, G, K and M stars (some of them discovered during this thesis; see Alonso-Floriano et al. 2011, 2015b), together with the methodology presented in Alonso-Floriano et al. (2015a).

References

Allard, F., Homeier, D., & Freytag, B. 2011, ASPC, 448, 91

Alonso-Floriano, F. J., Caballero, J. A., & Montes, D. 2011, Stellar Clusters & Associations: A RIA Workshop on Gaia, 344

Alonso-Floriano, F. J., Morales, J. C., Caballero, J. A., et al. 2015a, A&A, 577, A12

Alonso-Floriano, F. J., Caballero, J. A., Cortés-Contreras, M., et al. 2015b, A&A, in press, arXiv:1508.06929, doi:10.1051/0004-6361/201526795

Amado, P. J., & CARMENES Consortium 2015, Highlights of Spanish Astrophysics VIII, 701

Anglada-Escudé, G., Boss, A. P., Weinberger, A. J., et al. 2012a, ApJ, 746, 37

Anglada-Escudé, G., Arriagada, P., Vogt, S. S., et al. 2012b, ApJ, 751, L16

Anglada-Escudé, G., Tuomi, M., Gerlach, E., et al. 2013, A&A, 556, A126

Anglada-Escudé, G., Arriagada, P., Tuomi, M., et al. 2014, MNRAS, 443, L89

Apps, K., Clubb, K. I., Fischer, D. A., et al. 2010, PASP, 122, 156

Artigau, É., Kouach, D., Donati, J.-F., et al. 2014, Proc. SPIE, 9147, 914715

Astudillo-Defru, N., Bonfils, X., Delfosse, X., et al. 2015, A&A, 575, A119

Baraffe, I., Chabrier, G., Allard, F., & Hauschildt, P. H. 1998, A&A, 337, 403

Baraffe, I., Homeier, D., Allard, F., & Chabrier, G. 2015, A&A, 577, A42

Barnes, S. A. 2009, IAU Symposium, 258, 345

Bean, J. L., Seifahrt, A., Hartman, H., et al. 2010, ApJ, 713, 410

Becerril, S., Lizon, J. L., Sánchez-Carrasco, M. A., et al. 2012, Proc. SPIE, 8450, 84504L

Binks, A. S., & Jeffries, R. D. 2014, MNRAS, 438, L11

Bonnarel, F., Fernique, P., Bienaymé, O., et al. 2000, A&AS, 143, 33

Bonnefoy, M., & Chauvin, G. 2013, Mem. Soc. Astron. Italiana, 84, 992

Bonfils, X., Mayor, M., Delfosse, X., et al. 2007, A&A, 474, 293

Bonfils, X., Gillon, M., Forveille, T., et al. 2011, A&A, 528, A111

Bonfils, X., Gillon, M., Udry, S., et al. 2012, A&A, 546, A27

Bonfils, X., Delfosse, X., Udry, S., et al. 2013a, A&A, 549, A109

Bonfils, X., Lo Curto, G., Correia, A. C. M., et al. 2013b, A&A, 556, A110

Boeshaar, P. C. 1976, PhD Thesis, Ohio State Univ., Columbus

Boeshaar, P. C., & Tyson, J. A. 1985, AJ, 90, 817

Boisse, I., Bouchy, F., Hébrard, G., et al. 2011, A&A, 528, A4

Boyajian, T. S., von Braun, K., van Belle, G., et al. 2011, 16th Cambridge Workshop on Cool Stars, Stellar Systems, and the Sun, 448, 811

Boyajian, T. S., von Braun, K., van Belle, G., et al. 2012, ApJ, 757, 112

Boyajian, T. S., van Belle, G., & von Braun, K. 2014, AJ, 147, 47

Brandl, B. R., Lenzen, R., Pantin, E., et al. 2010, Proc. SPIE, 7735, 77352

Brandl, B. R., Lenzen, R., Pantin, E., et al. 2012, Proc. SPIE, 8446, 84461M

Bryden, G., Beichman, C. A., Carpenter, J. M., et al. 2009, ApJ, 705, 1226

Burrows, A., Hubbard, W. B., Lunine, J. I., et al. 1997, Planets Beyond the Solar System and the Next Generation of Space Missions, 119, 9

Burt, J., Vogt, S. S., Butler, R. P., et al. 2014, ApJ, 789, 114

Butler, R. P., Vogt, S. S., Marcy, G. W., et al. 2004, ApJ, 617, 580

Butler, R. P., Johnson, J. A., Marcy, G. W., et al. 2006, PASP, 118, 1685

Caballero, J. A. 2007, ApJ, 667, 520

Caballero, J. A. 2009, A&A, 507, 251

Caballero, J. A. 2010a, A&A, 514, A18

Caballero, J. A. 2010b, A&A, 514, A98

Caballero, J. A. 2012, The Observatory, 132, 1

Caballero, J. A., Cortés-Contreras, M., Alonso-Floriano, F. J., et al. 2013, Protostars and Planets VI Posters, 20

Caballero, J. A., Suvrath, M., Kopparapu, R. 2015, SatMeet4–Habitable planets, M dwarfs and NIR spectrographs, Pathways towards habitable planets II, published on-line

Cassan, A., Kubas, D., Beaulieu, J.-P., et al. 2012, Nature, 481, 167

Chabrier, G., & Küker, M. 2006, A&A, 446, 10271

Chabrier, G., Baraffe, I., Allard, F., & Hauschildt, P. 2000, ApJ, 542, 464

Charbonneau, D., Berta, Z. K., Irwin, J., et al. 2009, Nature, 462, 891

Chereul, E., Creze, M., & Bienayme, O. 1998, A&A, 340, 384

Chereul, E., Crézé, M., & Bienaymé, O. 1999, A&AS, 135, 5

Cortés-Contreras , M., Caballero, J. A., & Montes, D. 2014, The Observatory, 134, 348

Cortés-Contreras , M., Caballero, J. A., Bejar, V. J. S., et al. 2015, 18th Cambridge Workshop on Cool Stars, Stellar Systems, and the Sun, 18, 805

Cossou, C., Raymond, S. N., & Pierens, A. 2013, A&A, 553, L2

Crossfield, I. J. M. 2014, A&A, 566, A130

Cruz, K. L., & Reid, I. N. 2002, AJ, 123, 2828

Cruz, K. L., Reid, I. N., Liebert, J., Kirkpatrick, J. D., & Lowrance, P. J. 2003, AJ, 126, 2421

Cruz, K. L., Reid, I. N., Kirkpatrick, J. D., et al. 2007, AJ, 133, 439

Cruz, B., Lépine, S., Stone, J., & Jordan, C. 2010, Bulletin of the American Astronomical Society, 42, #419.25

de la Reza, R., Torres, C. A. O., Quast, G., Castilho, B. V., & Vieira, G. L. 1989, ApJ, 343, L61

Delfosse, X., Forveille, T., Mayor, M., et al. 1998, A&A, 338, L67

Delfosse, X., Bonfils, X., Forveille, T., et al. 2013, A&A, 553, A8

Desidera, S., Covino, E., Messina, S., et al. 2011, A&A, 529, A54

Desort, M., Lagrange, A.-M., Galland, F., Udry, S., & Mayor, M. 2007, A&A, 473, 983

de Zeeuw, P. T., Hoogerwerf, R., de Bruijne, J. H. J., Brown, A. G. A., & Blaauw, A. 1999, AJ, 117, 354

Donnison, J. R. 2010, MNRAS, 406, 1918

Dotter, A., Chaboyer, B., Jevremović, D., et al. 2008, ApJS, 178, 89

Dressing, C. D., & Charbonneau, D. 2013, ApJ, 767, 95

Durney, B. R., De Young, D. S., & Roxburgh, I. W. 1993, Sol. Phys, 145, 207

Eggen, O. J. 1958, MNRAS, 118, 65

Eggen, O. J. 1984, AJ, 89, 1350

Eggen, O. J. 1989, Fund. Cosmic Phys., 13, 1

Eggen, O. J. 1994, Galactic and Solar System Optical Astrometry, 191

Eggen, O. J. 1995, AJ, 110, 1749

Eisenbeiss, T., Ammler-von Eiff, M., Roell, T., et al. 2013, A&A, 556, A53

Elkins-Tanton, L. 2008, Bulletin of the American Astronomical Society, 40, 503

Elkins-Tanton, L. T. 2011, Ap&SS, 332, 359

Elliott, P., Bayo, A., Melo, C. H. F., et al. 2014, A&A, 568, A26

Elliott, P., Huélamo, N., Bouy, H., et al. 2015, A&A, 580, A88

Endl, M., Cochran, W. D., Wittenmyer, R. A., & Boss, A. P. 2008, ApJ, 673, 1165

Facchini, S., Ricci, L., & Lodato, G. 2014, MNRAS, 442, 3700

Famaey, B., Pont, F., Luri, X., et al. 2007, A&A, 461, 957

Figueira, P., Pepe, F., Melo, C. H. F., et al. 2010a, A&A, 511, A55

Figueira, P., Pepe, F., Santos, N. C., et al. 2010b, EAS Publications Series, 42, 125

Figueira, P., Marmier, M., Bonfils, X., et al. 2010c, A&A, 513, L8

Follert, R., Dorn, R. J., Oliva, E., et al. 2014, Proc. SPIE, 9147, 914719

Forveille, T., Bonfils, X., Delfosse, X., et al. 2009, A&A, 493, 645

Forveille, T., Bonfils, X., Lo Curto, G., et al. 2011a, A&A, 526, A141

Forveille, T., Bonfils, X., Delfosse, X., et al. 2011b, arXiv:1109.2505

Frink, S. 1999, PhD Thesis, Ruprecht-Karls-Univ., Heidelberg

Gagné, J., Lafrenière, D., Doyon, R., Malo, L., & Artigau, É. 2014, ApJ, 783, 121

Garcia-Piquer, A., Guàrdia, J., Colomé, J., et al. 2014, Proc. SPIE, 9152, 915221

Gizis, J. E., Monet, D. G., Reid, I. N., et al. 2000a, MNRAS, 311, 385

Gizis, J. E. & Reid, I. N., 1997, PASP, 109, 1233

Gizis, J. E., Reid, I. N., & Hawley, S. L. 2002, AJ, 123, 3356

Gliese, W., & Jahreiss, H. 1991, *Preliminary Version of the Third Catalogue of Nearby Stars*, NASA/Astronomical Data Center, Goddard Space Flight Center, Greenbelt

Gray, R. O., & Corbally, C., J. 2009, Stellar Spectral Classification by Richard O. Gray and Christopher J. Corbally. Princeton University Press, 2009. ISBN: 978-0-691-12511-4

Gregorio-Hetem, J., Lepine, J. R. D., Quast, G. R., Torres, C. A. O., & de La Reza, R. 1992, AJ, 103, 549

Griffin, R. F. 1998, The Observatory, 118, 223

Guàrdia, J., Colomé, J., Ribas, I., et al. 2012, Proc. SPIE, 8451, 84512S

Haghighipour, N., Vogt, S. S., Butler, R. P., et al. 2010, ApJ, 715, 271

Hamano, K., Abe, Y., & Genda, H. 2013, Nature, 497, 607

Hansen, B. M. S. 2015, International Journal of Astrobiology, 14, 267

Hawley, S. L., Gizis, J. E., & Reid, I. N. 1996, AJ, 112, 2799

Hejazi, N., De Robertis, M. M., & Dawson, P. C. 2015, AJ, 149, 140

Helling, C., Ackerman, A., Allard, F., et al. 2008, MNRAS, 391, 1854

Henry, T. J., Kirkpatrick, J. D., & Simons, D. A. 1994, AJ, 108, 1437

Hernán-Obispo, M., Gálvez-Ortiz, M. C., Anglada-Escudé, G., et al. 2010, A&A, 512, A45

Hernán-Obispo, M., Tuomi, M., Gálvez-Ortiz, M. C., et al. 2015, A&A, 576, A66

Hillenbrand, L. A. 1997, AJ, 113, 1733

Høg, E., Bässgen, G., Bastian, U., et al. 1997, A&A, 323, L57

Høg, E., Fabricius, C., Makarov, V. V., et al. 2000, A&A, 355, L27

Howard, A. W., Johnson, J. A., Marcy, G. W., et al. 2010, ApJ, 721, 1467

Howard, A. W., Marcy, G. W., Fischer, D. A., et al. 2014, ApJ, 794, 51

Huélamo, N., Figueira, P., Bonfils, X., et al. 2008, A&A, 489, L9

Ida, S., & Lin, D. N. C. 2008a, ApJ, 673, 487

Ida, S., & Lin, D. N. C. 2008b, ApJ, 685, 584

Ikoma, M., Nakazawa, K., & Emori, H. 2000, ApJ, 537, 1013

Jaffe, D. T., Mar, D. J., Warren, D., & Segura, P. R. 2006, Proc. SPIE, 6269, 62694

Jeffries, R. D., Maxted, P. F. L., Oliveira, J. M., & Naylor, T. 2006, MNRAS, 371, L6

Johnson, J. A., Butler, R. P., Marcy, G. W., et al. 2007, ApJ, 670, 833

Johnson, J. A., Howard, A. W., Marcy, G. W., et al. 2010, PASP, 122, 149

Jones, H. R. A., Rayner, J., Ramsey, L., et al. 2008, Proc. SPIE, 7014, E0Y

Joshi, M. M., Haberle, R. M., & Reynolds, R. T. 1997, Icarus, 129, 450

Joy, A. H. 1947, ApJ, 105, 96

Kasting, J. F., Whitmire, D. P., & Reynolds, R. T. 1993, Icarus, 101, 108

Kastner, J. H., Huenemoerder, D. P., Schulz, N., et al. 1997, Bulletin of the American Astronomical Society, 29, 1361

Käufl, H.-U., Ballester, P., Biereichel, P., et al. 2004, Proc. SPIE, 5492, 1218

Kirkpatrick, J. D. 2005, ARA&A, 43, 195

Kirkpatrick, J. D., Henry, T. J., & McCarthy, D. W., Jr. 1991, ApJS, 77, 417

Kirkpatrick, J. D., Henry, T. J., & Simons, D. A. 1995, AJ, 109, 797

Kirkpatrick, J. D., Henry, T. J., & Simons, D. A. 1995, AJ, 109, 797

Kirkpatrick, J. D., Beichman, C. A., & Skrutskie, M. F. 1997, ApJ, 476, 311

Kirkpatrick, J. D., Cushing, M. C., Gelino, C. R., et al. 2011, ApJS, 197, 19

Kiss, L. L., Moór, A., Szalai, T., et al. 2011, MNRAS, 411, 117

Klutsch, A., Freire Ferrero, R., Guillout, P., et al. 2014, A&A, 567, A52

Kopparapu, R. K. 2013, ApJ, 767, L8

Kotani, T., Tamura, M., Suto, H., et al. 2014, Proc. SPIE, 9147, 914714

Kraus, A. L., Shkolnik, E. L., Allers, K. N., & Liu, M. C. 2014, AJ, 147, 146

Kuiper, G. P. 1942, ApJ, 95, 201

Kürster, M., Endl, M., Els, S., et al. 2000, A&A, 353, L33

Lammer, H. 2013, Origin and Evolution of Planetary Atmospheres: Implications for Habitability, SpringerBriefs in Astronomy. ISBN 978-3-642-32086-6. The Author(s), 2013

Lammer, H., Lichtenegger, H. I. M., Kulikov, Y. N., et al. 2007, Astrobiology, 7, 185

Lammer, H., Stökl, A., Erkaev, N. V., et al. 2014, MNRAS, 439, 3225

Laymand, M., & Vauclair, S. 2006, Mem. Soc. Astron. Italiana, 77, 176

Lee, S., Yuk, I.-S., Lee, H., et al. 2010, Proc. SPIE, 7735, 77352K

Lépine, S. 2011, 16th Cambridge Workshop on Cool Stars, Stellar Systems, and the Sun, 448, 1375

Lépine, S., & Simon, M. 2009, AJ, 137, 3632

Lépine, S., & Gaidos, E. 2011, AJ, 142, 138

Lépine, S., & Gaidos, E. 2013, American Astronomical Society Meeting Abstracts #221, 221, #423.01

Lépine, S., Shara, M. M., & Rich, R. M. 2002, AJ, 124, 1190

Lépine, S., Rich, R. M., & Shara, M. M. 2003, AJ, 125, 1598

Lépine, S., Thorstensen, J. R., Shara, M. M., & Rich, R. M. 2009, AJ, 137, 4109

Lépine, S., Hilton, E. J., Mann, A. W., et al. 2013, AJ, 145, 102

Lissauer, J. J. 2007, ApJ, 660, L149

López, E. D., & Fortney, J. J. 2014, ApJ, 792, 1

López-Santiago, J., Montes, D., Crespo-Chacón, I., & Fernández-Figueroa, M. J. 2006, ApJ, 643, 1160

Lowrance, P. J., Kirkpatrick, J. D., & Beichman, C. A. 2002, ApJ, 572, L79

Luger, R., & Barnes, R. 2015, Astrobiology, 15, 119

Luger, R., Barnes, R., Lopez, E., et al. 2015, Astrobiology, 15, 57

Mahadevan, S., Ramsey, L. W., Terrien, R., et al. 2014, Proc. SPIE, 9147, 91471G

Maiolino, R., Haehnelt, M., Murphy, M. T., et al. 2013, arXiv:1310.3163

Maldonado, J., Affer, L., Micela, G., et al. 2015, A&A, 577, A132

Mamajek, E. E. 2015, Proceedings IAU Symposium No. 314, Young Stars & Planets Near the Sun, 2015, J. H. Kastner, B. Stelzer, & S. A. Metchev, eds, in press, arXiv:1507.06697

Mann, A. W., Brewer, J. M., Gaidos, E., Lépine, S., & Hilton, E. J. 2013a, AJ, 145, 52

Mann, A. W., Gaidos, E., & Ansdell, M. 2013b, ApJ, 779, 188

Mann, A. W., Deacon, N. R., Gaidos, E., et al. 2014, AJ, 147, 160

Mann, A. W., Feiden, G. A., Gaidos, E., Boyajian, T., & von Braun, K. 2015, ApJ, 804, 64

Marcy, G. W., Butler, R. P., Fischer, D., et al. 2001, ApJ, 556, 296

Martín, E. L., Guenther, E., Zapatero Osorio, M. R., Bouy, H., & Wainscoat, R. 2006, ApJ, 644, L75

Martín, E. L., Guenther, E., Del Burgo, C., et al. 2010, Pathways Towards Habitable Planets, 430, 181

Mayor, M., & Queloz, D. 1995, Nature, 378, 355

Mayor, M., Bonfils, X., Forveille, T., et al. 2009, A&A, 507, 487

Matsui, T., & Abe, Y. 1986, Nature, 319, 303

Mirabet, E., Carvas, P., Lizon, J.-L., et al. 2014, Proc. SPIE, 9151, 91513Y

Mizuno, H., Nakazawa, K., & Hayashi, C. 1978, Progress of Theoretical Physics, 60, 699

Mohanty, S., & Basri, G. 2003, ApJ, 583, 451

Monet, D. G., Levine, S. E., Canzian, B., et al. 2003, AJ, 125, 984

Montes, D., López-Santiago, J., Gálvez, M. C., et al. 2001, MNRAS, 328, 45

Montes, D., Caballero, J. A., Gallardo, I., et al. 2015, Proceedings IAU Symposium No. 314, Young Stars & Planets Near the Sun, 2015, J. H. Kastner, B. Stelzer, & S. A. Metchev, eds, in press

Montet, B. T., Crepp, J. R., Johnson, J. A., Howard, A. W., & Marcy, G. W. 2014, ApJ, 781, 28

Morgan, W. W. 1938, ApJ, 87, 589

Mülläri, A., Flynn, C., & Orlov, V. 2000, Astronomische Gesellschaft Meeting Abstracts, 16, 12

Ochsenbein, F., Bauer, P., & Marcout, J. 2000, A&AS, 143, 23

O'Donnell, C., Lepine, S., & Rojas Ayala, B. D. 2013, American Astronomical Society Meeting Abstracts #221, 221, #158.13

Ogihara, M., & Ida, S. 2009, ApJ, 699, 824

Oliva, E., Origlia, L., Maiolino, R., et al. 2012, Proc. SPIE, 8446, 84463T

Ortega, V. G., de la Reza, R., Jilinski, E., & Bazzanella, B. 2002, ApJ, 575, L75

Passegger, V. M.. Wende, S., Reiners, A., et al. 2014, Towards other Earths II: the star-planet connection, http://carmenes.caha.es/ext/conferences/CARMENES_TOEII2014_Passegger.pdf

Perryman, M. A. C., Lindegren, L., Kovalevsky, J., et al. 1997, A&A, 323, L49

Pizzolato, N., Maggio, A., Micela, G., Sciortino, S., & Ventura, P. 2003, A&A, 397, 147

Quirrenbach, A., Amado, P. J., Mandel, H., et al. 2010, Proc. SPIE, 7735, 37Q

Quirrenbach, A., Amado, P. J., Seifert, W., et al. 2012, Proc. SPIE, 8446

Quirrenbach, A., Amado, P. J., Caballero, J. A., et al. 2014, Proc. SPIE, 9147, E1F

Rafikov, R. R. 2006, ApJ, 648, 666

Rajpurohit, A. S., Reylé, C., Allard, F., et al. 2013, A&A, 556, A15

Ramírez, R. M., & Kaltenegger, L. 2014, ApJ, 797, L25

Raymond, S. N., Scalo, J., & Meadows, V. S. 2007, ApJ, 669, 606

Reid, I. N., & Hawley, S. L. 2005, New Light on Dark Stars Red Dwarfs, Low-Mass Stars, Brown Stars, by I.N. Reid and S.L. Hawley. Springer-Praxis books in astrophysics and astronomy. Praxis Publishing Ltd, 2005, ISBN 3-540-25124-3

Reid, I. N., Hawley, S. L., & Gizis, J. E. 1995, AJ, 110, 1838

Reid, I. N., Gizis, J. E., & Hawley, S. L. 2002, AJ, 124, 2721

Reid, I. N., Cruz, K. L., Allen, P., et al. 2003, AJ, 126, 3007

Reid, I. N., Cruz, K. L., Allen, P., et al. 2004, AJ, 128, 463

Reid, I. N., Cruz, K. L., Kirkpatrick, J. D., et al. 2008, AJ, 136, 1290

Reiners, A. 2007, A&A, 467, 259

Reiners, A. 2008, Reviews in Modern Astronomy, 20, 40

Reiners, A., & Basri, G. 2008, ApJ, 684, 1390

Reiners, A., & Basri, G. 2009, ApJ, 705, 1416

Reiners, A., Bean, J. L., Huber, K. F., et al. 2010, ApJ, 710, 432

Reiners, A., Shulyak, D., Anglada-Escudé, G., et al. 2013, A&A, 552, A103

Reiners, A., Schüssler, M., & Passegger, V. M. 2014, ApJ, 794, 144

Riedel, A. R., Finch, C. T., Henry, T. J., et al. 2014, AJ, 147, 85

Riedel, A. R. 2015, Proceedings IAU Symposium No. 314, Young Stars & Planets Near the Sun, 2015, J. H. Kastner, B. Stelzer, & S. A. Metchev, eds, in press, arXiv:1506.06685

Rivera, E. J., Lissauer, J. J., Butler, R. P., et al. 2005, ApJ, 634, 625

Rivera, E. J., Laughlin, G., Butler, R. P., et al. 2010, ApJ, 719, 890

Rodríguez, D. R., Bessell, M. S., Zuckerman, B., & Kastner, J. H. 2011, ApJ, 727, 62

Röser, S., Demleitner, M., & Schilbach, E. 2010, AJ, 139, 2440

Rojas-Ayala, B. 2013, European Physical Journal Web of Conferences, 47, 09004

Roth, M. M., Kelz, A., Fechner, T., et al. 2005, PASP, 117, 620

Sánchez-Blázquez, P., Peletier, R. F., Jiménez-Vicente, J., et al. 2006, MNRAS, 371, 703

Santerne, A., Díaz, R. F., Moutou, C., et al. 2012, A&A, 545, A76

Sanz-Forcada, J. 2015, SatMeet4–Stellar activity of M dwarfs with planets, Pathways towards habitable planets II, published on-line

Sarmiento, L. F., Reiners, A., Seemann, U., et al. 2014, Proc. SPIE, 9147, 914754

Scalo, J., Kaltenegger, L., Segura, A. G., et al. 2007, Astrobiology, 7, 85

Schlieder, J. E., Lépine, S., & Simon, M. 2010, AJ, 140, 119

Schlieder, J. E., Lépine, S., Rice, E., et al. 2012, AJ, 143, 114

Secchi, A. 1866, *CR Acd. Sci. Paris*, 63, 621

Segura, A., Walkowicz, L. M., Meadows, V., Kasting, J., & Hawley, S. 2010, Astrobiology, 10, 751

Setiawan, J., Weise, P., Henning, T., et al. 2007, ApJ, 660, L145

Setiawan, J., Henning, T., Launhardt, R., et al. 2008, Nature, 451, 38

Shaya, E. J., & Olling, R. P. 2011, ApJS, 192, 2

Scholz, R.-D., Meusinger, H., & Jahreiß, H. 2005, A&A, 442, 211

Shkolnik, E. L., Liu, M. C., Reid, I. N., Dupuy, T., & Weinberger, A. J. 2011, ApJ, 727, 6

Shkolnik, E., Liu, M. C., & Reid, I. N. 2009, ApJ, 699, 649

Shkolnik, E. L., Anglada-Escudé, G., Liu, M. C., et al. 2012, ApJ, 758, 56

Shulyak, D., Reiners, A., Seemann, U., Kochukhov, O., & Piskunov, N. 2014, A&A, 563, A35

Skidmore, W., Dell'Antonio, I., Fukugawa, M., et al. 2015, TMT.PSC.TEC 07.007.REL02, arXiv:1505.01195

Sills, A., Pinsonneault, M. H., & Terndrup, D. M. 2000, ApJ, 534, 335

Soderblom, D. R. 2010, ARA&A, 48, 581

Soderblom, D. R., & Mayor, M. 1993, AJ, 105, 226

Song, I., Zuckerman, B., & Bessell, M. S. 2003, ApJ, 599, 342

Southworth, J. 2010, MNRAS, 408, 1689

Soto, M. G., Jenkins, J. S., & Jones, M. I. 2015, MNRAS, 451, 3131

Stassun, K. G., Hebb, L., Covey, K., et al. 2011, 16th Cambridge Workshop on Cool Stars, Stellar Systems, and the Sun, 448, 505

Stürmer, J., Stahl, O., Schwab, C., et al. 2014, Proc. SPIE, 9151, 915152

Taylor, M. B. 2006, Astronomical Data Analysis Software and Systems XV, 351, 666

Tarter, J. C., Backus, P. R., Mancinelli, R. L., et al. 2007, Astrobiology, 7, 30

Taylor, B. J. 2000, A&A, 362, 56

Tian, F., & Ida, S. 2015, Nature Geoscience, 8, 177

Tsuji, T. 2002, ApJ, 575, 264

Tsuji, T., Ohnaka, K., Aoki, W., & Nakajima, T. 1996, A&A, 308, L29

Tuomi, M., Jones, H. R. A., Barnes, J. R., Anglada-Escudé, G., & Jenkins, J. S. 2014, MNRAS, 441, 1545

Torra, J., Fernández, D., & Figueras, F. 2000, A&A, 359, 82

Torres, C. A. O., da Silva, L., Quast, G. R., de la Reza, R., & Jilinski, E. 2000, AJ, 120, 1410

Torres, C. A. O., Quast, G. R., da Silva, L., et al. 2006, A&A, 460, 695

Torres, C. A. O., Quast, G. R., Melo, C. H. F., & Sterzik, M. F. 2008, Handbook of Star Forming Regions, Volume II, 757

Torres, C. A. O., Quast, G. R., & Montes, D. 2015, Proceedings IAU Symposium No. 314, Young Stars & Planets Near the Sun, 2015, J. H. Kastner, B. Stelzer, & S. A. Metchev, eds, in press

Udry, S., Bonfils, X., Delfosse, X., et al. 2007, A&A, 469, L43

van Leeuwen, F. 2007, A&A, 474, 653

Wang, J., & Ford, E. B. 2011, MNRAS, 418, 1822

Wenger, M., Ochsenbein, F., Egret, D., et al. 2000, A&AS, 143, 9

West, A. A., Hawley, S. L., Walkowicz, L. M., et al. 2004, AJ, 128, 426

Wilking, B. A., & Lada, C. J. 1983, ApJ, 274, 698

Winters, J. G., Henry, T. J., Lurie, J. C., et al. 2014, AJ, 149, 5

Wittenmyer, R. A., Wang, S., Horner, J., et al. 2013, ApJS, 208, 2

Wuchterl, G. 1993, Icarus, 106, 323

Zacharias, N., Finch, C. T., Subasavage, J. P., et al. 2015, American Astronomical Society Meeting Abstracts, 225, #433.01

Zahnle, K. J., Kasting, J. F., & Pollack, J. B. 1988, Icarus, 74, 62

Zapatero Osorio, M. R., Martín, E. L., Bouy, H., et al. 2006, ApJ, 647, 1405

Zechmeister, M., Kürster, M., & Endl, M. 2009, A&A, 505, 859

Zechmeister, M., Kürster, M., Endl, M., et al. 2013, A&A, 552, A78

Zhao, B., Ge, J., Nguyen, D. C., Wang, J., & Groot, J. 2010, Proc. SPIE, 7735, 773554

Zuckerman, B., & Webb, R. A. 2000, ApJ, 535, 959

Zuckerman, B., & Song, I. 2004, ARA&A, 42, 685

Zuckerman, B., Song, I., & Webb, R. A. 2001a, ApJ, 559, 388

Zuckerman, B., Song, I., Bessell, M. S., & Webb, R. A. 2001b, ApJ, 562, L87

2

Low-resolution spectroscopy of CARMENES M dwarfs with CAFOS

This chapter corresponds to the published paper *CARMENES input catalogue of M dwarfs. I. Low-resolution spectroscopy with CAFOS* (Alonso-Floriano et al. 2015, A&A, 577, A128).

As was previously pointed, the CARMENES consortium will observe a final sample of 300 M-dwarfs along 600 nights starting on early 2016. The selection of this final sample needs of a intense science preparation using low- and high resolution spectra and high-resolution imaging that provide the necessary information. Some preliminary results have been already presented at international conferences: the input catalogue description and selection (Caballero et al. 2013; Morales et al. 2013), low-resolution spectroscopy (Klutsch et al. 2012; Alonso-Floriano et al. 2013a), high-resolution spectroscopy (Alonso-Floriano et al. 2013b; Passegger et al. 2014), resolved multiplicity (Béjar et al. 2012; Cortés-Contreras et al. 2013), X-rays (Lalitha et al. 2012), exploitation of public databases (Montes et al. 2015), or synergies with *Kepler* K2 (Rodríguez-López et al. 2014). This chapter include the first item of the CARMENES science-preparation series detailing the low-resolution optical spectroscopy of M dwarfs with the CAFOS spectrograph at the Zeiss 2.2 m Calar Alto telescope.

The research presented below has not only served for the goals of this thesis. It is a reference work for the various publications that the consortium is preparing. For example, some of the objects studied on this chapter formed part of the sample used in Chapter 3, others were followed-up with high-resolution spectra or imaging on the others science preparation works of CARMENES. It might be also useful for other exoplanetary surveys around M dwarf, such as HPF or SPIRou (see Sect. 1.4). In addition, the methodology used to characterise low-mass objects in this chapter, is being used to perform a metallicity calibration of M-dwarfs using wide pairs of F,G,K and M stars (see Chapter 4).

We have noticed, after the interaction with a reader of the paper presented in this chapter, that the Table 5 (of the publication) can be improved by adding more significant figures to the coefficients of the cubic polynomial fits, which is shown in Table 2.1. **In addition, we report in Table 2.2 other six young stars after a revision of the sample, which should be added to the 49 young stars reported in Table 7 of the publication.**

The full version of the tables presented on the paper included in this chapter, correspond to the tables of the Appendix B; Table B.1, Table B.2 and Table B.3 respectively.

TABLE 2.1— Coefficients and standard deviation (in spectral subtypes) of the cubic polynomial fits of the five spectral-typing indices[a].

Index	a	b	c	d	σ
TiO 2	+10.984	–21.872	+27.920	–19.632	0.83
TiO 5	+9.5725	–20.123	+17.234	–9.4960	0.57
PC1	–49.542	+97.258	–58.952	+12.380	0.52
VO-7912	–520.19	+1295.6	–1073.6	+299.06	0.59
Color-M	+1.9771	+13.123	–15.616	+10.314	0.53

Notes. [a]We used the relation $\mathrm{SpT}(i) = a + b\,i + c\,i^2 + d\,i^3$ for the cubic fits. For the Color-M index we used the relation $\mathrm{SpT}(i) = a + b\,\log i + c\,(\log i)^2 + d\,(\log i)^3$.

TABLE 2.2— Six new reported young stars in our sample.

Karmn	Moving group/ association/cluster/ star-forming region	Ref
J03375+178N AB	Hyades	Gol13
J03375+178S AB	Hyades	Gol13
J03565+319	Hyades	Gol13
J04224+036	Hyades	Gol13
J05223+305	Hyades	Gol13
J06102+225	Hyades	Gol13

References. Gol13: Goldman, B., Röser, S., Schilbach, E., et al., 2013, A&A, 559, A43

A&A 577, A128 (2015)
DOI: 10.1051/0004-6361/201525803

Astronomy & Astrophysics

CARMENES input catalogue of M dwarfs

I. Low-resolution spectroscopy with CAFOS⋆

F. J. Alonso-Floriano[1], J. C. Morales[2,3], J. A. Caballero[4], D. Montes[1], A. Klutsch[5,1], R. Mundt[6], M. Cortés-Contreras[1], I. Ribas[2], A. Reiners[7], P. J. Amado[8], A. Quirrenbach[9], and S. V. Jeffers[7]

[1] Departamento de Astrofísica y Ciencias de la Atmósfera, Facultad de Ciencias Físicas, Universidad Complutense de Madrid, 28040 Madrid, Spain
e-mail: fjalonso@fis.ucm.es
[2] Institut de Ciències de l'Espai (CSIC-IEEC), Campus UAB, Facultat Ciències, Torre C5 – parell – 2ª, 08193 Bellaterra, Barcelona, Spain
[3] LESIA-Observatoire de Paris, CNRS, UPMC Univ. Paris 06, Univ. Paris-Diderot, 5 Pl. Jules Janssen, 92195 Meudon Cedex, France
[4] Departamento de Astrofísica, Centro de Astrobiología (CSIC–INTA), PO Box 78, 28691 Villanueva de la Cañada, Madrid, Spain
[5] INAF−Osservatorio Astrofisico di Catania, via S. Sofia 78, 95123 Catania, Italy
[6] Max-Planck-Institut für Astronomie, Königstuhl 17, 69117 Heidelberg, Germany
[7] Institut für Astrophysik, Friedrich-Hund-Platz 1, 37077 Göttingen, Germany
[8] Instituto de Astrofísica de Andalucía (CSIC), Glorieta de la Astronomía s/n, 18008 Granada, Spain
[9] Landessternwarte, Zentrum für Astronomie der Universität Heidelberg, Königstuhl 12, 69117 Heidelberg, Germany

Received 4 February 2015 / Accepted 18 February 2015

ABSTRACT

Context. CARMENES is a stabilised, high-resolution, double-channel spectrograph at the 3.5 m Calar Alto telescope. It is optimally designed for radial-velocity surveys of M dwarfs with potentially habitable Earth-mass planets.
Aims. We prepare a list of the brightest, single M dwarfs in each spectral subtype observable from the northern hemisphere, from which we will select the best planet-hunting targets for CARMENES.
Methods. In this first paper on the preparation of our input catalogue, we compiled a large amount of public data and collected low-resolution optical spectroscopy with CAFOS at the 2.2 m Calar Alto telescope for 753 stars. We derived accurate spectral types using a dense grid of standard stars, a double least-squares minimisation technique, and 31 spectral indices previously defined by other authors. Additionally, we quantified surface gravity, metallicity, and chromospheric activity for all the stars in our sample.
Results. We calculated spectral types for all 753 stars, of which 305 are new and 448 are revised. We measured pseudo-equivalent widths of Hα for all the stars in our sample, concluded that chromospheric activity does not affect spectral typing from our indices, and tabulated 49 stars that had been reported to be young stars in open clusters, moving groups, and stellar associations. Of the 753 stars, two are new subdwarf candidates, three are T Tauri stars, 25 are giants, 44 are K dwarfs, and 679 are M dwarfs. Many of the 261 investigated dwarfs in the range M4.0–8.0 V are among the brightest stars known in their spectral subtype.
Conclusions. This collection of low-resolution spectroscopic data serves as a candidate target list for the CARMENES survey and can be highly valuable for other radial-velocity surveys of M dwarfs and for studies of cool dwarfs in the solar neighbourhood.

Key words. stars: activity – stars: late-type – stars: low-mass

1. Introduction

The Calar Alto high-Resolution search for M dwarfs with Exo-earths with Near-infrared and optical Échelle Spectrographs (hereafter CARMENES[1]) is a next-generation instrument close to completion for the Zeiss 3.5 m Calar Alto telescope, which is located in the Sierra de Los Filabres, Almería, in southern Spain, at a height of about 2200 m (Sánchez et al. 2007, 2008). CARMENES is the name used for the instrument, the consortium of 11 German and Spanish institutions that builds it, and of the scientific project to be carried out during guaranteed time observations. The instrument consists of two separated, highly stable, fibre-fed spectrographs covering the wavelength ranges from 0.55 to 0.95 μm and from 0.95 to 1.70 μm at spectral resolution $R \approx 82\,000$, each of which shall perform high-accuracy radial-velocity measurements with long-term stability of ~1 m s^{-1} (Quirrenbach et al. 2010, 2012, 2014, and references therein; Amado et al. 2013). First light is scheduled for the summer of 2015, followed by the commission of the instrument in the second half of that year.

The main scientific objective for CARMENES is the search for very low-mass planets (i.e., super- and exo-earths) orbiting mid- to late-M dwarfs, including a sample of moderately active M-dwarf stars. Dwarf stars of M spectral type have effective temperatures between 2300 and 3900 K (Kirkpatrick et al. 2005; Rajpurohit et al. 2013). For stars with ages greater than

⋆ Full Tables A.1, A.2, and A.3 are only available at the CDS via anonymous ftp to cdsarc.u-strasbg.fr (130.79.128.5) or via http://cdsarc.u-strasbg.fr/viz-bin/qcat?J/A+A/577/A128

[1] http://carmenes.caha.es – Pronunciation: /kαr'·mεn·εs/

A&A 577, A128 (2015)

that of the Hyades, of about 0.6 Ga, these effective temperatures translate in the main sequence into a mass interval from 0.09 to 0.55 $M_\odot$, approximately (Baraffe et al. 1998; Chabrier et al. 2000; Allard et al. 2011). Of particular interest is the detection of very low-mass planets in the stellar habitable zone, the region around the star within which a planet can support liquid water (Kasting et al. 1993; Joshi et al. 1997; Lammer et al. 2007; Tarter et al. 2007; Scalo et al. 2007). In principle, the lower the mass of a host star, the higher the radial-velocity amplitude velocity induced (i.e., $K_{\rm star}$ is proportional to $M_{\rm planet}\, a^{-1/2}\, (M_{\rm star} + M_{\rm planet})^{-1/2} \approx (a\, M_{\rm star})^{-1/2}$ when $M_{\rm star} \gg M_{\rm planet}$). In addition, the lower luminosity of an M dwarf with respect to a star of earlier spectral type causes its habitable zone to be located very close to the host star, which makes detecting habitable planets around M dwarfs (at ∼0.1 au) easier than detections around solar-like stars (at ∼1 au).

From transit surveys with the NASA 0.95 m *Kepler* space observatory, very small planet candidates are found to be relatively more abundant than Jupiter-type candidates as the host stellar mass decreases (Howard et al. 2012; Dressing & Charbonneau 2013, 2015; Kopparapu 2013; Kopparapu et al. 2013). For early-M dwarf stars in the field, some radial-velocity studies have already been carried out (ESO CES, UVES and HARPS by Zechmeister et al. 2009, 2013; CRIRES by Bean et al. 2010; HARPS by Bonfils et al. 2013), but the much-sought value of $\eta_\oplus$, that is, the relative abundance of Earth-type planets in the habitable zone, is as yet only poorly constrained from radial-velocity data (e.g., $\eta_\oplus = 0.41^{+0.54}_{-0.13}$ from Bonfils et al. 2013).

Highly stable, high-resolution spectrographs in the near-infrared currently under construction, such as SPIRou (Artigau et al. 2014), IRD (Kotani et al. 2014), HPF (Mahadevan et al. 2014), and CARMENES, are preferable over visible for targets with spectral types M4 V or later (see Table 1 in Crossfield 2014). This is because the spectral energy distribution of late-M dwarfs approximately peaks at 1.0−1.2 μm (Reiners et al. 2010), while HARPS and its copy in the northern hemisphere, HARPS-N, cover the wavelength interval from 0.38 to 0.69 μm. That faintness in the optical is quantitatively illustrated with the tabulated V magnitudes of the brightest M dwarfs in the northern hemisphere (HD 79210/GJ 338 A, HD 79211/GJ 338 B, and HD 95735/GJ 411) at 7.5−7.7 mag, far from the limit of the naked human eye.

The specific advantage of CARMENES is the wide wavelength coverage and high spectral resolution in both visible and near-infrared channels. Simultaneous observation from 0.5 to 1.7 μm is a powerful tool for distinguishing between genuine planet detections and false positives caused by stellar activity, which have plagued planet searches employing spectrographs with a smaller wavelength coverage, especially in the M-type spectral domain (Reiners et al. 2010; Barnes et al. 2011). A substantial amount of guaranteed time for the completion of the key project is also an asset.

A precise knowledge of the targets is critical to ensure that most of the CARMENES guaranteed time is spent on the most promising targets. This selection involves not only a comprehensive data compilation from the literature, but also summarises our observational effort to achieve new low- and high-resolution optical spectroscopy and high-resolution imaging. The present publication on low-resolution spectroscopy is the first paper of a series aimed at describing the selection and characterisation of the CARMENES sample. We have shown some preliminary results at conferences before that described the input catalogue description and selection (Caballero et al. 2013; Morales et al. 2013), low-resolution spectroscopy (Klutsch et al. 2012; Alonso-Floriano et al. 2013a), high-resolution spectroscopy (Alonso-Floriano et al. 2013b; Passegger et al. 2014), resolved multiplicity (Béjar et al. 2012; Cortés-Contreras et al. 2013), X-rays (Lalitha et al. 2012), exploitation of public databases (Montes et al. 2015), or synergies with *Kepler* K2 (Rodríguez-López et al. 2014). This first item of the CARMENES science-preparation series details the low-resolution optical spectroscopy of M dwarfs with the CAFOS spectrograph at the Zeiss 2.2 m Calar Alto telescope.

Table 1. Completeness and limiting J-band magnitudes per spectral type for the CARMENES input catalogue.

Spectral type	J [mag]	
	Completeness	Limiting
M0.0–0.5 V	7.3	8.5
M1.0–1.5 V	7.8	9.0
M2.0–2.5 V	8.3	9.5
M3.0–3.5 V	8.8	10.0
M4.0–4.5 V	9.3	10.5
M5.0–5.5 V	9.8	11.0
M6.0–6.5 V	10.3	11.5
M7.0–7.5 V	10.8	11.5
M8.0–9.5 V	11.3	11.5

2. CARMENES sample

To prepare the CARMENES input catalogue with the best targets, we systematically collected all published M dwarfs in the literature that fulfilled two simple criteria:

- They had to be observable from Calar Alto with target declinations $\delta > -23$ deg (i.e., zenith distances <60 deg, air masses at culmination <2.0).
- They were selected according to late spectral type and brightness. We only catalogued confirmed dwarf stars with an accurate spectral type determination from spectroscopic data (i.e., not from photometry) between M0.0 V and M9.5 V. Additionally, we only compiled the brightest stars of each spectral type. Our database contains virtually all known M dwarfs that are brighter than the completeness magnitudes shown in Table 1, and most of them brighter than the limiting magnitudes. No target fainter than $J = 11.5$ mag is in our catalogue.

We started to fill the CARMENES database with the M dwarfs from the Research Consortium on Nearby Stars[2], which catalogues all known stars with measured astrometric parallaxes that place them within 10 pc (e.g., Henry et al. 1994; Kirkpatrick et al. 1995; Riedel et al. 2014; Winters et al. 2015). The RECONS stellar compilation was next completed with the Palomar/Michigan State University survey catalogue of nearby stars (PMSU – Reid et al. 1995, 2002; Hawley et al. 1996; Gizis et al. 2002). Afterwards, we gave special attention to the comprehensive proper-motion catalogues of Lépine et al. (2003, 2009, 2013) and Lépine & Gaidos (2011), and the "Meeting the Cool Neighbors" series of papers (Cruz & Reid 2002; Cruz et al. 2003, 2007; Reid et al. 2003, 2004, 2008). Table 2 provides the sources of our information on M dwarfs. Until we start our survey at the

[2] http://www.recons.org

Table 2. Sources of the CARMENES input catalogue.

Source	Reference[a]	Number of stars
The Palomar/MSU nearby star spectroscopic survey	PMSU[b]	676
A spectroscopic catalog of the brightest ($J < 9$) M dwarfs in the northern sky	Lépine et al. (2013)	446
G. P. Kuiper's spectral classifications of proper-motion stars	Bidelman (1985)	285
An all-sky catalog of bright M dwarfs[c]	Lépine & Gaidos (2011)	248
Spectral types of M dwarf stars	Joy & Abt (1974)	223
Spectral classification of high-proper-motion stars	Lee (1984)	118
Meeting the cool neighbors	RECONS[d]	22
Search for nearby stars among proper... III. Spectroscopic distances of 322 NLTT stars	Scholz et al. (2005)	19
New neighbors: parallaxes of 18 nearby stars selected from the LSPM-North catalog	Lépine et al. (2009)	13
Near-infrared metallicities, radial velocities and spectral types for 447 nearby M dwarfs	Newton et al. (2014)	10

Notes. [(a)] Some other publications and meta-archives that we have searched for potential CARMENES targets are Kirkpatrick et al. (1991), Gizis (1997), Gizis & Reid (1997), Gizis et al. (2000b), Henry et al. (2002, 2006), Mochnacki et al. (2002), Gray et al. (2003), Bochanski et al. (2005), Crifo et al. (2005), Lodieu et al. (2005), Scholz et al. (2005), Phan-Bao & Bessell (2006), Reylé et al. (2006), Riaz et al. (2006), Caballero (2007, 2009, 2012), Gatewood & Coban (2009), Shkolnik et al. (2009, 2012), Bergfors et al. (2010), Johnson et al. (2010), Boyd et al. (2011), Irwin et al. (2011), West et al. (2011), Avenhaus et al. (2012), Deacon et al. (2012), Janson et al. (2012, 2014), Frith et al. (2013), Jódar et al. (2013), Malo et al. (2013), Aberasturi et al. (2014), Dieterich et al. (2014), Riedel et al. (2014), Yi et al. (2014), Gaidos et al. (2014), and the DwarfArchive at `http://dwarfarchive.org`. [(b)] PMSU: Reid et al. (1995, 2002); Hawley et al. (1996); Gizis et al. (2002). [(c)] With spectral types derived from spectroscopy in this work. [(d)] RECONS: Henry et al. (1994, 2006); Kirkpatrick et al. (1995); Jao et al. (2011); Riedel et al. (2014); Winters et al. (2015) and references therein.

end of 2015, we will still include some new, particularly bright, late, single, M dwarfs[3].

As of February 2015, our input catalogue, dubbed CARMENCITA (CARMENES Cool dwarf Information and daTa Archive), contains approximately 2200 M dwarfs. For each target star, we tabulate a number of parameters compiled from the literature or measured by us with new data: accurate astrometry and distance, spectral type, photometry in 20 bands from the ultraviolet to the mid-infrared, rotational, radial, and Galactocentric velocities, Hα emission, X-ray count rates and hardness ratios, close and wide multiplicity data, membership in open clusters and young moving groups, target in other radial-velocity surveys, and exoplanet candidacy (Caballero et al. 2013). The private on-line catalogue, including preparatory science observations (i.e., low- and high-resolution spectroscopy, high-resolution imaging), will become public as a CARMENES legacy.

Of the 2200 stars, we discard all spectroscopic binaries and multiples, and resolved systems with physical or visual companions at less than 5 arcsec to our targets. The size of the CARMENES optical fibres projected on the sky is 1.5 arcsec (Seifert et al. 2012; Quirrenbach et al. 2014), and consequently any companion at less than 5 arcsec may induce real or artificial radial-velocity variations that would contaminate our measurements (Guenther & Wuchterl 2003; Ehrenreich et al. 2010; Guenther & Tal-Or 2010). About 1900 single stars currently remain after discarding all multiple systems.

2.1. CAFOS sample

The aim of our low-resolution spectroscopic observations is twofold: (i) to increase the number of bright, late-M dwarfs in CARMENCITA and (ii) to ensure that the compiled spectral types used for the selection and pre-cleaning are correct. With this double objective in mind, we observed the following:

- High proper-motion M-dwarf candidates from Lépine & Shara (2005) and Lépine & Gaidos (2011) with spectral types with large uncertainties or derived only from photometric colours. Spectral types from $V^* - J$ colours are not suitable for our purposes (Alonso-Floriano et al. 2013a; Mundt et al. 2013; Lépine et al. 2013 – V^* is an average of photographic magnitudes B_J and R_F from the Digital Sky Survey; cf. Lépine & Gaidos 2011). In collaboration with Sebastien Lépine, we observed and analysed an extension of the Lépine & Gaidos (2011) catalogue of high proper-motion candidates brighter than $J = 10.5$ mag. The spectra of stars brighter than $J = 9.0$ mag were published by Lépine et al. (2013), while most of the remaining fainter ones are published here.
- M dwarf candidates in nearby young moving groups (e.g., Montes et al. 2001; Zuckermann & Song 2004; da Silva et al. 2009; Shkolnik et al. 2012; Gagné et al. 2014; Klutsch et al. 2014), in multiple systems containing FGK-type primaries that are subjects of metallicity studies (Gliese & Jahreiss 1991; Poveda et al. 1994; Gould & Chanamé 2004; Rojas-Ayala et al. 2012; Terrien et al. 2012; Mann et al. 2013; Montes et al. 2013), in fragile binary systems at the point of disruption by the Galactic gravitational field (Caballero 2012, and references therein), and resulting from new massive virtual-observatory searches (Jiménez-Esteban et al. 2012; Aberasturi et al. 2014). Such a broad diversity of sources allowed us to widen the investigated intervals of age, activity, multiplicity, metallicity, and dynamical evolution.
- Known M dwarfs with well-determined spectral types from PMSU (see above) and Lépine et al. (2013). The comparison of these two samples with ours was a sanity check for determining the spectral types (see Sect. 4.1).
- M dwarfs in our input catalogue with uncertain or probably incorrect spectral types based on apparent magnitudes, $r' - J$ colours, and heliocentric distances, including resolved

[3] Please contribute to the comprehensiveness of our input catalogue by sending an e-mail with suggestions to José A. Caballero, e-mail: `caballero@cab.inta-csic.es`.

A&A 577, A128 (2015)

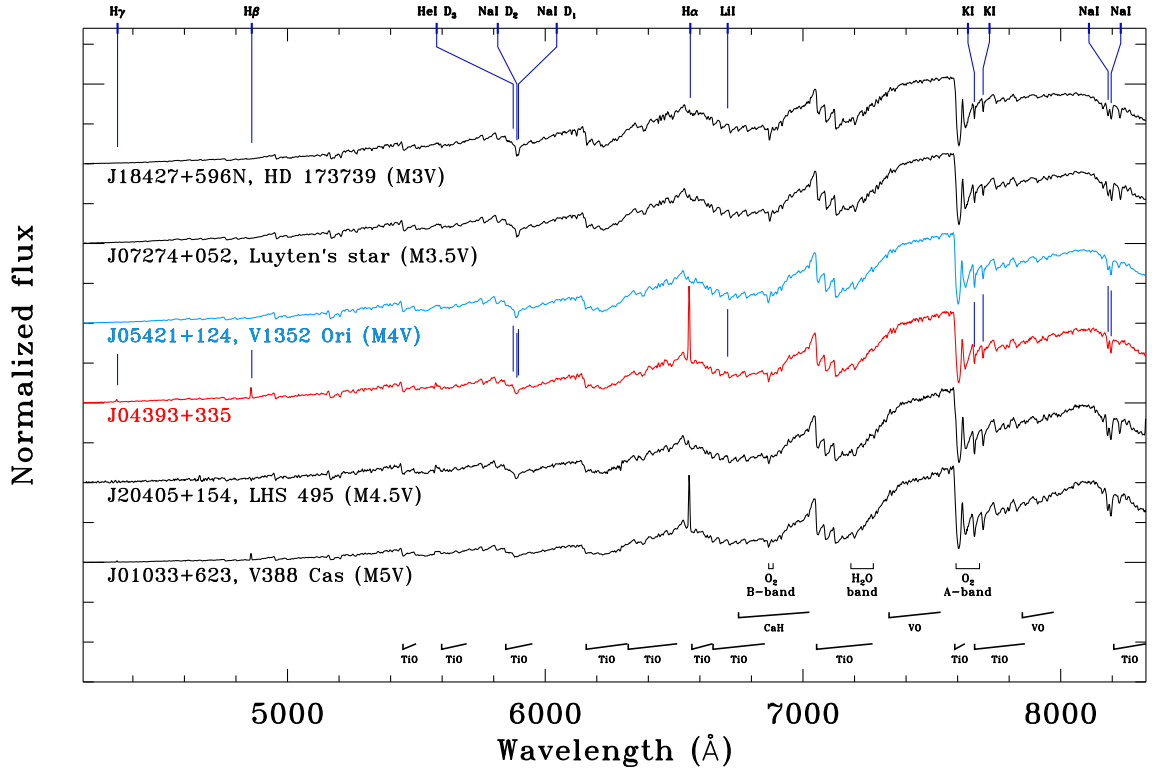

Fig. 1. Six representative CAFOS spectra. From top to bottom, spectra of standard stars with spectral type 1.0 and 0.5 subtypes earlier than the target (black), standard star with the same spectral type as the target (cyan), the target star (red; in this case, J04393+335 – M4.0 V, Simbad name: V583 Aur B), and standard stars with spectral type 0.5 and 1.0 subtypes later than the target (black). We mark activity-, gravity-, and youth-sensitive lines and doublets at the top of the figure (Hγ, Hβ, He I D_3, Na I D_2 and D_1, Hα, Li I, K I, and Na I, from left to right) and molecular absorption bands at the bottom. Note the three first lines of the Balmer series in emission in the spectrum of the target star.

physical binaries. See some examples in Cortés-Contreras et al. (2014).

– Numerous standard stars. For an accurate determination of spectral type and class, we also included approximately 50 stars with well-determined spectral types from K3 to M8 for both dwarf (Johnson & Morgan 1953; Kirkpatrick et al. 1991; PMSU) and giant classes (e.g., Moore & Paddock 1950; Ridgway et al. 1980; Jacoby et al. 1984; García 1989; Keenan & McNeil 1989; Kirkpatrick et al. 1991; Sánchez-Blázquez et al. 2006; Jiménez-Esteban et al. 2012).

3. Observations and analysis

3.1. Low-resolution spectroscopic data

Observations were secured with the Calar Alto Focal reductor and Spectrograph (CAFOS) mounted on the Ritchey-Chrétien focus of the Zeiss 2.2 m Calar Alto telescope (Meisenheimer 1994). We obtained more than 900 spectra of 745 targets during 38 nights over four semesters from 2011 November to 2013 April. All observations were carried out in service mode with the G-100 grism, which resulted in a useful wavelength coverage of 4200–8300 Å at a resolution $\mathcal{R} \sim 1500$. Exposure times ranged from shorter than 1 s to 1 h. The longest exposures were split into up to four sub-exposures. On some occasions, another star fell in the slit aperture (usually the primary of a close multiple system containing our M-dwarf candidate main target). We also added the 13 red dwarfs and giants observed in 2011 March by Jiménez-Esteban et al. (2012), which made a total of 758 targets.

We reduced the spectra using typical tasks within the IRAF environment. The reduction included bias subtraction, flat fielding, removal of sky background, optimal aperture extraction, wavelength calibration (with Hg-Cd-Ar, He, and Rb lamps), and instrumental response correction. For the latter, we repeatedly observed the spectrophotometric standards G 191–B2B (DA0.8), HD 84937 (sdF5), Feige 34 (sdO), BD+25 3941 (B1.5 V), and BD+28 421 (sdO) at different air masses. In the end, we only used the spectra with the highest signal-to-noise ratio of the hot subdwarf Feige 34, which gave the best-behaved instrumental response correction. We extracted all traces in the spectra, including those of other stars in the slit aperture. We did not remove telluric absorption lines from the spectra that were due to the variable meteorological conditions during two years of observation (see Sect. 3.2.2). All our spectra had a signal-to-noise ratio higher than 50 near the Hα λ6562.8 Å line, which together with the wide wavelength coverage allowed us to make a comprehensive analysis and to measure numerous spectral indices and activity indicators.

Table 3. Standard and prototype stars.

SpT		Karmn	Name
M0.0 V	*	J09143+526	HD 79210
		J07195+328	BD+33 1505
		J09144+526	HD 79211
M0.5 V	*	J18353+457	BD+45 2743
		J04329+001S	LP 595–023
		J22021+014	HD 209290
M1.0 V	*	J00183+440	GX And
		J05151–073	LHS 1747
		J11054+435	BD+44 2051A
M1.5 V	*	J05314–036	HD 36395
		J00136+806	G 242–048
		J01026+623	BD+61 195
		J11511+352	BD+36 2219
M2.0 V	*	J08161+013	GJ 2066
		J03162+581N	Ross 370 B
		J03162+581S	Ross 370 A
M2.5 V	*	J11421+267	Ross 905
		J10120–026 AB	LP 609–071
		J19169+051N	V1428 Aql
		J21019–063	Wolf 906
M3.0 V	*	J18427+596N	HD 173739
		J17364+683	BD+68 946
		J22524+099	σ Peg B
M3.5 V	*	J07274+052	Luyten's star
		J17199+265	V647 Her
		J17578+046	Barnard's star
		J18427+596S	HD 173740
M4.0 V	*	J05421+124	V1352 Ori
		J04308–088	Koenigstuhl 2 A
		J06246+234	Ross 64
		J10508+068	EE Leo
M4.5 V	*	J20405+154	G 144–025
		J04153–076	o^{02} Eri C
		J16528+610	GJ 625
		J17198+265	V639 Her
M5.0 V	*	J01033+623	V388 Cas
		J16042+235	LSPM J1604+2331
		J23419+441	HH And
M5.5 V	*	J02022+103	LP 469–067
		J21245+400	LSR J2124+4003
M6.0 V	*	J10564+070	CN Leo
		J07523+162	LP 423–031
		J16465+345	LP 276–022
M6.5 V	*	J08298+267	DX Cnc
		J09003+218	LP 368–128
		J10482–113	LP 731–058
M7.0 V	*	J16555-083	V1054 Oph D (vB 8)
		J02530+168	Teegarden's star
M8.0 V	*	J19169+051S	V1298 Aql (vB 10)

Notes. Prototype stars are marked with an asterisk.

We list in Table A.1 the 753 observed K and M dwarf and giant candidates according to identification number, our CARMENCITA identifier, discovery name, Gliese or Gliese & Jahreiß number, J2000.0 coordinates and J-band magnitude from the Two-Micron All-Sky Survey (Skrutskie et al. 2006), observation date, and exposure time. The five stars not tabulated are the spectrophotometric standards.

In Table A.1, our CARMENCITA identifier follows the nomenclature format "Karmn JHHMMm±DDd(X)", where "Karmn" is the acronym, "m" and "d" in the sequence are the truncated decimal parts of a minute or degree of the corresponding equatorial coordinates for the standard equinox of J2000.0 (IRAS style for right ascension, PKS quasar style for declination), and X is an optional letter (N, S, E, W) to distinguish between physical or visual pairs with the same HHMMm±DDd sequence within CARMENCITA. We use the discovery name for every target, except for M dwarfs with variable names (e.g., EZ PSc, GX And, V428 And) or those that are physical companions to bright stars (e.g., BD–00 109 B, η Cas B, HD 6440 B). We associate for the first time many X-ray events with active M dwarfs (e.g., Lalitha et al. 2012; Montes et al. 2015). In these cases, we use the precovery[4] *Einstein* 2E or *ROSAT* RX/1RXS event identifications instead of the names given by the proper-motion survey that recovered the stars.

Additionally, we always indicate whether the star is a known close binary or triple unresolved in our spectroscopic data (with "AB", "BC", "ABC"). There are 75 such close multiple systems in our sample (70 double and 5 triple), of which the widest unresolved pair is J09045+164 AB (BD+16 1895), with $\rho \approx 4.1$ arcsec. A comprehensive study on the multiplicity of M dwarfs in CARMENCITA, including spectral-type estimate of companions from magnitude differences in high-resolution imaging data, will appear in a forthcoming paper of this series (preliminary data were presented in Cortés-Contreras et al. 2015).

3.2. Spectral typing

We followed two widely used spectral classification schemes that require an accurate, wide grid of reference stars. The first strategy relies on least-squares minimisation and best-fitting to spectra of the standard stars, while the second scheme uses spectral indices that quantify the strength of the main spectral features in M dwarfs, notably molecular absorption bands (again, preliminary data were presented in Klutsch et al. 2012 – least-squares minimisation – and Alonso-Floriano et al. 2013a – spectral indices).

Before applying the two spectral-typing strategies, we normalised our spectra by dividing by the observed flux at 7400 Å. We also corrected for spatial distortions at the reddest wavelengths (with $R \sim 1500$, there is no need for a stellar radial-velocity correction). For that, we shifted our spectra until the K I $\lambda\lambda$7664.9, 7699.0 Å doublet was placed at the laboratory wavelengths. This correction, often of 1−2 Å, was critical for the definition of spectral indices, some of which are very narrow.

3.2.1. Spectral standard and prototype stars

We list the used standard stars in Table 3 (see also Sect. 3.2.4), most of which were taken from Kirkpatrick et al. (1991) and PMSU (Table 2). Our intention was to provide one prototype star and up to four reference stars per half subtype, but this was not always possible, especially at the latest spectral types. The prototype stars, shown in Fig. 2, are the brightest, least active reference stars that have spectra with the highest signal-to-noise ratio, and that do not deviate significantly from the general trend during fitting. In Table 3, the first star of each subtype is the prototype for that subtype. In the case of standard stars with different reported spectral types in the bibliography (with maximum

[4] "Pre-discovery recovery".

A&A 577, A128 (2015)

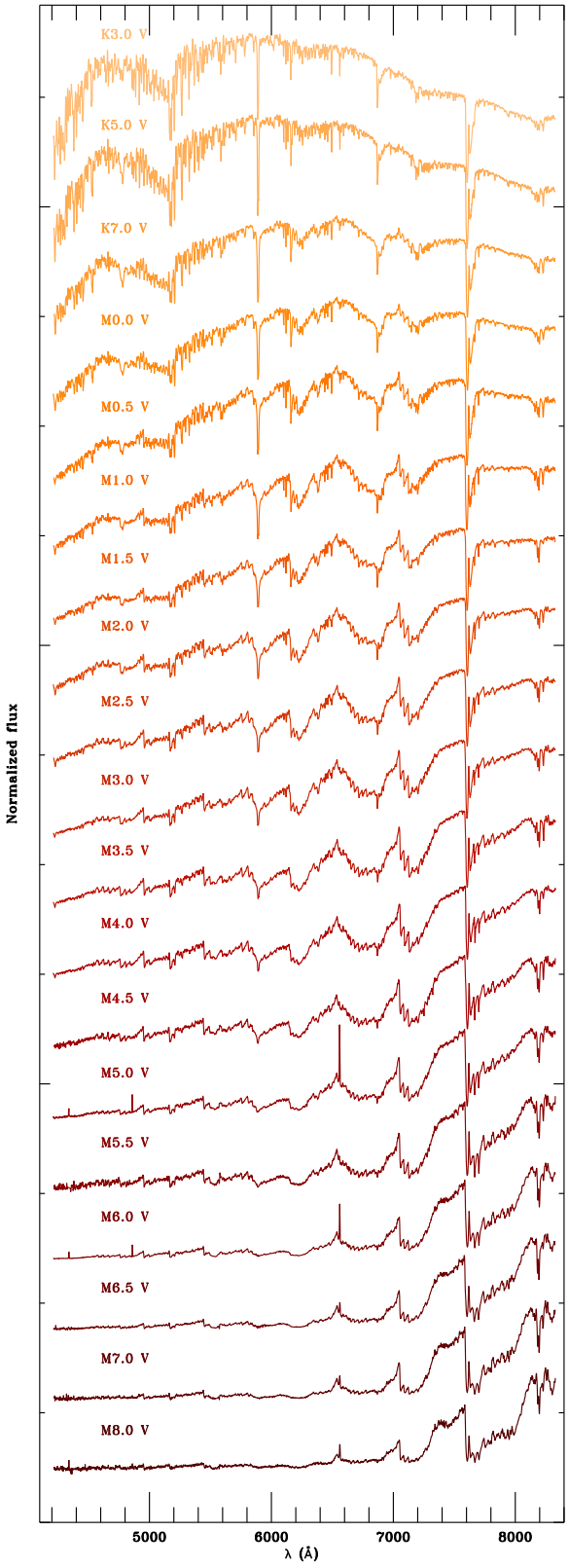

Fig. 2. CAFOS spectra of our prototype stars. From top to bottom, K3 V, K5 V, K7 V, M0.0–7.0 V in steps of 0.5 subtypes, and M8.0 V.

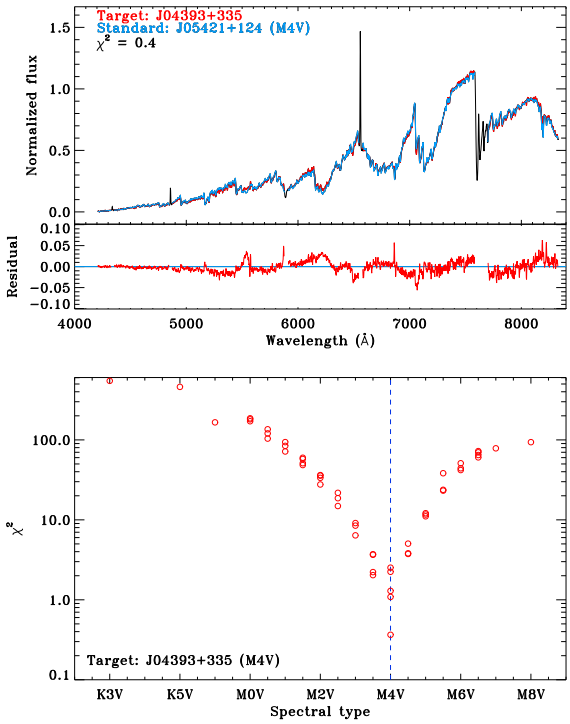

Fig. 3. Spectral typing of J04393+335 with best-match and $\chi^2_{\rm min}$ methods. *Top panel*: best-match. CAFOS normalised spectra of the target star and of the standard star that fits best (*top*) and the difference (*bottom*). *Bottom panel*: $\chi^2_{\rm min}$. Values of χ^2 as a function of the spectral type (open red circles). The vertical dashed line marks the spectral type at the lowest χ^2 value. Note the logarithmic scale in the Y axis.

differences of 0.5 subtypes), we chose the value that gave us less scatter in our fits.

We also used three K dwarfs from Kirkpatrick et al. (1991), not listed in Table 3, to extend our grid of standard stars towards warmer effective temperatures. The three K-dwarf standard stars are HD 50281 (K3 V), 61 Cyg A (K5 V), and η Cas B (K7 V). The standard star LP 609–071 AB is a close binary composed of an M2.5 V star and a faint companion separated by $\rho = 0.18 \pm 0.02$ arcsec (Delfosse et al. 1999). With $\Delta K = 0.95 \pm 0.05$ mag, the faint companion flux barely affects the primary spectrum in the optical.

3.2.2. Best-match and $\chi^2_{\rm min}$ methods

Before any least-squares minimisation, we discarded five narrow (20–30 Å) wavelength ranges influenced by activity indicators (Hα, Hβ, Hγ, and the Na I doublet – Fraunhofer C, F, and G′ lines) and by strong telluric lines (O_2 band around 7594 Å – Fraunhofer A line). Next, in the full remaining spectral range, we compared the normalised spectrum of every target star with those of all our standard stars in Table 3 and computed a χ^2 value for each fit. In the best-match method, we assigned the spectral type of the standard star that best fitted our target spectrum (i.e., with the lowest χ^2 value); in the $\chi^2_{\rm min}$ method, we assigned the spectral type that corresponded to the minimum of the curve resulting from the (sixth-order) polynomial fit of all the χ^2-spectral type pairs. As expected, the best-match and $\chi^2_{\rm min}$ methods give the same result in most cases. In the representative case shown

Table 4. Spectral indices used in this work.

Index	$\Delta\lambda_{num}$ [Å]	$\Delta\lambda_{den}$ [Å]	Reference
CaOH	6230:6240	6345:6354	Reid et al. (1995)
CaH 1	6380:6390	∑ 6345:6355, 6410:6420	Reid et al. (1995)
I2 (CaH)	6510:6540	6370:6400	Martín & Kun (1996)
I3 (TiO)	6510:6540	6660:6690	Martín & Kun (1996)
Hα	6560:6566	6545:6555	Reid et al. (1995)
TiO 1	6718:6723	6703:6708	Reid et al. (1995)
CaH 2	6814:6846	7042:7046	Reid et al. (1995)
CaH 3	6960:6990	7042:7046	Reid et al. (1995)
TiO-7053	7000:7040	7060:7100	Martín et al. (1999)
Ratio A (CaH)	7020:7050	6960:6990	Kirkpatrick et al. (1991)
TiO-7140	7015:7045	7125:7155	Wilking et al. (2005)
PC1	7030:7050	6525:6550	Martín et al. (1996)
CaH Narr	7044:7049	6972.5:6977.5	Shkolnik et al. (2009)
TiO 2	7058:7061	7043:7046	Reid et al. (1995)
TiO 3	7092:7097	7079:7084	Reid et al. (1995)
TiO 5	7126:7135	7042:7046	Reid et al. (1995)
TiO 4	7130:7135	7115:7120	Reid et al. (1995)
VO-a	∑ 7350:7370, 7550:7570	7430:7470	Kirkpatrick et al. (1999)
VO	∑ α7350:7400, β7510:7560[a]	7420:7470	Kirkpatrick et al. (1995)
Ratio B (Ti I)	7375:7385	7353:7363	Kirkpatrick et al. (1991)
VO-7434	7430:7470	7550:7570	Hawley et al. (2002)
PC2	7540:7580	7030:7050	Martín et al. (1996)
VO 1	7540:7580	7420:7460	Martín et al. (1999)
TiO 6	7550:7570	7745:7765	Lépine et al. (2003)
VO-b	∑ 7860:7880, 8080:8100	7960:8000	Kirkpatrick et al. (1999)
VO 2	7920:7960	8130:8150	Lépine et al. (2003)
VO-7912	7990:8030	7900:7940	Martín et al. (1999)
Ratio C (Na I)	8100:8130	8174:8204	Kirkpatrick et al. (1991)
Color-M	8105:8155	6510:6560	Lépine et al. (2003)
Na-8190	8140:8165	8173:8210	Hawley et al. (2002)
PC3	8235:8265	7540:7580	Martín et al. (1996)

Notes. [a] $\alpha = 0.5625, \beta = 0.4375$.

in Figs. 1 and 3, the target dwarf has an M4.0 V spectral type using both the best match and χ^2_{min} methods.

3.2.3. Spectral indices

The spectral indices methodology for spectral typing is based on computing flux ratios at certain wavelength intervals in low-resolution spectra (e.g., Kirkpatrick et al. 1991; Reid et al. 1994; Martín et al. 1996, 1999). In the present analysis, we compiled 31 spectral indices defined in the literature to determine spectral types of late-K dwarfs and M dwarfs that occur in the useable wavelength interval of our CAFOS spectra. In general, a spectral index I_i is defined by the ratio of numerator and denominator fluxes (i.e., $I_i = F_{i,num}/F_{i,den}$). Table 4 lists the 31 wavelength intervals of fluxes in the numerator and denominator, $\Delta\lambda_{num}$ and $\Delta\lambda_{den}$, and corresponding reference for each index. Some flux wavelength intervals are the linear combination of two subintervals (CaH 1, VO-a, VO-b) or, in the case of the VO index, a non-linear combination. Additionally, there are wavelength intervals of fluxes in the numerator that are either redder and bluer than the one in the denominator, which translates into different slopes in the index-spectral type relations. Of the 31 tabulated indices, nine are related to TiO features, seven to VO, six to CaH, three to the "pseudo-continuum" (i.e., relative absence of features), and the rest to H and neutral metallic lines (Ti, Na).

For every star observed with CAFOS, we computed the stellar numerator and denominator fluxes using an automatic trapezoidal integration procedure. When all indices were available, we plotted all spectral index vs. spectral type diagrams for the standard stars listed in Table 3 and fitted low-order polynomials to the data points. Although some spectral indices allowed linear (e.g., I2, Ratio B) or parabolic fits, most of the fits were to cubic polynomials of the form $\mathrm{SpT}(i) = a + b\,i + c\,i^2 + d\,i^3$, where i was the index. In all cases, we checked our diagrams and fits with those in the original papers and found no significant differences (of less than 0.5 subtypes). We also took special care in defining the range of application of our fits in spectral type. The different shapes of fitting curves, ranges of application, and internal dispersion of the data points are illustrated in Fig. 4.

Some indices are sensitive not only to spectral type (i.e., effective temperature), but also to surface gravity (e.g., I2, Ratio A, CaH Narr, Ratio C, Na-8190 – Sect. 4.2), metallicity (e.g., CaOH, CaH 1, CaH 2, CaH 3 – Sect. 4.3), or activity (Hα – Sect. 4.4). We identified the spectral indices with the widest range of application and least scatter. Table 5 lists the coefficients of the cubic polynomial fits of the five spectral indices that we eventually chose for spectral typing (note the logarithmic scale of the Color-M index). The spectral index vs. spectral type diagrams of VO-7912 and Color-M are very similar to those of PC, TiO 2, and TiO 5, shown in Fig. 4. All of them are valid from

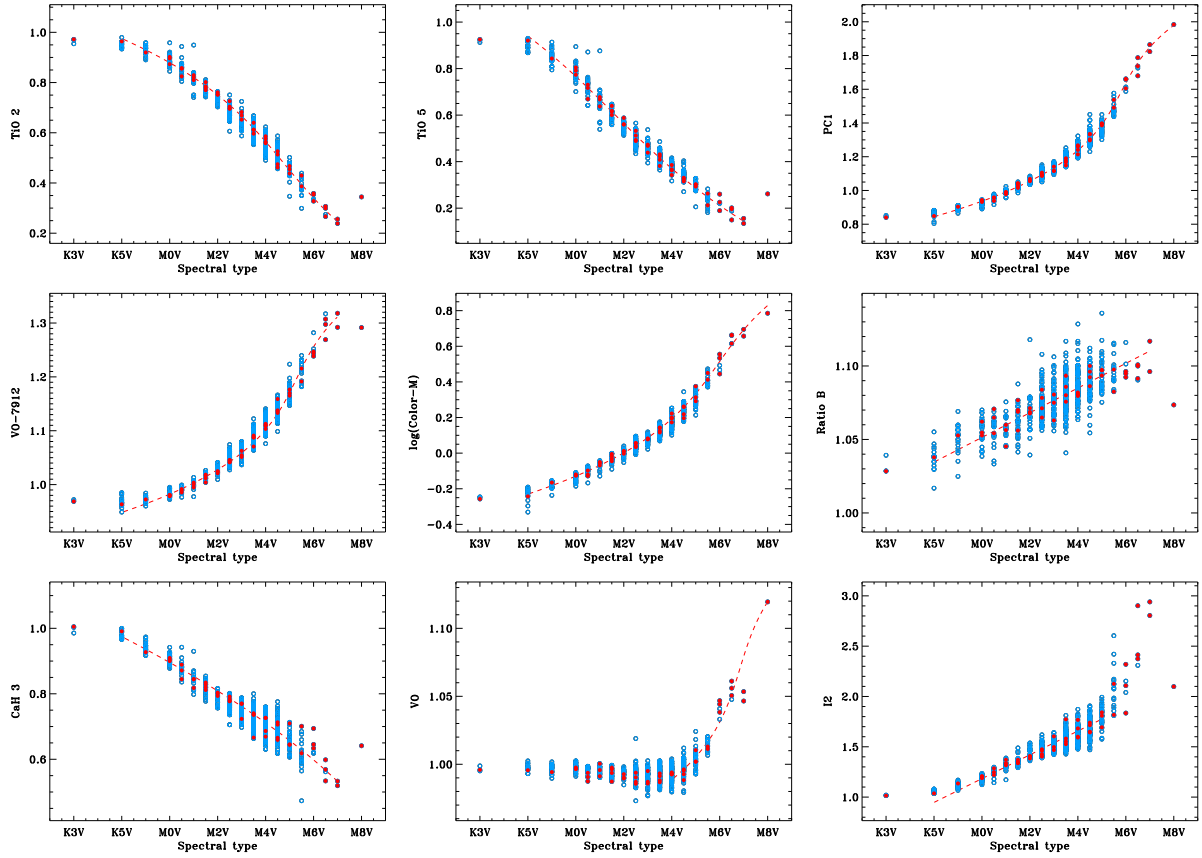

Fig. 4. Nine representative spectral indices as a function of spectral type. Filled (red) circles: standard stars. Open (blue) circles: remaining target stars. Dashed (red) line: fit to straight line, parabola, or cubic polynomial, drawn only in the range of application of the fit. *Top left and middle*: TiO 2 and TiO 5 (Reid et al. 1995), with negative slopes and useable up to M7 V; *top right*: PC1 (Martín et al. 1996), a monotonous spectral indicator from K5 V to M8 V; *centre left and middle*: VO-7912 (Martín et al. 1999) and Color-M (Lépine et al. 2003), two indices very similar to the PC1. Note the logarithmic scale in Color-M; *centre right*: ratio B (Kirkpatrick et al. 1991), sensitive to several stellar parameters and, thus, with a large scatter in the spectral type relation; *bottom left*: CaH 3 (Reid et al. 1995), with a slightly larger scatter than pseudo-continuum or titanium oxide indices, due to metallicity; *bottom middle*: VO (Kirkpatrick et al. 1995), useable only for determining spectral types later than M4 V; *bottom right*: I2 (Martín & Kun 1996), with a linear range of variation from mid-K to mid-M and a sudden increase (or high dispersion) at late-M.

K7 V to M7 V (to M8 V in the case of PC1 and Color-M), while the dispersion of the fits is of about 0.5 subtypes. The TiO 5 has been a widely used index for spectral typing (Reid et al. 1995; Gizis 1997; Seeliger et al. 2011; Lépine et al. 2013) but, to our knowledge, we propose here for the first time to use it with a nonlinear fit.

In Table A.2, we list the values of the five spectral-typing indices of all CAFOS stars together with the CaH 2 and CaH 3 indices that are used to compute the ζ metallicity index (Sect. 4.3) and the pseudo-equivalent width of the Hα line (Sect. 4.4).

3.2.4. Adopted spectral types

After applying the best-match and $\chi^2_{\rm min}$ methods and using the five spectral-index-type relations in Table 5, we obtained seven complementary spectral-type determinations for each star. In Table A.3, we assigned a value between 0.0 and 8.0 in steps of 0.5 to each M spectral subtype for all stars of dwarf luminosity class (there are no stars later than M8.0 V in our CAFOS sample). In addition, we used the values –2.0 and –1.0 for referring to K5 V and K7 V spectral types (there are no K6, 8, 9 spectral types in the standard K-dwarf classification – Johnson & Morgan 1953; Keenan & McNeil 1989). In some cases, we were able to identify dwarfs earlier than K5 V with the best-match and $\chi^2_{\rm min}$ methods. For giant stars, we only provide a visual estimation

Table 5. Coefficients and standard deviation (in spectral subtypes) of the cubic polynomial fits of the five spectral-typing indices.

Index	a	b	c	d	σ
TiO 2	+11.0	–22	+28	–20	0.83
TiO 5	+9.6	–20	+17.0	–9.0	0.57
PC1	–50	+97	–59	+12.4	0.52
VO-7912	–520	+1300	–1070	+300	0.59
Color-M	+1.98	+13.1	–15.6	+10.3	0.53

Notes. We used the relation SpT(i) = $a + b\,i + c\,i^2 + d\,i^3$ for the cubic fits. For the Color-M index we used the relation SpT(i) = $a + b\,\log i + c\,(\log i)^2 + d\,(\log i)^3$.

(K III, M III) based on the spectral types of well-known giant standard stars observed with CAFOS.

For all late-K and M dwarfs, we calculated one single spectral type per star based on the information provided by the seven individually determined spectral indices. We used a median of the seven values for cases where they were identical within 0.5 subtypes. To avoid any bias, we carefully checked the original spectra if the spectral types from the best-match and $\chi^2_{\rm min}$ methods and from the spectral indices were different by 0.5 subtypes, or if any spectral type deviated by 1.0 subtypes or more (which occurred very rarely). In these cases, we adopted the spectral type of the closest (visually and in χ^2) standard star. The uncertainty of the adopted spectral types is 0.5 subtype, except for some odd spectra indicated with a colon (probably young dwarfs of low gravity or subdwarfs of low metallicity; see below).

4. Results and discussion

4.1. Spectral types

Among the 753 investigated stars with adopted spectral types from CAFOS data, there were 23 late-K dwarfs at the K/M boundary (K7 V), 21 early- and intermediate-K dwarfs (K0−5 V), 22 M-type giants (M III), three K-type giants (K III), and one star without class determination (i.e., J04313+241 AB). This left 683 M-type dwarfs (and subdwarfs) in our CAFOS sample.

As shown in Table A.3, we searched for previous spectral type determinations in the literature for the 753 investigated stars (small "m" and "k" denote spectral types estimated from photometry). Taking previous determinations and estimations into account, we derived spectral types from spectra for the first time for 305 stars, and revised typing for most of the remaining 448 stars.

The agreement in spectral typing with previous large spectroscopic surveys of M dwarfs is shown in Fig. 5. The standard deviations of the differences between the spectral types derived by us and by PMSU (with a narrower wavelength interval; 100 stars in common) and by Lépine et al. (2013; 95 stars in common) were 0.55 and 0.38 subtypes, respectively, which are of the order of our internal uncertainty (0.5 subtypes). The standard deviation of the differences between our spectral types and those estimated from photometry by Lépine & Gaidos (2011; 576 stars in common) is larger, of up to 1.32 subtypes. The bias towards later spectral types in Lépine & Gaidos (2011) and the scatter of the spectral type differences is obvious from the bottom panel in Fig. 5. In particular, we measured maximum differences of up to 7 subtypes, by which some late-M dwarf candidates become actual K dwarfs (probably due to the use by Lépine & Gaidos of B_J and R_F from photographic plates for the spectral type estimation; see references in Sect. 2). However, over 93% of the compared stars have disagreements lower than or equal to 2 subtypes. We emphasize that our CARMENCITA data base is very homogeneous because more than 95% of the spectral type determinations come from either PMSU, Lépine et al. (2013), or our CAFOS data, which are consistent with each other, as shown above.

Of the 683 CAFOS M-type dwarfs (and subdwarfs), 414 and 106 M dwarfs satisfy our criteria in Table 1 of restrictive J-band spectral type limiting and completeness, respectively. In total, 261 dwarfs have spectral type M4.0 V or later. The brightest, latest of them are being followed-up with high-resolution spectrographs and imagers and with data from the bibliography to identify the most suitable targets for CARMENES (no physical or visual companions at less than 5 arcsec, low $v \sin i$; see forthcoming papers of this series). Furthermore, there are 61 relatively bright ($J < 10.9$ mag) CAFOS stars with spectral types

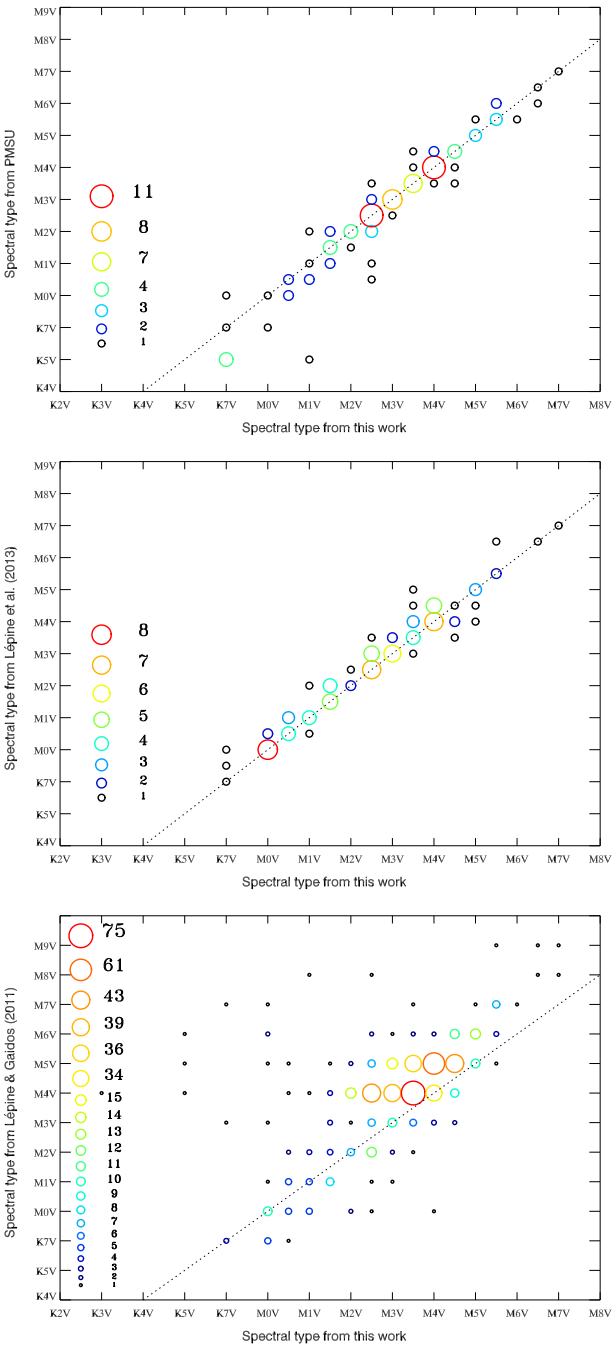

Fig. 5. Spectral type comparison between our results and those from PMSU (*top panel*), Lépine et al. (2013; *middle panel*), and Lépine & Gaidos (2011; from $V^* - J$ photometry, *bottom panel*). The larger a circle, the greater the number of stars on a data point. Dotted lines indicate the one-to-one relationship.

A&A 577, A128 (2015)

Table 6. Giant stars observed with CAFOS.

Karmn	Name	Giant
J00146+202	χ Peg	Standard
J00367+444	V428 And	Standard
J00502+601	HD 236547	Standard
J01012+571	1RXS J010112.8+570839	New
J01097+356	Mirach	Standard
J02479–124	Z Eri	Standard
J02558+183	ρ^{02} Ari	Standard
J03319+492	TYC 3320–337–1	LG11[a]
J04206–168	DG Eri	Standard
J07420+142	NZ Gem	Standard
J10560+061	56 Leo	Standard
J11018–024	p^{02} Leo	Standard
J11201+301	HD 98500	Standard
J11458+065	ν Vir	Standard
J12322+454	BW CVn	Standard
J12456+271	HD 110964	Standard
J12533+466	BZ CVn	Standard
J13587+465	HD 122132	Standard
J17126–099	Ruber 7	JE12[b]
J17216–171	TYC 6238–480–1	JE12[b]
J18423–013	Ruber 8	JE12[b]
J22386+567	V416 Lac	Standard
J23070+094	55 Peg	Standard
J23177+490	8 And	Standard
J23266+453	2MASS J23263798+4521054	Background

References. [(a)] LG11: Lépine & Gaidos (2011). [(b)] JE12: Jiménez-Esteban et al. (2012).

between M5.0 V and M8.0 V that are also suitable targets for any other near-infrared radial-velocity monitoring programmes with the instruments mentioned above (i.e., HPF, SPIRou, IRD).

4.2. Gravity

Table 6 lists the 25 giants observed with CAFOS. Of these, 17 stars have previously been tabulated as M giant standard stars (e.g., Keenan & McNeil 1989; García 1989; Kirkpatrick et al. 1991; Sánchez-Blázquez et al. 2006). They are bright ($J \lesssim 5.0$ mag; down to −1.0 mag in the case of Mirach, β And) and show the low-gravity spectral features typically found in M giants: faint alkali lines (K I $\lambda\lambda$7665, 7699 Å and Na I $\lambda\lambda$8183, 8195 Å), a tooth-shaped feature produced by MgH/TiO blend near 4770 Å, and a decrease of CaH in the A-band at 6908−6946 Å with the increase of luminosity (Kirkpatrick et al. 1991; Martín et al. 1999; Riddick et al. 2007; Gray & Corbally 2009). Two other stars, V428 And and HD 236547, are well-known K giant standard stars (Jacoby et al. 1984; García 1989; Kirkpatrick et al. 1991).

Of the other six giant stars in Table 6, three have J-band magnitudes of 6.1−6.2 mag and were identified by Jiménez-Esteban et al. (2012) as some of the reddest Tycho-2 stars with proper motions $\mu > 50$ mas a^{-1}, namely Ruber 7, TYC 6238–480–1, and Ruber 8 (which seems to be also one of the brightest metal-poor M giants ever identified). The remaining three giant stars, with faint J-band magnitudes between 8.2 and 10.0 mag, are listed below.

– J01012+571 (1RXS J010112.8+570839). It is a previously unknown distant M giant close to the Galactic plane (b = −5.7 deg). It was serendipitously identified in an unpublished photometric survey by one of us (J.A.C.), and was observed with CAFOS because of its very red optical and near-infrared colours and possible association with an X-ray event catalogued by *ROSAT* at a separation of only 6.4 arcsec.
– J03319+492 (TYC 3320–337–1). From photographic magnitudes, Pickles & Depagne (2010) and Lépine & Gaidos (2011) classified it as an M1.9 and M3 dwarf, respectively. However, it appears to be an early-K giant with a significant proper motion of 56 mas a^{-1}. It is not possible to separate it from the main sequence in a reduced proper-motion diagram.
– J23266+453 (2MASS J23263798+4521054). Our intention was to observe BD+44 4419 B (G 216–43), an M4.5 dwarf of roughly the same V-band magnitude (10.3 vs. 10.9 mag). Unfortunately, we incorrectly observed instead a background giant at a separation of about 20 arcsec.

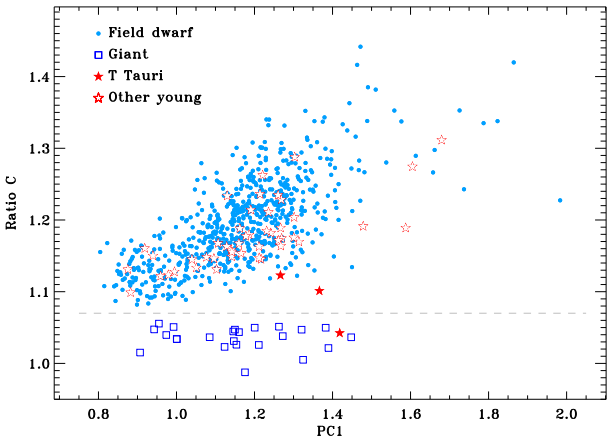

Fig. 6. Ratio C vs. PC1 index-index diagram. The different symbols represent field dwarfs (small dots, blue), giants (open squares, dark blue), Taurus stars (filled stars, red), and other young stars (open stars, red). All giants are below the dashed line at Ratio C = 1.07. The dashed line is the empirical border of the giant star region.

In a Ratio C vs. PC1 index-index diagram as the one shown in Fig. 6, where Ratio C is highly sensitive to gravity and PC1 is an effective temperature proxy (PC1 was indeed one of the five indices used for deriving spectral types), all giants are below the dashed line at Ratio C = 1.07. There is only one star not classified as a giant that lies below that empirical boundary. It is J04313+241 (V927 Tau AB), a T Tauri star for which we did not provide a luminosity class in Sect. 4.1. We discuss this in detail in Sect. 4.4. Ratio C, which contains the sodium doublet at 8193, 8195 Å, can also be used as a youth indicator (e.g., Schlieder et al. 2012b).

4.3. Metallicity

In F-, G-, and K-type stars whose photospheric continua are well-defined in high-resolution spectra, stellar metallicity is computed through spectral synthesis (McWilliam 1990; Valenti & Piskunov 1996; González 1997; González Hernández et al. 2004; Valenti & Fischer 2005; Recio-Blanco et al. 2006) or measuring equivalent widths, especially of iron lines (Sousa et al. 2008, 2011; Magrini et al. 2010; Adibekyan et al. 2012; Tabernero et al. 2012; Bensby et al. 2014). However, it is

not possible to measure a photospheric continuum in M-type stars and, thus, their metallicity is studied through other techniques. Since the first determinations from broad-band photometry by Stauffer & Hartmann (1986), there have been three main observational techniques employed to determine metallicity in M dwarfs:

- Photometry calibrated with M dwarfs in physical double and multiple systems with warmer companions, typically F, G, K dwarfs, of known metallicity (Bonfils et al. 2005; Casagrande et al. 2008; Schlaufman & Laughlin 2010; Neves et al. 2012).
- Low-resolution spectroscopy, also calibrated with M dwarfs with earlier primaries, in the optical (Dhital et al. 2012), in the near infrared (Rojas-Ayala et al. 2010, 2012; Terrien et al. 2012; Mann et al. 2014; Newton et al. 2014), or in both wavelength ranges (Mann et al. 2013, 2015).
- High-resolution spectroscopy in the optical (from spectral synthesis: Woolf & Wallerstein 2005; from spectral indices: Woolf & Wallerstein 2006; and Bean et al. 2006; from the measurement of pseudo-equivalent widths: Neves et al. 2013, 2014), in the near-infrared (Shulyak et al. 2011, in the *Y* band; Önehag et al. 2012, in the *J* band; Tsuji & Nakajima 2014, in the *K* band), or in the optical and near-infrared simultaneously (Gaidos & Mann 2014). The novel mid-resolution spectroscopy study in the optical aided with spectral synthesis by Zboril & Byrne (1998) also belongs in this item.

For the 753 CAFOS stars, we computed the $\zeta_{\mathrm{TIO/CaH}}$ metallicity parameter (denoted ζ for short) described by Lépine et al. (2007):

$$\zeta = \frac{1 - \mathrm{TiO\,5}}{1 - [\mathrm{TiO\,5}]_{Z_\odot}}, \quad (1)$$

where $[\mathrm{TiO\,5}]_{Z_\odot} = 0.571 - 1.697\mathrm{CaH} + 1.841\mathrm{CaH}^2 - 0.454\mathrm{CaH}^3$ is a third-order fit of CaH = CaH 2 + CaH 3 for *our* standard stars, and TiO 5, CaH 2, and CaH 3 are the spectral indices of Reid et al. (1995) (see also Gizis & Reid 1997; and Lépine et al. 2003). The ζ index is correlated with metallicity in metal-poor M subdwarfs (Woolf et al. 2009) and metal-rich dwarfs (Lépine et al. 2007; Mann et al. 2014). For completeness, we also tabulate the ζ index for our 25 giants, but they are not useful for a comparison. We made the same assumption of standard stars having solar metallicity ($\zeta \approx 1$) as in Lépine et al. (2007), which was later justified by the small dispersion of the data points.

We looked for M dwarfs (and subdwarfs) in our sample with abnormal metallicity, which could be spotted in a CaH 2 + CaH 3 vs. TIO 5 index-index diagram as in Fig. 7. Lépine et al. (2007) defined the classes subdwarf (sd), $0.5 < \zeta < 0.825$, and extreme subdwarf (esd), $\zeta < 0.5$. All our non-giant stars except two have ζ values greater than 0.825, which is the empirical boundary between dwarfs and subdwarfs. The spectra of the two exceptions show shallower molecular bands and lines than M dwarfs of the same spectral type.

One of our two subdwarf candidates is J19346+045 (sdM1:, $\zeta = 0.775$ – HD 184489). Some authors have reported features of low metallicity (e.g., Maldonado et al. 2010), but none had classified it as a subdwarf (but see Sandage & Kowal 1986). Its low effective temperature has prevented spectral synthesis analyses on high-resolution spectra.

The other new subdwarf candidate is J16354–039 (sdM0:, $\zeta = 0.664$ – HD 149414 B, BD–03 3968B). Giclas et al. (1959)

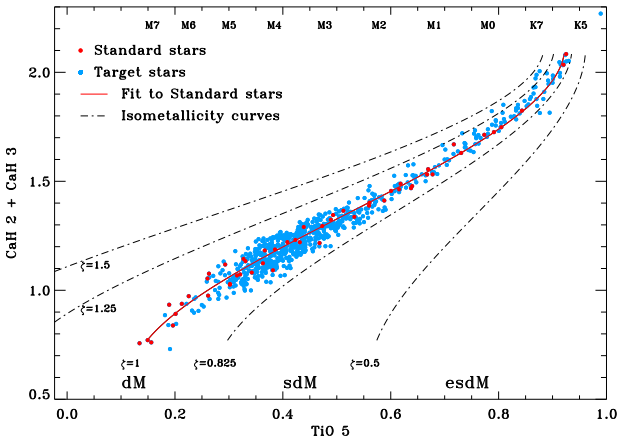

Fig. 7. CaH 2 + CaH 3 vs. TIO 5 index-index diagram of our CAFOS stars, after discarding giants. The spectral types at the top are indicative, but follow the TiO 5 fit given in Table 5. The solid and dash-dotted lines are iso-metallicity curves of the ζ index.

discovered it and associated it with the G5 Ve single-line spectroscopic binary HD 149414 Aa,Ab. Afterwards, its membership in the very wide system has been investigated by Poveda et al. (1994), Tokovinin (2008), and Dhital et al. (2010), for example, and confirmed and quantified by Caballero (2009). The projected physical separation between Aa,Ab and B amounts to 53 000 au (about a quarter of a parsec). Remarkably, the primary is a halo binary of low metallicity ([Fe/H] ~ –1.4 – Strom & Strom 1967; Sandage 1969; Cayrel de Strobel et al. 1997; Holmberg et al. 2009). This explains the low ζ metallicity index of J16354–039 for its spectral type and the wide separation of the system (due to gravitational disruption by the Galactic gravitational potential or to common origin and ejection from the same cluster; cf. Caballero 2009, and references therein).

In addition, J12025+084 (M1.5 V; ζ = 0.898 – LHS 320) was classified by Gizis (1997) as an sdM2.0 star and was investigated extensively afterwards with high-resolution imagers (Gizis & Reid 2000; Riaz et al. 2008; Jao et al 2009; Lodieu et al. 2009). However, we failed to detect any subdwarf signpost in our high signal-to-noise spectrum, which is partly consistent with the metallicity [Fe/H] = −0.6±0.3 measured by Rajpurohit et al. (2014).

No CAFOS star showed a very high metallicity index greater than ζ = 1.5. In spite of the dispersion of the ζ index around unity, we considered that all our 726 dwarfs (753 stars in total minus the 25 giants and the two subdwarfs) *approximately* have solar metallicity ([Fe/H] ≈ 0.0). This assumption is relevant for instance to derive the mass from absolute magnitudes, the spectral types, and theoretical models that need metallicity as an input.

4.4. Activity

Chromospheric activity is one of the main relevant parameters for exoplanet detection around M dwarfs. The heterogeneities on the stellar surface of the almost-fully convective, rotating, M dwarfs, such as dark spots, may induce spurious radial-velocity variations at visible wavelengths

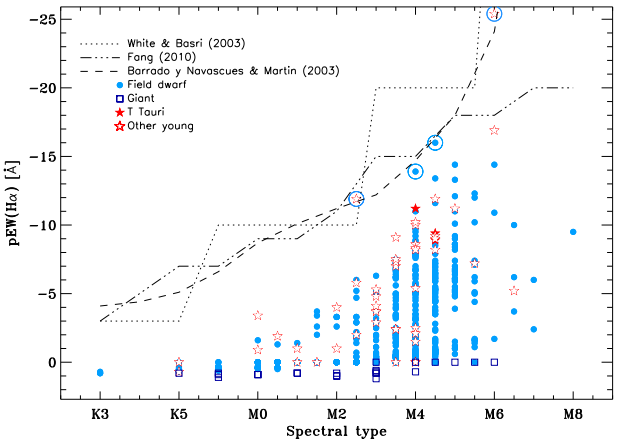

Fig. 8. Pseudo-equivalent width of Hα line vs. spectral type diagram. Measurement errors are 0.5 subtypes for the spectral type and are of the order of 10% with a minimum of 0.1 Å for pEW(Hα) (but scatter due to variability is probably larger than 10%). Dotted, dash-dotted, and dashed lines indicate the boundaries between chromospheric and accretion emission for different authors. Giants, plotted with open squares, have filled Hα lines or in absorption. None of the young stars, plotted with open and filled stars, show accretion emission. The four stars at the accretion boundary discussed in the text are encircled.

(Bonfils et al. 2007; Reiners et al. 2010; Barnes et al. 2011; Andersen & Korhonen 2015; Robertson et al. 2015). Near-infrared observations are expected to improve the precision of radial-velocity measurements with respect to the visible for stars cooler than M3, and CARMENES will cover the wavelength range from 0.55 to 1.70 μm. In spite of this, we plan to identify the least active stars for our exoplanet search. Moreover, several authors have identified significant differences between colours and spectral indices of active and inactive stars of similar properties that may affect the spectral typing of M dwarfs (Stauffer & Hartmann 1986; Hawley et al. 1996; Bochanski et al. 2007; Morales et al. 2008).

4.4.1. Hα emission

The Hα index (Reid et al. 1995) was one of the 31 indices measured on our CAFOS spectra (Table 4). For a better reliability on the activity determination and comparison with other works, we also measured the pseudo-equivalent width of the Hα line, pEW(Hα), of all the CAFOS stars (Table A.2). We here used pEW(Hα) as the proxy for activity (we used the pseudo-equivalent width of the line measured with respect to a local pseudo-continuum instead of the equivalent width because in M – and L, T, and Y – dwarfs the spectral continuum is not observable – e.g. Tsuji & Nakajima 2014).

We plot in Fig. 8 the pEW(Hα) vs. spectral type diagram for the whole sample. M dwarfs with late spectral types tend to show the Hα line in (strong) emission more often than earlier stars (see e.g. Hawley et al. 1996; West et al. 2004; or Reiners et al. 2013). There is a significant number of M4.0 V stars and later, however, that show very low Hα emission below 5 Å (in absolute values).

A few stars stand out in the pEW(Hα) vs. spectral type diagram in Fig. 8. Four of them lie at the boundary between chromospheric and accretion emission, as defined by Barrado y Navascués & Martín (2003), White & Basri (2003), and Fang (2010). Their high activity led us to investigate them in detail.

- J04290+186 (M2.5 V, pEW(Hα) = $-11.9^{+0.5}_{-0.3}$ Å, V1103 Tau). It is a member of the 600 Ma-old Hyades cluster (Johnson et al. 1962; Griffin et al. 1988; Stauffer et al. 1991; Reid 1992).
- J04544+650 (M4.0 V, pEW(Hα) = $-13.9^{+0.8}_{-0.5}$ Å, 1RXS J045430.9+650451). It is an anonymous Tycho-2 star (TYC 4087–1172–1; Lépine & Gaidos 2011) that we cross-matched with an aperiodic, variable, X-ray source identified by Fuhrmeister & Schmitt (2003). This X-ray variability and the presence of He I λ5875.6 Å in emission indicates that J04544+650 was flaring during our observations.
- J01567+305 (M4.5 V, pEW(Hα) = –16.0 ± 0.4 Å, NLTT 6496, Koenigstuhl 4 A). It forms a loosely bound common-proper-motion pair together with the M6.5: V star NLTT 6491 (Koenigstuhl 4 B), and is associated with an X-ray source (Caballero 2012). Interestingly, Aberasturi et al. (2014) collected low-resolution spectroscopy for J01567+305 just two months earlier, for which they determined a spectral type identical to ours within the uncertainties, but measured pEW(Hα) = –9.3 ± 0.3 Å, which is significantly lower than our measurement. Our CAFOS spectrum also shows He I in emission, so the mid-M dwarf likely underwent a flare during our observations.
- J07523+162 (M6.0 V, pEW(Hα) = $-25.4^{+1.4}_{-1.0}$ Å, LP 423–031). It has also been classified as a single M7 Ve star from optical spectra (Cruz et al. 2003; Reid et al. 2003; Gatewood & Coban 2009; Reiners & Basri 2009), but as an M6 V with surface gravity consistent with normal field dwarfs from near-infrared spectra (Allers & Liu 2013). From high-resolution spectroscopy (pEW(Hα) = –22.3 Å) and *ROSAT* X-ray count rates, Shkolnik et al. (2009) assigned J07523+162 an age of about 100 Ma, younger than the Pleiades. However, Reiners & Basri (2010) observed flaring activity in a J07523+162 spectrum (pEW(Hα) = –44.4 Å) and Gagné et al. (2014) and Klutsch et al. (2014) were not able to determine membership in any known stellar kinematic group.

There is an additional fifth active dwarf that stands out among the remaining stars in Fig. 8. It is J03332+462 (M0.0 V, pEW(Hα) = $-3.4^{+0.5}_{-0.3}$ Å, V577 Per B), a confirmed member of the ∼70 Ma-old AB Doradus moving group (Zuckerman et al. 2004; da Silva et al. 2009; Schlieder et al. 2012a). Its relatively bright primary at about 9 arcsec is a young K2 V star with strong ultraviolet and X-ray emission and lithium in absorption (Pounds et al. 1993; Jeffries 1995; Montes et al. 2001; Zuckerman & Song 2004; Xing & Xing 2012).

4.4.2. Young (and very young) stars

The identification of one open cluster member, one moving group member, and one purported young star in the field among five M dwarfs led us to examine the bibliography for other young star candidates in our CAFOS sample. The result of this bibliographic search is summarised in Table 7. In total, 49 spectroscopically investigated stars in this work have been reported to belong to the Taurus-Auriga star-forming region (∼1–10 Ma, three stars), β Pictoris moving group (∼12–22 Ma, five stars), Carina or Columba associations (∼15–50 Ma, two stars), Argus

Table 7. Reported young stars in our sample.

Karmn	Moving group/ association/cluster/ star-forming region	Ref.
J03332+462	AB Dor MG	See text
J03466+243 AB	Pleiades	vMa45
J03473–019	AB Dor MG	Zuc04
J03548+163 AB	Hyades	Gic62
J04123+162 AB	Hyades	Gic62
J04177+136 AB	Hyades	Gic62
J04206+272	Taurus	Sce07
J04207+152 AB	Hyades	Gic62
J04227+205	Hyades	Reid93
J04238+149 AB	Hyades	Gic62
J04238+092 AB	Hyades	Gic62
J04252+172 ABC	Hyades	Gic62
J04290+186	Hyades	Gic62
J04313+241 AB	Taurus	HR72
J04360+188	Hyades	Pels75
J04366+186	Hyades	See text
J04373+193	Hyades	Reid93
J04393+335	Taurus	Wic96
J04425+204 AB	Hyades	Reid93
J04430+187 AB	Hyades	Gic62
J05019+011	β Pic MG	Sch12
J05062+046	β Pic MG	Sch12
J05256–091 AB	AB Dor MG	Shk12
J05320–030	β Pic MG	daS09
J05415+534	Her-Lyr MG?	Eis13
J05457–223	UMa MG	Tab15
J06075+472	AB Dor MG	Sch12
J06246+234	Young	Mon01
J07319+362N	Castor MG	Cab10
J07319+362S AB	Castor MG	Cab10
J07361–031	Castor MG	Cab10
J07523+162	Young	See text
J08298+267	Castor MG	Cab10
J09328+269	Her-Lyr MG	Eis13
J09362+375	Young	Malo14
J10196+198 AB	Castor MG	Cab10
J10359+288	β Pic MG	Sch12
J10508+068	Her-Lyr MG?	Eis13
J11046–042S AB	Her-Lyr MG	Eis13
J13143+133 AB	Young	Sch14
J15079+762	IC 2391 MG	Mon01
J17198+265	Hyades SC	Klu14
J17199+265	Hyades SC	Klu14
J18313+649	AB Dor	Sch12
J21376+016	β Pic MG	Sch12
J22160+546	Her-Lyr MG?	Eis13
J22234+324 AB	AB Dor MG	Malo14
J23194+790	Carina/Columba Ass.	Klu
J23209–017 AB	Argus Ass.	Malo14
J23228+787	Carina/Columba Ass.	Klu

References. vMa45: van Maanen (1945); Gic62: Giclas et al. (1962); HR72: Herbig & Rao (1972); Pels75: Pels et al. (1975); Reid93: Reid (1993); Wic96: Wichmann et al. (1996); Mon01: Montes et al. (2001); Zuc04: Zuckerman et al. (2004); Sce07: Scelsi et al. (2007); daS09: da Silva et al. (2009); Cab10: Caballero (2010); Sch12: Schlieder et al. (2012a); Shk12: Shkolnik et al. (2012); Eis13: Eisenbeiss et al. (2013); Klu14: Klutsch et al. (2014); Malo14: Malo et al. (2014); Sch14: Schlieder et al. (2014); Tab15: Tabernero et al. (2015); Klu: Klutsch, priv. comm. Part of the content of this table was extracted from Hidalgo (2014).

association (~40 Ma, one star), AB Doradus moving group (~70−120 Ma, five stars), Pleiades cluster (~120 Ma, one star − with a relatively early K5 V spectral type), IC 2391 supercluster (~100−200 Ma, one star), Hercules-Lyra moving group (~200−300 Ma, four stars − note the question marks), Castor moving group (~200−300 Ma, six stars), Ursa Major moving group (~300−500 Ma, one star), and Hyades cluster and supercluster (~600 Ma, 14 and 2 stars, respectively), and four to the young ($\tau \lesssim 600$ Ma) field star population in the solar neighbourhood. See Zuckerman & Song (2004) and Torres et al. (2008) for reviews on young moving groups.

The actual existence of some of the entities above (e.g., Hercules-Lyra and Castor moving groups, and IC 2391 and Hyades superclusters) is questioned by several authors. Three of the five stars with the lowest Hα emission for their spectral type belong to the hypothetical Castor moving group (Barrado y Navascués 1998; Montes et al. 2001; Ribas 2003; Caballero 2010; Mamajek 2013; Zuckerman et al. 2013), and the other two to the Hyades (super-) cluster (van Altena 1966; Hanson 1975; Legget & Hawkins 1988; Hawley et al. 1996; Stauffer et al. 1997; Montes et al. 2001; Klutsch et al. 2014). However, the extreme youth of some targets is confirmed by detection of lithium in absorption, X-ray in emission, and common proper-motion to bona fide primaries in nearby young moving groups.

Eleven of the 16 Hyads are known to be binaries. The relatively large number and (apparent) high binary frequency is a natural consequence of the Malmquist bias, which leads to the preferential detection of intrinsically bright objects. Equal-mass binaries are brighter than single stars of the same spectral type (by up to 0.75 mag) and, thus, the frequency of binarity in our magnitude-limited sample is higher than in a bias-free, volume-limited sample. While most of our targets lie at 20−30 pc (Cortés-Contreras et al. 2015), the overbrightness of binary Hyads makes them to look as if they were located roughly at 30 pc instead at the nominal distance of the Hyades at about 46 pc. We suggest to investigate the actual multiplicity status of the five remaining *single* M dwarfs with a mid-resolution spectroscopic monitoring.

At $d \sim 140$ pc, the three Taurus stars in Table 7 are *not* in the solar neighbourhood. Since they are still on the Hayashi track of contraction, their radii are larger than those of dwarfs of the same effective temperature. As a result, they are also much more luminous, which explains why we were able to observe them even though they are located an order of magnitude farther away than the rest of our dwarf targets. As expected from their extreme youth, the three T Tauri stars have Hα emissions in the highest quartile (pEW(Hα)s between –9 and –11 Å, and spectral types between M4.0 and M4.5) and have been investigated spectroscopically earlier (Herbig & Rao 1972; Mathieu 1994; Wichmann et al. 1996; Kenyon et al. 1998; Scelsi et al. 2008; Sestito et al. 2008). The three of them displayed not only Hα in emission, but also Hβ and Hγ (we used one of them, J04393+335, in Fig. 3 to illustrate best the discarded wavelength ranges that are contaminated by activity in Sect. 3.2.2).

A large radius also translates into low gravity. Indeed, the brightest of the trio of T Tauri stars, J04313+241 AB (V927 Tau AB, $J = 9.73$ mag) was the only non-giant target with spectral index Ratio C < 1.07 (Fig. 6) and the only one to which we did not assign a luminosity class in Table A.3. Its optical spectrum is intermediate between those of giants and dwarfs of the same spectral type (M4.0:). Something similar is true for the other two T Tauri stars, which also have very low Ratio C indices for their spectral type (but all giant stars in our sample display

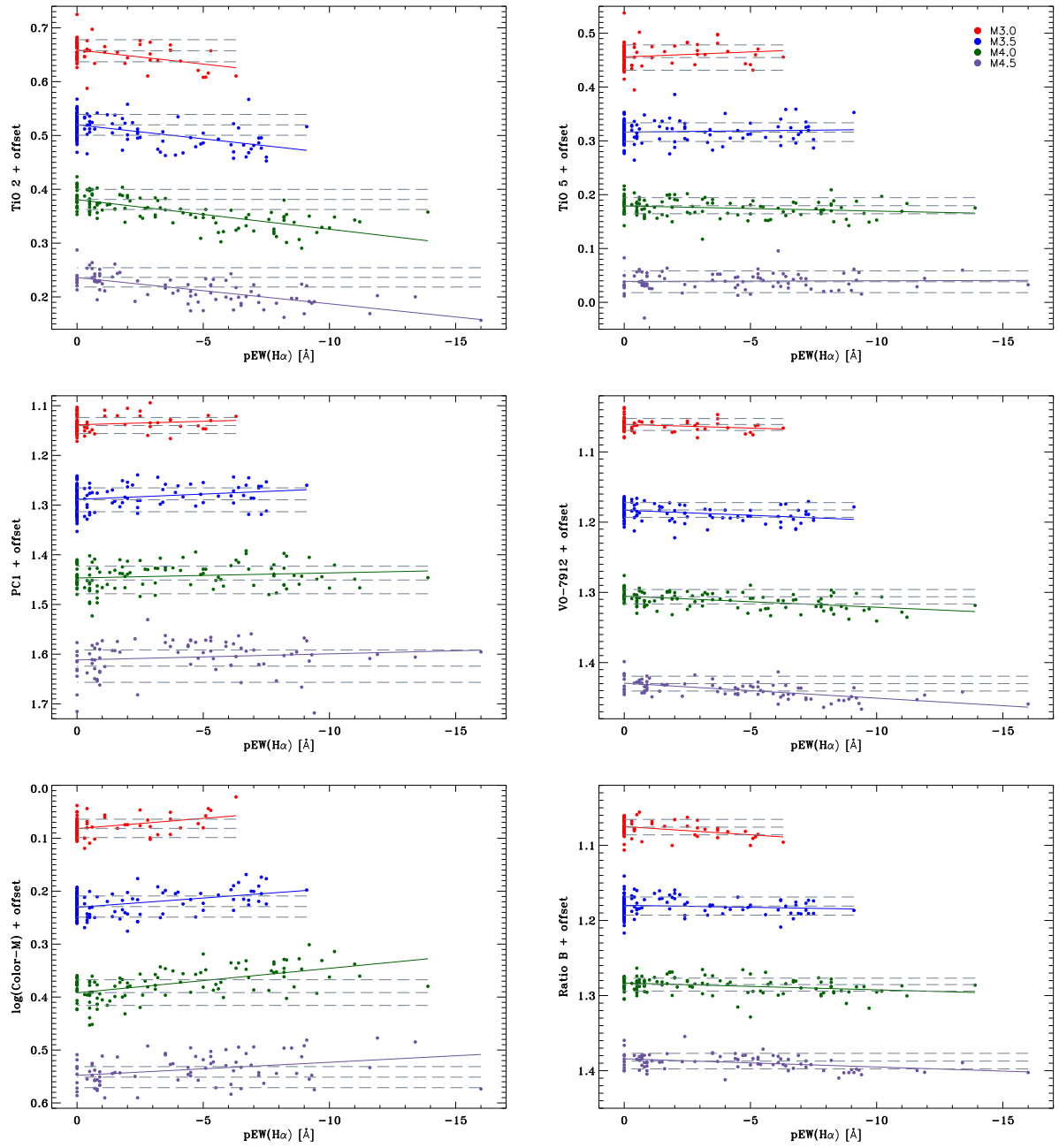

Fig. 9. Spectral-typing indices TiO 2, TiO 5 (*top*), PC1, VO-7912 (*middle*), Color-M, and Ratio B (*bottom*) as a function of Hα pseudo-equivalent width for spectral types M3.0 V, M3.5 V, M4.0 V, and M4.5 V, from top to bottom. For clarity, the indices are offset in steps of 0.1 in the vertical axis. Solid lines are linear fits of the indices as a function of $pEW(\alpha)$. Dashed lines indicate the mean and $\pm 1\sigma$ index at quiescence ($pEW(\alpha) > -1$ Å).

Hα in absorption). Although T Tauri stars are not natural targets for radial-velocity searches of low-mass exoplanets and none of the trio satisfies our criteria to be considered in the CARMENES sample (Table 1), a monitoring of bright, young, M dwarfs could shed light on the process of exoplanet formation (e.g., Crockett et al. 2012). Furthermore, young, nearby, very late stars are also ideal targets for direct-imaging surveys for Jupiter-like planetary companions at wide separations (Masciadri et al. 2005; Daemgen et al. 2007; Chauvin et al. 2010; Biller et al. 2013; Delorme et al. 2013, and references therein). Some of these targets are J13143+733 AB (NLTT 33370, M6.0 V in AB Doradus) and J09328+269 (DX Leo B, M5.5 V in Hercules-Lyra).

4.4.3. Effect of activity on spectral typing

As pointed out above, chromospheric activity could affect spectral typing. To study the validity of our results, we plot in Fig. 9 four of the five indices that we used for spectral typing as a function of $pEW(\mathrm{H}\alpha)$. We investigated the four spectral type intervals with the largest number of stars (in parenthesis): M3.0 V (72), M3.5 V (134), M4.0 V (113), and M4.5 V (84). Grouping by spectral type minimised the natural variation of the spectral index with effective temperature. The effect of activity on the TiO 5 and PC1 indices is not significant. However, strong activity in the largest quartile of $pEW(\mathrm{H}\alpha)$ has an appreciable effect on the indices VO-7912 and Color-M, but they fortuitously compensate each other because of the opposite slopes in their index vs. $pEW(\mathrm{H}\alpha)$ relations. The effect of activity on the TiO 2 index is more appreciable in the top left panel of Fig. 9, which agrees with the results shown by Hawley et al. (1996), who found that active M dwarfs tended to have lower values of TiO 2 (more absorption) than inactive dwarfs with the same TiO 5 indices (spectral types). However, this level of activity translates into a variation in spectral type of less than 0.8 subtypes for the most active stars, after using the coefficients in Table 5. In the end, the counter-weighting combination of five spectral indices and, especially, the use of the χ^2 and best-match methods guarantee that our adopted spectral types are free from the effect of chromospheric activity (for the investigated interval of $pEW(\mathrm{H}\alpha)$).

Our results on quantifying the variation of some spectral types as a function of activity are seemingly in contrast to some previous works, such as Morales et al. (2008). However, a direct comparison should be avoided because they grouped the stars by absolute magnitude, for which a determination of the distance is needed. A specific work on activity in M dwarfs will be another item of this series of papers on the science preparation of the CARMENES sample. It will be supported on one hand by new measurements of the emission of Hα, Hβ, and the Ca II H & K doublet and near-infrared triplet from high-resolution spectra and on the other hand by a comprehensive parallax distance compilation and accurate spectro-photometric distance determination.

5. Summary

CARMENES, the new spectrograph at the 3.5 m Calar Alto telescope, will spectroscopically monitor a sample of M dwarfs to detect exoplanets with the radial-velocity method. We are selecting the best planet host star candidates. For that, we are compiling a comprehensive list of dwarf stars coming from existing spectroscopic and photometric catalogues, as well as from late-type star studies. Currently, we are gathering all available information and determine fundamental properties from observations for approximately 2200 targets. Here we presented the first paper of a series that explains in detail the characterisation of our sample of targets for the CARMENES survey. This paper detailed optical low-resolution spectroscopy.

One of the key stellar astrophysical parameters that we need for each target is its spectral type. From the spectral type we estimate the stellar mass and infer planet detectability thresholds, and we ensure that we collate an even sampling of early-, mid-, and late-M dwarfs. Here, we undertook low-resolution spectroscopic observations of 753 targets with the CAFOS spectrograph on the 2.2 m Calar Alto telescope. This CAFOS sample contained M-dwarf candidates with poorly constrained spectral types, cool stars in multiple systems, and numerous comparison and standard stars. We classified our targets using both least-squares fitting techniques and 31 spectral indices, of which we chose five indices with small dispersion to empirically calibrate spectral types (TiO 2, TiO 5, PC1, VO-7912 and Color-M).

Additionally, we investigated the relation of spectral indices with surface gravity. We classified 25 of the observed targets as giant stars using the CaH series of related spectral indices, which are useful indicators to segregate giant stars from dwarfs. Metallicity was estimated through the ζ parameters (Lépine et al. 2007). We concluded that all our field dwarf stars except two new subdwarf candidates have solar metallicity. We identified 49 late-type stars as young dwarfs in star-forming regions or moving groups already reported in the bibliography.

Finally, we also computed stellar activity indicators. Stellar activity is a fundamental property for the CARMENES survey because activity features, such as photospheric spots, can mimic the signature of exoplanets or increase the stellar intrinsic jitter that can mask real exoplanet signals. We computed the pseudo-equivalent width of the Hα line of each target as an activity indicator, and analysed the effect of activity on spectral typing through indices. Although we have identified significant trends for some indices, the spectral type variation due to stellar activity is below one subtype level.

In summary, from the 753 targets that we observed with CAFOS, we obtained for the first time spectral types for 305 stars and improved it for 448 stars. We estimated gravity, metallicity, and activity indices for all targets. We identified 683 M dwarfs, of which 520 fulfill the CARMENES requirements and, therefore, will be included in the list of input targets. A more detailed investigation of these targets with high-resolution spectroscopic and imaging observations to select the best candidates for the CARMENES survey will produce the largest compilation of fully characterised M-type stars.

Acknowledgements. CARMENES is funded by the German Max-Planck-Gesellschaft (MPG), the Spanish Consejo Superior de Investigaciones Científicas (CSIC), the European Union through European Regional Fund (FEDER/ERF), the Spanish Ministry of Economy and Competitiveness, the state of Baden-Württemberg, the German Science Foundation (DFG), and the Junta de Andalucía, with additional contributions by the members of the CARMENES Consortium (Max-Planck-Institut für Astronomie, Instituto de Astrofísica de Andalucía, Landessternwarte Königstuhl, Institut de Ciències de l'Espai, Institut für Astrophysik Göttingen, Universidad Complutense de Madrid, Thüringer Landessternwarte Tautenburg, Instituto de Astrofísica de Canarias, Hamburger Sternwarte, Centro de Astrobiología, and the Centro Astronómico Hispano-Alemán). Financial support was also provided by the Universidad Complutense de Madrid, the Comunidad Autónoma de Madrid, the Spanish Ministerios de Ciencia e Innovación and of Economía y Competitividad, and the Fondo Europeo de Desarrollo Regional (FEDER/ERF) under grants AP2009-0187, SP2009/ESP-1496, AYA2011-30147-C03-01, -02, and -03, AYA2012-39612-C03-01, and ESP2013-48391-C4-1-R. Based on observations collected at the Centro Astronómico Hispano Alemán (CAHA) at Calar Alto, operated jointly by the Max–Planck Institut für Astronomie and the Instituto de Astrofísica de Andalucía. This research made use of the SIMBAD, operated at Centre de Données astronomiques de Strasbourg, France, the NASA's Astrophysics Data System, the RECONS project database (`http://www.recons.org`), the M, L, T, and Y dwarf compendium housed at `http://dwarfarchives.org` maintained by C. Gelino, J. D. Kirkpatrick and A. Burgasser, and the Washington Double Star Catalog maintained at the US Naval Observatory. We thank S. Lépine and E. Gaidos for sharing unpublished data with us, J. I. González-Hernández, E. W. Guenther, A. Hatzes, and M. R. Zapatero Osorio of the CARMENES Consortium for helpful comments, and the anonymous referee for the quick and encouraging report.

A&A 577, A128 (2015)

Appendix A: Long tables

Table A.1. Observed stars: identification, common name, Gliese number, 2MASS coordinates and J magnitude, observing date, and exposure time.

No.	Karmn	Name	Gl/GJ	α (J2000)	δ (J2000)	J [mag]	Observation date	$N \times t_{exp}$ [s]
1	J00066–070 AB	2MASS J00063925–0705354	...	00:06:39.20	–07:05:35.3	9.83	04 Aug. 2012	1×1000
2	J00077+603 AB	G 217–032	...	00:07:42.60	+60:22:54.3	8.91	24 Sep. 2012	1×600
3	J00115+591	LSR J0011+5908	...	00:11:31.82	+59:08:40.0	9.95	11 Jan. 2012	2×700
4	J00118+229	LP 348–40	...	00:11:53.03	+22:59:04.7	8.86	07 Dec. 2011	1×250
5	J00119+330	G 130–053	...	00:11:56.54	+33:03:17.8	9.07	07 Dec. 2011	1×220
6	J00122+304	1RXS J001213.6+302906	...	00:12:13.41	+30:28:44.3	10.24	12 Nov. 2011	1×600
7	J00133+275	[ACM2014] J0013+2733	...	00:13:19.52	+27:33:31.1	10.43	12 Nov. 2011	1×900
8	J00136+806	G 242–048	3014 A	00:13:38.71	+80:39:56.8	7.76	01 Sep. 2012	1×300
9	J00146+202	χ Peg	...	00:14:36.16	+20:12:24.1	1.76	11 Jan. 2012	1×1
10	J00152+530	G 217–040	...	00:15:14.53	+53:04:45.7	10.82	14 Feb. 2013	1×800

Notes. The full table is available at the CDS.

Table A.2. Seven representative spectral indices, ζ metallicity index, and Hα pseudo-equivalent width.

Karmn	PC1	TiO 2	TiO 5	VO-7912	Color-M	CaH 2	CaH 3	ζ	pEW(Hα) [Å]
J00066–070 AB	1.269	0.492	0.317	1.148	1.778	0.404	0.654	0.973	$-2.3^{+0.3}_{-0.5}$
J00077+603 AB	1.198	0.532	0.369	1.111	1.405	0.408	0.631	0.883	$-6.7^{+0.3}_{-0.4}$
J00115+591	1.511	0.378	0.202	1.222	2.902	0.281	0.564	0.970	$-1.6^{+0.2}_{-0.4}$
J00118+229	1.215	0.606	0.405	1.090	1.404	0.492	0.751	1.052	$-0.5^{+0.2}_{-0.2}$
J00119+330	1.167	0.634	0.427	1.072	1.293	0.503	0.748	1.023	$-0.3^{+0.1}_{-0.2}$
J00122+304	1.296	0.497	0.354	1.154	1.755	0.427	0.685	0.972	$-8.7^{+0.4}_{-0.5}$
J00133+275	1.296	0.512	0.339	1.144	1.805	0.425	0.686	0.994	$-4.0^{+0.2}_{-0.4}$
J00136+806	1.027	0.770	0.601	1.012	0.901	0.644	0.812	1.002	$+0.0^{+0.2}_{-0.2}$
J00146+202	0.955	0.729	0.520	1.005	0.643	0.839	0.946	2.754	$+0.8^{+0.1}_{-0.1}$
J00152+530	1.090	0.728	0.540	1.031	1.076	0.575	0.787	0.975	$+0.0^{+0.2}_{-0.2}$

Notes. The full table is available at the CDS.

Table A.3. Spectral types of observed stars.

Karmn	Sp. type biblio.	Ref.	Sp. type Best-fit	χ^2	Sp. type TiO2	TiO5	PC1	VO-7912	Color-M	Sp. type adopted
J00066–070 AB	M3.5 V+m4.5:	Reid07, Jan12	4.5	4.5	4.5	4.5	4.0	4.5	4.5	M4.5 V
J00077+603 AB	M4.5 V	Lep13	4.0	4.0	4.5	4.0	3.5	4.0	3.5	M4.0 V
J00115+591	M5.5 V	Lep03	6.0	6.0	5.5	6.0	5.5	5.5	5.5	M5.5 V
J00118+229	M3.5 V	Reid04	3.5	3.5	3.5	3.5	4.0	4.0	3.5	M3.5 V
J00119+330	M3.5 V	Giz97	3.5	3.0	3.5	3.5	3.5	3.5	3.5	M3.5 V
J00122+304	M5.0 V	Abe14	4.5	4.5	4.5	4.0	4.5	5.0	4.5	M4.5 V
J00133+275	M4.5 V	Abe14	4.5	4.5	4.5	4.5	4.5	4.5	4.5	M4.5 V
J00136+806	M1.5 V	PMSU	1.5	1.5	1.5	1.5	1.5	1.5	1.5	M1.5 V
J00146+202	M2 III	Gar89, Kir91	...	...	...	...	...	...	...	M III
J00152+530	M2.2 V	Mann13	2.5	2.0	2.5	2.0	2.5	2.0	2.5	M2.5 V

Notes. The full table is available at the CDS.

References. PMSU: Palomar/Michigan State University survey (see text); Simbad: spectral type as reported by Simbad; MP50: Moore & Paddock (1950); Vys56: Vyssotsky (1956); JM53: Johnson & Morgan (1953); Lee84: Lee (1984); Bid85: Bidelman (1985); Ste86: Stephenson (1986); SP88: Sanduleak & Pesch (1988); Gar89: García (1989); KMc89: Keenan & McNeil et al. (1989); Kir91: Kirkpatrick et al. (1991); Kri93: Krisciunas et al. (1993); Hen94: Henry et al. (1994); Jac94: Jacoby et al. (1994); Mar94: Martín et al. (1994); Giz97: Gizis (1997); GR97: Gizis & Reid (1997); Mot97: Motch et al. (1997); App98: Appenzeller et al. (1998); Gig98: Gigoyan et al. (1998); Mot98: Motch et al. (1998); Cut00: Cutispoto et al. (2000); Giz00: Gizis et al. (2000a); Li00: Li et al. (2000); CrRe02: Cruz & Reid (2002); Gray03: Gray et al. (2003); Lep03: Lépine et al. (2003); Reid03: Reid et al. (2003); Tee03: Teegarden et al. (2003); Reid04: Reid et al. (2004); Boc05: Bochanski et al. (2005); Scho05: Scholz et al. (2005); Gray06: Gray et al. (2006); Mon06: Montagnier et al. (2006); Riaz06: Riaz et al. (2006); SB06: Sánchez-Blázquez et al. (2006); Dae07: Daemgen et al. (2007); Eis07: Eisenbeiss et al. (2007); Reid07: Reid et al. (2007); BS08: Bender & Simon (2008); Jah08: Jahreiß et al. (2008); Law08: Law et al. (2008); LC08: López-Corredoira et al. (2008); Sce08: Scelsi et al. (2008); Cab09: Caballero (2009); Shk09: Shkolnik et al. (2009); Cab10: Caballero et al. (2010); Shk10: Shkolnik et al. (2010); LG11: Lépine & Gaidos (2011); Jan12: Janson et al. (2012); JE12: Jiménez-Esteban et al. (2012); RA12: Rojas-Ayala et al. (2012); Fri13: Frith et al. (2013); Lep13: Lépine et al. (2013); Mann13: Mann et al. (2013); Abe14: Aberasturi et al. (2014); Lam14: Lamert (2014); New14: Newton et al. (2014); RS14: Reyes-Sánchez (2014).

References

Aberasturi, M., Caballero, J. A., Montesinos, B., et al. 2014, AJ, 148, 36
Adibekyan, V. Zh., Sousa, S. G., Santos, N. C., et al. 2012, A&A, 545, A32
Allard, F., Homeier, D., & Freytag, B. 2011, ASP Conf. Ser., 448, 91
Allers, K. N., & Liu, M. C. 2013, ApJ, 772, 79
Alonso-Floriano, F. J., Caballero, J. A., & Montes, D. 2013a, Highlights of Spanish Astrophysics VII, 431
Alonso-Floriano, F. J., Montes, D., Jeffers, S. V., et al. 2013b, Protostars and Planets VI, 021
Amado, P. J., Quirrenbach, A., Caballero, J. A., et al. 2013, Highlights of Spanish Astrophysics VII, 842
Andersen, J. M., & Korhonen, H. 2015, MNRAS, 448, 3053
Appenzeller, I., Thiering, I., Zickgraf, F.-J., et al. 1998, ApJS, 117, 319
Artigau, É., Kouach, D., Donati, J.-F., et al. 2014, Proc. SPIE, 9147, E15
Avenhaus, H., Schmidt, H. M., & Meyer, M. R. 2012, A&A, 548, A105
Baraffe, I., Chabrier, G., Allard, F., & Hauschildt, P. H. 1998, A&A, 337, 403
Barnes, J. R., Jeffers, S. V., & Jones, H. R. A. 2011, MNRAS, 412, 1599
Barrado y Navascués, D. 1998, A&A, 339, 831
Barrado y Navascués, D., & Martín, E. L.2003, AJ, 126, 2997
Bean, J. L., Sneden, C., Hauschildt, P. H., Johns-Krull, C. M., & Benedict, G. F. 2006, ApJ, 652, 1604
Bean, J. L., Seifahrt, A., Hartman, H., et al. 2010, ApJ, 713, 410
Béjar, V. J. S., Gauza, B., Caballero, J. A., et al. 2012, 17th Cambridge Workshop on Cools Stars, Stellar Systems and the Sun, published on-line at http://www.coolstars17.net
Bender, C. F., & Simon, M. 2008, ApJ, 689, 416
Bensby, T., Feltzing, S., & Oey, M. S. 2014, A&A, 562, A71
Bergfors, C., Brandner, W., Janson, M., et al. 2010, A&A, 520, A54
Bidelman, W. P. 1985, ApJS, 59, 197
Biller, B. A., Liu, M. C., Wahhaj, Z., et al. 2013, ApJ, 777, 160
Bochanski, J. J., Hawley, S. L., Reid, I. N., et al. 2005, AJ, 130, 1871
Bochanski, J. J., West, A. A., Hawley, S. L., & Covey, K. R. 2007, AJ, 133, 531
Bonfils, X., Delfosse, X., Udry, S., et al. 2005, A&A, 442, 635
Bonfils, X., Mayor, M., Delfosse, X., et al. 2007, A&A, 474, 293
Bonfils, X., Delfosse, X.l, Udry, S., et al. 2013, A&A, 549, A109
Boyd, M. R., Winters, J. G., Henry, T. J., et al. 2011, AJ, 142, 10
Caballero, J. A. 2007, ApJ, 667, 520
Caballero, J. A. 2009, A&A, 507, 251
Caballero, J. A. 2010, A&A, 514, A98
Caballero, J. A. 2012, The Observatory, 132, 1
Caballero, J. A., Montes, D., Klutsch, A., et al. 2010, A&A, 520, A91
Caballero, J. A., Cortés-Contreras, M., López-Santiago, J., et al. 2013, Highlights of Spanish Astrophysics VII, 645
Casagrande, L., Flynn, C., & Bessell, M. 2008, MNRAS, 389, 585
Cayrel de Strobel, G., Soubiran, C., Friel, E. D., Ralite, N., & Francois, P. 1997, A&AS, 124, 299
Chabrier, G., Baraffe, I., Allard, F., & Hauschildt, P. 2000, ApJ, 542, 464
Chauvin, G., Lagrange, A.-M., Bonavita, M., et al. 2010, A&A, 509, A52
Cortés-Contreras, M., Caballero, J. A., Alonso-Floriano, F. J., et al. 2013, Highlights of Spanish Astrophysics VII, 646
Cortés-Contreras, M., Caballero, J. A., & Montes, D. 2014, The Observatory, 134, 348
Cortés-Contreras, M., Béjar, V. J. S., Caballero, J. A., et al. 2015, 18th Cambridge Workshop on Cools Stars, Stellar Systems and the Sun, in press
Crifo, F., Phan-Bao, N., Delfosse, X., et al. 2005, A&A, 441, 653
Crockett, C. J., Mahmud, N. I., Prato, L., et al. 2012, ApJ, 761, 164
Crossfield, I. J. M. 2014, A&A, 566, A130
Cruz, K. L., & Reid, I. N. 2002, AJ, 123, 2828
Cruz, K. L., Reid, I. N., Liebert, J., Kirkpatrick, J. D., & Lowrance, P. J. 2003, AJ, 126, 2421
Cruz, K. L., Reid, I. N., Kirkpatrick, J. D., et al. 2007, AJ, 133, 439
Cutispoto, G., Pastori, L., Guerrero, A., et al. 2000, A&A, 364, 205
Daemgen, S., Siegler, N., Reid, I. N., & Close, L. M. 2007, ApJ, 654, 558
da Silva, L., Torres, C. A. O., de La Reza, R., et al. 2009, A&A, 508, 833
Deacon, N. R., Liu, M. C., Magnier, E. A., et al. 2012, ApJ, 757, 100
Delfosse, X., Forveille, T., Beuzit, J.-L., et al. 1999, A&A, 344, 897
Delorme, P., Gagné, J., Girard, J. H., et al. 2013, A&A, 553, L5
Dhital, S., West, A. A., Stassun, K. G., & Bochanski, J. J. 2010, AJ, 139, 2566
Dhital, S., West, A. A., Stassun, K. G., et al. 2012, AJ, 143, 67
Dieterich, S. B., Henry, T. J., Jao, W.-C., et al. 2014, AJ, 147, 94
Dressing, C. D., & Charbonneau, D. 2013, ApJ, 767, 95
Dressing, C. D., & Charbonneau, D. 2015, ApJ, submitted [arXiv:1501.01623]
Ehrenreich, D., Lagrange, A.-M., Montagnier, G., et al. 2010, A&A, 523, A73
Eisenbeiss, T., Seifahrt, A., Mugrauer, M., et al. 2007, Astron. Nachr., 328, 521
Eisenbeiss, T., Ammler-von Eiff, M., Roell, T., et al. 2013, A&A, 556, A53
Fang, M. 2010, Ph.D. Thesis, Universität Heidelberg, Germany
Frith, J., Pinfield, D. J., Jones, H. R. A., et al. 2013, MNRAS, 435, 2161
Fuhrmeister, B., & Schmitt, J. H. M. M. 2003, A&A, 403, 247
Gagné, J., Lafrenière, D., Doyon, R., Malo, L., & Artigau, É. 2014, ApJ, 783, 121
Gaidos, E., & Mann, A. W. 2014, ApJ, 791, 54
Gaidos, E., Mann, A. W., Lépine, S., et al. 2014, MNRAS, 443, 2561
García, B. 1989, Bulletin d'Information du Centre de Données Stellaires, 36, 27
Gatewood, G., & Coban, L. 2009, AJ, 137, 402
Giclas, H. L., Slaughter, C. D., & Burnham, R. 1959, Lowell Observatory Bulletin, 4, 136
Giclas, H. L., Burnham, R., & Thomas, N. G. 1962, Lowell Observatory Bulletin, 5, 257
Gigoyan, K. S., Hambaryan, V. V., & Azzopardi, M. 1998, Astrophys., 41, 356
Gizis, J. E. 1997, AJ, 113, 806
Gizis, J. E., & Reid, I. N. 1997, PASP, 109, 1233
Gizis, J. E., & Reid, I. N. 2000, PASP, 112, 610
Gizis, J. E., Monet, D. G., Reid, I. N., et al. 2000a, MNRAS, 311, 385
Gizis, J. E., Monet, D. G., Reid, I. N., et al. 2000b, AJ, 120, 1085
Gizis, J. E., Reid, I. N., & Hawley, S. L. 2002, AJ, 123, 3356
Gliese, W., & Jahreiss, H. 1991, Preliminary Version of the Third Catalogue of Nearby Stars, NASA/Astronomical Data Center, Goddard Space Flight Center, Greenbelt
González, G. 1997, MNRAS, 285, 403
González Hernández, J. I., Rebolo, R., Israelian, G., et al. 2004, ApJ, 609, 988
Gould, A., & Chanamé, J. 2004, ApJS, 150, 455
Gray, R. O., Corbally, C. J., Garrison, R. F., McFadden, M. T., & Robinson, P. E. 2003, AJ, 126, 2048
Gray, R. O., & Corbally, C. J. 2009, Stellar Spectral Classification (Princeton University Press)
Gray, R. O., Corbally, C. J., Garrison, R. F., et al. 2006, AJ, 132, 161
Griffin, R. F., Griffin, R. E. M., Gunn, J. E., & Zimmerman, B. A. 1988, AJ, 96, 172
Guenther, E. W., & Tal-Or, L. 2010, A&A, 521, A83
Guenther, E. W., & Wuchterl, G. 2003, A&A, 401, 677
Hanson, R. B. 1975, AJ, 80, 379
Hawley, S. L., Gizis, J. E., & Reid, I. N. 1996, AJ, 112, 2799
Hawley, S. L., Covey, K. R., Knapp, G. R., et al. 2002, AJ, 123, 3409
Henry, T. J., Kirkpatrick, J. D., & Simons, D. A. 1994, AJ, 108, 1437
Henry, T. J., Walkowicz, L. M., Barto, T. C., & Golimowski, D. A. 2002, AJ, 123, 2002
Henry, T. J., Jao, W.-C., Subasavage, J. P., et al. 2006, AJ, 132, 2360
Herbig, G. H., & Rao, N. K. 1972, ApJ, 174, 401
Hidalgo, D. 2014, MSc Thesis, Universidad Complutense de Madrid, Spain
Holmberg, J., Nordström, B., & Andersen, J. 2009, A&A, 501, 941
Howard, A. W., Marcy, G. W., Bryson, S. T., et al. 2012, ApJS, 201, 15
Irwin, J., Berta, Z. K., Burke, C. J., et al. 2011, ApJ, 727, 56
Jacoby, G. H., Hunter, D. A., & Christian, C. A. 1984, ApJS, 56, 257
Jahreiß, H., Meusinger, H., Scholz, R.-D., & Stecklum, B. 2008, A&A, 484, 575
Jao, W.-C., Mason, B. D., Hartkopf, W. I., Henry, T. J., & Ramos, S. N. 2009, AJ, 137, 3800
Jao, W.-C., Henry, T. J., Subasavage, J. P., et al. 2011, AJ, 141, 117
Janson, M., Hormuth, F., Bergfors, C., et al. 2012, ApJ, 754, 44
Janson, M., Bergfors, C., Brandner, W., et al. 2014, ApJ, 789, 102
Jeffries, R. D. 1995, MNRAS, 273, 559
Jiménez-Esteban, F. M., Caballero, J. A., Dorda, R., Miles-Páez, P. A., & Solano, E. 2012, A&A, 539, A86
Jódar, E., Pérez-Garrido, A., Díaz-Sánchez, A., et al. 2013, MNRAS, 429, 859
Johnson, H. L., & Morgan, W. W. 1953, ApJ, 117, 313
Johnson, J. A., Aller, K. M., Howard, A. W., & Crepp, J. R. 2010, PASP, 122, 905
Joshi, M. M., Haberle, R. M., & Reynolds, R. T. 1997, Icarus, 129, 450
Joy, A. H., & Abt, H. A. 1974, ApJS, 28, 1
Kasting, J. F., Whitmire, D. P., & Reynolds, R. T. 1993, Icarus, 101, 108
Keenan, P. C., & McNeil, R. C. 1989, ApJS, 71, 245
Kenyon, S. J., Brown, D. I., Tout, C. A., & Berlind, P. 1998, AJ, 115, 2491
Kirkpatrick, J. D. 2005, ARA&A, 43, 195
Kirkpatrick, J. D., Henry, T. J., & McCarthy, D. W., Jr. 1991, ApJS, 77, 417
Kirkpatrick, J. D., Henry, T. J., & Simons, D. A. 1995, AJ, 109, 797
Kirkpatrick, J. D., Reid, I. N., Liebert, J., et al. 1999, ApJ, 519, 802

Klutsch, A., Alonso-Floriano, F. J., Caballero, J. A., et al. 2012, SF2A-2012: Proc. Annual meeting French Soc. Astron. Astrophys., 357
Klutsch, A., Freire Ferrero, R., Guillout, P., et al. 2014, A&A, 567, A52
Kopparapu, R. K. 2013, ApJ, 767, L8
Kopparapu, R. K., Ramírez, R., Kasting, J. F., et al. 2013, ApJ, 765, 131
Kotani, T., Tamura, M., Suto, H., et al. 2014, Proc. SPIE, 9147, E14
Krisciunas, K., Aspin, C., Geballe, T. R., et al. 1993, MNRAS, 263, 781
Lalitha, S., Czesla, S., Schmitt, J. H. M. M., et al. 2012, 17th Cambridge Workshop on Cools Stars, Stellar Systems and the Sun, published on-line at http://www.coolstars17.net
Lamert, A. 2014, MSc Thesis, Georg-August-Universität Göttingen, Germany
Lammer, H., Lichtenegger, H. I. M., Kulikov, Y. N., et al. 2007, Astrobiology, 7, 185
Law, N. M., Hodgkin, S. T., & Mackay, C. D. 2008, MNRAS, 384, 150
Lee, S.-G. 1984, AJ, 89, 702
Leggett, S. K., & Hawkins, M. R. S. 1988, MNRAS, 234, 1065
Lépine, S., & Gaidos, E. 2011, AJ, 142, 138
Lépine, S., & Shara, M. M. 2005, AJ, 129, 1483
Lépine, S., Rich, R. M., & Shara, M. M. 2003, AJ, 125, 1598
Lépine, S., Rich, R. M., & Shara, M. M. 2007, 669, 1235
Lépine, S., Thorstensen, J. R., Shara, M. M., & Rich, R. M. 2009, AJ, 137, 4109
Lépine, S., Hilton, E. J., Mann, A. W., et al. 2013, AJ, 145, 102
Li, J. Z., Hu, J. Y., & Chen, W. P. 2000, A&A, 356, 157
Lodieu, N., Scholz, R.-D., McCaughrean, M. J., et al. 2005, A&A, 440, 1061
Lodieu, N., Zapatero Osorio, M. R., & Martín, E. L. 2009, A&A, 499, 729
López-Corredoira, M., Gutiérrez, C. M., Mohan, V., Gunthardt, G. I., & Alonso, M. S. 2008, A&A, 480, 61
Magrini, L., Randich, S., Zoccali, M., et al. 2010, A&A, 523, A11
Mahadevan, S., Ramsey, L. W., Terrien, R., et al. 2014, Proc. SPIE, 9147
Maldonado, J., Martínez-Arnáiz, R. M., Eiroa, C., Montes, D., & Montesinos, B. 2010, A&A, 521, A12
Malo, L., Doyon, R., Lafrenière, D., et al. 2013, ApJ, 762, 88
Malo, L., Doyon, R., Feiden, G. A., et al. 2014, ApJ, 792, 37
Mamajek, E. E., Bartlett, J. L., Seifahrt, A., et al. 2013, AJ, 146, 154
Mann, A. W., Brewer, J. M., Gaidos, E., Lépine, S., & Hilton, E. J. 2013, AJ, 145, 52
Mann, A. W., Deacon, N. R., Gaidos, E., et al. 2014, AJ, 147, 160
Mann, A. W., Feiden, G. A., Gaidos, E., & Boyajian, T. 2015, ApJ, 804, 64
Martín, E. L., & Kun, M. 1996, A&AS, 116, 467
Martín, E. L., Rebolo, R., & Magazzù, A. 1994, ApJ, 436, 262
Martín, E. L., Rebolo, R., & Zapatero Osorio, M. R. 1996, ApJ, 469, 706
Martín, E. L., Delfosse, X., Basri, G., et al. 1999, AJ, 118, 2466
Masciadri, E., Mundt, R., Henning, T., Álvarez, C., & Barrado y Navascués, D. 2005, ApJ, 625, 1004
Mathieu, R. D. 1994, ARA&A, 32, 465
McWilliam, A. 1990, ApJS, 74, 1075
Meisenheimer, K. 1994, Sterne und Weltraum, 33, 516
Mochnacki, S. W., Gladders, M. D., Thomson, J. R., et al. 2002, AJ, 124, 2868
Montagnier, G., Ségransan, D., Beuzit, J.-L., et al. 2006, A&A, 460, L19
Montes, D., López-Santiago, J., Gálvez, M. C., et al. 2001, MNRAS, 328, 45
Montes, D., Alonso-Floriano, F. J., Tabernero, H. M., et al. 2013, Protostars and Planets VI, 2K022
Montes, D., Caballero, J. A., Alonso-Floriano, A. F., et al. 2015, 18th Cambridge Workshop on Cools Stars, Stellar Systems and the Sun, in press
Moore, J. H., & Paddock, G. F. 1950, ApJ, 112, 48
Morales, J. C., Ribas, I., & Jordi, C. 2008, A&A, 478, 507
Morales, J. C., Ribas, I., Caballero, J. A., et al. 2013, Highlights of Spanish Astrophysics VII, 664
Motch, C., Guillout, P., Haberl, F. , et al. 1997, A&A, 318, 111
Motch, C., Guillout, P., Haberl, F. , et al. 1998, A&AS, 132, 341
Mundt, R., Alonso-Floriano, F. J., Caballero, J. A., et al. 2013, Protostars and Planets VI, 2K055
Neves, V., Bonfils, X., Santos, N. C., et al. 2012, A&A, 538, A25
Neves, V., Bonfils, X., Santos, N. C., et al. 2013, A&A, 551, A36
Neves, V., Bonfils, X., Santos, N. C., et al. 2014, A&A, 568, A121
Newton, E. R., Charbonneau, D., Irwin, J., et al. 2014, AJ, 147, 20
Önehag, A., Heiter, U., Gustafsson, B., et al. 2012, A&A, 542, A33
Passegger, V.-M.. Wende, S., Reiners, A., et al. 2014, Towards other Earths II: the star-planet connection, in press
Pels, G., Oort, J. H., & Pels-Kluyver, H. A. 1975, A&A, 43, 423
Phan-Bao, N., & Bessell, M. S. 2006, A&A, 446, 515
Pickles, A., & Depagne, É. 2010, PASP, 122, 1437
Pounds, K. A., Allan, D. J., Barber, C., et al. 1993, MNRAS, 260, 77
Poveda, A., Herrera, M. A., Allen, C., Cordero, G., & Lavalley, C. 1994, Rev. Mex. Astron. Astrophys., 28, 43
Quirrenbach, A., Amado, P. J., Mandel, H., et al. 2010, Proc. SPIE, 7735, E13
Quirrenbach, A., Amado, P. J., Seifert, W., et al. 2012, Proc. SPIE, 8446
Quirrenbach, A., Amado, P. J., Caballero, J. A., et al. 2014, Proc. SPIE, 9147, E1F
Rajpurohit, A. S., Reylé, C., Allard, F., et al. 2013, A&A, 556, A15
Rajpurohit, A. S., Reylé, C., Allard, F., et al. 2014, A&A, 564, A90
Recio-Blanco, A., Bijaoui, A., & de Laverny, P. 2006, MNRAS, 370, 141
Reid, N. 1992, MNRAS, 257, 257
Reid, N. 1993, MNRAS, 265, 785
Reid, I. N., Hawley, S. L., & Gizis, J. E. 1995, AJ, 110, 1838
Reid, I. N., Gizis, J. E., & Hawley, S. L. 2002, AJ, 124, 2721
Reid, I. N., Cruz, K. L., Allen, P., et al. 2003, AJ, 126, 3007
Reid, I. N., Cruz, K. L., Allen, P., et al. 2004, AJ, 128, 463
Reid, I. N., Cruz, K. L., & Allen, P. 2007, AJ, 133, 2825
Reid, I. N., Cruz, K. L., Kirkpatrick, J. D., et al. 2008, AJ, 136, 1290
Reiners, A., & Basri, G. 2009, ApJ, 705, 1416
Reiners, A., & Basri, G. 2010, ApJ, 710, 924
Reiners, A., Bean, J. L., Huber, K. F., et al. 2010, ApJ, 710, 432
Reiners, A., Shulyak, D., Anglada-Escudé, G., et al. 2013, A&A, 552, A103
Reyes-Sánchez, K. P. 2014, MSc Thesis, Universidad Internacional de Valencia, Spain
Reylé, C., Scholz, R.-D., Schultheis, M., Robin, A. C., & Irwin, M. 2006, MNRAS, 373, 705
Riaz, B., Gizis, J. E., & Harvin, J. 2006, AJ, 132, 866
Riaz, B., Gizis, J. E., & Samaddar, D. 2008, ApJ, 672, 115
Ribas, I. 2003, A&A, 400, 297
Riddick, F. C., Roche, P. F., & Lucas, P. W. 2007, MNRAS, 381, 1067
Ridgway, S. T., Joyce, R. R., White, N. M., & Wing, R. F. 1980, ApJ, 235, 126
Riedel, A. R., Finch, C. T., Henry, T. J., et al. 2014, AJ, 147, 85
Robertson, P., Endl, M., Henry, G. W., et al. 2015, ApJ, 801, 79
Rodríguez-López, C., Anglada-Escudé, G., Amado, P. J., et al. 2014, Highlights of Spanish Astrophysics VIII, in press
Rojas-Ayala, B., Covey, K. R., Muirhead, P. S., & Lloyd, J. P. 2010, ApJ, 720, L113
Rojas-Ayala, B., Covey, K. R., Muirhead, P. S., & Lloyd, J. P. 2012, ApJ, 748, 93
Sánchez, S. F., Aceituno, J., Thiele, U., Pérez-Ramírez, D., & Alves, J. 2007, PASP, 119, 118
Sánchez, S. F., Thiele, U., Aceituno, J., et al. 2008, PASP, 120, 1244
Sánchez-Blázquez, P., Peletier, R. F., Jiménez-Vicente, J., et al. 2006, MNRAS, 371, 703
Sandage, A. 1969, ApJ, 158, 1115
Sandage, A., & Kowal, C. 1986, AJ, 91, 1140
Sanduleak, N., & Pesch, P. 1988, ApJS, 66, 387
Scalo, J., Kaltenegger, L., Segura, A. G., et al. 2007, Astrobiology, 7, 85
Scelsi, L., Maggio, A., Michela, G., et al. 2007, A&A, 468, 405
Scelsi, L., Sacco, G., Affer, L., et al. 2008, A&A, 490, 601
Schlaufman, K. C., & Laughlin, G. 2010, A&A, 519, A105
Schlieder, J. E., Lépine, S., & Simon, M. 2012a, AJ, 143, 80
Schlieder, J., Lépine, S., Rice, E., et al. 2012b, AJ, 143, 114
Schlieder, J., Bonnefoy, M., Herbst, T. M., et al. 2014, ApJ, 783, 27
Scholz, R.-D., Meusinger, H., & Jahreiß, H. 2005, A&A, 442, 211
Seeliger, M., Neuhäuser, R., & Eisenbeiss, T. 2011, AN, 332, 821
Seifert, W., Sánchez Carrasco, M. A., Xu, W., et al. 2012, Proc. SPIE, 8446, E33
Sestito, P., Palla, F., & Randich, S. 2008, A&A, 487, 965
Shkolnik, E., Liu, M. C., & Reid, I. N. 2009, ApJ, 699, 649
Shkolnik, E. L., Hebb, L., Liu, M. C., Reid, I. N., & Collier Cameron, A., 2010, ApJ, 716, 1522
Shkolnik, E. L., Anglada-Escudé, G., Liu, M. C., et al. 2012, ApJ, 758, 56
Shulyak, D., Seifahrt, A., Reiners, A., Kochukhov, O., & Piskunov, N. 2011, MNRAS, 418, 2548
Skrutskie, M. F., Cutri, R. M., Stiening, R., et al. 2006, AJ, 131, 1163
Sousa, S. G., Santos, N. C., Mayor, M., et al. 2008, A&A, 487, 373
Sousa, S. G., Santos, N. C., Israelian, G., Mayor, M., & Udry, S. 2011, A&A, 533, A141
Stauffer, J. R., & Hartmann, L. W. 1986, ApJS, 61, 531
Stauffer, J. R., Giampapa, M. S., Herbst, W., et al. 1991, ApJ, 374, 142
Stephenson, C. B. 1986, AJ, 91, 144
Strom, S. E., & Strom, K. M. 1967, ApJ, 150, 501
Tabernero, H. M., Montes, D., & González Hernández, J. I. 2012, A&A, 547, A13
Tabernero, H. M., Montes, D., González Hernández, J. I., & Ammler-von Eiff, M. 2015, A&A, in press [arXiv:1409.2348]
Tarter, J. C., Backus, P. R., Mancinelli, R. L., et al. 2007, Astrobiology, 7, 30
Teegarden, B. J., Pravdo, S. H., Hicks, M., et al. 2003, ApJ, 589, L51
Terrien, R. C., Mahadevan, S., Bender, C. F., et al. 2012, ApJ, 747, L38
Tokovinin, A. 2008, MNRAS, 389, 925
Torres, C. A. O., Quast, G. R., Melo, C. H. F., & Sterzik, M. F. 2008, in Handbook of Star Forming Regions, Volume II, 757

Tsuji, T., & Nakajima, T. 2014, PASJ, 66, 98
Valenti, J. A., & Fischer, D. A. 2005, ApJS, 159, 141
Valenti, J. A., & Piskunov, N. 1996, A&AS, 118, 595
van Altena, W. F. 1966, AJ, 71, 482
van Maanen, A. 1945, ApJ, 102, 26
Vyssotsky, A. N. 1956, AJ, 61, 201
West, A. A., Hawley, S. L., Walkowicz, L. M., et al. 2004, AJ, 128, 426
West, A. A., Morgan, D. P., Bochanski, J. J., et al. 2011, AJ, 141, 97
White, R., & Basri, G. 2003, ApJ, 582, 1109
Wichmann, R., Krautter, J., Schmitt, J. H. M. M., et al. 1996, A&A, 312, 439
Wilking, B. A., Meyer, M. R., Robinson, J. G., & Greene, T. P. 2005, AJ, 130, 1733
Winters, J. G., Henry, T. J., Lurie, J. C., et al. 2015, AJ, 149, 5
Woolf, V. M., & Wallerstein, G. 2005, MNRAS, 356, 963
Woolf, V. M., & Wallerstein, G. 2006, PASP, 118, 218
Woolf, V. M., Lépine, S., & Wallerstein, G. 2009, PASP, 121, 117
Xing, L.-F., & Xing, Q.-F. 2012, A&A, 537, A91
Yi, Z., Luo, A., Song, Y., et al. 2014, AJ, 147, 33
Zboril, M., & Byrne, P. B. 1998, MNRAS, 299, 753
Zechmeister, M., Kürster, M., & Endl, M. 2009, A&A, 505, 859
Zechmeister, M., Kürster, M., Endl, M., et al. 2013, A&A, 552, A78
Zuckerman, B., & Song, I. 2004, ARA&A, 42, 685
Zuckerman, B., Song, I., & Bessell, M. S. 2004, ApJ, 613, L65
Zuckerman, B., Vican, L., Song, I., & Schneider, A. 2013, ApJ, 778, 5

3

Search for common proper motion companions in the β Pictoris moving group

This chapter includes the paper accepted for publication in A&A titled *Reaching the boundary between stellar kinematic groups and very wide binaries III. Sixteen new stars and eight new wide systems in the β Pictoris moving group* (Alonso-Floriano et al. 2015, A&A, in press, arXiv:1508.06929, doi:10.1051/0004-6361/201526795).

This publication presents a research focused on the young close moving group β Pictoris. As was explained in the introduction, there are only a few exoplanets discovered around young objects, and none of those discovered by radial velocity technique are orbiting M-type stars. The study of young M-stars by radial velocity surveys is necessary to understand the formation and evolution of exoplanets, and the habitability of those exoplanets found in the HZs of M dwarfs. The following work presents a compilation of previously identify β Pictoris members and candidates members along the whole mass range, and proposes new candidates –mostly on the low-mass regimen– through the common proper motion technique. This study provides a highly valuable list of young targets for exoplanetary projects like CARMENES. Several objects, studied in this publication, have been characterised in our previous low-resolution spectroscopic study (see Chapter 2, Table 7), or were already included in the input catalogue of CARMENES. However, this investigation not only provides useful information for radial velocity planetary surveys, but for other works, such the ones on debris disk, star formation, metallicity calibration yardstick (see Chapter 4, Sect. 4.2), evolutionary models, membership of dubious objects, etc.

We presented preliminary results of the publication included in this chapter at several conferences (see Appendix A), of which we point out Alonso-Floriano et al. (2011) that have been cited in three refereed publications (Bowler et al. 2015, Eisenbeiss et al. 2013 and Shkolnik et al. 2012).

Table A.1 to Table A.5 of the paper included in this chapter, are showed on the Appendix C as Table C.1 to Table C.5.

Astronomy & Astrophysics manuscript no. bp17
September 6, 2015

Reaching the boundary between stellar kinematic groups and very wide binaries

III. Sixteen new stars and eight new wide systems in the β Pictoris moving group

F. J. Alonso-Floriano[1], J. A. Caballero[2], M. Cortés-Contreras[1], E. Solano[2,3], and D. Montes[1]

[1] Departamento de Astrofísica y Ciencias de la Atmósfera, Facultad de Ciencias Físicas, Universidad Complutense de Madrid, 28040 Madrid, Spain
e-mail: fjalonso@ucm.es
[2] Centro de Astrobiología (CSIC-INTA), ESAC PO box 78, 28691 Villanueva de la Cañada, Madrid, Spain
[3] Spanish Virtual Observatory, ESAC PO box 78, 28691 Villanueva de la Cañada, Madrid, Spain

Received 19 June 2015 / Accepted 8 August 2015

ABSTRACT

Aims. We look for common proper motion companions to stars of the nearby young β Pictoris moving group.
Methods. First, we compiled a list of 185 β Pictoris members and candidate members from 35 representative works. Next, we used the Aladin and STILTS virtual observatory tools and the PPMXL proper motion and Washington Double Star catalogues to look for companion candidates. The resulting potential companions were subjects of a dedicated astro-photometric follow-up using public data from all-sky surveys. After discarding 67 sources by proper motion and 31 by colour-magnitude diagrams, we obtained a final list of 36 common proper motion systems. The binding energy of two of them is perhaps too small to be considered physically bound.
Results. Of the 36 pairs and multiple systems, eight are new, 16 have only one stellar component previously classified as a β Pictoris member, and three have secondaries at or below the hydrogen-burning limit. Sixteen stars are reported here for the first time as moving group members. The unexpected large number of high-order multiple systems, 12 triples and two quadruples among 36 systems, may suggest a biased list of members towards close binaries or an increment of the high-order-multiple fraction for very wide systems.

Key words. stars: binaries: general – stars: binaries: visual – Galaxy: kinematics and dynamics – open clusters and associations: individual: β Pictoris

1. Introduction

Wide binaries provide valuable information about key questions in astrophysics; for example, halo-wide pairs contribute to constraining the properties of dark matter (Weinberg et al. 1987; Yoo et al. 2004; Quinn et al. 2009), some star formation theories depend on the frequency and separation of wide young binaries (Parker et al. 2009; Ward-Duong et al. 2015; Marks et al. 2015), and relatively bright FGK-type primaries with M-dwarf companions provide a metallicity calibration yardstick for cool stars (Bonfils et al. 2005; Rojas-Ayala et al. 2012; Newton et al. 2014; Li et al. 2014). However, the maximum projected physical separation of a wide binary is still a matter of discussion: Some authors consider a cutoff in the number of wide binaries at $2\,10^4$ au (∼0.1 pc), which is the typical size of protostellar cores (Tolbert 1964; Abt 1988; Wasserman & Weinberg 1991; Allen et al. 2000; Tokovinin & Lépine 2012), while others contemplate separations of $2\,10^5$ au (∼1 pc) or more (Jiang & Tremaine 2009; Caballero 2009; Shaya & Olling 2011). Such wide common proper-motion pair candidates, which give their name to the title of this series of papers, can be either unbound members of the same young stellar kinematic group that by chance are co-moving (Tokovinin 2014a) or bound "binaries" of very low binding energies at the limit of disruption (Caballero 2010).

The younger a weakly bound system is, the less time it has had to be disrupted (Bahcall & Soneira 1981; Retterer & King 1982; Weinberg et al. 1987; Saarinen & Gilmore 1989; Poveda & Allen 2004). As a result, a search for multiple systems within a young stellar kinematic group (moving group or stellar association) offers a unique opportunity for finding new faint benchmark objects hardly influenced by the Galactic gravitational potential, but instead by their formation process. In other words, the shape of young wide binaries is dominated by nature instead of by nurture.

In this work, we use the profitable technique of searching for common proper-motion pairs of wide separation (e.g., Luyten 1979; Chanamé & Gould 2004) in a close and very young moving group, namely β Pictoris (Zuckerman et al. 2001b; Ortega et al. 2002; Song et al. 2003). Although there is no consensus in the literature, the β Pictoris age lies in a relatively narrow interval between 11 Ma and 26 Ma (Barrado y Navascués 1998; Torres et al. 2006; Yee & Jensen 2010; Binks & Jeffries 2014; Mamajek & Bell 2014 and references therein). Known moving group members and member candidates lie at between 6 pc and 80 pc from our Sun with a median distance of 40 pc.

Because of its youth and proximity, the β Pictoris moving group has been relevant for studying resolved debris discs with high angular resolution observations (Smith & Terrile 1984; Metchev et al. 2005; Boccaletti et al. 2009; Churcher et al. 2011; Wahhaj et al. 2013; Dent et al. 2013) and exoplanets through direct imaging (Mouillet et al. 1997; Neuhäuser et al. 2003; Kasper et al. 2007; Lagrange et al. 2009, 2010; Bonnefoy et al. 2011, 2013; Biller et al. 2013; Rameau et al. 2013; Males et al.

Table 1. Sources of the β Pictoris stellar sample.

Title	References
Search for associations containing young stars (I, III, V, VI)	SACY [a]
Bayesian analysis to identify new star candidates in nearby young stellar... (I–V)	BANYAN [b]
A dusty M5 binary in the β Pictoris moving group	Rodríguez et al. 2014
On the age of the β Pictoris moving group	Mamajek & Bell 2014
The Solar Neighborhood. XXXIII. Parallax results from the CTIOPI 0.9 m program...	Riedel et al. 2014
A lithium depletion boundary age of 21 Myr for β Pictoris moving group	Binks & Jeffries 2014
Unveiling new members in five nearby young moving groups	Moór et al. 2013
Identifying the young low-mass stars within 25 pc (I, II)	Shkolnik et al. 2009, 2012
Likely memebers of the β Pictoris and AB Doradus moving groups in the north	Schlieder et al. 2012b
Cool young stars in the northern hemisphere: β Pictoris and AB Doradus moving...	Schlieder et al. 2012a
The sizes of the nearest young stars	McCarthy & White 2012
Potential members of stellar kinematic groups within 30 pc of the Sun	Nakajima & Morino 2012
A search for new members of the β Pictoris, Tucana-Horologium and η Cha	Kiss et al. 2011
β Pictoris and AB Doradus moving groups: likely new low-mass members	Schlieder et al. 2010
The lowest-mass member of the β Pictoris moving group	Rice et al. 2010
Potential members of stellar kinematic groups within 20 pc of the Sun	Nakajima et al. 2010
Kinematic analysis and membership status of TWA22 AB	Teixeira et al. 2009
Nearby young stars selected by proper motion. I. Four new members of the β Pictoris...	Lépine & Simon 2009
Young nearby loose associations	Torres et al. 2008
Unraveling the origins of nearby young stars	Makarov 2007
Nearby debris disk systems with high fractional luminosity reconsidered	Moór et al. 2006
Young stars near the Sun	Zuckerman & Song 2004
New aspects of the formation of the β Pictoris moving group	Ortega et al. 2004
New memeber of the TW Hydrae association, β Pictoris moving group and Tucana...	Song et al. 2003
The origin of the β Pictoris moving group	Ortega et al. 2002
The β Pictoris moving group	Zuckerman et al. 2001b
The age of β Pictoris	Barrado y Navascués et al. 1999

Notes. [(a)] SACY: Torres et al. (2006); da Silva et al. (2009); Elliott et al. (2014, 2015). [(b)] BANYAN: Malo et al. (2013, 2014a, 2014b); Gagné et al. (2014, 2015). We only collected BANYAN candidates with membership probability $P > 50\%$.

2014; Bowler et al. 2015; Macintosh et al. 2015) or for comparing observations with evolutionary models (Crifo et al. 1997; Song et al. 2002; Cruz et al. 2009; Biller et al. 2010; Mugrauer et al. 2010; Jenkins et al. 2012; Montet et al. 2015). Therefore, increasing the number of members via common proper-motion companionship, especially at low masses, can help to inform the previously mentioned fields and to constrain the age of the group. Besides that, identiying bright M-dwarf targets of ∼10–30 Ma for extremely precise radial velocity surveys is becoming critical for understanding the formation and early evolution of terrestrial planets in habitable zones (Lissauer 2007; Ramírez & Kaltenegger 2014; Luger et al. 2015; Tian 2015; Tian & Ida 2015). Preliminary results of this work, including the discovery of two new stellar members in the β Pictoris moving group, were given in Alonso-Floriano et al. (2011).

2. Analysis

2.1. Stars sample

We have compiled in Table A.1 a list of 185 β Pictoris members and member candidates around which we looked for common proper-motion companions. We gathered them from 35 previous works published in the past 16 years from the first articles of Barrado y Navascués et al. (1999) and Zuckerman et al. (2001b) to the last investigations published in the SACY (Search for Associations Containing Young stars – Torres et al. 2006; Elliott et al. 2014, 2015) and BANYAN series (Bayesian Analysis for Nearby Young AssociatioNs – Malo et al. 2014a,b; Gagné et al. 2015). Table 1 lists all works that we searched through.

We cross-matched our list with the latest Geneva-Copenhagen catalogue (Holmberg et al. 2009) and identified 17 bright stars for which metallicity was available. From these data, we determined a solar metallicity of the β Pictoris moving group of [Fe/H] = –0.2±0.2. In Table A.1, we provide for each star: discovery (or recommended) name, right ascension and declination from the Two-Micron All-Sky Survey (Skrutskie et al. 2006), heliocentric distance, its uncertainty when available, and corresponding reference. We follow the nomenclature convention of Alonso-Floriano et al. (2015). In particular, we provide for the first time the *ROSAT* precovery names (1RXS) for several stars for which no X-ray counterpart had been identified by subsequent proper-motion surveys.

In the last column, we also list a flag indicating the quality of the star membership in β Pictoris:

1. Uncontrovertible moving group members for which at least two independent research groups have declared them to be bona fide moving group members and whose memberships have not been put in doubt afterwards. In general, these objects have coherent kinematics (with reliable distance and radial velocity determination) and youth features (coronal X-ray and chromospheric Hα emission, lithium in absorption and, in some cases, debris discs).
2. Moving-group member candidates for which there is no definitive confirmation of true membership.

3. Dubious moving group member candidates that have also been proposed as belonging to other young moving groups of similar kinematics, or even to the field. We include them in our work for completeness.

2.2. Proper motion companion candidates

For this search, we made extensive use of virtual observatory tools. We used the comprehensive PPMXL proper motion catalogue (Roeser et al. 2010), the Aladin sky atlas (Bonnarel et al. 2000), and the Starlink Tables Infrastructure Library Tool Set (STILTS; Taylor 2006) to look for common proper-motion companions to the 185 β Pictoris stars in Table A.1. The PPMXL catalogue is complete down to the visual magnitude $V \approx 20$ mag and has typical individual mean errors of the proper motions between 4 and 10 mas/a, approximately. We applied the following selection criteria in our search.

- We looked for companion candidates in a circular area of angular radius $\rho = s/d$ (in arcsec) centred on each sample star, where s is the maximum projected physical separation, fixed at $s = 10^5$ au, and d (in pc) is the heliocentric distance shown in Table A.1. At the given distances, the search radii varied between over 4 deg for the closest β Pictoris stars (e.g., YZ CMi AB at 5.96±0.08 pc) and 12 to 23 arcmin for the most distant ones (e.g., LP 58–170 at 140±40 pc and V4046 Sgr AB and C at 73±18 pc). The median search radius was 44 arcmin.
- We discarded from the survey 24 stars with total PPMXL proper motions $\mu < 50$ mas/a (19) or no proper motions at all (5). Therefore, we looked for companions of 161 β Pictoris stars. Stars slower than $\mu = 50$ mas/a were not considered at this step because of the large number of potential candidates with relative uncertainties of 10 %–30 % in proper motion that would fall in the surveyed area and pass the filter. As proper motion companion candidates, we classified only the PPMXL sources with a 2MASS counterpart for which the values of $\mu_\alpha \cos\delta$ and μ_δ lie within 10 % of those of the primary target (see Fig. 1).
- We retained objects brighter than $J = 15.5$ mag. In general, fainter sources in the near-infrared also have very faint magnitudes in the optical, close to the limit of the USNO-B1 (Monet et al. 2003) digitisations of B_J, R_F, and I_N photographic plates, which were used by PPMXL. This faintness translates into large astrometric errors in the PPMXL proper motions. Keeping relatively bright sources assures the quality of the compiled astro-photometric measurements (see below), although prevents detecting fainter and, thus, low-mass β Pictoris members in, perhaps, the substellar domain.

Once we had a preliminary list of candidates, we inspected all of them visually with Aladin and the images and data of various all-sky surveys (Palomar Observatory Sky Survey I and II; 2MASS; SDSS-DR9, Ahn et al. 2012; *WISE*, Cutri et al. 2012, 2014; CMC14 and CMC15, Evans et al. 2002). In particular, we checked that the companion candidates have a unique and reliable entry in the PPMXL catalogue (e.g., at least four astrometric detections, no other PPMXL source at less than 2 arcsec, smooth variation of the magnitudes from B_J, through R_J, I_N, J, H, K_s, to *WISE* $W1$–4). In this step, we discarded a number of preliminary companion candidates with erroneous PPMXL proper motions (i.e., with incorrect USNO-B1 matches) owing to close visual multiplicity or source confusion in very crowded fields at low Galactic latitudes. Some of the mistaken sources were identified around α Cir, 1RXS J171502.4–333344,

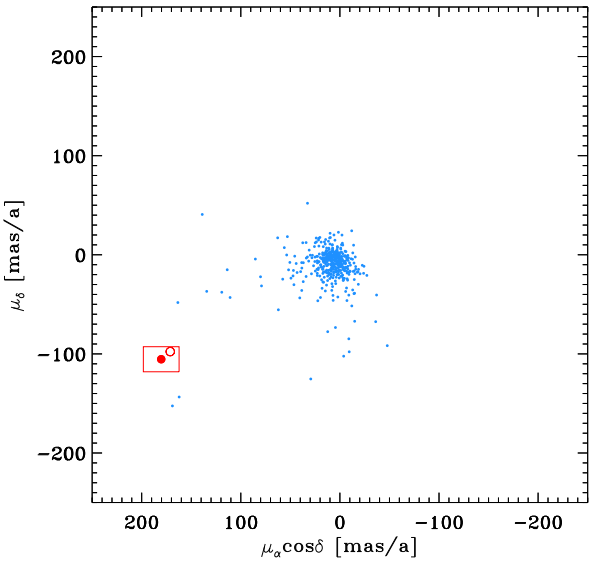

Fig. 1. Representative proper-motion diagram of all PPMXL sources brighter than $J = 15.5$ mag in a 30 arcmin-radius circular area centred on LP 648–20. The red square box in the bottom left indicates the proper-motion search area around LP 648–20, marked with a filled circle. The open circle corresponds to the bright, young G5 V star EX Cet.

V4046 Sgr, 1RXS J184956.1–013402, which have $|b| < 7$ deg, and, especially, V343 Nor, which is at less than 2 deg of the Galactic plane and, besides this, towards the Galactic centre. After this visual pre-cleaning, we obtained a list of 92 proper motion companion candidates to 65 β Pictoris stars.

Next, we performed a 10 arcsec-radius cross-match on our initial 185-star sample with the Washington Double Star catalogue (WDS – Mason et al. 2001, 2015). We got 163 positive cross-matches in 55 WDS systems. Of the cross-matches, 136 corresponded to close physical binaries not resolved by 2MASS nor PPMXL ($\rho \lesssim 2.5$ arcsec) or to wider multiple systems, but with large magnitude differences measured with powerful adaptive optics systems (e.g., Lafrenière et al. 2007; Chauvin et al. 2010). The list of WDS systems unresolved or unidentified in our search are shown in Table A.2, which provides the star name, WDS discovery name (for resolved pairs) or reference (for spectroscopic binaries), multiplicity status (physical, visual –non-common proper motion–, single/double-line spectroscopic binaries), angular separation (interval of ρ when several visual companions are tabulated), position angle (θ), and WDS identifier (only for resolved pairs). For the physical and visual pairs in Table A.2, ρ and θ correspond to the latest epoch listed by WDS.

Thanks to the cross-match with WDS, we were able to add another 15 previously known secondaries detected by 2MASS to our list of 92 proper motion companion candidates. They did not pass our filters above because they have PPMXL proper motions that deviate more than 10 % from those of the "primary", probably because of relative orbital motion, erroneous measurements in right ascension and/or declination, proper motions with 1σ lower limits below the 50 mas/a boundary, or no proper motions at all.

Finally, we also added to our list the companion candidates of three additional pairs of β Pictoris stars that were not in WDS and that were not detected because of the reasons explained above: [SLS2012] PYC J02017+0117N & S

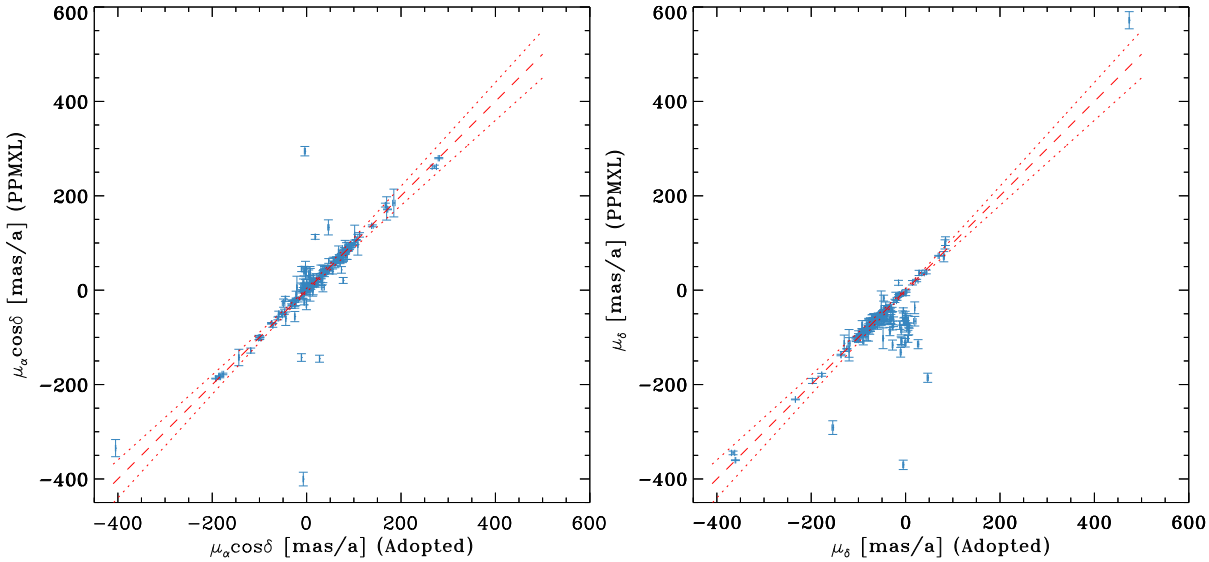

Fig. 2. PPMXL vs. adopted proper-motion diagrams in right ascension (*left panel*) and declination (*right panel*). The red dashed and dotted lines mark the one-to-one relationship and the 10 % error area above and below it, respectively.

($\rho \sim 10$ arcsec and equal brightness) and TYC 112–917–1 & 2E 1249 AB ($\mu \approx 41$ mas/a), which have the same predicted or measured distances and radial velocities (Schlieder et al. 2012a; Elliott et al. 2014) and are quite obvious proper motion companion candidates in Aladin, and V4046 Sgr AB and C, which was presented by Kastner et al. (2011).

In Table A.3, we list the 110 (92+15+3) proper motion companion candidates that passed on to the next analysis stage.

2.3. Astro-photometric follow-up

2.3.1. Astrometry

We performed a dedicated astro-photometric follow-up of the 110 companion candidates in two steps. In the first one, we confirmed true common proper motion of the pairs with a precise astrometric study. This step was necessary because PPMXL used the astro-photometric USNO-B1 catalogue as input, which is known to be affected by systematics at the fainter optical magnitudes, especially when dealing with high proper motion stars.

Of the 184 objects in Table A.3 (74 primaries and 110 companion candidates), 55 had reliable proper motions measured by *Hipparcos* (TYC, Høg et al. 2000; HIP2, van Leeuwen 2007). For the remaining 129 objects, we measured precise proper motions from public data in virtual observatory catalogues as in Caballero (2010, 2012). In particular, we used astrometric epochs from the following catalogues: AC2000.2 (Urban et al. 1998), USNO-A2 (Monet 1998), GSC2.3 (Lasker et al. 2008), DENIS (Epchtein et al. 1997), CMC14 and CMC15, 2MASS, SDSS, and *WISE*. To maximise the number of astrometric epochs, N, and time baseline, Δt, of the follow-up, which translates into reducing the uncertainty in proper motion, we also used the SuperCOSMOS digitisations of Palomar Observatory Sky Survey photographic plates, especially for the faintest objects (Hambly et al. 2001; cf., Caballero 2012). The addition of SuperCOSMOS data allowed us to get at least four accurate astrometric epochs spread over a minimum of 11.5 a for all targets except for one star (2MASS J05113065–2155189, $N = 3$). The average number of astrometric epochs and time baseline were five and 34 a, respectively. In the extreme case of TYC 4571–1414–1, we measured its proper motion with eight astrometric epochs spread over almost 115 a. Table A.3 lists the 2MASS coordinates of the 184 "primaries" and companion candidates, and their PPMXL and adopted proper motions. For the adopted proper motions that do not come from TYC or HIP2, Table A.3 also provides the time baseline and number of epochs used in our astrometric follow-up. Except for partially resolved close binaries (e.g., AT Mic AB) or faint sources ($r' \gtrsim 16$ mag), we were able to measure proper motions with typical uncertainties of 1 mas a^{-1} or less, which are comparable to or even better than TYC or HIP2.

We show a comparison of the original PPMXL proper motion values and the ones adopted by us in Fig. 2. While the values of proper motions in right ascension provided by PPMXL have in general good agreement with our adopted values, many PPMXL proper motions in declination have greater absolute values.

With the new data, we made a second, more precise, astrometric filtering and discarded 43 visual companions with adopted proper motions that deviate more than 10 % from the proper motion of the system. This step of the follow-up thus left 67 physical companion candidates for the second step. In general, the astrometrically rejected objects are distant background stars with fake high proper motions in the PPMXL catalogue, which are located close to bright stars and were reported previously as companion candidates or which are located at large angular separations to our primary targets and have by chance similar, but not identical, proper motions. Of the rejected stars, four were catalogued companion candidates of c Eri, α Cir, CD–24 16238, and AF Psc, and one was a faint companion candidate to [SLS2012] PYC J10175+5542 (Schlieder et al. 2012a) that had been reported by W. J. Luyten (LDS 2851, WDS 10176+5542).

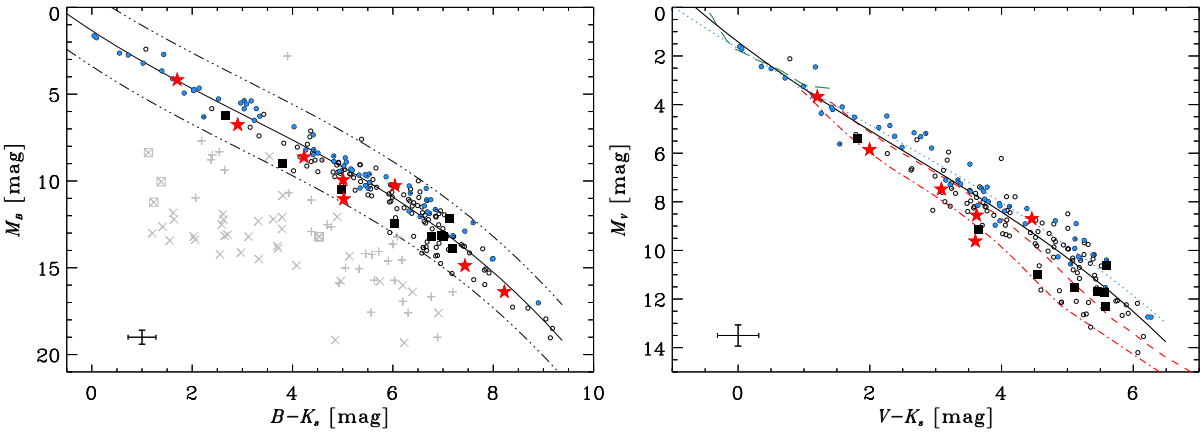

Fig. 3. Optical-to-near-infrared colour-magnitude diagrams of our β Pictoris stars and common proper-motion companion candidates. In both panels, blue filled circles mark bona fide moving group members with membership flag 1 in Table A.1 (see Section 2.1), and open circles indicate other member candidates with flags 2 and 3. Black filled squares denote companions previously known in the literature that had not been reported as belonging to β Pictoris. Red filled stars mark our eight new proper motion companions. Typical error bars are shown in the bottom left corner. The black solid line is the average β Pictoris sequence computed with all candidate members as in the left panel (flags 1, 2, and 3). *Left panel*: M_B vs. $B-K_s$ diagram. The dash-dotted lines are the β Pictoris sequence shifted by $\pm 3\sigma$. Grey times ($\times$) and crosses (+) indicate discarded companion candidates from astrometry and photometry, respectively; squared symbols mark companion candidates in the WDS. *Right panel*: M_V vs. $V-K_s$ diagram. The blue dotted line is the sequence with only bona fide members (flag 1). Red dashed and dash-dotted lines are the 20 and 100 Ma isochrones from Baraffe et al. (2015). Green long dashed line is the 20 Ma isochrone from Siess et al. (2000) plotted only at highest masses. For clarity, we do not draw the discarded companion candidates. Some remarkable stars do not have V photometry.

2.3.2. Photometry

In the second step of the follow-up, we studied the membership in the β Pictoris moving group of the 67 companion candidates that passed the previous astrometric filter with the help of colour-magnitude diagrams and theoretical isochrones.

First, we compiled B, V, r', J, H, K_s, and $W1$–4 magnitudes for all the sources investigated in this work. While infrared JHK_sW1–4 photometry came in all cases from 2MASS and *WISE*, the origin of the optical BVr' photometry was diverse. When available, we collected BVr' photometry from UCAC4 (Zacharias et al. 2013). If not available, we got it from a number of sources: Tycho-2 (B and V, after transformation from B_T and V_T magnitudes), USNO-B1 (B, after average of two photographic B_J magnitudes), AC2000.2 (only one star), SPM4 (Girard et al. 2011 – V, only one star), CMC 15 (r'), SDSS DR9 (r'), or the literature (Voges et al. 1999; Bakos et al. 2002; Torres et al. 2006; Beichman et al. 2010; Smart 2013).

We were not able to compile optical BVr' photometry for all our targets. Since we were able to compile magnitudes for more stars in the B band, we applied our photometric filtering using the reddest near-infrared band, K_s, and the bluest optical one, B. Actually, we failed to find reliable B photometry for only six stars: five low-mass stars or brown-dwarf candidates with spectral types at the M/L boundary, of which four are from Gagné et al. (2014, 2015), one is the known companion of L 186–67 A (see below), and the sixth one is a star close to the bright primary V343 Nor A. The reddest and faintest object in our sample with B and K_s photometry is 2MASS J06085283-2753583 (M8.5 V, Luhman et al. 2009; $B-K_s = 9.1$ mag). The use of *WISE* photometry did not provide significant improvement over the use of 2MASS K_s.

We performed our photometric filtering in a recursive scheme:

- First we computed the B-band absolute magnitude M_B with the heliocentric distances in Table A.1 and built the M_B vs. $B-K_s$ diagram in left-hand panel of Fig. 3. Any new companion candidate would have to be located at the same distance as the target star.
- We defined an average β Pictoris sequence with all members and candidates in Table A.1 (flags 1, 2, and 3). All sources that did not pass the astrometric filter lie in the locus of background stars in the colour-magnitude diagram.
- We checked the reliability of our average sequence by comparing it with the latest evolutionary models by Baraffe et al. (2015). Since BT-Settl does not provide M_B magnitudes, we used M_V ones instead. We built the M_V vs. $V-K_s$ diagram in right-hand panel of Fig. 3 and plotted the corresponding BT-Settl 20 and 100 Ma isochrones. The acceptable match between our average M_V vs. $V-K_s$ sequence and the 20 Ma isochrone encouraged us to use our average M_B vs. $B-K_s$ sequence for the photometric filter.
- We discarded stars with absolute magnitudes M_B and colours $B-K_s$ inconsistent with the β Pictoris sequence. Most discarded stars lie outside the $\pm 3\sigma$ area around the sequence. The systematic error introduced by mixing different photometric systems for the blue magnitude seems to be smaller than the intrinsic scatter in the β Pictoris sequence, mostly due to uncertainties in distance.

Of the previous 67 stars, 31 did not pass the photometric filter. One known system, L 186–67 Aa,Ab,B, could not be studied photometrically because of the lack of reliable data in the optical, but the short angular separation between components and the large common proper motions ensured that it is a physical system.

3. Results and discussion

3.1. Known and new common proper motion pairs

From the initial list of 184 common proper motion companion candidates to β Pictoris stars in Section 2.2, only 36 targets passed the two filters of our astro-photometric follow-up in

Section 2.3. Our final list of confirmed common-proper motion systems in the β Pictoris moving group, as shown in Table A.5, consists of

- Eighteen known systems in which the two stars had been reported previously to belong to the moving group. All of them except one are listed by WDS; the exception is the wide system formed by V4046 Sgr AB and V4046 Sgr C, which was proposed and investigated by the first time by Kastner et al. (2011). Some of the 17 WDS systems have been known for decades, such as five pairs in the W. J. Luyten's Double Star catalogue or the HD 14082 AB pair, which was resolved for the first time by F. G. W. Struve in 1821.
- Ten known systems in which only one star had been reported previously as belonging to the moving group. Of the ten stars that had not been reported as belonging to β Pictoris (i.e., not listed in Table A.1), four displayed significant X-ray emission in *ROSAT* observations (Voges et al. 1999; Riaz et al. 2006; Kaplan et al. 2006; Haakonsen & Rutledge 2009) and two showed intense Hα emission at the chromospheric/accretion boundary for their spectral types (pEW(Hα) $\approx$ –12 to –16 Å – Reid et al. 1995; Riaz et al. 2006). Since there is one star that is an Hα *and* X-ray emitter (2MASS J00193931+1951050), half of the ten new stars have known signposts of youth, which supports membership in β Pictoris. Besides this, another one has a similar radial velocity to the primary in the system (CD–44 753 A and B – Kordopatis et al. 2013). For the other four new young stars, there are only photometric data available (and, in the case of 2MASS J07293670+3554531, mass and spectral type derived from photometry – Pickles & Depagne 2010; Janson et al. 2012).
- Eight new common proper motion systems with β Pictoris stars. In reality, there are WDS entries for two β Pictoris pairs that were presented for the first time by Alonso-Floriano et al. (2011): EX Cet A,B (CAB 3) and HD 173167 A,B (CAB 8). Although the results from this preliminary publication have already been used by other authors (Shkolnik et al. 2012; Eisenbeiss et al. 2013; Bowler et al. 2015), we consider their discovery as part of this work. Moór et al. (2003) "rediscovered" the pair HD 173167 A,B, although they did not report ρ or θ. The optical spectra of these two stars and of TYC 112–917–1 and 2E 1249 AB in the new pair *WDS 05200+0613* display intense Li I λ6707.8 Å line in absorption for their spectral type (Alcalá et al. 2000; Torres et al. 2006), which supports their extremely young age. Six of these stars are reported here as new member candidates in the β Pictoris moving group.

On some occasions we use the term "pair" to refer to multiple systems that contain only two components resolvable from the ground with standard imaging (i.e., no adaptive optics or lucky imaging) and spectroscopic devices. Most of our systems are such pairs. However, Table A.5 lists 12 triple and two quadruple hierarchical systems that contain one or two close pairs unresolved by public catalogues (Table A.2). The two quadruple systems are MV Vir Aa,Ab,B,C and HD 199143 AB,CD (for which the close components were resolved first by Jayawardhana & Brandeker 2001). The latter has an "A. Tokovinin" WDS entry dated after 2011, but the wide multiplicity was previously reported by Alonso-Floriano et al. (2011) and, especially, Zuckerman et al. (2001b).

The existence of 14 triples and quadruples in a list of 36 multiples provides a high-order-multiple ratio of about 1:3, which is unexpectedly high. Law et al. (2010) found a similar ratio of about 1:2 for wide M-dwarf binaries of the field and suggest that some of the binaries with large separations are actually triple and quadruple systems. (Actually, Caballero 2007 and Burgasser et al. 2007 pointed it out before.) The increment of the high-order-multiple fraction for the widest systems is supported by the work of Reipurth & Mikkola (2012), who used N-body simulations of the dynamical evolution of triple systems to suggest that loosely bound triple systems might appear to be very wide binaries. However, recent dedicated surveys for multiplicity of F, G, K (Tokovinin et al. 2014b; Elliott et al. 2015) and M dwarfs in the field (Cortés-Contreras et al. 2014) have found lower ratios of about 1:10. Although our sample comprises a wide range of masses and separations, it is not large enough to do an appropriate comparison with the previously mentioned works. Another explanation might be an observational effect of a biased sample in which surveys for nearby young stars are naturally slanted towards detecting intrinsically bright binaries and multiple stars (Malmquist bias), and active spectroscopic binaries (very close separations enhances stellar activity). The discovery of new moving groups members only based on astrometry, as in this survey, may help to alleviate this observational bias.

In Table A.5 we list our WDS identifiers in italics if they are not included in the WDS catalogue at the time of writing these lines (i.e., V4046 Sgr AB,C and six of the eight new pairs). In total, in this survey we propose 16 new stellar members of the β Pictoris moving group: six in new pairs and ten in known systems with only one reported young star. One of the new β Pictoris stars in a new pair is HD 173167 A, which was discovered by Alonso-Floriano et al. (2011) and classified afterwards as a moving group member by Moór et al. (2013). These values represent an increase of 9 % in the total number of reported β Pictoris stars and of almost 30 % in the number of wide proper motion systems in the moving group. We ran the on-line BANYAN tool[1] (Malo et al. 2013) on the 16 new proposed members of β Pictoris and calculated approximate membership probabilities (Table 2). We used the distances of the systems provided in Table A.5, our proper motion measurements in Table A.3, and radial velocities from the literature (for those objects without radial velocity measurements, we assumed the values of their companions). Although only seven of the 16 pairs showed high-probability memberships to β Pictoris (see Table 2), these results should be used with caution because most of the new candidates lack accurate distances or radial velocities.

None of the new reported wide systems have parallax measurements for both components. However, the location of the 16 stars (eight primaries and eight secondaries) in the colour-magnitude diagrams suggests that both components are located at similar distances. Definitive parallactic confirmation of common distance will have to wait until early 2016 with the second *Gaia* release. In the meantime, we can infer the true physical binding of the systems with the computation of the reduced gravitational binding energy.

3.2. Projected separations and binding energies

In Table A.5 we list the angular separations, ρ, and position angles, θ, at the 2MASS epoch of observation of the 36 wide pairs in the β Pictoris moving group. Angular separations vary from 8.2 arcsec for BD–21 1074A,Ba,Bb to about 1.3 deg for the triple system AU Mic–AT Mic AB (Luyten 1941; Caballero 2009). Among our new pairs, ρ varies from 10.6 arcsec to 24.5 arcmin.

[1] http://www.astro.umontreal.ca/~malo/banyan.php

Table 2. Membership probabilities for the 16 new β Pictoris candidates using the BANYAN on-line tool.

Simbad name	β Pic prob. [%]	Highest prob. [%]	V_r [kms^{-1}]	Reference of V_r
2MASS J00193931+1951050	83.9	β Pic	-1.7 ± 1.0^P	Schlieder et al. 2012a
EX Cet	99.9	β Pic	$+41.8 \pm 0.7$	Soubiran et al. 2013
CD–44 753 B	0.1	Tuc-Hor (99.4)	$+12.4 \pm 1.9$	Kordopatis et al. 2013
2MASS J07293670+3554531	23.4	Field (50.8)	$+10.4 \pm 0.9^P$	Schlieder et al. 2012a
L 186–67 B	0.0	Field (100)	$+40 \pm 9^P$	Kordopatis et al. 2013
2MASS J08274412+1122029	16.0	Field (84.0)	$+11.2 \pm 1.7^P$	Schlieder et al. 2012a
HD 82939 A	1.1	Field (98.9)	-0.5 ± 0.4	Gontcharov 2006
2MASS J12120849+1248050	0.0	Field (99.9)	-4.0 ± 1.0^P	Schlieder et al. 2012a
MV Vir C	0.0	AB Dor (86.0)	$+0.0 \pm 0.8^P$	Malo et al. 2014a
2MASS J16170673+7734028	0.0	Field (100)	-14.4 ± 1.0^P	Schlieder et al. 2012a
2MASS J18420483–5554126	99.9	β Pic	$+1.0 \pm 0.7^P$	Malo et al. 2013
HD 173167 A	99.9	β Pic	$+0.8 \pm 7.0$	Moór et al. 2013
HDE 331149 B	95.3	β Pic	-19.2 ± 1.1^P	Schlieder et al. 2012a
BPS CS 22898–0066	0.0	Field (100)	$+0.6 \pm 3.0$	Kordopatis et al. 2013
2MASS J21551738–0046231	75.2	β Pic	...	...
2MASS J23301129–0237227	91.2	β Pic	-5.3 ± 0.2^P	Malo et al. 2014b

Notes. $^{(P)}$ Radial velocity adopted from the primary component.

To distinguish between true very wide physical binaries and co-moving pairs of "single" stars that belong to the same kinematic group, we computed the reduced gravitational binding energies, $U_g^* = -G\mathcal{M}_1\mathcal{M}_2 s^{-1}$ (Caballero 2009), of the 36 systems. With the angular separations and distances, we obtained the projected physical separations, s, which vary from merely 100–120 au for the known pairs WDS 08228–5727 (L 186–67 Aa,Ab,B) and WDS 10596+2527 (HD 95174 AB) to about $7\,10^4$ au (0.34 pc) for the new pair WDS 08290+1125. Given the uncertainties in the distance (Table A.1), we provide only two significant figures for s.

We derived masses $\mathcal{M}_1$ and $\mathcal{M}_2$ from J-band absolute magnitudes M_J and the Baraffe et al. (2015) or Siess et al. (2000) evolutionary models at 20 Ma for solar metallicity and the appropriate mass intervals. When available, we gathered masses of single early type stars and close binaries from the literature (e.g., Strassmeier & Rice 2000; Neuhäuser et al. 2002; Caballero 2009; Donati et al. 2011; Janson et al. 2012; Elliott et al. 2015; Montet et al. 2015) or suitable information that allowed us to make a precise derivation (e.g., magnitude differences from adaptive optics or lucky imaging, mass ratios from spectroscopic monitoring – Chauvin et al. 2010; Neuhäuser et al. 2011; Janson et al. 2012; Messina et al. 2014; Bowler et al. 2015; Elliott et al. 2015). Masses range approximately from 2.4 $M_\odot$ for η Tel A to well below the substellar boundary for L 186–67 B with a broad maximum of the distribution at 0.5–1.0 $M_\odot$. Derived masses reasonably match those expected from spectral types, when available. For the sake of completeness, we also list spectral types compiled from a number of sources in Table A.5 (Riaz et al. 2006; Reid et al. 2007; Pickles & Depagne 2010; R. Caballero 2012; Janson et al. 2012; Kraus et al. 2014; Messina et al. 2014; Rodríguez et al. 2014; Mason et al. 2015; I. Gallardo & M. Gómez Garrido, priv. comm.; SIMBAD).

The greatest absolute value of reduced binding energy among the 36 systems in Table A.5, of $-U_g^* = 9800\ 10^{33}$ J, corresponds to the strongly bound pair HD 95174 AB, which is not only the tightest one, but also contains two stars of ~0.8 $M_\odot$. On the other hand, there are two very fragile system candidates with binding energies of 0.57–2.7 10^{33} J, almost one order of magnitude lower than that of the Luyten's system AU Mic+AT Mic AB, which lies at the boundary between very wide binaries and couples of single stars that are co-moving within the same stellar kinematic group (Caballero 2010; see the title of this series of papers). As a result, it is likely that the components in the two new fragile system candidates *WDS 08290+1125* and *WDS 23317–0245*, which includes the flaring star AF Psc (Bond 1976; Kraus et al. 2014; Ramsay & Doyle 2014), originated in the same parental cloud and were ejected at the same time, in the same direction, and at the same velocity, but they are not physically bound. The six other new pairs have binding energies between 13 and 1400 10^{33} J and may survive the eventual disruption by the Galactic gravitational potential for some billion years (Weinberg et al. 1987; Close et al. 2007). In any case, detecting features of youth in the spectra of *WDS 08290+1125* A and B and the wide M6.0 V companion candidate to AF Psc (Reid et al. 2007) would shed light on their actual membership in the β Pictoris moving group.

3.3. Benchmark objects and probable members in other young moving groups

The 36 wide systems tabulated by us can help to constrain the actual membership of some controversial candidate members in β Pictoris:

- WDS 01367–0645. Some authors have also classified the primary of the system, EX Cet (G5 V), as a member of the Hercules-Lyra association (~100–200 Ma – Montes et al. 2001; López-Santiago et al. 2006; Shkolnik et al. 2012; Eisenbeiss et al. 2013).
- WDS 02305–4342. The primary CD–44 753 A is also a member candidate of the Columba association (~15–50 Ma – Torres et al. 2006, 2008; Elliott et al. 2014; Malo et al. 2014a).
- WDS 08228–5727. The membership of the primary L 186–67 Aa,Ab to β Pictoris is ambiguous (Malo et al. 2013, 2014a). The late-M common proper motion companion, L 186–67 B, whose physical binding in the system had been

confirmed earlier (Bakos et al. 2002; Bergfors et al. 2010; Janson et al. 2012, 2014), would have a mass close to the deuterium-burning mass limit if it were 20 Ma old. If membership in β Pictoris were confirmed, the triple system would be a benchmark for very low-mass substellar astrophysics.
- WDS 09361+3733. While there are no membership studies for the primary, the homonymous secondary HD 82939 Ba,Bb was listed not only as a β Pictoris star by Schlieder et al. (2012a, 2012b), but also as a young field star by Malo et al. (2014b).
- *WDS 16172+7734*. Schlieder et al. (2012a) listed the primary TYC 4571–1414–1 as a probable member of both β Pictoris and AB Doradus (~70 Ma) moving groups.
- WDS 21214–6655. The primary star V390 Pav A has also been classified as a member of the Tucana-Horologium association (~30 Ma – Zuckerman et al. 2001a; Mamajek et al. 2004; Rojas et al. 2008).

If the six systems above were eventually discarded as true β Pictoris "pairs", 30 systems would still remain for further investigation in the young moving group, of which six (20 %) are reported here for the first time.

Certain systems in Table A.5 are also particularly important in the low-mass domain, because they can be used to test evolutionary models. Just to cite one example, the secondary of the pairs *WDS 16172+7734* (presented here for the first time) and WDS 21105–2711 (Bergfors et al. 2010; Malo et al. 2013, 2014b) lie close to the substellar limit and, therefore, to the lithium depletion boundary. As a result, a high-resolution spectroscopic analysis of both primaries and secondaries could shed more light on the debated age of β Pictoris.

4. Conclusions

We searched through 35 previous publications and compiled an exhaustive list of 185 members and member candidates in the nearby, young (~20 Ma) β Pictoris moving group, around which we looked for common proper-motion companions at projected physical separations of up to 10^5 au. For that, we made extensive use of the Aladin and STILTS virtual observatory tools and numerous public all-sky catalogues (e.g., WDS, PPMXL, 2MASS).

Of the 184 initial common proper-motion companion candidates, 129 were the subject of a precise astrometric follow-up, by which we measured proper motions with typical uncertainties of only 1 mas/a, and 67 of a multi-band photometric study. Eventually, we discarded five previously reported pairs and retained 36 reliable pair candidates. Of them, 18 and 10 are known systems with both components or only one component classified as β Pictoris members, respectively, and eight are new pairs in the moving group. We also report 16 new star and brown dwarf candidates in β Pictoris for the first time. These values represent an increase of 9 % in the total number of reported objects in the moving group and of almost 30 % in the number of wide proper motion systems.

We investigated the 36 pairs with available public information in detail. Among them, there are 12 triple and two quadruple systems, which points out to a greater incidence of high-order multiplicity in β Pictoris than in the field, possibly ascribed to a member list biased towards close binaries or an increment of the high-order, multiple fraction for very wide systems.

We measured angular separations and projected physical separations, compiled or derived masses for components in all systems, and computed reduced gravitational binding energies. Two of the new pair candidates could be unbound couples of single stars that are co-moving within β Pictoris, while at least one of the components in six (new and known) pairs have also been reported to belong to other young moving groups and associations (four in Hercules-Lyra, Columba, AB Doradus, Tucana-Horologium) or to the field (two). There are three pairs (one presented here) with masses of secondaries at or below the hydrogen-burning limit, and they can be used as benchmarks for upcoming age-dating works in β Pictoris. Our study provides a comprehensive analysis of the wide multiplicity in one of the closest and youngest moving groups known and, therefore, also serves as input to models of moving-group evolution and eventual dissipation by the Galactic gravitational field.

Acknowledgements. We thank the anonymous referee for the report. This research made use of the Washington Double Star Catalogue, maintained at the U.S. Naval Observatory, the SIMBAD database and VizieR catalogue access tool, operated at Centre de Données astronomiques de Strasbourg, France, and the Spanish Virtual Observatory (`http://svo.cab.inta-csic.es`). Financial support was provided by the Universidad Complutense de Madrid, the Comunidad Autónoma de Madrid, and the Spanish Ministerios de Ciencia e Innovación and of Economía y Competitividad under grants AP2009-0187, AYA2011-24052, and AYA2011-30147-C03-02, and -03.

References

Abt, H. A. 1988, Ap&SS, 142, 111
Ahn, C. P., Alexandroff, R., Allende Prieto, C., et al. 2012, ApJS, 203, 21
Alcalá, J. M., Covino, E., Torres, G., et al. 2000, A&A, 353, 186
Allen, C., Poveda, A., & Herrera, M. A. 2000, A&A, 356, 529
Alonso-Floriano, F. J., Caballero, J. A., & Montes, D. 2011, Stellar Clusters & Associations: A RIA Workshop on Gaia, 344
Alonso-Floriano, F. J., Morales, J. C., Caballero, J. A., et al. 2015, A&A, 577, A128
Bahcall, J. N., & Soneira, R. M. 1981, ApJ, 246, 122
Bakos, G. Á., Sahu, K. C., & Németh, P. 2002, ApJS, 141, 187
Baraffe, I., Homeier, D., Allard, F., & Chabrier, G. 2015, A&A, 577, A42
Barrado y Navascués, D. 1998, Ap&SS, 263, 235
Barrado y Navascués, D., Stauffer, J. R., Song, I., & Caillault, J.-P. 1999, ApJ, 520, L123
Beichman, C. A., Krist, J., Trauger, J. T., et al. 2010, PASP, 122, 162
Bergfors, C., Brandner, W., Janson, M., et al. 2010, A&A, 520, A54
Biller, B. A., Liu, M. C., Wahhaj, Z., et al. 2010, ApJ, 720, L82
Biller, B. A., Liu, M. C., Wahhaj, Z., et al. 2013, ApJ, 777, 160
Binks, A. S., & Jeffries, R. D. 2014, MNRAS, 438, L11
Boccaletti, A., Augereau, J.-C., Baudoz, P., Pantin, E., & Lagrange, A.-M. 2009, A&A, 495, 523
Bond, H. E. 1976, Information Bulletin on Variable Stars, 1160, 1
Bonfils, X., Delfosse, X., Udry, S., et al. 2005, A&A, 442, 635
Bonnarel, F., Fernique, P., Bienaymé, O., et al. 2000, A&AS, 143, 33
Bonnefoy, M., Lagrange, A.-M., Boccaletti, A., et al. 2011, A&A, 528, L15
Bonnefoy, M., Boccaletti, A., Lagrange, A.-M., et al. 2013, A&A, 555, A107
Bowler, B. P., Liu, M. C., Shkolnik, E. L., & Tamura, M. 2015, ApJS, 216, 7
Burgasser, A. J., Reid, I. N., Siegler, N., et al. 2007, Protostars and Planets V, 427
Caballero, J. A. 2007, A&A, 462, L61
Caballero, J. A. 2009, A&A, 507, 251
Caballero, J. A. 2010, A&A, 514, AA98
Caballero, J. A. 2012, The Observatory, 132, 1
Caballero, R. 2012, Journal of Double Star Observations, 8, 58
Chanamé, J., & Gould, A. 2004, ApJ, 601, 289
Chauvin, G., Lagrange, A.-M., Bonavita, M., et al. 2010, A&A, 509, A52
Churcher, L., Wyatt, M., & Smith, R. 2011, MNRAS, 410, 2
Close, L. M., Zuckerman, B., Song, I., et al. 2007, ApJ, 660, 1492
Cortés-Contreras, M., Caballero, J. A., & Montes, D. 2014, The Observatory, 134, 348
Crifo, F., Vidal-Madjar, A., Lallement, R., Ferlet, R., & Gerbaldi, M. 1997, A&A, 320, L29
Cruz, K. L., Kirkpatrick, J. D., & Burgasser, A. J. 2009, AJ, 137, 3345
Cutri, R. M. et al. 2012, VizieR on-line catalogue II/311
Cutri, R. M. et al. 2014, VizieR on-line catalogue II/328
da Silva, L., Torres, C. A. O., de La Reza, R., et al. 2009, A&A, 508, 833
Delfosse, X., Forveille, T., Beuzit, J.-L., et al. 1999, A&A, 344, 897
Dent, W. R. F., Thi, W. F., Kamp, I., et al. 2013, PASP, 125, 477
Donati, J.-F., Gregory, S. G., Montmerle, T., et al. 2011, MNRAS, 417, 1747
Eisenbeiss, T., Ammler-von Eiff, M., Roell, T., et al. 2013, A&A, 556, A53

Elliott, P., Bayo, A., Melo, C. H. F., et al. 2014, A&A, 568, A26
Elliott, P., Huélamo, N., Bouy, H., et al. 2015, A&A, 580, A88
Epchtein, N., de Batz, B., Capoani, L. et al. 1997, The Messenger, 87, 27
Evans, D. W., Irwin, M. J., & Helmer, L. 2002, A&A, 395, 347
Faherty, J. K., Burgasser, A. J., Walter, F. M., et al. 2012, ApJ, 752, 56
Gagné, J., Lafrenière, D., Doyon, R., Malo, L., & Artigau, É. 2014, ApJ, 783, 121
Gagné, J., Lafrenière, D., Doyon, R., Malo, L., & Artigau, É. 2015, ApJ, 798, 73
Girard, T. M., van Altena, W. F., Zacharias, N., et al. 2011, AJ, 142, 15
Haakonsen, C. B., & Rutledge, R. E. 2009, ApJS, 184, 138
Hambly, N. C., MacGillivray, H. T., Read, M. A., et al. 2001, MNRAS, 326, 1279
Høg, E., Fabricius, C., Makarov, V. V., et al. 2000, A&A, 355, L27
Holmberg, J., Nordström, B., & Andersen, J. 2009, A&A, 501, 941
Janson, M., Hormuth, F., Bergfors, C., et al. 2012, ApJ, 754, 44
Janson, M., Bergfors, C., Brandner, W., et al. 2014, ApJS, 214, 17
Jayawardhana, R., & Brandeker, A. 2001, ApJ, 561, L111
Jenkins, J. S., Pavlenko, Y. V., Ivanyuk, O., et al. 2012, MNRAS, 420, 3587
Jiang, Y.-F., & Tremaine, S. 2010, MNRAS, 401, 977
Kaplan, D. L., Gaensler, B. M., Kulkarni, S. R., & Slane, P. O. 2006, ApJS, 163, 344
Kasper, M., Apai, D., Janson, M., & Brandner, W. 2007, A&A, 472, 321
Kastner, J. H., Sacco, G. G., Montez, R., et al. 2011, ApJ, 740, L17
Kiss, L. L., Moór, A., Szalai, T., et al. 2011, MNRAS, 411, 117
Kordopatis, G., Gilmore, G., Steinmetz, M., et al. 2013, AJ, 146, 134
Kraus, A. L., Shkolnik, E. L., Allers, K. N., & Liu, M. C. 2014, AJ, 147, 146
Lafrenière, D., Doyon, R., Marois, C., et al. 2007, ApJ, 670, 1367
Lagrange, A.-M., Gratadour, D., Chauvin, G., et al. 2009, A&A, 493, L21
Lagrange, A.-M., Bonnefoy, M., Chauvin, G., et al. 2010, Science, 329, 57
Lasker, B. M., Lattanzi, M. G., McLean, B. J., et al. 2008, AJ, 136, 735
Law, N. M., Dhital, S., Kraus, A., Stassun, K. G., & West, A. A. 2010, ApJ, 720, 1727
Lépine, S., & Simon, M. 2009, AJ, 137, 3632
Lépine, S., & Gaidos, E. 2011, AJ, 142, 138
Li, T., Marshall, J. L., Lépine, S., Williams, P., & Chavez, J. 2014, AJ, 148, 60
Lissauer, J. J. 2007, ApJ, 660, L149
López-Santiago, J., Montes, D., Crespo-Chacón, I., & Fernández-Figueroa, M. J. 2006, ApJ, 643, 1160
Luger, R., Barnes, R., Lopez, E., et al. 2015, Astrobiology, 15, 57
Luhman, K. L., Mamajek, E. E., Allen, P. R., & Cruz, K. L. 2009, ApJ, 703, 399
Luyten, W. J. 1941, Bruce proper motion survey, Minneapolis
Luyten, W. J. 1979, New Luyten catalogue of stars with proper motions larger than two tenths of an arcsecond and first supplement (Minneapolis)
Macintosh, B., Graham, J. R., Barman, T., et al. 2015, Science, in press (eprint arXiv:1508.03084)
Makarov, V. V. 2007, ApJS, 169, 105
Males, J. R., Close, L. M., Morzinski, K. M., et al. 2014, ApJ, 786, 32
Malo, L., Doyon, R., Lafrenière, D., et al. 2013, ApJ, 762, 88
Malo, L., Artigau, É., Doyon, R., et al. 2014a, ApJ, 788, 81
Malo, L., Doyon, R., Feiden, G. A., et al. 2014b, ApJ, 792, 37
Mamajek, E. E., & Bell, C. P. M. 2014, MNRAS, 445, 2169
Marks, M., Janson, M., Kroupa, P., Leigh, N., & Thies, I. 2015, MNRAS, 452, 1014
Mason, B. D., Wycoff, G. L., Hartkopf, W. I., Douglass, G. G., & Worley, C. E. 2001, AJ, 122, 3466
Mason, B. D., Wycoff, G. L., Hartkopf, W. I., Douglass, G. G., & Worley, C. E. 2015, VizieR on-line catalogue, B/WDS
McCarthy, K., & White, R. J. 2012, AJ, 143, 134
Messina, S., Monard, B., Biazzo, K., Melo, C. H. F., & Frasca, A. 2014, A&A, 570, A19
Metchev, S. A., Eisner, J. A., Hillenbrand, L. A., & Wolf, S. 2005, ApJ, 622, 451
Monet, D. G., Canzian, B., Harris, H. et al. 1998, VizieR on-line catalogue I/243
Monet, D. G., Levine, S. E., Canzian, B., et al. 2003, AJ, 125, 984
Montes, D., López-Santiago, J., Gálvez, M. C., et al. 2001, MNRAS, 328, 45
Montet, B. T., Bowler, B. P., Shkolnik, E. L., et al. 2015, ApJL, in press (eprint arXiv:1508.05945)
Moór, A., Ábrahám, P., Derekas, A., et al. 2006, ApJ, 644, 525
Moór, A., Szabó, G. M., Kiss, L. L., et al. 2013, MNRAS, 435, 1376
Mouillet, D., Larwood, J. D., Papaloizou, J. C. B., & Lagrange, A. M. 1997, MNRAS, 292, 896
Mugrauer, M., Vogt, N., Neuhäuser, R., & Schmidt, T. O. B. 2010, A&A, 523, L1
Nakajima, T., Morino, J.-I., & Fukagawa, M. 2010, AJ, 140, 713
Nakajima, T., & Morino, J.-I. 2012, AJ, 143, 2
Newton, E. R., Charbonneau, D., Irwin, J., et al. 2014, AJ, 147, 20
Neuhäuser, R., Guenther, E., Mugrauer, M., Ott, T., & Eckart, A. 2002, A&A, 395, 877
Neuhäuser, R., Guenther, E. W., Alves, J., et al. 2003, AN, 324, 535
Neuhäuser, R., Ginski, C., Schmidt, T. O. B., & Mugrauer, M. 2011, MNRAS, 416, 1430
Nordström, B., Mayor, M., Andersen, J., et al. 2004, A&A, 418, 989
Ortega, V. G., de la Reza, R., Jilinski, E., & Bazzanella, B. 2002, ApJ, 575, L75
Ortega, V. G., de la Reza, R., Jilinski, E., & Bazzanella, B. 2004, ApJ, 609, 243
Parker, R. J., Goodwin, S. P., Kroupa, P., & Kouwenhoven, M. B. N. 2009, MNRAS, 397, 1577
Pickles, A., & Depagne, É. 2010, PASP, 122, 1437
Poveda, A., & Allen, C. 2004, RMxAC, 21, 49
Gontcharov, G. A. 2006, Astronomy Letters, 32, 759
Quinn, D. P., Wilkinson, M. I., Irwin, M. J., et al. 2009, MNRAS, 396, L11
Rameau, J., Chauvin, G., Lagrange, A.-M., et al. 2013, A&A, 553, A60
Ramírez, R. M., & Kaltenegger, L. 2014, ApJ, 797, L25
Ramsay, G., & Doyle, J. G. 2014, MNRAS, 442, 2926
Reid, I. N., Hawley, S. L., & Gizis, J. E. 1995, AJ, 110, 1838
Reid, I. N., Cruz, K. L., & Allen, P. R. 2007, AJ, 133, 2825
Reipurth, B., & Mikkola, S. 2012, Nature, 492, 221
Retterer, J. M., & King, I. R. 1982, ApJ, 254, 214
Riaz, B., Gizis, J. E., & Harvin, J. 2006, AJ, 132, 866
Rice, E. L., Faherty, J. K., & Cruz, K. L. 2010, ApJ, 715, L165
Riedel, A. R., Finch, C. T., Henry, T. J., et al. 2014, AJ, 147, 85
Rodríguez, D. R., Zuckerman, B., Faherty, J. K., & Vican, L. 2014, A&A, 567, A20
Roeser, S., Demleitner, M., & Schilbach, E. 2010, AJ, 139, 2440
Rojas, G., Gregorio-Hetem, J., & Hetem, A. 2008, MNRAS, 387, 1335
Rojas-Ayala, B., Covey, K. R., Muirhead, P. S., & Lloyd, J. P. 2012, ApJ, 748, 93
Saarinen, S., & Gilmore, G. 1989, MNRAS, 237, 311
Schlieder, J. E., Lépine, S., & Simon, M. 2010, AJ, 140, 119
Schlieder, J. E., Lépine, S., & Simon, M. 2012a, AJ, 143, 80
Schlieder, J. E., Lépine, S., & Simon, M. 2012b, AJ, 144, 109
Shaya, E. J., & Olling, R. P. 2011, ApJS, 192, 2
Shkolnik, E., Liu, M. C., & Reid, I. N. 2009, ApJ, 699, 649
Shkolnik, E. L., Anglada-Escudé, G., Liu, M. C., et al. 2012, ApJ, 758, 56
Siess, L., Dufour, E., & Forestini, M. 2000, A&A, 358, 593
Skrutskie, M. F., Cutri, R. M., Stiening, R., et al. 2006, AJ, 131, 1163
Smart, R. L. 2013, VizieR on-line catalogues I/324
Smith, B. A., & Terrile, R. J. 1984, Science, 226, 1421
Song, I., Bessell, M. S., & Zuckerman, B. 2002, ApJ, 581, L43
Song, I., Zuckerman, B., & Bessell, M. S. 2003, ApJ, 599, 342
Strassmeier, K. G., & Rice, J. B. 2000, A&A, 360, 1019
Taylor, M. B. 2006, Astronomical Data Analysis Software and Systems XV, 351, 666
Teixeira, R., Ducourant, C., Chauvin, G., et al. 2009, A&A, 503, 281
Tian, F. 2015, Icarus, 258, 50
Tian, F., & Ida, S. 2015, Nature Geoscience, 8, 177
Tokovinin, A. 2014a, AJ, 147, 86
Tokovinin, A. 2014b, AJ, 147, 87
Tokovinin, A., & Lépine, S. 2012, AJ, 144, 102
Tolbert, C. R. 1964, ApJ, 139, 1105
Torres, C. A. O., Quast, G. R., da Silva, L., et al. 2006, A&A, 460, 695
Torres, C. A. O., Quast, G. R., Melo, C. H. F., & Sterzik, M. F. 2008, Handbook of Star Forming Regions, Volume II, 757
Urban, S. E., Corbin, T. E., Wycoff, G. L., et al. 1998, AJ, 115, 1212
van Altena, W. F., Lee, J. T., & Hoffleit, E. D. 1995, New Haven, CT: Yale University Observatory, 4th ed.
van Leeuwen, F. 2007, A&A, 474, 653
Voges, W., Aschenbach, B., Boller, T., et al. 1999, A&A, 349, 389
Wahhaj, Z., Liu, M. C., Nielsen, E. L., et al. 2013, ApJ, 773, 179
Ward-Duong, K., Patience, J., de Rosa, R. J., et al. 2015, MNRAS, 449, 2618
Wasserman, I., & Weinberg, M. D. 1991, ApJ, 382, 149
Weinberg, M. D., Shapiro, S. L., & Wasserman, I. 1987, ApJ, 312, 367
Yee, J. C., & Jensen, E. L. N. 2010, ApJ, 711, 303
Yoo, J., Chanamé, J., & Gould, A. 2004, ApJ, 601, 311
Zacharias, N., Finch, C. T., Girard, T. M., et al. 2013, AJ, 145, 44
Zuckerman, B., & Song, I. 2004, ARA&A, 42, 685
Zuckerman, B., Song, I., & Webb, R. A. 2001a, ApJ, 559, 388
Zuckerman, B., Song, I., Bessell, M. S., & Webb, R. A. 2001b, ApJ, 562, L87

4

Conclusions and future work

"Less is more"
— Ludwig Mies van der Rohe (1960s)

4.1 Conclusions

This dissertation is mainly focused on providing a list of target candidates to detect exoplanets with CARMENES. Two journal publications are presented on this PhD thesis work. The first publication is related with the low-resolution characterisation of low-mass candidates. It was basically addressed to obtain accurate spectral types used to provide a robust sample of M dwarfs, while the second paper compiled a sample of β Pictoris members and candidates members for studying and searching for wide binaries using the common proper motion technique. The young low-mass objects obtained are highly interesting for the study of exoplanetary formation, evolution and habitability in young M-type stars. However, the two publications presented can be understood independently and, therefore, both of them presented particular conclusions beyond the general goal of CARMENES.

The conclusions derived from this PhD thesis work can be summarised as follow:

- Low-resolution spectroscopy observations were carried out with the CAFOS spectrograph for 753 objects. Most of them were M-dwarf candidates with poorly constrained spectral types. We studied the sample combining two least-squares minimisation techniques and 31 spectral indices. We identified the best five indices for spectral typing (TiO 2, TiO 5, PC1, VO-7912 and Color-M). We provided for the whole sample: spectral types, chromospheric activity levels ($pEW(\mathrm{H}\alpha)$ measurements) and quantification of gravity and metallicity (ζ index).
- Accurate spectral types, with a typical error of 0.5 subtypes, were provided from mid-K to late-M dwarfs. The comparisons with the widely used catalogues of M-type stars, PMSU and Lépine et al (2013), supported the quality of the spectral typing results and the homogeneity of the spectral types used for the CARMENCITA input catalogue.
- Giant stars and very young objects were identified using the Ratio C and the CaH series of related spectral indices, which were also used for the spectroscopic characterisation and are sensitive to surface gravity. The metallicity of the stars were quantified using the parameter ζ, which is based on the TiO 5, CaH 2 and CaH 3 spectral indices. The use of the parameter ζ showed that most of the sample objects present a solar metallicity.

- The $pEW(\mathrm{H}\alpha)$ measurements quantified the chromospheric activity level of the studied stars, which is interesting for CARMENES due to the possible radial velocity variations induced by starspots. We also found that none of the studied stars showed $pEW(\mathrm{H}\alpha)$ measurements compatible with an accretion process. Moreover, the activity levels of the sample did not induce significant variation on the determined spectral types and, therefore, this effect can be neglected.

- In summary, the characterisation allowed us to identify 25 K and M giants, three T Tauri stars, two subdwarfs candidates, 44 K dwarfs and 679 M dwarfs. We also identified **49 late-type stars (including the T Tauri stars)** as young dwarfs in star-forming regions or moving groups. From the 683 M-type stars (including subdwarfs and T Tauri stars), 520 fulfilled the CARMENES requirements to be included in the list of input targets.

- An unprecedented list of 185 β Pictoris members and candidate members were collected from 35 previous publications. We searched for common proper motion companions, especially low-mass stars, around the objects of this list. The search made use of virtual observatory tools and public all-sky catalogues to find companions up to 10^5 au. We provided short- and long-term multiplicity information for the whole sample, as well as a catalogue of accurate proper motions.

- The catalogue of proper motions provided accurate measurements for 184 companion candidates, of which 129 were computed by us. This catalogue can be useful for several astronomical purposes, such as the determination of moving group membership of those objects with young indicators.

- Five previously catalogued companions were rejected after the astrometric study and we were able to recover 36 reliable pair candidates after the photometric study. Of them, 18 and 10 were known systems with both components or only one component classified as β Pictoris members. In addition, eight systems were presented for first time, two of them with both components classified as β Pictoris members. We also reported 16 new star and brown dwarf candidates in this association. These values represent and increase of 9 % in the total number of reported objects in the moving group and almost a 30 % in the number of wide proper motion systems. Therefore, the methodology developed to search for proper motion companions is highly profitable for study long term multiplicity.

- Twelve of the wide pairs studied are triples and other two are quadruple systems. This unexpected large number of high-order multiple systems may suggest a biased list of members towards close binaries (Malmquist bias) or an increment of the high-order-multiple fraction for very wide systems at young ages.

- The new pairs presented need a deeper investigation (especially distance determinations) to confirm their binary nature and their membership to β Pictoris. Meanwhile, we measured angular separations and projected physical separations, compiled or derived masses for components in all systems, and computed reduced gravitational binding energies. Two of the new pair candidates could be unbound couples of single stars that are co-moving within the moving group. Moreover, six pairs (new and known) presented at least one component that has also been reported to belong to other young moving groups and associations (four in Hercules-Lyra, Columba, AB Doradus, Tucana-Horologium) or to the field (two).

- There are three pairs with masses of secondaries at or below the hydrogen burning limit, which can be used as benchmarks for next age-dating investigations in β Pictoris.

- Our study provides a comprehensive analysis of the wide multiplicity in one of the closest and youngest moving groups known and, therefore, also serves as an input to models of moving-group evolution and eventual dissipation by the Galactic gravitational field.

- In addition, the low-mass objects studied in this research (compiled or presented for the first time) are highly valuable as targets for exoplanetary studies in order to investigate the formation, evolution and habitability of exoplanets in M-type stars.

4.2 Future work

The present thesis is part of the science preparation for CARMENES. Therefore, the information provided in the two publications was stored in the input catalogue of CARMENES and will be used to develop other investigations inside the CARMENES consortium, such as the sample characterisation using high-resolution spectroscopy and imaging.

High-resolution spectroscopy provides other fundamental information for the selection of the final sample, such as the rotational velocity ($v \sin i$) and the identification of single- and double-line spectroscopic binaries. It is fundamental to identify fast rotator stars and spectroscopic binaries, because they should be removed from the CARMENES target list. We have observed ∼500 M dwarfs using high-resolution spectrographs (FEROS, CAFE, HRS; $R = 30{,}000$–$48{,}000$), from which we are determining rotational velocities with an accuracy better than 0.5-0.2 $\mathrm{km\,s^{-1}}$, and radial velocities with a stability better than 0.2-0.1 $\mathrm{km\,s^{-1}}$. Our aim is to have at least two spectra at different epochs of the final 300 CARMENES targets. Part of this task was developed during this PhD thesis in a three-month stay at the Institut für Astrophysik Göttingen, which is the CARMENES institution responsible of the characterisation of M dwarfs using high-resolution spectra. We presented some preliminary high-resolution spectroscopy results for ∼200 M dwarfs at the Protostar & Planets VI conference (see Alonso-Floriano et al. 2013b). This high-resolution study is still on going and we keep our collaboration (see Alonso-Floriano et al. 2015a; Montes et al. 2015; Jeffers et al. in prep.). Furthermore, the CARMENES consortium will also use the high-resolution spectra and Phoenix models to obtain fundamental parameters of the observed M dwarfs (Passegger et al. 2014).

However, the data provided in Alonso-Floriano et al. (2015b,c) might be used for other investigations outside the CARMENES consortium. For example, in Alonso-Floriano et al. (2015b) we realised that young objects present smaller Ratio C values than older stars of the same spectral type. The Ratio C index is an indicator of the Na I $\lambda\lambda$8183,8195 Å strength, which is very sensitive to the surface gravity of the star and, therefore –until the end of the star contraction– to the age (see Schlieder et al. 2012). This index might be useful not only for detecting very young objects and giant stars, but to provide an age estimation of the objects after an appropriate calibration.

We have already started another project to develop a metallicity calibration yardstick for cool stars using relatively bright F-,G-,K-type primaries with M dwarf companions. Some authors have made use of some tens of these wide pairs and photometric data or spectral features to obtain metallicity calibrations (Rojas-Ayala et al. 2012; Mann et al. 2013, 2014). However, we aim to use a large sample of wide pairs and spectroscopic data to obtain more accurate measurements. The tools developed in this thesis will be used to study more CAFOS spectra, already obtained, to measure the indices and spectral types. In addition, we will obtain chemical abundances using high-resolution spectra of the hotter primaries, also already observed (Tabernero et al. 2012; Tabernero 2014). We will use the metallicity values of the primaries as if they were the metallicity values of the cooler

objects for calibrating the parameter ζ or other suitable index. Some preliminary results have been presented at the 17^{th} Cool stars conference (Montes et al. 2012) and at the Protostar & Planets conference (Montes et al. 2013; see Fig. 4.1).

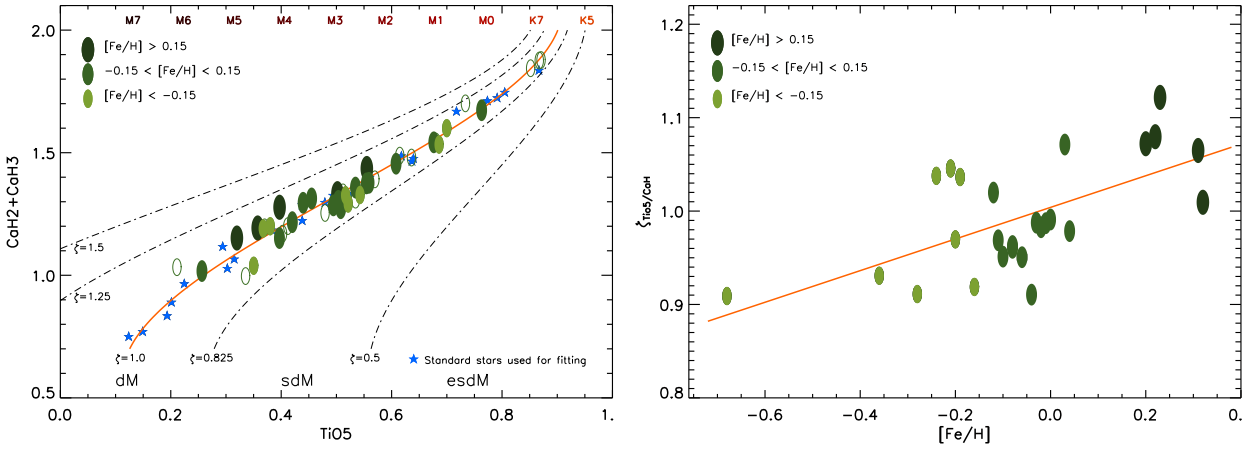

FIGURE 4.1— Preliminary results on the metallicity calibration future work, presented by Montes et al. (2013). *Left panel:* CaH 2 + CaH 3 vs. TIO 5 index-index diagram of standard stars and M-dwarfs in wide systems (green ellipses). The values of [Fe/H] come from measurements on high-resolution spectra of F,G, K primary companions. The indices are obtained from low-resolution CAFOS spectra using the same technique presented in Chapter 2. The indices are combined to obtain the metallicity sensitive index, ζ (The solid and dash-dotted lines are iso-metallicity curves of this index). The spectral types at the top are indicative. *Right panel:* ζ index vs. [Fe/H]. It shows the relationship between the ζ index and the metallicity values used for the M dwarfs. The calibration of this relationship will provide metallicity values, [Fe/H], from the CH 2, CH 3 and TiO 5 indices.

Finally, the methodology used by Alonso-Floriano et al. (2015c) can be applied to other stellar kinematic groups to obtain samples of different ages. These possible samples are interesting for a number of investigations on astrophysics, e.g., star formation theories, exoplanetary evolution, age-dating of moving groups (see, Binks & Jeffries 2014). We have already tested a similar methodology in the Local Association and its subgroups AB Doradus and Tucana-Horologium (Alonso-Floriano et al. 2011, 2013a), finding unknown proper motion pairs with low-mass companions –some of them, such as HD 143809 B, have been observed in the CARMENES science preparation. However, all the new candidates, or even some of the previous known ones, will need of deeper investigations that provide important data, such as distances, radial velocity, age by lithium detection, spectral types, etc.

References

Alonso-Floriano, F. J., Caballero, J. A., & Montes, D. 2011, Stellar Clusters & Associations: A RIA Workshop on Gaia, 344

Alonso-Floriano, F. J., Caballero, J. A., & Montes, D. 2013b, Highlights of Spanish Astrophysics VII, 432

Alonso-Floriano, F. J., Montes, D., Jeffers, S., et al. 2013a, Protostars and Planets VI Posters, 21

Alonso-Floriano, F. J., Montes, D., Caballero, J. A., et al. 2015a, 18th Cambridge Workshop on Cool Stars, Stellar Systems, and the Sun, 18, 796

Alonso-Floriano, F. J., Morales, J. C., Caballero, J. A., et al. 2015b, A&A, 577, A128

Alonso-Floriano, F. J., Caballero, J. A., Cortés-Contreras, M, et al. 2015c, A&A, in press, arXiv:1508.06929, doi:10.1051/0004-6361/201526795

Binks, A. S., & Jeffries, R. D. 2014, MNRAS, 438, L1

Lépine, S., Hilton, E. J., Mann, A. W., et al. 2013, AJ, 145, 102

Mann, A. W., Brewer, J. M., Gaidos, E., Lépine, S., & Hilton, E. J. 2013, AJ, 145, 52

Mann, A. W., Deacon, N. R., Gaidos, E., et al. 2014, AJ, 147, 160

Montes, D., Alonso-Floriano, F. J., Caballero, J. A., et al. 2012, Proceedings of the Cool stars 17, The 17th Cool Stars, Stellar Systems and the Sun workshop

Montes, D., Alonso-Floriano, F. J., Tabernero, H. M., et al. 2013, Protostars and Planets VI Posters, 22

Montes, D., Caballero, J. A., Jeffers, S., et al. 2015, Highlights of Spanish Astrophysics VIII, 605

Passegger, V. M.. Wende, S., Reiners, A., et al. 2014, Towards other Earths II: the star-planet connection, http://carmenes.caha.es/ext/conferences/CARMENES_TOEII2014_Passegger.pdf

Rojas-Ayala, B. 2013, European Physical Journal Web of Conferences, 47, 09004

Schlieder, J. E., Lépine, S., Rice, E., et al. 2012, AJ, 143, 114

Tabernero, H. M. 2014, PhD Thesis, Universidad Complutense de Madrid

Tabernero, H. M., Montes, D., & González Hernández, J. I. 2012, A&A, 547, A13

A

List of publications

A.1 Published in refereed journals

A.1.1 In this thesis

1. *CARMENES input catalogue of M dwarfs. I. Low-resolution spectroscopy with CAFOS.*
   Alonso-Floriano, F. J., Morales, J. C., Caballero, J. A., et al. 2015, A&A, 577, A128.

2. *Reaching the boundary between stellar kinematic groups and very wide binaries III. Sixteen new stars and eight new wide systems in the β Pictoris moving group.*
   Alonso-Floriano, F. J., Caballero, J. A., Cortés-Contreras, M, et al. 2015, A&A, in press, arXiv:1508.06929, doi:10.1051/0004-6361/201526795.

A.1.2 Additional publications

1. *CARMENES. I: instrument and survey overview.*
   A. Quirrenbach, P. J. Amado, W. Seifert, et al. (including Alonso-Floriano) 2012, SPIE, 8446, E0R

2. *CARMENES instrument overview.*
   A. Quirrenbach, P. J. Amado, J. A. Caballero et al. (including Alonso-Floriano) 2014, SPIE, 9147, E1F

3. *CARMENES input catalogue of M dwarfs II. High-resolution imaging with FastCam.*
   M. Cortés-Contreras, V. J. S. Béjar, J. A. Caballero, et al. (including Alonso-Floriano) A&A, in prep.

4. *CARMENES input catalogue of M dwarfs III. High-resolution spectroscopy with FEROS, CAFE and HRS.*
   S. Jeffers. et al. (including Alonso-Floriano), A&A, in prep.

A.2 Conference proceedings

1. *An Aladin-based search for proper-motion companions to young stars in the Local Association, Tucana-Horologium and β Pictoris.*

Alonso-Floriano, F. J., Caballero, J. A., & Montes, D. 2011, Stellar Clusters & Associations: A RIA Workshop on Gaia, 344 (23–27 May 2011, Granada, Spain).

2. *Spectral characterisation of the CARMENES input catalogue.*
   Klutsch, A., Alonso-Floriano, F. J., Caballero, J. A., et al. 2012, SF2A-2012: Proceedings of the Annual meeting of the French Society of Astronomy and Astrophysics, 357 (5–8 June 2012, Nice, France).

3. *Calibrating the metallicity of M-dwarfs with wide visual binaries.*
   Montes, D., Alonso-Floriano, F. J., Caballero, J. A., et al. 2012, The 17th Cool Stars, Stellar Systems and the Sun workshop (24–29 June 2012, Barcelona, Spain).

4. *CARMENES. II. CARMENCITA, the input catalogue archive.*
   Caballero, J.A., Cortés-Contreras, M., López-Santiago, J., et al. 2012, The 17th Cool Stars, Stellar Systems and the Sun workshop (24–29 June 2012, Barcelona, Spain).

5. *CARMENES. IV. Preliminary low resolution spectroscopic characterisation.*
   Alonso-Floriano, F. J., Montes, D., Caballero, J. A., et al. 2012, The 17th Cool Stars, Stellar Systems and the Sun workshop (24–29 June 2012, Barcelona, Spain).

6. *CARMENES. II. Characterisation of the stellar sample.*
   Montes, D., Alonso-Floriano, F. J., Caballero, J. A., et al. Proceedings of the IAU Symposium 293 (27–31 August 2012, Beijing, China).

7. *CARMENES. IV. Preliminary low-resolution spectroscopic characterisation.*
   Alonso-Floriano, F. J., Montes, D., Caballero, J. A., et al. 2013, Highlights of Spanish Astrophysics VII, 43. Proceedings of the X Reunión Científica de la Sociedad Espaola de Astronomía (9–13 July 2012, Valencia, Spain).

8. *Searching for common proper-motion companions in the Local Association and its young kinematic subgroups.*
   Alonso-Floriano, F. J., Montes, D., Caballero, J. A., et al. 2013, Highlights of Spanish Astrophysics VII, 431. Proceedings of the X Reunión Científica de la Sociedad Espaola de Astronomía (9–13 July 2012, Valencia, Spain).

9. *CARMENES. III. CARMENCITA, the input catalogue.*
   Caballero, J. A., Cortés-Contreras, M., López-Santiago, J., et al. 2013, Highlights of Spanish Astrophysics VII, 645. Proceedings of the X Reunión Científica de la Sociedad Espaola de Astronomía (9–13 July 2012, Valencia, Spain).

10. *CARMENES. V. M dwarfs in multiple systems.*
    Cortés-Contreras, M., Caballero, J. A., Alonso-Floriano, F. J., et al. 2013, Highlights of Spanish Astrophysics VII, 646. Proceedings of the X Reunión Científica de la Sociedad Espaola de Astronomía (9–13 July 2012, Valencia, Spain).

11. *CARMENES. II. Science case and M-dwarf sample.*
    Morales, J. C., Ribas, I., Caballero, J. A., et al. 2013, Highlights of Spanish Astrophysics VII, 664. Proceedings of the X Reunión Científica de la Sociedad Espaola de Astronomía (9–13 July 2012, Valencia, Spain).

12. *CARMENES at PPVI. CARMENCITA Herbs and Spices to Help you Prepare a Genuine Target Sample.*
Caballero, J. A., Cortés-Contreras, M., Alonso-Floriano, F. J., et al. 2013, Protostars and Planets VI Posters, 20 (15–20 July 2013, Heidelberg, Germany).

13. *CARMENES at PPVI. High-Resolution Spectroscopy of M Dwarfs with FEROS, CAFE and HRS.*
Alonso-Floriano, F. J., Montes, D., Jeffers, S., et al. 2013, Protostars and Planets VI Posters, 21 (15–20 July 2013, Heidelberg, Germany).

14. *CARMENES at PPVI. Calibrating the Metallicity of M-Dwarfs with Wide Visual Binaries.*
Montes, D., Alonso-Floriano, F. J., Tabernero, H. M., Caballero, J. A., González Hernández, J. I., Klutsch, A., Cortés-Contreras, M., et al. Protostars and Planets VI Posters, 22 (15–20 July 2013, Heidelberg, Germany).

15. *CARMENES at PPVI. Low-Resolution Spectroscopy of M Dwarfs with CAFOS at Calar Alto.*
Mundt, R., Alonso-Floriano, F. J., Caballero, J. A., et al. 2013, Protostars and Planets VI Posters, 55 (15–20 July 2013, Heidelberg, Germany).

16. *CARMENES: Blue planets orbiting red dwarfs.*
Quirrenbach, A., Amado, P. J., Caballero, J. A., et al. 2014, IAU Symposium, 299, 395 (2–7 June 2013, Victoria, Canada).

17. *Preparation of the CARMENES Input Catalogue: Mining Public Archives for Stellar Parameters and Spectra of M Dwarfs with Master Thesis Students.*
Montes, D., Caballero, J. A., Alonso-Floriano, F. J., et al. 2015, 18th Cambridge Workshop on Cool Stars, Stellar Systems, and the Sun, 18, 651 (7–12 June 2014, Flagstaff, US).

18. *Preparation of the CARMENES Input Catalogue: Low- and High-resolution Spectroscopy of M dwarfs.*
Alonso-Floriano, F. J., Montes, D., Caballero, J. A., et al. 2015, 18th Cambridge Workshop on Cool Stars, Stellar Systems, and the Sun, 18, 796 (7–12 June 2014, Flagstaff, US).

19. *Preparation of the CARMENES Input Catalogue: Multiplicity of M dwarfs from Tenths of Arcseconds to Hundreds of Arcminutes.*
Cortés-Contreras, M., Caballero, J. A., Bejar, V. J. S., et al. 2015, 18th Cambridge Workshop on Cool Stars, Stellar Systems, and the Sun, 18, 805 (7-12 June 2014, Flagstaff, US).

20. *CARMENES science preparation: low-resolution spectroscopy of M dwarfs.*
Alonso-Floriano, F. J., Montes, D., Caballero, J. A., et al. 2015, Highlights of Spanish Astrophysics VIII, 441. Proceedings of the XI Reunión Científica de la Sociedad Espaola de Astronomía (8–12 September 2014, Teruel, Spain).

21. *CARMENES. Mining public archives for stellar parameters and spectra of M dwarfs with master thesis students.*
Caballero, J. A., Montes, D., Alonso-Floriano, F. J., et al. 2015, Highlights of Spanish Astrophysics VIII, 595. Proceedings of the XI Reunión Científica de la Sociedad Espaola de Astronomía (8–12 September 2014, Teruel, Spain).

22. *CARMENES. Multiplicity of M dwarfs from tenths of arcseconds to hundreds of arcminutes.*
Cortés-Contreras, M., J. S. Béjar, V., Caballero, J. A., et al. 2015, Highlights of Spanish

Astrophysics VIII, 597. Proceedings of the XI Reunión Científica de la Sociedad Espaola de Astronomía (8–12 September 2014, Teruel, Spain).

23. *CARMENES science preparation. High-resolution spectroscopy of M dwarfs.*
Montes, D., Caballero, J. A., Jeffers, S., et al. 2015, Highlights of Spanish Astrophysics VIII, 605. Proceedings of the XI Reunión Científica de la Sociedad Espaola de Astronomía (8–12 September 2014, Teruel, Spain).

24. *Kinematics of M dwarfs in the CARMENES input catalogue: membership in young moving groups.*
D. Montes, J.A. Caballero, I. Gallardo, et al. 2015, Proceedings IAU Symposium No. 314, Young Stars & Planets Near the Sun, 2015, J. H. Kastner, B. Stelzer, & S. A. Metchev, eds, in press (11–15 May 2015, Atlanta, US).

B

Long tables of Chapter 2

This is the on-line material of the paper included in Chapter 2, available at VizieR:
http://vizier.cfa.harvard.edu/viz-bin/VizieR?-source=J/A+A/577/A128

- Table B.1: basic star data, observing date and exposure time for the sample observed with CAFOS. It corresponds to Table A.1 of the article. Col. 1 object number; Col. 2 CARMENES identification (JHHMMm+DDdAAA), which consists in the truncate coordinates of the object preceded by the letter J, also ends by the cardinal positions, N, S, E or W when is needed to discriminate between close objects; Col. 3 discovery or most common name; Col. 4 Gliese or Gliese & Jahreiss star number; Col. 5-6 infrared coordinates of the object (J2000.0); Col. 7 J-band magnitude; Col. 8 date of CAFOS observation; Col. 9 number of exposure and exposure time.

- Table B.2: some spectral indices used for the spectral typing, activity and metallicity characterisation. It corresponds to Table A.2 of the article. Col. 1 CARMENES identification; Col. 2-6 indices used for the spectra typing; Col. 7-8 indices used to calculate the metallic index ζ; Col. 9 ζ metallicity index; Col. 10 pseudo-equivalent width of Hα line measured by us.

- Table B.3: spectral types adopted. We assigned a value between 0.0 and 8.0 in steps of 0.5 to each M spectral subtype of dwarf luminosity class. In addition, the K5 V and K7 V spectral types correspond to -2 and -1 respectively (we follow the standard classification where there are no K6, 8, 9 subtypes). It corresponds to Table A.3 of the article. Col. 1 CARMENES identification; Col. 2 spectral type from literature, small "m" and "k" denote spectral types estimated from photometry; Col. 3 reference for the spectral type; Col. 4-5 numeric spectral types determined by best-match and χ^2 methods; Col.6-10 numeric spectral types determined by indices technique; Col. 11 adopted spectral type, some odd spectra are indicated with a colon (probably young dwarfs of low gravity or subdwarfs of low metallicity).

Table B.1: Observed stars: identification, common name, Gliese number, 2MASS coordinates and J magnitude, observing date, and exposure time.

No.	Karmn	Name	Gl/GJ	α (J2000)	δ (J2000)	J [mag]	Observation date	$N \times t_{\mathrm{exp}}$ [s]
1	J00066–070 AB	2MASS J00063925–0705354	...	00:06:39.20	–07:05:35.3	9.83	04 Aug 2012	1×1000
2	J00077+603 AB	G 217–032	...	00:07:42.60	+60:22:54.3	8.91	24 Sep 2012	1×600
3	J00115+591	LSR J0011+5908	...	00:11:31.82	+59:08:40.0	9.95	11 Jan 2012	2×700
4	J00118+229	LP 348–40	...	00:11:53.03	+22:59:04.7	8.86	07 Dec 2011	1×250
5	J00119+330	G 130–053	...	00:11:56.54	+33:03:17.8	9.07	07 Dec 2011	1×220
6	J00122+304	1RXS J001213.6+302906	...	00:12:13.41	+30:28:44.3	10.24	12 Nov 2011	1×600
7	J00133+275	[ACM2014] J0013+2733	...	00:13:19.52	+27:33:31.1	10.43	12 Nov 2011	1×900
8	J00136+806	G 242–048	3014 A	00:13:38.71	+80:39:56.8	7.76	01 Sep 2012	1×300
9	J00146+202	χ Peg	...	00:14:36.16	+20:12:24.1	1.76	11 Jan 2012	1×1
10	J00152+530	G 217–040	...	00:15:14.53	+53:04:45.7	10.82	14 Feb 2013	1×800
11	J00162+198W	EZ Psc	1006 A	00:16:14.63	+19:51:37.6	7.88	22 Sep 2012	1×100
12	J00162+198E	LP 404–062	1006 B	00:16:16.08	+19:51:51.5	8.89	22 Sep 2012	1×180
13	J00183+440	GX And	15 A	00:18:22.57	+44:01:22.2	5.25	11 Nov 2011	1×40
14	J00228–164	PM I00228–1627	...	00:22:50.20	–16:27:44.3	10.25	02 Aug 2012	3×500
15	J00240+264	LSPM J0024+2626	...	00:24:03.77	+26:26:29.9	10.22	12 Nov 2011	1×700
16	J00253+235	LP 349–017	...	00:25:19.60	+23:32:51.2	9.79	08 Dec 2011	1×800
17	J00297+012	LP 585–038	...	00:29:43.22	+01:12:38.5	9.15	08 Dec 2011	1×700
18	J00313+336	G 130–073	...	00:31:20.10	+33:37:37.5	8.75	08 Dec 2011	1×700
19	J00313+001	LP 585–046	...	00:31:21.50	+00:09:29.4	9.76	03 Aug 2012	1×650
20	J00322+544	G 217–056	...	00:32:15.74	+54:29:02.7	9.39	08 Dec 2011	1×350
21	J00328–045 AB	GR* 50	...	00:32:53.14	–04:34:06.8	9.28	08 Dec 2011	1×350
22	J00358+526	NLTT 1920	...	00:35:53.22	+52:41:12.4	8.93	01 Sep 2012	1×350
23	J00367+444	V428 And	...	00:36:46.44	+44:29:18.9	2.26	11 Jan 2012	1×4
24	J00380+169	PM I00380+1656	...	00:38:03.86	+16:56:02.9	9.38	08 Dec 2011	1×800
25	J00389+306	Wolf 1056	26	00:38:58.79	+30:36:58.4	7.45	22 Sep 2012	1×30
26	J00395+149S	LP 465–061	...	00:39:33.49	+14:54:18.9	9.96	07 Dec 2011	1×700
27	J00395+149N	LP 465–062	...	00:39:33.74	+14:54:34.8	9.83	09 Jan 2012	1×700
28	J00452+002 AB	HD 4271 BC	...	00:45:13.59	+00:15:51.0	10.11	04 Sep 2012	1×800
29	J00464+506	G 172–022	...	00:46:29.90	+50:38:38.9	9.96	03 Jan 2012	1×800
30	J00467–044	HD 4449 B	...	00:46:43.36	–04:24:45.5	11.20	02 Sep 2012	2×800
31	J00484+753	LSPM J0048+7518	...	00:48:29.71	+75:18:48.0	9.49	03 Jan 2012	1×300
32	J00490+657	PM I00490+6544	...	00:49:04.77	+65:44:37.8	9.30	03 Jan 2012	1×300
33	J00490+578	η Cas B	34 B	00:49:05.20	+57:49:03.8	7.17	04 Aug 2012	1×25
34	J00502+601	HD 236547	...	00:50:16.44	+60:07:55.8	5.50	11 Jan 2012	1×40
35	J00502+086	RX J0050.2+0837	...	00:50:17.53	+08:37:34.1	9.75	10 Jan 2012	1×750
36	J00540+691	Ross 317	...	00:54:00.49	+69:11:01.3	9.46	07 Dec 2011	1×300

Table B.1: Observed stars: identification, common name, Gliese number, 2MASS coordinates and J magnitude, observing date, and exposure time (cont.).

No.	Karmn	Name	Gl/GJ	α (J2000)	δ (J2000)	J [mag]	Observation date	$N \times t_{\rm exp}$ [s]
37	J00548+275	G 069–032	...	00:54:48.03	+27:31:03.6	10.34	24 Sep 2012	2×600
38	J00580+393	1RXS J005802.4+391912	...	00:58:01.16	+39:19:11.2	9.56	09 Jan 2012	1×800
39	J01009–044	LP 646–077	1025	01:00:56.44	–04:26:56.1	9.04	22 Sep 2012	1×200
40	J01012+571	1RXS J010112.8+570839	...	01:01:13.46	+57:08:44.4	10.05	11 Jan 2012	1×700
41	J01014–010	LP 586–043	...	01:01:24.60	–01:05:58.6	9.27	03 Aug 2012	1×210
42	J01014+188	G 033–032	...	01:01:26.70	+18:53:10.0	9.63	08 Dec 2011	1×400
43	J01026+623	BD+61 195	49 A	01:02:38.96	+62:20:42.2	6.23	02 Sep 2012	1×80
44	J01028+189	RX J0102.8+1857	...	01:02:51.00	+18:56:54.2	9.51	03 Aug 2012	1×600
45	J01028+470	G 172–035	...	01:02:53.50	+47:03:03.0	9.35	03 Aug 2012	1×600
46	J01032+712	LP 29–70	...	01:03:14.50	+71:13:12.7	9.69	03 Jan 2012	1×600
47	J01033+623	V388 Cas	51 B	01:03:19.72	+62:21:55.7	8.61	10 Feb 2012	1×700
48	J01055+153	HD 6440 B	9038 B	01:05:29.75	+15:23:18.6	7.15	15 Feb 2013	2×150
49	J01069+804	NLTT 3583	...	01:06:54.74	+80:27:24.4	9.35	03 Jan 2012	1×500
50	J01074–025	RAVE J010727.5–023326	...	01:07:27.50	–02:33:26.4	10.38	25 Sep 2012	3×900
51	J01076+229E	HD 6660 B	53.1 B	01:07:38.50	+22:57:21.9	9.53	04 Sep 2012	1×300
52	J01097+356	Mirach	53.3	01:09:43.92	+35:37:14.0	–0.96	11 Jan 2012	1×0.3
53	J01186–008	HD 7895 B	56.3 B	01:18:40.18	–00:52:27.6	8.01	04 Sep 2012	1×100
54	J01214+313	BD+30 206 B	...	01:21:27.40	+31:20:32.7	9.98	04 Sep 2012	1×500
55	J01226+127	BD+12 168	...	01:22:36.60	+12:45:03.4	7.86	12 Feb 2013	1×400 $+1 \times 300$
56	J01342–015	LP 588–009	...	01:34:12.35	–01:34:26.0	11.72	04 Sep 2012	2×700
57	J01356–200 AB	G 272–050	...	01:35:39.90	–20:03:42.6	8.99	24 Sep 2012	3×600
58	J01390–179 AB	BL Cet + UV Cet	65 AB	01:39:01.20	–17:57:02.7	6.28	11 Nov 2011	1×900
59	J01406–081	PM I01406–0808	...	01:40:39.60	–08:08:54.4	10.37	25 Sep 2012	1×900
60	J01431+210	RX J0143.1+2101	...	01:43:11.90	+21:01:10.6	9.25	03 Aug 2012	1×450
61	J01541–156	LP 768–670	...	01:54:08.00	–15:36:22.3	9.81	01 Sep 2012	1×600
62	J01551–162	PM I01551–1615	...	01:55:06.60	–16:15:52.3	9.94	10 Jan 2012	1×700
63	J01562+001	RX J0156.2+0006	...	01:56:14.90	+00:06:08.9	9.49	03 Aug 2012	1×700
64	J01567+305	Koenigstuhl 4 A	...	01:56:45.71	+30:33:28.8	10.32	12 Nov 2011	1×900
65	J01571–102	HD 11964 B	81.1 B	01:57:11.00	–10:14:53.3	8.41	04 Sep 2012	1×150
66	J02000+135 AB	LP 469–041 AB	...	02:00:02.30	+13:34:50.7	9.31	03 Aug 2012	1×300
67	J02002+130	TZ Ari	83.1	02:00:12.79	+13:03:11.2	7.51	11 Nov 2011	1×500
68	J02019+342	PM I02019+3413	...	02:01:58.70	+34:13:45.0	9.51	07 Dec 2011	1×900
69	J02022+103	LP 469–067	3128	02:02:16.21	+10:20:13.7	9.84	03 Aug 2012	1×1200
70	J02023+012	LP 589–023	...	02:02:22.40	+01:15:42.8	9.81	07 Dec 2011	1×600
71	J02100–088	LP 709–043	...	02:10:03.70	–08:52:59.7	8.95	14 Feb 2013	1×400
72	J02133+368 AB	EUVE J0213+36.8	...	02:13:20.62	+36:48:50.7	9.37	07 Dec 2011	1×400
73	J02142–039	LP 649–072	...	02:14:12.51	–03:57:43.4	10.48	04 Aug 2012	3×900

Table B.1: Observed stars: identification, common name, Gliese number, 2MASS coordinates and J magnitude, observing date, and exposure time (cont.).

No.	Karmn	Name	Gl/GJ	α (J2000)	δ (J2000)	J [mag]	Observation date	$N \times t_{\rm exp}$ [s]
74	J02159–094 ABC	EUVE J0215–09.5	...	02:15:58.90	–09:29:12.2	8.43	14 Feb 2013	1×150
75	J02274+031	PM I02274+0310	...	02:27:27.56	+03:10:54.8	9.98	10 Jan 2012	1×800
76	J02285–200	HD 15468 C	100 C	02:28:31.89	–20:02:26.5	9.18	12 Nov 2011	1×300
77	J02291+228	BD+22 353B	...	02:29:06.99	+22:52:01.9	8.73	12 Feb 2013	1×300
78	J02362+068	BX Cet	105 B	02:36:15.36	+06:52:19.1	7.33	12 Nov 2011	1×300
79	J02367+226	G 036–026	...	02:36:44.13	+22:40:26.5	10.08	22 Sep 2012	2×600
80	J02412–045	G 075–035	...	02:41:15.11	–04:32:17.7	9.20	08 Dec 2011	1×400
81	J02441+492	θ Per B	107 B	02:44:10.25	+49:13:54.1	6.69	12 Nov 2011	1×120
82	J02456+449	G 078–004	3178 A	02:45:39.63	+44:56:55.7	7.82	22 Sep 2012	1×30
83	J02479–124	Z Eri	...	02:47:55.92	–12:27:38.3	1.59	09 Feb 2012	1×2
84	J02502+628	G 246–012	...	02:50:16.44	+62:51:19.8	9.37	08 Dec 2011	1×400
85	J02530+168	Teegarden's star	...	02:53:00.85	+16:52:53.3	8.39	22 Sep 2012	2×500
86	J02555+268	HD 18143 C	118.2 C	02:55:35.73	+26:52:20.9	9.56	09 Jan 2012	1×500
87	J02558+183	ρ^{02} Ari	...	02:55:48.50	+18:19:53.9	0.23	08 Dec 2011	1×2
88	J02562+239	LSPM J0256+2359	...	02:56:13.96	+23:59:10.5	9.98	08 Dec 2011	1×900
89	J03026–181	LP 771–72	121.1	03:02:38.01	–18:09:58.7	8.21	22 Sep 2012	1×50
90	J03033–080	StM 20	...	03:03:21.32	–08:05:15.4	9.12	08 Dec 2011	1×200
91	J03047+617	HD 18757 B	3195 B	03:04:43.35	+61:44:09.7	8.88	09 Jan 2012	1×300
92	J03110–046	LP 652–062	...	03:11:04.89	–04:36:35.8	9.41	08 Dec 2011	1×250
93	J03147+114	RX J0314.7+1127	...	03:14:47.02	+11:27:27.2	9.35	03 Jan 2012	1×250
94	J03154+578	G 246–030	...	03:15:29.44	+57:51:33.0	11.12	01 Sep 2012	1×800
95	J03162+581S	Ross 370 A	130.1 A	03:16:13.82	+58:10:02.4	7.34	01 Sep 2012	1×300
96	J03162+581N	Ross 370 B	130.1 B	03:16:13.90	+58:10:07.3	7.50	01 Sep 2012	1×300
97	J03167+389	HAT 168–01565	...	03:16:46.13	+38:55:27.4	9.16	03 Jan 2012	1×210
98	J03174–011	LP 592–031	...	03:17:28.12	–01:07:29.7	9.73	14 Feb 2013	1×300
99	J03179–010	G 077–042	...	03:17:55.33	–01:05:44.2	10.81	14 Feb 2013	1×900
100	J03181+426	Wolf 140	...	03:18:07.01	+42:40:09.1	9.25	09 Jan 2012	1×300
101	J03194+619	G 246–033	...	03:19:28.80	+61:56:04.4	9.51	07 Dec 2011	1×650
102	J03236+476	Koenig 33	...	03:23:37.70	+47:37:26.5	9.48	07 Dec 2011	1×750
103	J03236+056	1RXS J032338.7+054117	...	03:23:39.16	+05:41:15.3	9.87	10 Jan 2012	1×800
104	J03263+171	TYC 1237–889–1	...	03:26:23.62	+17:09:30.9	9.77	08 Dec 2011	1×650
105	J03275+222	[ACM2014] J0327+2212	...	03:27:30.84	+22:12:38.3	10.04	09 Jan 2012	1×800
106	J03294+117	PM I03294+1142	...	03:29:25.20	+11:42:11.3	9.34	03 Aug 2012	1×300
107	J03303+346	1RXS J033021.4+340444	...	03:30:23.32	+34:40:32.6	10.00	06 Mar 2012	1×650
108	J03309+706	LP 031–368	...	03:30:54.74	+70:41:14.6	9.49	03 Jan 2012	1×500
109	J03319+492	TYC 3320–337–1	...	03:31:57.00	+49:12:58.4	9.00	12 Feb 2013	1×300
110	J03320+436	HD 21727 B	...	03:32:05.99	+43:40:01.0	9.24	12 Feb 2013	1×500
111	J03325+287 ABC	RX J0332.6+2843	...	03:32:35.79	+28:43:55.5	9.36	07 Dec 2011	1×400

Table B.1: Observed stars: identification, common name, Gliese number, 2MASS coordinates and J magnitude, observing date, and exposure time (cont.).

No.	Karmn	Name	Gl/GJ	α (J2000)	δ (J2000)	J [mag]	Observation date	$N \times t_{\rm exp}$ [s]
112	J03332+462	V577 Per B	...	03:33:14.04	+46:15:19.4	8.38	04 Sep 2012	1×150
113	J03354+428	HD 22122 B	...	03:35:28.52	+42:53:35.0	10.83	12 Feb 2013	1×700
114	J03356–084	LP 653–013	...	03:35:38.50	–08:29:22.4	10.38	01 Sep 2012	3×600
115	J03361+313	[GBM90] Per 49	...	03:36:08.68	+31:18:39.8	9.19	03 Jan 2012	1×600
116	J03375+288	PM I03375+2852	...	03:37:30.30	+28:52:28.3	9.47	07 Dec 2011	1×250
117	J03375+178N AB	LP 413–018	3239 A	03:37:33.32	+17:51:14.6	9.10	24 Sep 2012	1×120
118	J03375+178S AB	LP 413–019	3240 B	03:37:33.87	+17:51:00.5	9.19	24 Sep 2012	1×200
119	J03392+565 AB	G 175–002	...	03:39:15.30	+56:32:05.9	9.99	07 Dec 2011	1×1100
120	J03430+459	NLTT 11633	...	03:43:02.07	+45:54:18.2	9.67	03 Jan 2012	1×600
121	J03466+243 AB	V642 Tau	...	03:46:37.30	+24:20:36.6	10.12	03 Jan 2012	1×500
122	J03473–019	G 080–021	...	03:47:23.30	–01:58:19.8	7.80	14 Feb 2013	1×90
123	J03480+405	HD 23596 B	...	03:48:05.88	+40:32:22.6	9.35	25 Sep 2012	1×300
124	J03510+142	PM I03510+1413 A	...	03:51:00.79	+14:13:39.9	9.44	06 Mar 2012	1×400
125	J03519+397	HDE 275867 B	...	03:51:58.14	+39:46:56.7	8.28	15 Feb 2013	1×150
126	J03548+163 AB	HG 7–33	...	03:54:53.20	+16:18:56.4	9.96	04 Jan 2012	1×800
127	J03556+522	HD 24421 B	...	03:55:36.89	+52:14:29.1	10.89	12 Feb 2013	1×1500
128	J03565+319	1RXS J035632.5+315746	...	03:56:33.08	+31:57:24.8	9.80	04 Jan 2012	1×600
129	J03566+507	43 Per B	...	03:56:40.57	+50:42:48.1	8.15	25 Sep 2012	1×300
130	J03574–011 AB	HD 24916 BC	157 BC	03:57:28.92	–01:09:23.4	7.77	10 Feb 2012	1×220
131	J03588+125	G 007–014	...	03:58:49.06	+12:30:24.2	9.76	04 Jan 2012	1×700
132	J04041+307	G 038–024	...	04:04:06.16	+30:42:45.5	9.26	13 Dec 2011	1×300
133	J04061–055	2MASS J04060688–0534444	...	04:06:06.88	–05:34:44.4	9.13	13 Dec 2011	1×300
134	J04079+142	HDE 286475 B	...	04:07:54.80	+14:13:00.7	9.22	10 Jan 2012	1×300
135	J04081+743	LP 032–016	...	04:08:11.01	+74:23:01.8	9.25	09 Jan 2012	1×400
136	J04083+691	LP 031–433	...	04:08:23.72	+69:10:59.3	10.26	11 Jan 2012	2×500
137	J04123+162 AB	HG 7–124	...	04:12:21.73	+16:15:03.3	9.74	09 Jan 2012	1×700
138	J04153–076	o^{02} Eri C	166 C	04:15:21.73	–07:39:17.4	6.75	09 Feb 2012	1×200
139	J04177+410	LSPM J0417+4103	...	04:17:44.31	+41:03:13.8	9.24	11 Jan 2012	1×300
140	J04177+136 AB	HG 7–153	...	04:17:47.70	+13:39:42.3	9.41	07 Dec 2011	1×300
141	J04191–074	LP 654–039	...	04:19:06.60	–07:27:44.8	9.97	07 Dec 2011	1×700
142	J04191+097	PM I04191+0944	...	04:19:08.09	+09:44:48.2	9.99	04 Jan 2012	1×700
143	J04205+815	PM I04205+8131	...	04:20:35.05	+81:31:55.6	9.48	11 Jan 2012	1×400
144	J04206+272	XEST 16–045	...	04:20:39.18	+27:17:31.7	10.50	02 Sep 2012	2×600
145	J04206–168	DG Eri	...	04:20:41.35	–16:49:47.9	2.99	13 Dec 2011	1×10
146	J04207+152 AB	HG 7–172	...	04:20:47.96	+15:14:09.2	9.49	04 Jan 2012	1×600
147	J04224+036	RX J0422.4+0337	...	04:22:25.04	+03:37:08.2	9.86	07 Dec 2011	1×900
148	J04227+205	LP 415–030	...	04:22:42.84	+20:34:12.5	10.46	11 Jan 2012	3×700
149	J04229+259	G 008–031	...	04:22:59.26	+25:59:14.8	9.65	11 Jan 2012	1×700

Table B.1: Observed stars: identification, common name, Gliese number, 2MASS coordinates and J magnitude, observing date, and exposure time (cont.).

No.	Karmn	Name	Gl/GJ	α (J2000)	δ (J2000)	J [mag]	Observation date	$N \times t_{\mathrm{exp}}$ [s]
150	J04234+809	1RXS J042323.2+805511	...	04:23:29.05	+80:55:10.2	9.41	06 Mar 2012	1×450
151	J04238+149 AB	IN Tau	...	04:23:50.33	+14:55:17.4	9.29	04 Jan 2012	1×400
152	J04238+092 AB	HG 7–192	...	04:23:50.70	+09:12:19.4	9.12	06 Mar 2012	1×220
153	J04247–067 ABC	1RXS J042441.9–064725	...	04:24:42.60	–06:47:31.3	9.57	06 Aug 2012	1×700
154	J04252+172 ABC	V805 Tau	...	04:25:13.53	+17:16:05.6	9.15	09 Jan 2012	1×300
155	J04290+186	V1103 Tau	...	04:29:01.00	+18:40:25.4	9.57	04 Jan 2012	1×500
156	J04308–088	Koeningstuhl 2 A	...	04:30:52.03	–08:49:19.3	9.85	02 Sep 2012	1×800
157	J04310+367	1RXS J043100.0+364800	...	04:31:00.10	+36:47:54.8	9.45	04 Jan 2012	1×800
158	J04313+241 AB	V927 Tau	...	04:31:23.82	+24:10:52.9	9.73	24 Sep 2012	1×350
159	J04329+001S	LP 595–023	...	04:32:56.24	+00:06:15.9	8.42	04 Sep 2012	1×250
160	J04347–004	G 082–033	...	04:34:45.32	–00:26:46.4	9.31	10 Jan 2012	1×300
161	J04360+188	LP 415–1582	...	04:36:04.17	+18:53:18.9	9.77	03 Jan 2012	1×500
162	J04366+186	LP 415–1619	...	04:36:38.90	+18:36:56.8	9.78	09 Feb 2012	1×568
163	J04373+193	LP 415–1644	...	04:37:21.89	+19:21:17.5	10.18	03 Jan 2012	1×500
164	J04386–115	LP 715–039	...	04:38:37.20	–11:30:14.8	8.67	14 Feb 2013	1×200
165	J04388+217	NLTT 13673	...	04:38:53.53	+21:47:54.9	9.55	10 Jan 2012	1×600
166	J04393+335	V583 Aur B	...	04:39:23.20	+33:31:49.4	9.92	10 Jan 2012	1×700
167	J04398+251	2MASS J04394898+2509262	...	04:39:48.98	+25:09:26.2	9.64	09 Feb 2012	1×450
168	J04413+327	NLTT 13733	...	04:41:23.88	+32:42:22.8	9.46	11 Jan 2012	1×500
169	J04425+204 AB	LP 415–345	...	04:42:30.30	+20:27:11.4	9.40	01 Sep 2012	1×500
170	J04430+187 AB	HD 285970	...	04:43:01.43	+18:42:41.9	7.75	25 Sep 2012	1×150
171	J04458–144	PM I04458–1426	...	04:45:52.70	–14:26:25.8	9.09	02 Sep 2012	1×300
172	J04468–112 AB	1RXS J044652.0–111658	...	04:46:51.70	–11:16:47.7	8.14	14 Feb 2013	1×150
173	J04472+206	RX J0447.2+2038	...	04:47:12.25	+20:38:10.9	9.38	10 Sep 2012	1×1200
174	J04494+484 AB	G 081–034	...	04:49:29.47	+48:28:45.9	9.06	10 Feb 2012	1×431
175	J04496–153	2MASS J04455273–1426259	...	04:49:37.00	–15:22:52.6	10.32	24 Sep 2012	4×900
176	J04499+711	NLTT 13933	...	04:49:55.70	+71:09:47.0	9.63	09 Jan 2012	1×500
177	J04536+623	G 247–039	...	04:53:40.12	+62:19:03.9	9.23	04 Jan 2012	1×800
178	J04538+158	LSPM J0453+1549	...	04:53:50.05	+15:49:15.6	9.43	09 Feb 2012	1×327
179	J04544+650	1RXS J045430.9+650451	...	04:54:29.82	+65:04:41.1	9.67	13 Dec 2011	1×700
180	J04559+046	HD 31412 B	9169 B	04:55:54.46	+04:40:16.4	5.97	09 Feb 2012	1×150
181	J04560+432	G 096–010	...	04:56:03.54	+43:13:55.6	9.30	10 Feb 2012	1×358
182	J05003+251 AB	HD 31867 B	...	05:00:19.52	+25:07:51.0	9.41	15 Feb 2013	1×250
183	J05019+011	1RXS J050156.7+010845	...	05:01:56.70	+01:08:42.9	8.53	24 Sep 2012	1×180
184	J05030+213 AB	HDE 285190 BC	...	05:03:05.63	+21:22:36.2	9.75	07 Dec 2011	1×1100
185	J05032+213	HDE 285190 A	...	05:03:16.08	+21:23:56.4	7.45	02 Sep 2012	1×300
186	J05050+442	PM I05050+4414	...	05:05:05.92	+44:14:03.8	9.83	07 Dec 2011	1×800
187	J05062+046	RX J0506.2+0439	...	05:06:12.90	+04:39:27.2	8.91	24 Sep 2012	1×280

Table B.1: Observed stars: identification, common name, Gliese number, 2MASS coordinates and J magnitude, observing date, and exposure time (cont.).

No.	Karmn	Name	Gl/GJ	α (J2000)	δ (J2000)	J [mag]	Observation date	$N \times t_{\rm exp}$ [s]
188	J05068+516	9 Aur C	187.2 C	05:06:49.19	+51:36:35.3	7.34	25 Sep 2012	1×200
189	J05072+375	1RXS J050714.8+373103	...	05:07:14.49	+37:30:42.1	10.28	04 Jan 2012	3×700
190	J05083+756	LP 015–315	...	05:08:18.41	+75:38:15.5	9.39	07 Dec 2011	1×600
191	J05151–073	LHS 1747	3340	05:15:08.05	–07:20:48.6	8.36	25 Sep 2012	1×700
192	J05152+236	[ACM2004] J0515+2336	...	05:15:17.54	+23:36:26.1	10.19	09 Jan 2012	1×1000
193	J05173+321	G 086–037	...	05:17:19.96	+32:07:35.0	9.24	11 feb 2012	1×250
194	J05175+487	HAT 94–03592	...	05:17:33.60	+48:46:14.5	9.97	08 Dec 2011	1×500
195	J05187+464	PM I05187+4629	...	05:18:44.56	+46:29:59.5	9.96	13 Dec 2011	1×900
196	J05187–213	HD 34751 B	199 B	05:18:47.54	–21:23:36.5	7.85	15 Feb 2013	1×250
197	J05195+649	1RXS J051929.3+645435	...	05:19:31.20	+64:54:33.8	8.95	24 Sep 2012	1×300
198	J05200–229	PM I05200–2257	...	05:20:03.50	–22:57:03.3	9.17	02 Sep 2012	1×200
199	J05223+305	PM I05223+3031	...	05:22:20.53	+30:31:09.7	9.41	10 Feb 2012	1×350
200	J05256–091 AB	LP 717–036	...	05:25:41.70	–09:09:12.5	8.45	14 Feb 2013	1×160
201	J05289+125	HD 35956 B	3348	05:28:56.50	+12:31:53.9	9.65	10 Feb 2012	1×600
202	J05294+155E	LP 417–212	2043 A	05:29:27.04	+15:34:38.4	7.56	24 Sep 2012	1×60
203	J05295–113	PM I05295–1119	...	05:29:32.90	–11:19:57.3	10.13	04 Jan 2012	1×900
204	J05300+121W	AHD 19 B	...	05:30:01.70	+12:07:26.5	9.65	03 Jan 2012	1×700
205	J05300+121E	AHD 19 A	...	05:30:02.30	+12:07:34.8	10.25	03 Jan 2012	1×700
206	J05314–036	HD 36395	205	05:31:27.35	–03:40:35.7	5.00	14 Dec 2011	1×300
207	J05320–030 AB	V1311 Ori	...	05:32:04.50	–03:05:29.4	7.88	14 Feb 2013	1×160
208	J05324–072	BD–07 1110	...	05:32:26.90	–07:14:19.0	7.95	14 Feb 2013	1×90
209	J05328+338	LHS 5108	...	05:32:51.95	+33:49:47.5	9.39	03 Jan 2012	1×300
210	J05342+103S	Ross 45 B	3353	05:34:15.08	+10:19:09.2	9.19	02 Sep 2012	1×300
211	J05342+103N	Ross 45 A	3354	05:34:15.14	+10:19:14.2	8.56	02 Sep 2012	1×300
212	J05394+747	NLTT 15320	...	05:39:25.41	+74:46:04.9	9.33	03 Jan 2012	1×350
213	J05415+534	HD 37394 B	212 B	05:41:30.73	+53:29:23.3	6.59	10 Feb 2012	1×90
214	J05421+124	V1352 Ori	213	05:42:08.98	+12:29:25.3	7.12	11 Jan 2012	1×300
215	J05424+506	LP 159–15	...	05:42:25.00	+50:38:41.4	9.91	03 Jan 2012	1×650
216	J05425+154	1RXS J054232.1+152459	...	05:42:31.78	+15:25:01.6	9.44	10 Jan 2012	1×300
217	J05427+026	HD 38014 B	...	05:42:45.50	+02:41:41.5	9.45	09 Feb 2012	1×300
218	J05455–119	PM I05455–1158	...	05:45:31.98	–11:58:03.5	9.59	11 feb 2012	1×600
219	J05456+729	PM I05456+7255	...	05:45:38.80	+72:55:12.7	9.4	13 Dec 2011	1×1200
220	J05456+111	PM I05456+1107	...	05:45:41.60	+11:07:48.5	9.90	09 Jan 2012	1×1200
221	J05457–223	γ Lep C (vB 1)	216 C	05:45:43.22	–22:20:03.5	11.13	12 Feb 2013	1×1200
222	J05458+729	PM I05458+7254	...	05:45:49.74	+72:54:07.2	9.34	02 Jan 2012	1×300
223	J05463+012	HD 38529 B	...	05:46:19.38	+01:12:47.2	9.72	09 Feb 2012	1×300
224	J05501+051	1RXS J055009.0+051154	...	05:50:08.60	+05:11:53.7	9.37	11 Jan 2012	1×300
225	J05511+122	PM I05511+1216	...	05:51:10.40	+12:16:10.2	9.45	11 feb 2012	1×350

Table B.1: Observed stars: identification, common name, Gliese number, 2MASS coordinates and J magnitude, observing date, and exposure time (cont.).

No.	Karmn	Name	Gl/GJ	α (J2000)	δ (J2000)	J [mag]	Observation date	$N \times t_{\rm exp}$ [s]
226	J05566–103	1RXS J055641.0-101837	...	05:56:40.66	–10:18:37.9	9.07	11 feb 2012	1×350
227	J05582–046	HD 40397 C	3377 C	05:58:17.17	–04:38:01.3	11.11	14 Feb 2013	4×800
228	J05588+213	LHS 6097	...	05:58:53.33	+21:21:01.1	9.97	09 Jan 2012	3×600
229	J05596+585	EG Cam	3371 A	05:59:37.75	+58:35:35.1	7.07	22 Sep 2012	1×150
230	J06024+663	LP 057–046	...	06:02:25.54	+66:20:40.4	9.86	08 Dec 2011	1×1000
231	J06024+498	G 192–015	3380	06:02:29.18	+49:51:56.2	9.35	06 Mar 2012	1×800
232	J06035+168	1RXS J060334.8+165128	...	06:03:34.62	+16:51:45.7	9.39	09 Feb 2012	1×358
233	J06035+155	TYC 1313–1482–1	...	06:03:34.80	+15:31:30.9	8.2	08 Dec 2011	1×1000
234	J06054+608	LP 086–173	...	06:05:29.36	+60:49:23.2	9.10	13 Dec 2011	1×300
235	J06065+045	vB 2	...	06:06:30.57	+04:30:32.7	11.16	15 Feb 2013	2×500
236	J06066+465	PM I06066+4633	...	06:06:37.89	+46:33:46.3	9.23	14 Dec 2011	1×300
237	J06075+472	EUVE J0607+47.2	...	06:07:31.85	+47:12:26.6	9.72	14 Dec 2011	1×900
238	J06102+225	2E 1607	...	06:10:17.76	+22:34:19.9	9.88	01 Jan 2012	1×683
239	J06103+722	LSPM J0610+7212	...	06:10:18.26	+72:12:00.6	9.27	04 Jan 2012	1×600
240	J06145+025	LP 564–051	...	06:14:34.91	+02:30:27.4	9.30	07 Dec 2011	1×650
241	J06151–164	LP 779–034	...	06:15:11.99	–16:26:15.2	9.28	06 Mar 2012	1×520
242	J06171+051 AB	HD 43587 BC	231.1 BC	06:17:10.65	+05:07:02.4	9.09	10 Feb 2012	1×300
243	J06185+250	NLTT 16348	...	06:18:34.80	+25:03:06.4	9.95	09 Jan 2012	1×700
244	J06236–096 AB	LP 720–010	...	06:23:38.50	–09:38:51.7	9.82	10 Jan 2012	1×700
245	J06238+456	LP 160–022	...	06:23:51.24	+45:40:05.1	10.35	01 Jan 2012	3×750
246	J06246+234	Ross 64	232	06:24:41.32	+23:25:58.6	8.66	24 Sep 2012	1×650
247	J06298–027 AB	G 108–004	...	06:29:50.28	–02:47:45.5	9.47	03 Jan 2012	1×250
248	J06307+397	PM I06307+3947	...	06:30:47.42	+39:47:37.1	9.41	03 Jan 2012	1×250
249	J06313+006	HDE 291725 B	...	06:31:23.74	+00:36:44.5	11.08	12 feb 2013	1×1500
250	J06314–016	G 106–054	...	06:31:28.52	–01:41:20.8	10.55	15 Feb 2013	1×500
251	J06323–097	PM I06323–0943	...	06:32:20.29	–09:43:29.0	9.85	13 Dec 2011	1×500
252	J06325+641	LP 057–192	...	06:32:30.61	+64:06:20.7	9.81	03 Jan 2012	1×600
253	J06332+054	HD 46375 B	...	06:33:12.09	+05:27:53.2	8.70	09 Feb 2012	1×220
254	J06354–040 AB	1RXS J063531.2–040314	...	06:35:29.87	–04:03:18.5	9.27	11 Feb 2012	1×500
255	J06361+201	LP 420–004	...	06:36:11.93	+20:08:14.2	9.43	03 Jan 2012	1×250
256	J06367+378	BD+37 1545B	...	06:36:43.22	+37:51:31.7	11.44	14 Feb 2013	3×800
257	J06401–164	LP 780–023	...	06:40:08.61	–16:27:26.9	9.12	03 Jan 2012	1×200
258	J06435+166	G 110–014	...	06:43:34.77	+16:41:34.9	9.78	04 Jan 2012	1×1000
259	J06461+325	HDE 263175 B	3409	06:46:07.50	+32:33:14.9	8.99	09 Feb 2012	1×250
260	J06474+054	G 108–027	...	06:47:27.51	+05:24:28.2	9.45	09 Feb 2012	1×272
261	J06489+211	1RXS J064855.9+210754	...	06:48:55.22	+21:08:03.9	9.37	03 Jan 2012	1×250
262	J06509–091	LP 661–002	...	06:50:59.48	–09:10:50.6	9.40	09 Feb 2012	1×250
263	J06522+627	G 250–025	...	06:52:16.60	+62:46:58.5	9.42	03 Jan 2012	1×350

Table B.1: Observed stars: identification, common name, Gliese number, 2MASS coordinates and J magnitude, observing date, and exposure time (cont.).

No.	Karmn	Name	Gl/GJ	α (J2000)	δ (J2000)	J [mag]	Observation date	$N \times t_{\rm exp}$ [s]
264	J06522+179	PM 06522+1756	...	06:52:16.80	+17:56:19.5	9.68	13 Dec 2011	1×350
265	J06523–051S AB	HD 50281 B	250 B	06:52:18.04	–05:11:24.1	6.58	14 Nov 2011	1×200
266	J06523–051N	HD 50281 A	250 A	06:52:18.05	–05:10:25.4	5.01	14 Nov 2011	1×200
267	J06548+332	HDE 265866	251	06:54:49.03	+33:16:05.9	6.10	06 Mar 2012	1×60
268	J06565+440	G 107–036	...	06:56:30.94	+44:01:56.8	9.92	13 Dec 2011	1×700
269	J07001–190	1RXS J070005.1–190115	...	07:00:06.83	–19:01:23.6	9.03	06 Mar 2012	1×900
270	J07009–023	PM I07009–0221	...	07:00:59.78	–02:21:33.0	9.30	13 Dec 2011	1×300
271	J07031+836	HD 48974 B	...	07:03:10.98	+83:38:58.9	11.11	15 Feb 2013	3×450
272	J07051–101	1RXS J070511.2–100801	...	07:05:11.95	–10:07:52.8	10.20	03 Jan 2012	3×500
273	J07105–087	1RXS J071032.6–084232	...	07:10:31.47	–08:42:48.5	9.05	10 Jan 2012	1×350
274	J07105+283	StKM 1–629	...	07:10:34.20	+28:22:41.9	8.92	13 Dec 2011	1×300
275	J07111–035	PM I07111–0334	...	07:11:09.00	–03:34:11.7	9.10	14 Dec 2011	3×700
276	J07111+434 AB	LP 206–011	...	07:11:11.38	+43:29:59.0	9.98	01 Jan 2012	3×700
277	J07172–050	SCR J0717–0501	...	07:17:17.10	–05:01:03.1	8.87	14 Feb 2013	1×500
278	J07182+137	PM I07182+1342	...	07:18:12.91	+13:42:16.7	9.36	13 Dec 2011	1×300
279	J07191+667	HD 55745 B	...	07:19:09.18	+66:44:29.8	8.88	12 Feb 2013	1×600
280	J07195+328	BD+33 1505	270	07:19:31.28	+32:49:48.3	7.18	03 Mar 2012	1×150
281	J07219–222	PM I07219–2216	...	07:21:57.50	–22:16:38.4	10.00	10 Jan 2012	1×800
282	J07274+052	Luyten's star	273	07:27:24.50	+05:13:32.9	5.71	12 Nov 2011	1×180
283	J07310+460	1RXS J073101.9+460030	...	07:31:01.29	+46:00:26.6	9.95	13 Dec 2011	1×700
284	J07319+362N	BL Lyn	277 B	07:31:57.35	+36:13:47.8	7.57	06 Mar 2012	1×200
285	J07319+362S AB	VV Lyn	277 A	07:31:57.74	+36:13:10.2	6.77	06 Mar 2012	1×200
286	J07321–088	HD 59984 B	3450	07:32:07.26	–08:53:01.7	8.03	12 Feb 2013	1×200
287	J07324–130	PM I07324–1304	...	07:32:28.40	–13:04:09.0	9.89	04 Jan 2012	1×1200
288	J07359+785	LP 017–066	...	07:35:58.15	+78:32:52.9	9.21	03 Jan 2012	1×210
289	J07361–031	HD 61606 C	282 C	07:36:07.10	–03:06:38.7	6.79	13 Dec 2011	1×300
290	J07365–006	PM I07365–0039	...	07:36:30.27	–00:39:35.2	9.42	10 Jan 2012	1×500
291	J07366+440	G 111–020	...	07:36:39.28	+44:04:48.9	9.96	13 Dec 2011	1×500
292	J07420+142	NZ Gem	...	07:42:02.22	+14:12:30.6	1.59	07 Dec 2011	1×8
293	J07429–107	PM I07429–1043	...	07:42:55.70	–10:43:45.2	9.52	10 Jan 2012	1×500
294	J07467+574	G 193–065	...	07:46:42.03	+57:26:53.4	9.70	14 Dec 2011	1×600
295	J07470+760	LP 017–075	...	07:47:05.83	+76:03:19.6	9.98	03 Jan 2012	1×700
296	J07497–033	2MASS J07494215–0320338	...	07:49:42.10	–03:20:33.9	8.89	14 Feb 2013	1×220
297	J07498–032	1RXS J074948.5–031712	...	07:49:50.90	–03:17:19.5	8.04	14 Feb 2013	1×120
298	J07523+162	LP 423–031	...	07:52:23.90	+16:12:15.7	10.88	22 Sep 2012	3×900
299	J07545–096	PM I07545–0941	...	07:54:32.73	–09:41:47.8	9.70	09 Feb 2012	1×623
300	J07545+085	LSPM J0754+0832	...	07:54:34.12	+08:32:25.3	8.54	14 Dec 2011	1×800
301	J07558+833	LP 005–088	1101	07:55:53.97	+83:23:05.0	8.74	19 Mar 2011	2×1000

Table B.1: Observed stars: identification, common name, Gliese number, 2MASS coordinates and J magnitude, observing date, and exposure time (cont.).

No.	Karmn	Name	Gl/GJ	α (J2000)	δ (J2000)	J [mag]	Observation date	$N \times t_{\rm exp}$ [s]
302	J07591+173	1RXS J075908.2+171957	...	07:59:07.19	+17:19:47.4	9.47	01 Jan 2012	1×327
303	J08025–130	LP 724–016	...	08:02:32.91	–13:05:29.1	9.42	13 Dec 2011	1×300
304	J08031+203 AB	2MASS J08031018+2022154	...	08:03:10.18	+20:22:15.5	9.24	07 Dec 2011	1×300
305	J08069+422	G 111–056	...	08:06:55.32	+42:17:33.4	9.72	07 Dec 2011	1×550
306	J08082+211N	BD+21 1764A	3481	08:08:13.18	+21:06:18.2	6.86	09 Jan 2012	1×200
307	J08082+211S AB	BD+21 1764B	3482	08:08:13.59	+21:06:09.4	7.34	10 Feb 2012	1×200
308	J08104–111	TYC 5430–1154–1	...	08:10:26.50	–11:09:37.0	8.29	14 Feb 2013	1×120
309	J08105–138 AB	18 Pup B	297.2 B	08:10:34.29	–13:48:51.4	8.28	09 Feb 2012	1×220
310	J08117+531	G 194–014	...	08:11:47.60	+53:11:51.3	9.29	07 Dec 2011	1×350
311	J08143+630	HD 67850 B	...	08:14:18.97	+63:04:39.8	9.91	15 Feb 2013	1×250
312	J08161+013	GJ 2066	2066	08:16:07.98	+01:18:09.2	6.63	03 Mar 2012	1×100
313	J08283+553	PM I08283+5522	...	08:28:18.81	+55:22:42.4	9.24	01 Jan 2012	1×248
314	J08286+660	2E 1987	...	08:28:41.22	+66:02:23.9	9.20	07 Dec 2011	1×400
315	J08298+267	DX Cnc	1111	08:29:49.50	+26:46:34.8	8.24	14 Nov 2011	1×1200
316	J08353+141	LSPM J0835+1408	...	08:35:19.93	+14:08:33.4	9.16	07 Dec 2011	1×450
317	J08375+035	LSPM J0837+0333	...	08:37:30.21	+03:33:45.8	9.85	13 Dec 2011	1×700
318	J08386–028	GWP 1056 A	...	08:38:37.31	–02:48:59.4	10.57	14 Feb 2013	1×120
319	J08394–028	GWP 1056 B	...	08:39:24.54	–02:49:11.4	12.14	14 Feb 2013	3×600
320	J08423–048	G 114–014	...	08:42:23.20	–04:53:55.1	9.05	13 Dec 2011	1×900
321	J08449–066 AB	2MASS J08445566–0637259	...	08:44:55.67	–06:37:25.9	9.33	14 Dec 2011	1×350
322	J08526+283	ρ Cnc B	324 B	08:52:40.85	+28:18:58.9	8.56	09 Feb 2012	1×300
323	J08531–202	RAVE J085310.9–201717	...	08:53:10.91	–20:17:17.3	9.32	13 Dec 2011	1×300
324	J08563-044	LP 666–044	...	08:56:18.80	–04:24:55.2	9.78	13 Dec 2011	1×900
325	J08572+194	LP 426–035	...	08:57:15.41	+19:24:17.8	9.45	02 Jan 2012	1×350
326	J08590+364	G 115–039	...	08:59:05.40	+36:26:31.9	8.85	08 Dec 2011	1×1000
327	J08595+537	G 194–047	...	08:59:35.93	+53:43:50.5	9.01	01 Jan 2012	1×226
328	J08599+042	PM I08599+0417	...	08:59:57.60	+04:17:55.3	9.93	14 Dec 2011	1×600
329	J09003+218	LP 368–128	...	09:00:23.59	+21:50:05.4	9.44	06 Mar 2012	3×800
330	J09008+237	HD 77052 B	...	09:00:53.23	+23:46:58.5	11.40	15 Feb 2013	3×500
331	J09023+177	2MASS J09022307+1746326	...	09:02:23.08	+17:46:32.6	9.65	03 Jan 2012	1×500
332	J09028+060	BD+06 2091B	...	09:02:53.20	+06:02:09.6	11.26	14 Feb 2013	1×900
333	J09040–159	1RXS J090406.8–155512	...	09:04:05.55	–15:55:18.4	9.16	03 Jan 2012	1×210
334	J09045+164 AB	BD+16 1895	...	09:04:31.00	+16:25:01.6	9.10	03 Jan 2012	1×300
335	J09058+555	HD 77599 B	...	09:05:51.18	+55:32:18.4	11.49	15 Feb 2013	3×450
336	J09091+227	[ACM2004] J0909+2247	...	09:09:07.99	+22:47:41.3	10.47	09 Jan 2012	3×450
337	J09115+126	LP 487–010	...	09:11:31.95	+12:37:23.7	9.41	01 Jan 2012	1×226
338	J09143+526	HD 79210	338 A	09:14:22.98	+52:41:12.5	4.89	10 Feb 2012	1×30
339	J09144+526	HD 79211	338 B	09:14:24.86	+52:41:11.8	4.78	10 Feb 2012	1×30

Table B.1: Observed stars: identification, common name, Gliese number, 2MASS coordinates and J magnitude, observing date, and exposure time (cont.).

No.	Karmn	Name	Gl/GJ	α (J2000)	δ (J2000)	J [mag]	Observation date	$N \times t_{\rm exp}$ [s]
340	J09151+233	HD 79498 B	...	09:15:10.12	+23:21:33.1	9.14	14 Feb 2013	1×300
341	J09156–105 AB	G 161–007	...	09:15:36.40	–10:35:47.2	8.61	14 Feb 2013	1×500
342	J09201+037	1RXS J092010.8+034731	...	09:20:10.87	+03:47:25.8	9.31	09 Jan 2012	1×300
343	J09206–169	PM I09206–1654	...	09:20:40.00	–16:54:58.4	9.57	10 Jan 2012	1×600
344	J09212+603	BD+61 1116B	...	09:21:17.62	+60:21:46.7	9.13	15 Feb 2013	1×250
345	J09218–023	RAVE J092148.1–021943	...	09:21:48.13	–02:19:43.4	8.44	13 Dec 2011	1×700
346	J09243+063	HD 81212 C	...	09:24:23.86	+06:22:41.8	10.60	14 Feb 2013	1×600
347	J09248+306	RX J0924.8+3041	...	09:24:50.83	+30:41:37.3	9.49	14 Dec 2011	1×400
348	J09256+634	G 235–025	...	09:25:40.33	+63:29:19.7	9.82	14 Dec 2011	1×900
349	J09301–009	LP 607–057	...	09:30:08.60	–00:57:58.8	8.76	13 Dec 2011	1×350
350	J09308+024	1RXS J093051.2+022741	...	09:30:50.85	+02:27:20.2	9.42	04 Jan 2012	1×700
351	J09328+269	DX Leo B	354.1 B	09:32:48.27	+26:59:44.3	10.36	09 Jan 2012	1×1000
352	J09351–103	HD 83008 B	...	09:35:11.84	–10:18:34.0	9.08	15 Feb 2013	1×220
353	J09362+375	HD 89239 B	9303	09:36:15.91	+37:31:45.5	8.09	15 Feb 2013	1×150
354	J09394+146	NLTT 22280	...	09:39:29.94	+14:38:49.8	9.39	03 Jan 2012	1×300
355	J09449–123	G 161–071	...	09:44:54.20	–12:20:54.4	8.50	13 Feb 2013	1×600
356	J09488+156	G 043–002	...	09:48:50.20	+15:38:44.9	9.30	03 Jan 2012	1×300
357	J09526–156	LP 728–071	...	09:52:41.77	–15:36:13.8	9.32	03 Mar 2012	1×700
358	J09538–073	TYC 4902–210–1	...	09:53:51.70	–07:20:07.9	7.83	13 Feb 2013	1×180
359	J09589+059	NLTT 23096	...	09:58:56.51	+05:58:00.1	9.94	02 Jan 2012	1×1100
360	J09597+721	Pul–3 620285	...	09:59:45.35	+72:11:59.8	9.06	03 Jan 2012	1×200
361	J10008+319	20 LMi B	376 B	10:00:50.31	+31:55:46.0	10.26	14 Feb 2013	3×700
362	J10020+697	LP 037–057	...	10:02:05.81	+69:45:29.4	9.77	03 Jan 2012	1×800
363	J10028+484	G 195–055	...	10:02:49.36	+48:27:33.4	9.96	03 Jan 2012	1×500
364	J10063–064	GWP 1102 A	...	10:06:20.56	–06:26:10.2	13.26	14 Feb 2013	3×700
365	J10068–127	2MASS J10065210–1246543	...	10:06:52.11	–12:46:54.3	9.75	10 Jan 2012	1×1200
366	J10098–007	BPM 73854	...	10:09:51.20	–00:46:18.9	9.01	10 Jan 2012	1×600
367	J10120–026 AB	LP 609–71	381 AB	10:12:04.66	–02:41:04.5	7.02	14 Nov 2011	1×300
368	J10130+233	G 054–018	...	10:13:00.26	+23:20:50.5	9.19	03 Jan 2012	1×250
369	J10148+213	G 054–019	...	10:14:53.15	+21:23:46.4	9.73	10 Jan 2012	1×900
370	J10155–164	WT 1774	...	10:15:35.40	–16:28:23.6	9.36	11 Jan 2012	1×400
371	J10196+198 AB	AD Leo	388 AB	10:19:36.35	+19:52:12.2	5.45	06 Mar 2012	1×40
372	J10200+289	G 118–051	...	10:20:00.88	+28:57:13.1	9.16	04 Jan 2012	1×400
373	J10238+438	LP 212–062	...	10:23:51.85	+43:53:33.2	10.04	04 Jan 2012	1×900
374	J10240+366	2MASS J10240507+3639326	...	10:24:05.07	+36:39:32.6	9.43	09 Jan 2012	1×400
375	J10278+028	LHS 5171	...	10:27:49.67	+02:51:36.9	9.44	11 Jan 2012	1×300
376	J10304+559	36 UMa B	394	10:30:25.31	+55:59:56.8	6.12	13 Feb 2013	1×120
377	J10359+288	RX J1035.9+2853	...	10:35:57.25	+28:53:31.7	9.25	10 Jan 2012	1×300

Table B.1: Observed stars: identification, common name, Gliese number, 2MASS coordinates and J magnitude, observing date, and exposure time (cont.).

No.	Karmn	Name	Gl/GJ	α (J2000)	δ (J2000)	J [mag]	Observation date	$N \times t_{\rm exp}$ [s]
378	J10368+509	LP 127–502	...	10:36:48.12	+50:55:04.1	9.87	04 Jan 2012	1×900
379	J10430–092 AB	WT 1827	...	10:43:02.93	–09:12:41.1	9.67	09 Jan 2012	1×500
380	J10443+124	LP 490–063	...	10:44:18.82	+12:25:11.7	9.42	10 Jan 2012	1×400
381	J10482–113	LP 731–058	3622	10:48:12.58	–11:20:08.2	8.86	06 Mar 2012	2×900
382	J10508+068	EE Leo	402	10:50:52.01	+06:48:29.3	7.32	06 Mar 2012	1×200
383	J10546–073	LP 671–008	...	10:54:42.00	–07:18:33.1	8.88	13 Feb 2013	1×600
384	J10560+061	56 Leo	...	10:56:01.47	+06:11:07.3	0.43	08 Dec 2011	1×3
385	J10563+042	PM I10563+0415	...	10:56:22.25	+04:15:45.9	9.18	10 Jan 2012	1×300
386	J10564+070	CN Leo	406	10:56:28.86	+07:00:52.8	7.09	02 Jan 2012	1×600
387	J10584–107	BD–10 3166B	...	10:58:28.00	–10:46:30.5	9.51	04 Jan 2012	1×900
388	J11018–024	p^{02} Leo	...	11:01:49.67	–02:29:04.5	1.78	13 Dec 2011	1×1
389	J11030+037	Wolf 360	...	11:03:04.27	+03:44:22.6	9.31	10 Jan 2012	1×300
390	J11033+359	HD 95735	411	11:03:20.24	+35:58:11.8	4.20	18 Mar 2011	1×10
391	J11046–042S AB	HH Leo BC	...	11:04:40.98	–04:13:24.7	7.27	06 Mar 2012	1×100
392	J11054+435	BD+44 2051A	412 A	11:05:29.03	+43:31:35.7	5.54	11 Feb 2012	1×50
393	J11055+435	BD+44 2051B (WX UMa)	412 B	11:05:31.33	+43:31:17.1	8.74	03 Mar 2012	1×900
394	J11075+437	HAT 141–00828	...	11:07:32.08	+43:45:56.4	9.94	09 Jan 2012	1×800
395	J11151+734N	HD 97584 B	420 B	11:15:11.06	+73:28:36.0	7.88	11 Jan 2012	1×220
396	J11151+734S	HD 97584 A	420 A	11:15:11.90	+73:28:30.7	5.78	11 Jan 2012	1×220
397	J11201–104 AB	LP 733–099	...	11:20:06.10	–10:29:46.8	7.81	13 Feb 2013	1×120
398	J11201+301	HD 98500	...	11:20:11.18	+30:07:13.7	4.34	19 Mar 2011	1×10
399	J11214–204S	SZ Crt A	425 A	11:21:26.56	–20:27:09.5	6.64	11 Jan 2012	1×200
400	J11214–204N	SZ Crt B	425 B	11:21:26.66	–20:27:13.6	6.10	11 Jan 2012	1×200
401	J11218+181	HD 98736 B	426 B	11:21:49.13	+18:11:28.0	7.65	12 Feb 2013	1×400
402	J11240+381	RX J1124.1+3808	...	11:24:04.35	+38:08:10.9	9.93	04 Jan 2012	1×900
403	J11306–080	LP 672–042	...	11:30:41.80	–08:05:43.1	8.03	13 Feb 2013	1×300
404	J11312+631	BD+63 695	430	11:31:13.09	+63:09:27.1	7.40	06 Mar 2012	1×60
405	J11378+418	BD+42 2230B	...	11:37:49.92	+41:49:59.5	11.04	15 Feb 2013	1×500
406	J11403+095	BD+10 2321B	...	11:40:20.84	+09:30:45.4	10.12	15 Feb 2013	1×400
407	J11421+267	Ross 905	436	11:42:10.55	+26:42:30.5	6.90	14 Nov 2011	1×200
408	J11451+183	LP 433–047	...	11:45:11.92	+18:20:58.7	9.16	10 Jan 2012	1×300
409	J11458+065	ν Vir	...	11:45:51.56	+06:31:45.7	1.18	14 Dec 2011	1×1
410	J11472+770	HD 102326 B	...	11:47:12.68	+77:02:35.9	9.20	15 Feb 2013	1×300
411	J11474+667	1RXS J114728.8+664405	...	11:47:28.57	+66:44:02.6	9.68	04 Jan 2012	1×1100
412	J11485+076	G 010–052	...	11:48:35.59	+07:41:40.4	9.48	10 Jan 2012	1×400
413	J11511+352	BD+36 2219	450	11:51:07.34	+35:16:19.2	6.42	11 Feb 2012	1×60
414	J11522+100	HD 103112 B	3690	11:52:17.93	+10:00:39.2	11.42	11 Feb 2012	2×900
415	J11549–021	PM I11549–0206	...	11:54:56.93	–02:06:09.2	9.55	10 Jan 2012	1×600

Table B.1: Observed stars: identification, common name, Gliese number, 2MASS coordinates and J magnitude, observing date, and exposure time (cont.).

No.	Karmn	Name	Gl/GJ	α (J2000)	δ (J2000)	J [mag]	Observation date	$N \times t_{\rm exp}$ [s]
416	J12025+084	LHS 320	...	12:02:33.65	+08:25:50.6	10.74	03 Jan 2012	1×600
417	J12049+174	HD 104923 B	...	12:04:56.11	+17:28:11.9	9.79	12 Feb 2013	1×600
418	J12069+058	HD 105219 B	...	12:06:56.94	+05:48:09.3	8.58	15 Feb 2013	1×300
419	J12088+217	BD+22 2442B	...	12:08:55.41	+21:47:31.6	11.15	13 Feb 2013	1×1800
420	J12093+210	StM 165	...	12:09:21.81	+21:03:07.7	9.47	04 Jan 2012	1×600
421	J12104–131	NLTT 29827	...	12:10:28.34	–13:10:23.5	9.29	10 Jan 2012	1×400
422	J12124+121	PM I12124+1211	...	12:12:26.06	+12:11:38.1	9.39	10 Jan 2012	1×300
423	J12162+508	RX J1216.2+5053	...	12:16:15.06	+50:53:37.7	9.29	09 Jan 2012	1×400
424	J12228–040	G 013–033	...	12:22:50.62	–04:04:46.2	9.66	10 Jan 2012	1×600
425	J12322+454	BW CVn	...	12:32:14.37	+45:29:50.4	4.81	19 Mar 2011	1×30
426	J12349+322	PM I12349+3214	...	12:34:54.01	+32:14:27.9	9.46	04 Jan 2012	1×600
427	J12364+352	G 123–045	...	12:36:28.70	+35:12:00.8	9.11	09 Jan 2012	1×350
428	J12368–019	RAVE J123652.2–015901	...	12:36:52.15	–01:59:00.7	9.44	10 Jan 2012	1×300
429	J12372+358	BD+36 2288B	...	12:37:15.47	+35:49:17.7	11.35	15 Feb 2013	1×1100
430	J12417+567	RX J1241.7+5645	...	12:41:47.37	+56:45:13.8	9.48	04 Jan 2012	1×600
431	J12440–111	LP 735–029	...	12:44:00.76	–11:10:30.2	9.52	10 Jan 2012	1×500
432	J12456+271	HD 110964	...	12:45:36.99	+27:07:44.3	5.09	06 Mar 2012	1×30
433	J12470+466	Ross 991	3748	12:47:01.02	+46:37:33.4	8.10	06 Mar 2012	1×200
434	J12488+120	HD 111398 B	...	12:48:53.45	+12:04:32.7	11.40	14 Feb 2013	3×1000
435	J12533–053	LP 676–026	...	12:53:19.40	–05:19:52.5	8.92	13 Feb 2013	1×400
436	J12533+466	BZ CVn	...	12:53:20.02	+46:39:22.9	3.36	19 Mar 2011	1×15
437	J12549–063	BD–05 3596B	488.2 B	12:54:55.12	–06:20:03.9	11.38	09 Feb 2012	3×800
438	J12593–001	LP 616–056	...	12:59:18.20	–00:10:33.4	8.79	14 Feb 2013	1×300
439	J13027+415	G 123–084	...	13:02:47.52	+41:31:09.9	9.03	10 Jan 2012	1×200
440	J13088–015	LP 617–004	...	13:08:51.20	–01:31:07.6	8.92	14 Feb 2013	1×300
441	J13102+477	G 177–025	...	13:10:12.69	+47:45:19.0	9.58	09 Jan 2012	1×1200
442	J13113+096	HD 114606 B	9431 B	13:11:22.44	+09:36:13.2	9.68	15 Feb 2013	1×400
443	J13143+133 AB	NLTT 33370	...	13:14:20.39	+13:20:01.2	9.75	09 Jan 2012	2×800
444	J13167–123	LP 737–014	...	13:16:45.46	–12:20:20.4	9.49	11 Jan 2012	1×300
445	J13168+170	HD 115404 B	505 B	13:16:51.54	+17:00:59.9	6.53	09 Feb 2012	1×60
446	J13179+362	GJ 1170	1170	13:17:58.40	+36:17:56.9	8.11	18 Mar 2011	1×800
447	J13182+733	PM I13182+7322	...	13:18:13.52	+73:22:07.4	9.54	11 Jan 2012	1×500
448	J13247–050	G 014–052	...	13:24:46.48	–05:04:19.4	9.47	11 Feb 2012	1×300
449	J13251–114	PM I13251–1126	...	13:25:11.72	–11:26:36.8	9.16	11 Jan 2012	1×250
450	J13253+426	BD+43 2328B	...	13:25:23.50	+42:41:29.6	9.08	15 Feb 2013	1×300
451	J13260+275	1RXS J132601.9+273449	...	13:26:02.68	+27:35:02.1	9.25	11 Jan 2012	1×250
452	J13294–143	1RXS J132923.9–142206	...	13:29:24.08	–14:22:12.3	9.06	11 Jan 2012	1×200
453	J13312+589	PM I13312+5857	...	13:31:12.50	+58:57:19.0	10.95	18 Apr 2013	2×500

Table B.1: Observed stars: identification, common name, Gliese number, 2MASS coordinates and J magnitude, observing date, and exposure time (cont.).

No.	Karmn	Name	Gl/GJ	α (J2000)	δ (J2000)	J [mag]	Observation date	$N \times t_{\rm exp}$ [s]
454	J13314–079	HD 117579 B	...	13:31:29.79	–07:59:59.4	9.60	15 Feb 2013	1×400
455	J13321–112	HD 117676 B	...	13:32:06.86	–11:16:40.8	9.45	15 Feb 2013	1×300
456	J13326+309	LP 323–169	...	13:32:39.08	+30:59:06.5	9.62	11 Jan 2012	1×900
457	J13335+704	2MASS J1333371+7029412	...	13:33:33.72	+70:29:41.3	9.23	11 Jan 2012	1×300
458	J13386–115	1RXS J133841.3–113137	...	13:38:40.87	–11:32:07.8	9.71	11 Jan 2012	1×600
459	J13394+461 AB	BD+46 1889	521 AB	13:39:24.10	+46:11:11.4	7.05	06 Mar 2012	1×90
460	J13413–091	PM I13413–0907	...	13:41:21.22	–09:07:17.1	9.44	11 Jan 2012	1×300
461	J13414+489	StM 186	...	13:41:27.70	+48:54:45.9	9.00	12 Feb 2013	1×500
462	J13474+063	HD 120066 B	...	13:47:28.80	+06:18:56.4	7.76	12 Feb 2013	1×200
463	J13503–216	LP 798–041	...	13:50:23.77	–21:37:19.3	9.46	09 Feb 2012	1×272
464	J13537+521 AB	1RXS J135348.0+521036	...	13:53:45.89	+52:10:29.9	9.13	11 Jan 2012	1×300
465	J13551–079	BPM 76486	...	13:55:10.80	–07:56:59.2	8.73	14 Feb 2013	1×250
466	J13555–073	G 064–028	...	13:55:35.10	–07:23:16.6	8.81	14 Feb 2013	1×150
467	J13582–120	LP 739–002	...	13:58:16.22	–12:02:59.2	9.73	11 Jan 2012	1×600
468	J13583–132	LP 739–003	...	13:58:19.56	–13:16:24.8	9.49	09 Feb 2012	1×518
469	J13587+465	HD 122132	...	13:58:45.70	+46:35:46.5	4.12	19 Mar 2011	1×10
470	J14019+432	PM I14019+4316	...	14:01:58.79	+43:16:42.7	9.28	09 Feb 2012	1×226
471	J14102–180	1RXS J141553.4–110227	...	14:10:12.70	–18:01:16.3	10.03	11 Feb 2012	3×500
472	J14159–110	PM I14159–1102	...	14:15:54.20	–11:02:44.6	9.00	12 Feb 2013	1×400
473	J14171+088	PM I14171+0851	...	14:17:07.31	+08:51:36.3	9.11	09 Feb 2012	1×431
474	J14175+025	RX J1417.5+0233	...	14:17:30.21	+02:33:43.6	9.27	11 Feb 2012	1×220
475	J14194+029	NLTT 36959	...	14:19:29.58	+02:54:36.5	9.95	09 Feb 2012	3×450
476	J14195–051	HD 125455 B	544 B	14:19:35.85	–05:09:08.0	10.49	12 feb 2013	1×900
477	J14215–079	PM I14215–0755	...	14:21:34.06	–07:55:16.6	9.46	11 Feb 2012	1×327
478	J14227+164	NLTT 37131	...	14:22:43.41	+16:24:46.4	10.30	09 Feb 2012	3×600
479	J14244+602	BD+60 1536B	...	14:24:27.44	+60:15:17.0	9.73	12 Feb 2013	1×1500
480	J14251+518	θ Boo B	549 B	14:25:11.61	+51:49:53.5	7.88	11 Feb 2012	1×200
481	J14255–118	LP 740–010	...	14:25:34.13	–11:48:51.5	9.35	11 Feb 2012	1×327
482	J14312+754	LSPM J1431+7526	...	14:31:13.49	+75:26:42.4	9.79	09 Feb 2012	1×568
483	J14336+093	HD 127871 B	...	14:33:39.86	+09:20:09.5	10.23	18 Apr 2013	1×700
484	J14415+136	HD 129290 B	...	14:41:30.25	+13:37:36.2	10.35	12 Feb 2013	1×800
485	J14446–222	HD 129715 B	3865	14:44:40.13	–22:14:45.5	10.57	12 Feb 2013	1×600
486	J14472+570	RX J1447.2+5701	...	14:47:13.54	+57:01:55.1	9.91	09 Feb 2012	1×623
487	J14480+384	BD+39 2801	563.1	14:48:01.43	+38:27:58.4	7.23	18 Mar 2011	1×340
488	J14485+101	G 066–027	...	14:48:33.16	+10:06:57.4	9.48	09 Feb 2012	1×272
489	J14492+498	PM I14492+4949	...	14:49:14.77	+49:49:39.1	10.24	18 Apr 2013	1×450
490	J14501+323	LP 326–034	...	14:50:11.12	+32:18:17.3	9.14	09 Feb 2012	1×206
491	J14544+161 ABC	CE Boo	569	14:54:29.23	+16:06:04.0	6.63	06 Mar 2012	1×90

Table B.1: Observed stars: identification, common name, Gliese number, 2MASS coordinates and J magnitude, observing date, and exposure time (cont.).

No.	Karmn	Name	Gl/GJ	α (J2000)	δ (J2000)	J [mag]	Observation date	$N \times t_{\rm exp}$ [s]
492	J14595+454	HD 132830 B	...	14:59:30.59	+45:26:52.9	8.10	15 Feb 2013	1×200
493	J15079+762	HD 135363 B	...	15:07:57.24	+76:13:59.0	9.24	11 Feb 2012	1×500
494	J15081+623	LSPM J1508+6221	...	15:08:11.93	+62:21:53.6	9.30	11 Feb 2012	1×300
495	J15118+395	HD 135144 B	...	15:11:51.45	+39:33:02.4	9.87	12 Feb 2013	1×1200
496	J15131+181	PM I15131+1808N	...	15:13:06.62	+18:08:44.2	11.02	18 Apr 2013	1×700
497	J15142–099	PM I15142–0958	...	15:14:16.90	–09:58:38.8	9.67	12 Feb 2013	1×1200
498	J15147+645	G 224–057	...	15:14:46.81	+64:33:43.9	9.79	11 Feb 2012	1×700
499	J15151+333	LP 272–063	...	15:15:07.06	+33:18:03.3	9.21	11 Feb 2012	1×200
500	J15157–074	LTT 6084	...	15:15:43.70	–07:25:21.1	8.57	14 Feb 2013	1×120
501	J15164+167	HD 135792 B	...	15:16:25.29	+16:47:41.5	7.82	15 Feb 2013	1×300
502	J15197+046	PM I15197+0439	...	15:19:45.85	+04:39:34.5	9.55	11 Feb 2012	1×500
503	J15204+001	HD 136378 B	...	15:20:28.30	+00:11:26.9	9.43	14 Feb 2013	1×300
504	J15210+255	HD 136655 B	...	15:21:04.80	+25:33:30.2	8.46	15 Feb 2013	1×220
505	J15238+584	G 224–065	...	15:23:51.44	+58:28:06.4	9.91	11 Feb 2012	1×650
506	J15277–090	HD 137763 C	586 C	15:27:45.03	–09:01:32.8	10.55	14 Feb 2013	3×500
507	J15290+467 AB	RX J1529.0+4646	...	15:29:02.97	+46:46:24.0	9.94	09 Feb 2012	3×450
508	J15291+574	HD 138367 B	...	15:29:09.36	+57:24:41.8	8.83	14 Feb 2013	1×300
509	J15305+094	NLTT 40406	...	15:30:30.33	+09:26:01.4	9.57	11 Feb 2012	3×450
510	J15340+513	LP 135–414	...	15:34:03.87	+51:22:02.4	9.37	11 Feb 2012	1×500
511	J15386+371	G 179–042	...	15:38:37.08	+37:07:24.7	9.98	11 Feb 2012	1×700
512	J15430–130	PM I15430–1302	...	15:43:05.68	–13:02:52.0	10.24	18 Apr 2013	1×300
513	J15474+451	LP 177–102	...	15:47:27.44	+45:07:51.2	9.08	11 Feb 2012	1×300
514	J15476+226	LSPM J1547+2241	...	15:47:40.71	+22:41:16.5	9.54	11 Feb 2012	1×600
515	J15480+043	RX J1548.0+0421	...	15:48:02.80	+04:21:39.3	9.06	11 Feb 2012	1×188
516	J15481+015	V382 Ser B	3917 B	15:48:09.30	+01:34:36.0	9.30	10 Feb 2012	1×500
517	J15499+796	G 256–025	...	15:49:55.18	+79:39:51.7	9.72	11 Feb 2012	1×900
518	J15552–101	RAVE J155514.5–101023	...	15:55:14.50	–10:10:23.1	8.48	13 Feb 2013	1×200
519	J15557–103	1RXS J155542.1–102012	...	15:55:42.30	–10:20:01.6	9.40	12 Feb 2013	1×600
520	J15558–118	LP 743–053	...	15:55:52.20	–11:54:19.6	8.98	13 Feb 2013	1×400
521	J15569+376	RX J1556.9+37381	...	15:56:58.24	+37:38:13.8	9.42	11 Feb 2012	1×250
522	J15578+090	LSPM J1557+0901	...	15:57:48.27	+09:01:09.9	9.28	11 Feb 2012	1×327
523	J16023+036	HD 143809 B	...	16:02:16.91	+03:38:41.2	10.35	10 Feb 2012	1×600
524	J16042+235	LSPM J1604+2331	...	16:04:13.20	+23:31:38.7	9.97	02 Aug 2012	3×350
525	J16048+391	HD 144579 B	611 B	16:04:50.93	+39:09:36.0	9.90	12 Feb 2013	1×1200
526	J16120+033N	1RXS J161204.8+031850	...	16:12:05.00	+03:18:53.3	9.96	23 Sep 2012	1×900
527	J16139+337 AB	σ CrB C	615.2 C	16:13:56.27	+33:46:24.3	8.60	12 Feb 2013	1×400
528	J16148+606 AB	HD 146868 B	...	16:14:52.97	+60:38:27.8	9.82	12 Feb 2013	1×1500
529	J16157+586	G 225–054	...	16:16:42.20	+58:39:43.1	10.18	04 Aug 2012	1×750

Table B.1: Observed stars: identification, common name, Gliese number, 2MASS coordinates and J magnitude, observing date, and exposure time (cont.).

No.	Karmn	Name	Gl/GJ	α (J2000)	δ (J2000)	J [mag]	Observation date	$N \times t_{\rm exp}$ [s]
530	J16167+672S	HD 147379	617 A	16:16:42.80	+67:14:19.7	5.78	18 Mar 2011	1×40
531	J16183+757	η UMi B	3951 B	16:18:20.95	+75:43:08.1	10.84	18 Apr 2013	3×500
532	J16243+199	RX J1624.3+1959	...	16:24:22.70	+19:59:22.6	9.32	06 Aug 2012	1×400
533	J16254+543	GJ 625	625	16:25:24.59	+54:18:14.9	6.61	02 Sep 2012	1×120
534	J16269+149	2E 3693	...	16:26:54.40	+14:57:50.2	9.75	23 Sep 2012	1×900
535	J16276–035 AB	MCC 765	...	16:27:39.20	–03:35:03.4	8.54	13 Feb 2013	1×400
536	J16299+048	PM I16299+0453	...	16:29:54.70	+04:53:25.4	9.15	03 Aug 2012	1×200
537	J16314+471	LSPM J1631+4710	...	16:31:28.10	+47:10:21.3	9.40	06 Aug 2012	1×500
538	J16330+031	HD 149162 C	9566 C	16:33:02.79	+03:11:37.2	10.63	18 Apr 2013	1×500
539	J16354–039	BD–03 3968B	629.2 B	16:35:29.11	-03:57:58.6	11.09	18 Apr 2013	1×350
540	J16365+287	G 169–019	...	16:36:30.30	+28:46:42.3	9.45	04 Sep 2012	1×330
541	J16459+609	LP 101–126	...	16:45:55.00	+60:57:04.1	9.39	06 Aug 2012	1×600
542	J16465+345	LP 276–022	...	16:46:31.55	+34:34:55.5	10.53	03 Aug 2012	3×900
543	J16480+453	RX J1648.0+4522	...	16:48:04.50	+45:22:43.0	9.35	06 Aug 2012	1×800
544	J16528+610	LSPM J1652+6304	...	16:52:49.50	+63:04:38.9	9.59	23 Sep 2012	1×900
545	J16536+560	G 226–033	...	16:53:39.20	+56:03:27.3	9.86	04 Sep 2012	1×600
546	J16543+256	LP 387–019	...	16:54:19.10	+25:37:36.5	9.39	25 Sep 2012	1×300
547	J16555–083	V1054 Oph D (vB 8)	644 C	16:55:35.29	–08:23:40.1	9.78	02 Aug 2012	2×1200 $+1 \times 900$
548	J17011+555	LP 138–020	...	17:01:11.60	+55:35:00.3	9.15	05 Aug 2012	1×240
549	J17017+741	LP 043–292	...	17:01:45.90	+74:11:51.3	9.44	04 Sep 2012	1×400
550	J17052–050	HD 154363 B	654	17:05:13.78	–05:05:39.2	6.78	18 Apr 2013	1×100
551	J17062+646	G 240–044	...	17:06:17.70	+64:38:09.1	9.38	05 Aug 2012	1×250
552	J17094+391	Wolf 648	...	17:09:26.00	+39:09:37.4	9.84	23 Sep 2012	1×900
553	J17126–099	Ruber 7	...	17:12:40.72	–09:54:12.1	6.19	19 Mar 2011	1×200
554	J17140+176	LP 447–021	...	17:14:01.50	+17:38:55.0	9.28	25 Sep 2012	1×250
555	J17154+308	G 181–032	...	17:15:28.00	+30:52:22.0	9.45	25 Sep 2012	1×250
556	J17163–053	LP 687–017	...	17:16:20.60	–05:23:51.4	8.70	13 Feb 2013	1×300
557	J17167+115	LSPM J1716+1133	...	17:16:47.80	+11:33:52.3	9.80	04 Sep 2012	1×600
558	J17176+524	HD 156985 B	...	17:17:38.60	+52:24:22.4	9.77	05 Aug 2012	1×700
559	J17198+265	V639 Her	669 B	17:19:52.98	+26:30:02.6	8.23	06 Aug 2012	1×800
560	J17199+265	V647 Her	669 A	17:19:54.20	+26:30:03.1	7.27	06 Aug 2012	1×600
561	J17199+242	V475 Her	...	17:19:59.50	+24:12:05.4	9.75	25 Sep 2012	1×570
562	J17216–171	TYC 6238–480–1	...	17:21:39.95	–17:11:29.5	6.15	19 Mar 2011	1×100
563	J17239+136	LSPM J1723+1338	...	17:23:56.80	+13:38:20.2	9.50	25 Sep 2012	1×500 $+1 \times 400$
564	J17246+617	LSPM J1724+6147	...	17:24:39.90	+61:47:50.8	9.45	05 Aug 2012	1×250
565	J17265–227	1RXS J172635.8-224359	...	17:26:35.40	–22:44:02.2	9.56	25 Sep 2012	1×600

Table B.1: Observed stars: identification, common name, Gliese number, 2MASS coordinates and J magnitude, observing date, and exposure time (cont.).

No.	Karmn	Name	Gl/GJ	α (J2000)	δ (J2000)	J [mag]	Observation date	$N \times t_{\rm exp}$ [s]
566	J17267–050	PM I17267–0500	...	17:26:46.80	–05:00:35.6	9.48	18 Apr 2013	1×280
567	J17270+422	HD 158415 B	...	17:27:03.09	+42:14:07.8	8.50	18 Apr 2013	1×160
568	J17281–017	SCR J1728–0143	...	17:28:11.10	–01:43:57.0	9.89	18 Apr 2013	1×700
569	J17299–209	LP 807–018	...	17:29:58.60	–20:59:24.6	9.78	25 sep 2012	1×900
570	J17301+546	LSPM J1730+5439	...	17:30:06.10	+54:39:32.2	9.04	05 Aug 2012	1×210
571	J17304+337	LSPM J1730+3344	...	17:30:26.70	+33:44:52.5	9.46	04 Sep 2012	1×300
572	J17364+683	BD+68 946	687	17:36:25.94	+68:20:22.0	5.34	11 Nov 2011	1×60
573	J17412+724	G 258–17	...	17:41:16.12	+72:26:32.0	10.28	18 Apr 2013	3×450
574	J17426+756	LP 024–054	...	17:42:41.60	+75:37:18.8	9.68	23 Sep 2012	1×900
575	J17428+167	BD+16 3268B	...	17:42:52.04	+16:43:47.9	10.40	14 Feb 2013	1×450
576	J17464+277 AB	μ Her BC	695 BC	17:46:25.08	+27:43:01.4	5.77	23 Sep 2012	1×180
577	J17477+277	BD+27 2891B	...	17:47:44.32	+27:47:07.4	11.42	14 Feb 2013	2×500
578	J17520+566	RX J1752.0+5636	...	17:52:02.90	+56:36:27.8	9.23	23 Sep 2012	1×500
579	J17559+294	PM I17559+2926	...	17:55:58.00	+29:26:09.8	9.76	24 Sep 2012	2×900
580	J17578+046	Barnard's star	699	17:57:48.49	+04:41:40.5	5.24	04 Aug 2012	1×80
581	J17578+465	G 204–039	4040 A	17:57:50.96	+46:35:18.2	7.85	19 Mar 2011	1×100
582	J18006+685	BD+68 971B	...	18:00:36.96	+68:32:54.0	9.67	18 Apr 2013	1×250
583	J18007+295	HD 164595 B	...	18:00:45.44	+29:33:56.7	9.06	12 Nov 2011	1×300
584	J18019+001	PM I18019+0007	...	18:01:58.30	+00:07:50.2	10.13	05 Aug 2012	3×500
585	J18022+642	LP 071–082	...	18:02:16.60	+64:15:44.3	8.54	24 Sep 2012	1×500
586	J18028–030	PM I18028–0300	...	18:02:49.40	–03:00:02.6	9.44	25 Sep 2012	1×250
587	J18036–189	G 154–043	...	18:03:36.10	–18:58:50.5	9.13	25 Sep 2012	1×400
588	J18041+838	LSPM J1804+8350	...	18:04:10.60	+83:50:28.1	9.02	24 Sep 2012	1×700
589	J18046+139	LSPM J1804+1354	...	18:04:38.70	+13:54:14.3	9.47	18 Apr 2013	1×300
590	J18054+015	G 140–036	...	18:05:29.10	+01:32:36.0	9.11	18 Apr 2013	1×350
591	J18057–143	PM I18057–1422	...	18:05:44.70	–14:22:42.4	9.78	02 Sep 2012	3×500
592	J18068+177	LP 449–010	...	18:06:48.60	+17:20:47.2	9.49	24 Sep 2012	1×900
593	J18090+241	HD 166301 B	...	18:09:01.93	+24:09:04.2	9.30	18 Apr 2013	1×240
594	J18112–010	1RXS J181115.2–010111	...	18:11:14.90	–01:01:11.7	10.19	04 Aug 2012	4×600
595	J18130+414	HD 167389 B	...	18:13:00.02	+41:29:19.6	10.21	15 Feb 2013	1×500
596	J18131+260 AB	LP 390–016	4044 AB	18:13:06.57	+26:01:51.9	8.90	23 Sep 2012	1×240
597	J18135+055	NLTT 46124	...	18:13:33.20	+05:32:12.0	9.70	25 Sep 2012	1×600
								$+1 \times 520$
598	J18149+196	Wolf 832	...	18:14:59.90	+19:39:26.0	9.44	06 Aug 2012	1×500
599	J18162+686	BD+68 986B	...	18:16:14.75	+68:40:27.8	11.53	15 Feb 2013	3×500
600	J18224+620	LP 103–305	1227	18:22:27.19	+62:03:02.5	8.64	18 Mar 2011	1×700
601	J18253+186	PM I18252+1839	...	18:25:18.00	+18:39:09.1	9.57	06 Aug 2012	1×900
602	J18306–039	PM I18306–0356	...	18:30:39.50	–03:56:19.0	9.72	25 Sep 2012	1×700

Table B.1: Observed stars: identification, common name, Gliese number, 2MASS coordinates and J magnitude, observing date, and exposure time (cont.).

No.	Karmn	Name	Gl/GJ	α (J2000)	δ (J2000)	J [mag]	Observation date	$N \times t_{\rm exp}$ [s]
603	J18313+649	RX J1831.3+6454	...	18:31:21.80	+64:54:13.3	9.36	06 Aug 2012	1×500
604	J18338+194	NLTT 46663	...	18:33:50.10	+19:26:11.2	9.16	25 Sep 2012	1×400
605	J18353+457	BD+45 2743	720 A	18:35:18.33	+45:44:37.9	6.88	11 Nov 2011	1×90
606	J18354+457	BD+45 2743B (vB 9)	720 B	18:35:27.23	+45:45:40.3	8.89	11 Nov 2011	1×500
607	J18400+726	LP 044–334	...	18:40:02.38	+72:40:54.0	10.97	02 Aug 2012	3×1200
608	J18409+315	BD+31 3330B	...	18:40:54.98	+31:32:04.8	6.80	15 Feb 2013	1×220
609	J18423–013	Ruber 8	...	18:42:20.54	–01:20:15.2	6.18	19 Mar 2011	1×150
610	J18427+596N	HD 173739	725 A	18:42:46.66	+59:37:49.9	5.19	12 Nov 2011	1×180
611	J18427+596S	HD 173740	725 B	18:42:46.88	+59:37:37.4	5.72	12 Nov 2011	1×180
612	J18453+188	G 184–024	...	18:45:22.90	+18:51:58.5	9.27	25 Sep 2012	1×500
613	J18467+007	1RXS J184646.9+004320	...	18:46:46.80	+00:43:26.1	9.59	04 Sep 2012	1×500
614	J18482+076	G 141–036	...	18:48:17.50	+07:41:21.1	8.85	25 Sep 2012	1×800
615	J18491–032	PM I18491–0315	...	18:49:06.40	–03:15:17.5	9.61	02 Sep 2012	1×900
616	J18499+186	G 184–031	...	18:49:54.49	+18:40:29.5	9.38	02 Sep 2012	1×300
617	J18542+109	PM I18542+1058	...	18:54:17.10	+10:58:09.2	9.38	04 Sep 2012	1×300
618	J18550+429	1RXS J185504.7+425952	...	18:55:04.50	+42:59:51.0	9.78	06 Aug 2012	1×900
619	J18570+473	G 205–048	...	18:57:00.50	+47:20:28.8	9.42	06 Aug 2012	1×400
620	J19052+387	2MASS J1901335+3845050	...	19:05:13.40	+38:45:05.3	9.35	04 Aug 2012	1×400
621	J19060–074	SCR J1906–0729	...	19:06:02.60	–07:29:41.2	9.50	05 Aug 2012	1×300
622	J19070+208	HD 349726	745 A	19:07:05.56	+20:53:16.8	7.30	02 Sep 2012	1×150
623	J19072+442	LP 230–029	...	19:07:12.70	+44:16:07.3	10.45	05 Aug 2012	3×660
624	J19105–075	PM I19105–0734	...	19:10:33.30	–07:34:04.3	9.88	04 Sep 2012	1×450
625	J19164+842	PM I19164+8413	...	19:16:24.80	+84:13:41.1	9.98	06 Aug 2012	3×600
626	J19168+003	1RXS J191650.3+002341	...	19:16:48.80	+00:23:32.1	9.96	02 Sep 2012	1×650
627	J19169+051N	V1428 Aql	752 A	19:16:55.26	+05:10:08.6	5.58	05 Aug 2012	1×70
628	J19169+051S	V1298 Aql (vB 10)	752 B	19:16:57.62	+05:09:02.2	9.91	03 Aug 2012	3×1200 $+1 \times 900$
629	J19243+426	PM I19243+4237	...	19:24:21.00	+42:37:25.6	9.34	05 Aug 2012	1×300
630	J19260+244	G 185–023	...	19:26:01.60	+24:26:17.2	9.63	05 Aug 2012	1×1000
631	J19271+770	NLTT 478944	...	19:27:09.10	+77:04:32.8	9.24	06 Aug 2012	1×400
632	J19282–001	PM I19282–0009	...	19:28:13.70	–00:09:51.9	9.72	04 sep 2012	1×700
633	J19312+361 AB	G 125–015	...	19:31:12.60	+36:07:29.9	9.61	05 Aug 2012	1×500
634	J19316–069	PM J19316–0658	...	19:31:38.70	–06:58:25.3	9.48	04 Sep 2012	1×360
635	J19327–068	SCR J1932–0652	...	19:32:46.30	–06:52:18.1	9.94	04 Sep 2012	1×500
636	J19346+045	HD 184489	763	19:34:39.84	+04:34:57.0	6.71	11 Nov 2011	1×60
637	J19390+338	PM I19390+3352	...	19:39:05.60	+33:52:02.1	9.39	05 Aug 2012	1×300
638	J19393+148	PM I19393+1448	...	19:39:22.10	+14:48:16.0	9.94	05 Aug 2012	1×600
639	J19421+656	G 260–031	...	19:42:10.00	+65:38:30.0	9.35	05 Aug 2012	1×240

Table B.1: Observed stars: identification, common name, Gliese number, 2MASS coordinates and J magnitude, observing date, and exposure time (cont.).

No.	Karmn	Name	Gl/GJ	α (J2000)	δ (J2000)	J [mag]	Observation date	$N \times t_{\rm exp}$ [s]
640	J19430+102	G 142–046	...	19:43:02.70	+10:12:39.6	9.25	23 Sep 2012	1×500
641	J19439–057	1RXS J194354.7–054634	...	19:43:54.30	–05:46:36.4	9.75	04 Sep 2012	1×450
642	J19452+407	TYC 3140–883–1	...	19:45:12.50	+40:43:18.4	8.96	25 Sep 2012	1×450
643	J19519+141	LSPM J1951+1408	...	19:51:55.50	+14:08:23.4	9.42	03 Aug 2012	1×250
644	J19524+603	PM I19524+6022	...	19:52:24.50	+60:22:14.5	9.79	03 Aug 2012	1×700
645	J19539+444W AB	V1581 Cyg	1245 AB	19:53:54.43	+44:24:54.2	7.79	02 Aug 2012	1×800
646	J19539+444E	G 208–045	1245 C	19:53:55.09	+44:24:55.0	8.28	02 Aug 2012	1×1000
647	J19547+844	1RXS J195446.2+842937	...	19:54:47.20	+84:29:29.6	9.51	24 Sep 2012	1×900
648	J19564+591	BD+58 2015B	9677 B	19:56:24.90	+59:09:21.7	9.65	23 Sep 2012	1×600
649	J19565+591	BD+58 2015A	9677 A	19:56:34.01	+59:09:42.1	7.42	23 Sep 2012	1×200
650	J19578–108	LP 754–008	...	19:57:52.00	–10:53:05.0	9.73	02 Sep 2012	1×900
651	J20021+130 AB	PM I20021+1300	...	20:02:10.60	+13:00:31.5	9.73	05 Aug 2012	1×600
652	J20033+672	G 262–003	...	20:03:23.30	+67:16:48.8	9.45	05 Aug 2012	1×500
653	J20034+298	HD 190360 B	777 B	20:03:26.52	+29:52:00.1	9.55	12 Nov 2011	1×600
654	J20047+512	Wolf 1129	...	20:04:47.40	+51:13:16.9	9.49	05 Aug 2012	2×300
655	J20065+159	G 143–029	...	20:06:31.10	+15:59:17.1	9.74	05 Aug 2012	1×500
656	J20077+189	Wolf 869	...	20:07:42.70	+18:59:00.4	9.43	04 Sep 2012	1×350
657	J20093–012	SCR J2009–0113	...	20:09:18.20	–01:13:38.2	9.40	02 Sep 2012	1×497
658	J20108+772	HD 193202	786	20:10:52.42	+77:14:20.3	6.41	04 Aug 2012	1×120
659	J20112+161	HD 191785 B	783.2 B	20:11:13.29	+16:11:07.5	9.63	12 Nov 2011	1×350
660	J20123–126	ξ Cap B	4139 B	20:12:20.30	–12:37:06.0	...	23 Sep 2012	1×600
661	J20177+059	LSPM J2017+0559	...	20:17:43.30	+05:59:17.3	9.32	04 Sep 2012	1×250
662	J20182–202	NLTT 49012	...	20:18:14.60	–20:12:47.7	9.46	04 Sep 2012	1×250
663	J20216–199	LP 815–004	...	20:21:41.10	–19:57:18.0	9.47	02 Sep 2012	1×300
664	J20254–198	PM I20254–1948	...	20:25:27.10	–19:48:03.4	10.04	04 Aug 2012	3×600
665	J20283+617	LP 106–101	...	20:28:19.20	+61:43:47.9	9.32	03 Aug 2012	1×450
666	J20300+003 AB	PM I20300+0023	...	20:30:01.90	+00:23:55.3	9.91	04 Sep 2012	1×700
667	J20332+283	G 210–026	...	20:33:15.80	+28:23:44.5	9.96	04 Aug 2012	1×1000
668	J20336+365	G 209–036	...	20:33:41.80	+36:35:58.7	9.42	02 Sep 2012	1×400
669	J20382+231	1RXS J203813.6+230750	...	20:38:14.40	+23:07:52.4	9.20	04 Aug 2012	1×240
670	J20405+154	G 144–25	1256	20:40:33.64	+15:29:57.2	8.64	31 Aug 2012	1×1000 $+ 1 \times 800$
671	J20407+199 AB	HD 197076 B	797 B	20:40:44.50	+19:54:02.3	8.16	12 Nov 2011	1×300
672	J20439+231	Wolf 1361	...	20:43:54.10	+23:07:13.7	9.28	02 Sep 2012	1×300
673	J20467–118	LP 756–003	...	20:46:43.60	–11:48:13.3	9.35	04 Aug 2012	1×360
674	J20510+399	G 210–038	...	20:51:01.60	+39:55:43.3	9.06	03 Aug 2012	1×200
675	J20540+603	1RXS J205405.4+601811	...	20:54:05.10	+60:18:04.1	10.10	04 Aug 2012	3×450
676	J20581+401 AB	HD 200007 B	...	20:58:11.47	+40:11:29.0	8.14	23 Sep 2012	1×400

Table B.1: Observed stars: identification, common name, Gliese number, 2MASS coordinates and J magnitude, observing date, and exposure time (cont.).

No.	Karmn	Name	Gl/GJ	α (J2000)	δ (J2000)	J [mag]	Observation date	$N \times t_{\rm exp}$ [s]
677	J20583+425	G 212–012	...	20:58:23.10	+42:35:03.4	9.49	04 Aug 2012	1×360
678	J20593+530 AB	LSPM J2059+5303	...	20:59:20.40	+53:03:04.9	9.91	03 Aug 2012	1×600
679	J21009+510	G 231–024	...	21:00:59.80	+51:03:14.7	9.88	07 Dec 2011	1×400
680	J21019–063	Wolf 906	816	21:01:58.66	–06:19:07.1	7.56	02 Sep 2012	1×400
681	J21027+349	G 211–009	...	21:02:46.06	+34:54:36.0	9.85	07 Dec 2011	1×600
682	J21053+208	G 144–063	...	21:05:22.20	+20:51:34.2	9.42	03 Aug 2012	1×350
683	J21057+502W	PM I21057+5015W	...	21:05:42.40	+50:15:57.7	9.97	02 Aug 2012	1×749
684	J21057+502E	PMI21057+5015E	...	21:05:45.38	+50:15:43.6	9.54	07 Dec 2011	1×750
685	J21068+387	61 Cyg A	820 A	21:06:53.42	+38:44:53.0	3.11	11 Nov 2011	1×4
686	J21069+387	61 Cyg B	820 B	21:06:54.74	+38:44:26.64	3.55	11 Nov 2011	1×10
687	J21074+198	LP 456–039	...	21:07:24.44	+19:50:52.3	9.18	07 Dec 2011	1×300
688	J21074+468	PM I21074+4651	...	21:07:28.10	+46:51:53.8	9.49	07 Dec 2011	1×300
689	J21109+469	G 212–027	...	21:10:58.80	+46:57:32.1	9.88	02 Aug 2012	3×600
690	J21114+658	LSPM J2111+6553	...	21:11:27.40	+65:53:26.5	9.48	03 Aug 2012	1×350
691	J21127–073	PM I21127–0719	...	21:12:45.60	–07:19:55.8	9.90	07 Dec 2011	1×1100
692	J21147+160	G 145–029	...	21:14:47.50	+16:04:49.7	9.22	03 Aug 2012	1×250
693	J21245+400	LSR J2124+4003	...	21:24:32.34	+40:04:00.0	10.34	02 Aug 2012	3×900
694	J21376+016	2E 4498	...	21:37:40.20	+01:37:13.8	8.80	24 Sep 2012	1×300
695	J21414+207	1RXS J214127.5+204302	...	21:41:26.60	+20:43:10.8	9.43	03 Aug 2012	1×250
696	J21466+668	G 264–012	...	21:46:40.20	+66:48:10.6	8.84	24 Sep 2012	1×480
697	J21467–212	LP 874–062	...	21:46:45.50	–21:17:46.9	9.29	04 Sep 2012	1×280
698	J21472–047	PM I21472–0444	...	21:47:17.50	–04:44:40.6	9.42	02 Aug 2012	1×749
699	J21554+596 AB	RX J2155.3+5938	...	21:55:24.40	+59:38:37.2	9.18	02 Aug 2012	1×431
700	J22021+014	HD 209290	846	22:02:10.27	+01:24:00.8	6.20	05 Aug 2012	1×60
701	J22035+036 AB	1RXS J220330.8+034001	...	22:03:33.38	+03:40:23.6	9.74	04 Jan 2012	1×700
702	J22088+117	PM I22088+1144	...	22:08:50.35	+11:44:13.2	9.90	03 Jan 2012	1×750
703	J22089–177	HD 210190 B	...	22:08:54.18	–17:47:52.2	11.97	04 Sep 2012	1×800
704	J22095+118	LP 519–038	...	22:09:31.68	+11:52:53.7	9.90	10 Jan 2012	1×650
705	J22114+409	1RXS J221124.3+410000	...	22:11:24.17	+40:59:58.7	9.73	03 Jan 2012	3×600
706	J22160+546	V447 Per B	4269 B	22:16:02.59	+54:39:59.5	9.72	05 Aug 2012	1×900
706	J22202+067	Wolf 1034	...	22:20:13.27	+06:43:32.1	9.50	10 Jan 2012	1×300
708	J22234+324 AB	Wolf 1225	856 AB	22:23:29.05	+32:27:33.4	6.90	23 Sep 2012	1×80
709	J22264+583	PM I22264+5823	...	22:26:24.98	+58:23:05.1	9.46	03 Jan 2012	1×300
710	J22300+488 AB	2E 4617	...	22:30:04.19	+48:51:34.7	9.52	04 Jan 2012	1×450
711	J22386+567	V416 Lac	...	22:38:37.92	+56:47:44.3	1.09	04 Jan 2012	1×2
712	J22387+252	G 127–042	...	22:38:44.26	+25:13:30.5	9.77	09 Jan 2012	1×700
713	J22396–125	NV Aqr C	867.1 C	22:39:41.59	–12:35:20.4	10.57	04 Aug 2012	1×1000
714	J22415+260	1RXS J224134.7+260210	...	22:41:35.78	+26:02:12.9	9.04	10 Jan 2012	1×250

Table B.1: Observed stars: identification, common name, Gliese number, 2MASS coordinates and J magnitude, observing date, and exposure time (cont.).

No.	Karmn	Name	Gl/GJ	α (J2000)	δ (J2000)	J [mag]	Observation date	$N \times t_{\rm exp}$ [s]
715	J22437+192	RX J2243.7+1916	...	22:43:43.78	+19:16:54.5	9.24	10 Jan 2012	1×300
716	J22476+184	LP 461–011	...	22:47:38.84	+18:26:36.5	9.10	10 Jan 2012	1×200
717	J22489+183	PM J22489+1819	...	22:48:54.59	+18:19:59.3	9.96	10 Jan 2012	1×1000
718	J22509+499	1RXS J225056.4+495906	...	22:50:55.05	+49:59:13.2	9.80	03 Jan 2012	1×850
719	J22524+099 AB	σ Peg B	9801 B	22:52:29.77	+09:54:04.3	9.66	04 Sep 2012	1×360
720	J22526+750	NLTT 55174	...	22:52:39.64	+75:04:19.0	9.09	07 Dec 2011	1×200
721	J22582–110	1RXS J225817.2–110434	...	22:58:16.40	–11:04:17.1	9.07	03 Aug 2012	1×200
722	J22588+690	BD+68 1345B	...	22:58:50.60	+69:01:37.1	10.59	04 Sep 2012	2×800
723	J23006+036	LP 641–057	...	23:00:36.10	+03:38:17.0	9.59	06 Aug 2012	1×600
724	J23028+436	LSPM J2302+4338	...	23:02:52.51	+43:38:15.7	9.32	08 Dec 2011	1×400
725	J23036–072	LP 701–066	...	23:03:36.40	–07:16:30.2	9.48	05 Aug 2012	2×400
726	J23036+097	PM I23036+0942	...	23:03:37.45	+09:42:58.5	9.99	08 Dec 2011	1×300
727	J23051+519	PM I23051+5159	...	23:05:06.32	+51:59:13.3	9.68	08 Dec 2011	1×250
728	J23051+452	LSPM J2305+4517	...	23:05:08.71	+45:17:31.8	9.30	03 Jan 2012	1×210
729	J23070+094	55 Peg	...	23:07:00.26	+09:24:34.2	1.58	07 Dec 2011	1×1
730	J23177+490	8 And	...	23:17:44.65	+49:00:55.1	1.62	11 Jan 2012	1×1
731	J23182+795	LP 012–069	...	23:18:17.06	+79:34:47.4	9.71	03 Jan 2012	1×520
732	J23194+790	V368 Cep B	...	23:19:24.47	+79:00:03.7	8.04	11 Feb 2012	1×250
733	J23209–017 AB	LP 642–048	...	23:20:57.70	–01:47:37.3	9.36	06 Aug 2012	1×400
734	J23220+569	G 217–006	...	23:22:00.71	+56:59:19.9	9.47	08 Dec 2011	1×400
735	J23228+787	NLTT 56725	...	23:22:53.85	+78:47:38.6	10.42	11 Feb 2012	3×800
736	J23235+457	HD 220445 B	...	23:23:30.68	+45:47:18.6	7.38	04 Sep 2012	1×60
737	J23261+170 AB	2MASS J23261182+1700082	...	23:26:11.82	+17:00:08.3	9.36	10 Jan 2012	1×300
738	J23266+453	2MASS J23263798+4521054	...	23:26:37.98	+45:21:05.5	8.20	04 Sep 2012	1×60
739	J23306+466	Ross 247	...	23:30:41.80	+46:39:56.2	9.97	08 Dec 2011	1×700
740	J23317–064	2MASS J23314763–0625502	...	23:31:47.60	–06:25:50.4	9.84	05 Aug 2012	1×900
741	J23376+163	LP 463–023	...	23:37:36.00	+16:22:03.2	10.48	24 Sep 2012	3×900
742	J23416–065	LP 703–042	...	23:41:39.30	–06:35:50.4	10.32	06 Aug 2012	3×700
743	J23417–059 AB	HD 222582 B	...	23:41:45.15	–05:58:14.7	10.39	12 Nov 2011	1×600
744	J23419+441	HH And	905	23:41:54.99	+44:10:40.8	6.88	11 Nov 2011	1×400
745	J23423+349	PM I23423+3458	...	23:42:22.11	+34:58:27.7	9.32	04 Jan 2012	1×350
746	J23425+392	LP 291–007	...	23:42:33.50	+39:14:23.3	9.64	09 Jan 2012	1×1000
747	J23438+610	G 217–018	...	23:43:53.10	+61:02:15.7	9.39	04 Jan 2012	1×500
748	J23490–086	G 273–144	...	23:49:02.30	–08:24:30.9	9.50	02 Aug 2012	1×272
749	J23559–133	NLTT 58441	...	23:55:55.20	–13:21:23.8	9.26	02 Sep 2012	1×250
750	J23560+150	LP 523–078	...	23:56:00.29	+15:01:40.9	9.38	07 Dec 2011	1×250
751	J23569+230	G 129-045	...	23:56:55.10	+23:05:02.7	9.15	07 Dec 2011	1×300
752	J23585+242	G 131–006	...	23:58:30.21	+24:12:04.8	9.13	04 Sep 2012	1×90

Table B.1: Observed stars: identification, common name, Gliese number, 2MASS coordinates and J magnitude, observing date, and exposure time (cont.).

No.	Karmn	Name	Gl/GJ	α (J2000)	δ (J2000)	J [mag]	Observation date	$N \times t_{\mathrm{exp}}$ [s]
753	J23590+208	G 129–051	...	23:59:00.42	+20:51:38.8	9.07	07 Dec 2011	1×180

Table B.2: Seven representative spectral indices, ζ metallicity index, and Hα pseudo-equivalent width.

Karmn	PC1	TiO 2	TiO 5	VO-7912	Color-M	CaH 2	CaH 3	ζ	pEW(Hα) [Å]
J00066–070 AB	1.269	0.492	0.317	1.148	1.778	0.404	0.654	0.973	$-2.3^{+0.3}_{-0.5}$
J00077+603 AB	1.198	0.532	0.369	1.111	1.405	0.408	0.631	0.883	$-6.7^{+0.3}_{-0.4}$
J00115+591	1.511	0.378	0.202	1.222	2.902	0.281	0.564	0.970	$-1.6^{+0.2}_{-0.4}$
J00118+229	1.215	0.606	0.405	1.090	1.404	0.492	0.751	1.052	$-0.5^{+0.2}_{-0.2}$
J00119+330	1.167	0.634	0.427	1.072	1.293	0.503	0.748	1.023	$-0.3^{+0.1}_{-0.2}$
J00122+304	1.296	0.497	0.354	1.154	1.755	0.427	0.685	0.972	$-8.7^{+0.4}_{-0.5}$
J00133+275	1.296	0.512	0.339	1.144	1.805	0.425	0.686	0.994	$-4.0^{+0.2}_{-0.4}$
J00136+806	1.027	0.770	0.601	1.012	0.901	0.644	0.812	1.002	$+0.0^{+0.2}_{-0.2}$
J00146+202	0.955	0.729	0.520	1.005	0.643	0.839	0.946	2.754	$+0.8^{+0.1}_{-0.1}$
J00152+530	1.090	0.728	0.540	1.031	1.076	0.575	0.787	0.975	$+0.0^{+0.2}_{-0.2}$
J00162+198E	1.271	0.559	0.367	1.121	1.663	0.451	0.731	1.032	$-0.5^{+0.1}_{-0.2}$
J00162+198W	1.260	0.553	0.363	1.122	1.553	0.450	0.708	1.010	$-4.5^{+0.4}_{-0.4}$
J00183+440	0.990	0.810	0.638	1.004	0.892	0.651	0.818	0.932	$+0.0^{+0.2}_{-0.2}$
J00228–164	1.229	0.564	0.378	1.105	1.478	0.443	0.691	0.960	$-2.7^{+0.3}_{-0.3}$
J00240+264	1.266	0.539	0.350	1.132	1.705	0.447	0.710	1.030	$-1.9^{+0.3}_{-0.3}$
J00253+235	1.006	0.811	0.644	1.011	0.934	0.672	0.840	1.001	$+0.0^{+0.4}_{-0.4}$
J00297+012	0.997	0.819	0.665	1.002	0.877	0.684	0.844	0.975	$+0.0^{+0.2}_{-0.2}$
J00313+336	0.945	0.882	0.778	0.988	0.779	0.809	0.895	1.001	$+0.0^{+0.2}_{-0.2}$
J00313+001	1.138	0.658	0.474	1.061	1.183	0.530	0.758	0.991	$-0.4^{+0.1}_{-0.1}$
J00322+544	1.338	0.554	0.349	1.129	1.798	0.452	0.738	1.072	$-0.4^{+0.1}_{-0.2}$
J00328–045 AB	1.293	0.561	0.358	1.131	1.748	0.451	0.723	1.038	$-1.5^{+0.7}_{-0.1}$
J00358+526	1.080	0.706	0.510	1.035	1.059	0.565	0.777	1.004	$+0.0^{+0.4}_{-0.4}$
J00367+444	0.993	0.751	0.546	1.013	0.758	0.854	0.963	2.888	$+0.8^{+0.1}_{-0.1}$
J00380+169	1.124	0.672	0.471	1.057	1.189	0.509	0.742	0.945	$+0.0^{+0.2}_{-0.2}$
J00389+306	1.090	0.715	0.526	1.035	1.079	0.570	0.790	1.001	$+0.0^{+0.2}_{-0.2}$
J00395+149N	1.321	0.503	0.344	1.153	1.749	0.416	0.672	0.963	$-7.2^{+0.2}_{-0.3}$
J00395+149S	1.237	0.590	0.399	1.100	1.487	0.467	0.722	0.989	$-1.7^{+0.2}_{-0.2}$
J00452+002 AB	1.227	0.584	0.392	1.104	1.437	0.424	0.713	0.942	$-3.1^{+0.2}_{-0.3}$
J00464+506	1.256	0.559	0.371	1.116	1.554	0.478	0.753	1.092	$-0.5^{+0.1}_{-0.2}$
J00467–044	1.274	0.546	0.359	1.112	1.593	0.450	0.711	1.022	$-0.8^{+0.2}_{-0.3}$
J00484+753	1.121	0.665	0.475	1.058	1.138	0.534	0.762	1.000	$-1.1^{+0.3}_{-0.2}$
J00490+578	0.904	0.920	0.843	0.972	0.683	0.897	0.927	1.017	$+0.3^{+0.1}_{-0.1}$
J00490+657	1.108	0.707	0.517	1.043	1.118	0.564	0.784	0.998	$+0.0^{+0.2}_{-0.2}$
J00502+086	1.294	0.501	0.343	1.145	1.609	0.437	0.701	1.019	$-6.7^{+0.2}_{-0.3}$
J00502+601	1.154	0.747	0.559	1.034	1.068	0.793	0.915	2.017	$+0.8^{+0.1}_{-0.2}$
J00540+691	1.066	0.740	0.542	1.033	1.096	0.548	0.759	0.887	$+0.0^{+0.2}_{-0.2}$
J00548+275	1.294	0.521	0.353	1.145	1.682	0.429	0.691	0.983	$-5.3^{+-5.3}_{-0.2}$
J00580+393	1.285	0.531	0.352	1.141	1.688	0.417	0.667	0.947	$-3.7^{+0.3}_{-0.2}$
J01009–044	1.212	0.605	0.378	1.090	1.492	0.429	0.677	0.931	$+0.0^{+0.2}_{-0.2}$
J01012+571	1.123	0.842	0.703	1.019	1.087	0.893	0.947	2.021	$+1.1^{+0.2}_{-0.2}$
J01014+188	1.067	0.710	0.513	1.033	1.018	0.580	0.794	1.052	$+0.0^{+0.2}_{-0.2}$
J01014–010	1.215	0.613	0.415	1.102	1.386	0.485	0.731	0.997	$+0.0^{+0.2}_{-0.2}$
J01026+623	1.043	0.778	0.615	1.017	0.960	0.643	0.820	0.979	$+0.0^{+0.2}_{-0.2}$

Table B.2: Seven representative spectral indices, ζ metallicity index, and Hα pseudo-equivalent width (cont.).

Karmn	PC1	TiO 2	TiO 5	VO-7912	Color-M	CaH 2	CaH 3	ζ	$pEW(\mathrm{H}\alpha)$ [Å]
J01028+189	1.244	0.529	0.349	1.124	1.352	0.450	0.712	1.038	$-9.7^{+0.3}_{-0.3}$
J01028+470	0.999	0.760	0.578	1.013	0.855	0.621	0.806	1.001	$+0.0^{+0.2}_{-0.2}$
J01032+712	1.323	0.589	0.395	1.108	1.785	0.453	0.719	0.975	$-0.6^{+0.2}_{-0.4}$
J01033+623	1.394	0.438	0.302	1.176	1.959	0.385	0.644	0.968	$-10.1^{+0.4}_{-0.1}$
J01055+153	0.865	0.918	0.836	0.965	0.579	0.916	0.935	1.160	$+0.4^{+0.1}_{-0.1}$
J01069+804	1.321	0.490	0.332	1.150	1.770	0.408	0.668	0.970	$-7.2^{+0.3}_{-0.2}$
J01074–025	0.860	0.937	0.876	0.981	0.603	1.027	0.979	1.386	$+0.7^{+0.4}_{-0.2}$
J01076+229E	1.189	0.569	0.393	1.097	1.355	0.508	0.743	1.084	$+2.2^{+0.8}_{-0.4}$
J01097+356	0.943	0.826	0.652	0.992	0.662	0.937	0.965	2.902	$+0.9^{+0.2}_{-0.3}$
J01186–008	0.903	0.917	0.810	0.970	0.674	0.869	0.917	1.093	$+0.5^{+0.1}_{-0.2}$
J01214+313	1.160	0.606	0.421	1.078	1.277	0.510	0.742	1.035	$+0.0^{+0.2}_{-0.2}$
J01226+127	0.886	0.896	0.795	0.973	0.635	0.863	0.918	1.162	$+0.4^{+0.1}_{-0.1}$
J01342–015	0.989	0.797	0.628	0.998	0.849	0.679	0.849	1.086	$+0.0^{+0.2}_{-0.2}$
J01356–200 AB	1.082	0.706	0.520	1.039	1.049	0.582	0.796	1.045	$+0.0^{+0.2}_{-0.2}$
J01390–179 AB	1.336	0.429	0.313	1.198	2.326	0.410	0.638	0.970	$-4.8^{+0.4}_{-0.2}$
J01406–081	0.882	0.940	0.892	0.972	0.641	0.996	0.966	1.082	$+0.7^{+0.2}_{-0.2}$
J01431+210	1.240	0.509	0.351	1.130	1.425	0.465	0.723	1.066	$-4.9^{+0.2}_{-0.2}$
J01541–156	1.236	0.572	0.356	1.127	1.612	0.449	0.688	0.997	$-1.3^{+0.2}_{-0.3}$
J01551–162	0.896	0.923	0.865	0.979	0.668	0.955	0.948	1.128	$+0.5^{+0.2}_{-0.2}$
J01562+001	1.120	0.616	0.460	1.063	1.107	0.500	0.713	0.917	$-5.2^{+0.3}_{-0.2}$
J01567+305	1.295	0.457	0.333	1.159	1.878	0.397	0.630	0.925	$-16.0^{+0.4}_{-0.4}$
J01571–102	0.944	0.869	0.758	0.981	0.745	0.809	0.889	1.073	$+0.4^{+0.1}_{-0.1}$
J02000+135 AB	1.169	0.618	0.417	1.076	1.244	0.505	0.749	1.046	$+0.0^{+0.2}_{-0.2}$
J02002+130	1.154	0.658	0.486	1.122	1.498	0.557	0.800	1.080	$-2.0^{+0.2}_{-0.3}$
J02019+342	0.964	0.861	0.738	0.990	0.821	0.774	0.882	1.037	$+0.4^{+0.2}_{-0.2}$
J02022+103	1.491	0.387	0.213	1.216	2.583	0.319	0.619	1.015	$-1.6^{+0.5}_{-0.3}$
J02023+012	1.082	0.751	0.565	1.027	1.092	0.574	0.783	0.912	$+0.0^{+0.2}_{-0.2}$
J02100–088	1.145	0.588	0.395	1.073	1.107	0.501	0.763	1.101	$-0.4^{+0.1}_{-0.1}$
J02133+368 AB	1.279	0.476	0.330	1.149	1.735	0.381	0.617	0.906	$-6.2^{+0.4}_{-0.2}$
J02142–039	1.558	0.350	0.236	1.240	2.800	0.335	0.625	1.002	$-12.3^{+0.9}_{-0.7}$
J02159–094 ABC	1.090	0.668	0.504	1.061	1.013	0.564	0.754	0.979	$-6.0^{+0.4}_{-0.4}$
J02274+031	1.205	0.556	0.384	1.111	1.432	0.440	0.676	0.933	$-4.2^{+0.4}_{-0.3}$
J02285–200	1.070	0.719	0.512	1.043	1.068	0.537	0.752	0.921	$+0.0^{+0.2}_{-0.2}$
J02291+228	0.899	0.935	0.865	0.976	0.680	0.968	0.962	1.229	$+0.6^{+0.2}_{-0.2}$
J02362+068	1.202	0.602	0.385	1.108	1.506	0.464	0.739	1.030	$-0.5^{+0.2}_{-0.2}$
J02367+226	1.406	0.428	0.280	1.178	2.158	0.361	0.627	0.964	$-5.5^{+0.5}_{-0.4}$
J02412–045	1.272	0.507	0.352	1.136	1.682	0.405	0.651	0.921	$-3.8^{+0.3}_{-0.4}$
J02441+492	1.017	0.782	0.607	1.011	0.932	0.634	0.821	0.983	$+0.0^{+0.2}_{-0.2}$
J02456+449	0.968	0.873	0.716	0.991	0.838	0.745	0.881	1.040	$+0.4^{+0.1}_{-0.2}$
J02479–124	1.382	0.747	0.459	1.227	2.418	0.779	1.455	5.825	$+0.0^{+0.2}_{-0.2}$
J02502+628	1.125	0.680	0.489	1.048	1.187	0.532	0.759	0.967	$+0.0^{+0.2}_{-0.2}$
J02530+168	1.823	0.256	0.134	1.292	4.540	0.224	0.533	1.012	$-2.4^{+0.6}_{-0.8}$
J02555+268	1.273	0.567	0.369	1.112	1.621	0.465	0.728	1.044	$-0.5^{+0.2}_{-0.2}$
J02558+183	1.573	1.008	0.415	1.222	2.599	0.453	0.855	1.134	$+0.0^{+0.2}_{-0.2}$

Table B.2: Seven representative spectral indices, ζ metallicity index, and Hα pseudo-equivalent width (cont.).

Karmn	PC1	TiO 2	TiO 5	VO-7912	Color-M	CaH 2	CaH 3	ζ	pEW(Hα) [Å]
J02562+239	1.357	0.478	0.328	1.156	1.896	0.402	0.679	0.980	$-6.6^{+0.4}_{-0.2}$
J03026–181	1.098	0.711	0.520	1.040	1.068	0.566	0.785	0.996	$+0.0^{+0.2}_{-0.2}$
J03033–080	1.138	0.634	0.444	1.072	1.187	0.536	0.776	1.085	$-1.9^{+0.2}_{-0.2}$
J03047+617	1.139	0.660	0.455	1.062	1.203	0.530	0.783	1.067	$-0.4^{+0.1}_{-0.1}$
J03110–046	1.133	0.676	0.480	1.059	1.171	0.534	0.765	0.997	$-0.4^{+0.1}_{-0.1}$
J03147+114	1.038	0.716	0.565	1.041	0.989	0.614	0.800	1.010	$-3.3^{+0.5}_{-0.4}$
J03154+578	1.141	0.608	0.437	1.065	1.265	0.473	0.710	0.920	$+0.0^{+0.2}_{-0.2}$
J03162+581N	1.059	0.752	0.560	1.021	0.993	0.595	0.794	0.975	$+0.0^{+0.2}_{-0.2}$
J03162+581S	1.069	0.761	0.588	1.024	1.028	0.611	0.800	0.951	$+0.0^{+0.2}_{-0.2}$
J03167+389	1.191	0.612	0.413	1.089	1.395	0.494	0.750	1.038	$+0.0^{+0.2}_{-0.2}$
J03174–011	0.954	0.820	0.682	0.990	0.760	0.710	0.855	1.007	$+0.0^{+0.2}_{-0.2}$
J03179–010	1.039	0.733	0.531	1.019	0.939	0.546	0.763	0.912	$+0.0^{+0.2}_{-0.2}$
J03181+426	1.224	0.605	0.401	1.092	1.442	0.494	0.757	1.069	$+0.0^{+0.2}_{-0.2}$
J03194+619	1.262	0.523	0.363	1.132	1.537	0.428	0.666	0.941	$-7.0^{+0.4}_{-0.3}$
J03236+056	1.354	0.488	0.320	1.164	1.755	0.417	0.693	1.022	$-7.9^{+0.2}_{-0.3}$
J03236+476	0.971	0.858	0.738	0.996	0.839	0.775	0.882	1.041	$+0.4^{+0.2}_{-0.2}$
J03263+171	1.227	0.603	0.390	1.101	1.503	0.491	0.760	1.091	$-0.8^{+0.2}_{-0.2}$
J03275+222	1.309	0.533	0.344	1.140	1.670	0.433	0.707	1.019	$-5.4^{+0.4}_{-0.3}$
J03294+117	1.064	0.684	0.474	1.055	0.981	0.561	0.777	1.071	$+0.0^{+0.4}_{-0.4}$
J03303+346	1.260	0.542	0.383	1.123	1.451	0.459	0.708	0.989	$-8.2^{+0.3}_{-0.3}$
J03309+706	1.157	0.625	0.429	1.074	1.345	0.477	0.714	0.942	$+0.0^{+0.3}_{-0.3}$
J03319+492	0.907	0.979	0.939	0.997	0.707	1.073	1.010	0.772	$+1.2^{+0.1}_{-0.2}$
J03320+436	0.906	0.913	0.832	0.972	0.699	0.902	0.932	1.125	$+0.4^{+0.2}_{-0.2}$
J03325+287 ABC	1.292	0.523	0.345	1.136	1.564	0.436	0.705	1.019	$-7.0^{+0.4}_{-0.2}$
J03332+462	0.919	0.866	0.789	0.995	0.705	0.875	0.903	1.182	$-3.4^{+0.5}_{-0.3}$
J03354+428	0.966	0.870	0.744	0.992	0.816	0.762	0.882	0.981	$+0.0^{+0.4}_{-0.4}$
J03356–084	1.443	0.424	0.238	1.182	2.405	0.339	0.628	1.003	$+0.0^{+0.3}_{-0.3}$
J03361+313	1.320	0.476	0.325	1.152	1.832	0.396	0.652	0.953	$-7.4^{+0.6}_{-0.3}$
J03375+288	0.944	0.869	0.756	0.981	0.769	0.820	0.914	1.200	$+0.0^{+0.4}_{-0.4}$
J03375+178N AB	1.085	0.728	0.542	1.045	1.099	0.573	0.784	0.962	$-1.4^{+0.4}_{-0.2}$
J03375+178S AB	1.145	0.667	0.459	1.109	1.309	0.517	0.777	1.029	$-6.8^{+0.6}_{-0.5}$
J03392+565 AB	1.141	0.673	0.479	1.058	1.185	0.556	0.795	1.084	$-0.4^{+0.1}_{-0.1}$
J03430+459	1.209	0.566	0.373	1.099	1.485	0.443	0.694	0.971	$-0.7^{+0.2}_{-0.3}$
J03466+243 AB	0.882	0.949	0.890	0.975	0.627	1.014	0.973	1.172	$+0.0^{+0.5}_{-0.5}$
J03473–019	1.129	0.658	0.498	1.047	1.124	0.532	0.747	0.933	$-3.7^{+0.4}_{-0.2}$
J03480+405	1.026	0.774	0.615	1.026	0.933	0.669	0.819	1.030	$-2.6^{+0.5}_{-0.4}$
J03510+142	1.306	0.500	0.360	1.142	1.530	0.439	0.692	0.984	$-13.4^{+0.6}_{-0.6}$
J03519+397	0.936	0.898	0.800	0.977	0.727	0.831	0.900	0.975	$+0.0^{+0.4}_{-0.4}$
J03548+163 AB	1.242	0.539	0.376	1.120	1.516	0.442	0.684	0.954	$-8.6^{+0.7}_{-0.4}$
J03556+522	1.075	0.717	0.514	1.033	1.059	0.536	0.751	0.913	$+0.0^{+0.2}_{-0.2}$
J03565+319	1.202	0.579	0.405	1.098	1.409	0.473	0.719	0.983	$-4.7^{+0.6}_{-0.3}$
J03566+507	0.879	0.948	0.893	0.971	0.648	0.985	0.961	1.025	$+0.4^{+0.2}_{-0.2}$
J03574–011 AB	1.082	0.722	0.543	1.037	1.053	0.566	0.761	0.915	$-2.2^{+0.2}_{-0.2}$
J03588+125	1.298	0.557	0.362	1.130	1.734	0.472	0.754	1.101	$-0.5^{+0.2}_{-0.3}$

Table B.2: Seven representative spectral indices, ζ metallicity index, and Hα pseudo-equivalent width (cont.).

Karmn	PC1	TiO 2	TiO 5	VO-7912	Color-M	CaH 2	CaH 3	ζ	$pEW(\mathrm{H}\alpha)$ [Å]
J04041+307	1.027	0.769	0.585	1.019	0.998	0.581	0.783	0.880	$+0.0^{+0.4}_{-0.4}$
J04061–055	1.199	0.619	0.407	1.081	1.442	0.465	0.715	0.966	$-0.4^{+0.1}_{-0.1}$
J04079+142	1.132	0.668	0.470	1.062	1.213	0.541	0.781	1.052	$+0.0^{+0.3}_{-0.3}$
J04081+743	1.181	0.640	0.436	1.076	1.389	0.477	0.719	0.937	$-0.4^{+0.2}_{-0.2}$
J04083+691	1.279	0.528	0.330	1.140	1.804	0.397	0.667	0.960	$-0.8^{+0.3}_{-0.2}$
J04123+162 AB	1.211	0.584	0.402	1.099	1.434	0.472	0.724	0.993	$-2.5^{+0.3}_{-0.3}$
J04153–076	1.297	0.475	0.315	1.133	1.653	0.402	0.666	0.986	$-5.0^{+0.6}_{-0.5}$
J04177+410	1.165	0.614	0.458	1.074	1.212	0.489	0.708	0.900	$-6.4^{+0.4}_{-0.3}$
J04177+136 AB	1.051	0.795	0.647	1.009	0.997	0.666	0.829	0.958	$+0.0^{+0.2}_{-0.2}$
J04191–074	1.228	0.566	0.364	1.112	1.428	0.489	0.748	1.115	$-0.4^{+0.1}_{-0.1}$
J04191+097	1.150	0.657	0.440	1.065	1.315	0.494	0.734	0.970	$-0.3^{+0.1}_{-0.2}$
J04205+815	1.120	0.725	0.537	1.043	1.194	0.551	0.768	0.913	$+0.0^{+0.3}_{-0.3}$
J04206+272	1.366	0.524	0.334	1.152	1.632	0.463	0.776	1.170	$-8.9^{+0.6}_{-0.3}$
J04206–168	1.325	1.042	0.546	1.071	1.416	0.571	0.893	1.160	$+0.0^{+0.5}_{-0.5}$
J04207+152 AB	1.231	0.563	0.387	1.105	1.512	0.468	0.729	1.020	$-1.5^{+0.2}_{-0.3}$
J04224+036	1.160	0.560	0.404	1.096	1.171	0.479	0.706	0.976	$-6.7^{+0.5}_{-0.4}$
J04227+205	1.269	0.547	0.378	1.125	1.538	0.455	0.703	0.986	$-5.4^{+0.3}_{-0.4}$
J04229+259	1.282	0.564	0.361	1.129	1.680	0.452	0.717	1.027	$-0.6^{+0.3}_{-0.2}$
J04234+809	1.227	0.580	0.409	1.097	1.399	0.460	0.687	0.925	$-8.2^{+0.8}_{-0.5}$
J04238+149 AB	1.160	0.616	0.453	1.078	1.252	0.511	0.729	0.963	$-9.1^{+0.4}_{-0.3}$
J04238+092 AB	1.166	0.668	0.497	1.053	1.238	0.527	0..749	0.931	$-3.7^{+0.3}_{-0.2}$
J04247–067 ABC	1.237	0.553	0.364	1.090	1.314	0.450	0.689	0.986	$-5.0^{+0.6}_{-0.4}$
J04252+172 ABC	1.186	0.581	0.416	1.102	1.260	0.486	0.712	0.973	$-7.0^{+0.4}_{-0.4}$
J04290+186	1.096	0.693	0.526	1.056	1.061	0.570	0.765	0.960	$-11.9^{+0.5}_{-0.3}$
J04308–088	1.267	0.564	0.363	1.109	1.581	0.437	0.686	0.972	$-1.5^{+0.5}_{-0.4}$
J04310+367	1.134	0.639	0.460	1.067	1.240	0.501	0.728	0.936	$-3.2^{+0.4}_{-0.2}$
J04313+241 AB	1.418	0.491	0.315	1.166	1.884	0.433	0.750	1.118	$-9.4^{+0.6}_{-0.5}$
J04329+001S	0.957	0.825	0.669	0.992	0.757	0.711	0.845	1.024	$+0.0^{+0.3}_{-0.3}$
J04347–004	1.213	0.588	0.391	1.105	1.517	0.443	0.691	0.940	$-2.0^{+0.2}_{-0.4}$
J04360+188	1.107	0.645	0.488	1.060	1.113	0.541	0.750	0.968	$-5.8^{+0.4}_{-0.4}$
J04366+186	1.077	0.722	0.540	1.033	1.049	0.582	0.790	0.989	$-1.0^{+0.2}_{-0.3}$
J04373+193	1.269	0.501	0.350	1.131	1.594	0.428	0.670	0.964	$-8.3^{+0.6}_{-0.2}$
J04386–115	1.193	0.643	0.432	1.070	1.282	0.504	0.769	1.046	$+0.0^{+0.3}_{-0.3}$
J04388+217	1.175	0.624	0.422	1.087	1.349	0.499	0.748	1.026	$-0.6^{+0.1}_{-0.2}$
J04393+335	1.266	0.540	0.384	1.135	1.447	0.470	0.718	1.014	$-11.2^{+0.5}_{-0.4}$
J04398+251	1.168	0.625	0.422	1.081	1.317	0.480	0.726	0.972	$+0.0^{+0.4}_{-0.4}$
J04413+327	1.252	0.599	0.403	1.103	1.571	0.490	0.758	1.062	$-0.4^{+0.2}_{-0.1}$
J04425+204 AB	1.140	0.621	0.443	1.074	1.182	0.514	0.731	0.987	$-4.8^{+0.3}_{-0.3}$
J04430+187 AB	0.875	0.934	0.868	0.985	0.631	1.005	0.967	1.351	$+0.7^{+0.2}_{-0.2}$
J04458–144	1.268	0.582	0.384	1.108	1.487	0.488	0.753	1.085	$-0.5^{+0.2}_{-0.2}$
J04468–112 AB	1.147	0.608	0.431	1.076	1.142	0.483	0.712	0.943	$-5.1^{+0.4}_{-0.2}$
J04472+206	1.349	0.440	0.302	1.181	1.773	0.394	0.654	0.985	$-14.4^{+1.0}_{-0.5}$
J04494+484 AB	1.252	0.538	0.378	1.107	1.500	0.440	0.680	0.944	$-5.5^{+0.5}_{-0.5}$
J04496–153	0.867	0.957	0.914	0.966	0.614	1.019	0.979	0.945	$+0.5^{+0.1}_{-0.2}$

Table B.2: Seven representative spectral indices, ζ metallicity index, and Hα pseudo-equivalent width (cont.).

Karmn	PC1	TiO 2	TiO 5	VO-7912	Color-M	CaH 2	CaH 3	ζ	pEW(Hα) [Å]
J04499+711	1.223	0.612	0.420	1.084	1.475	0.486	0.745	1.009	$-0.3^{+0.1}_{-0.2}$
J04536+623	1.195	0.619	0.408	1.089	1.445	0.474	0.731	0.994	$+0.0^{+0.2}_{-0.2}$
J04538+158	1.113	0.691	0.490	1.044	1.159	0.535	0.768	0.981	$-0.4^{+0.1}_{-0.1}$
J04544+650	1.246	0.558	0.375	1.119	1.513	0.434	0.681	0.943	$-13.9^{+0.8}_{-0.5}$
J04559+046	1.057	0.736	0.570	1.028	0.996	0.603	0.788	0.958	$-3.3^{+0.3}_{-0.2}$
J04560+432	1.228	0.597	0.386	1.104	1.479	0.462	0.718	1.001	$-0.5^{+0.2}_{-0.4}$
J05003+251 AB	1.006	0.800	0.644	0.999	0.883	0.677	0.847	1.025	$+0.0^{+0.3}_{-0.3}$
J05019+011	1.261	0.547	0.370	1.125	1.423	0.454	0.716	1.014	$-8.2^{+0.5}_{-0.3}$
J05030+213 AB	1.406	0.475	0.323	1.172	2.130	0.386	0.649	0.944	$-5.3^{+0.7}_{-0.5}$
J05032+213	1.025	0.743	0.561	1.022	0.901	0.610	0.799	1.008	$+0.0^{+0.2}_{-0.2}$
J05050+442	1.410	0.502	0.293	1.166	2.133	0.388	0.681	1.019	$-1.0^{+0.4}_{-0.2}$
J05062+046	1.267	0.529	0.353	1.141	1.453	0.437	0.696	0.997	$-10.0^{+0.6}_{-0.2}$
J05068+516	0.853	0.963	0.920	0.968	0.598	1.051	0.994	0.969	$+0.6^{+0.1}_{-0.2}$
J05072+375	1.319	0.442	0.296	1.174	1.957	0.360	0.606	0.927	$-9.0^{+0.6}_{-0.5}$
J05083+756	1.312	0.531	0.336	1.130	1.810	0.421	0.694	1.003	$-0.7^{+0.4}_{-0.3}$
J05151–073	0.990	0.821	0.667	1.000	0.880	0.687	0.844	0.975	$+0.0^{+0.3}_{-0.3}$
J05152+236	1.361	0.447	0.309	1.179	1.969	0.390	0.647	0.966	$-8.4^{+0.9}_{-0.8}$
J05173+321	1.173	0.639	0.437	1.073	1.317	0.507	0.764	1.033	$-1.2^{+0.5}_{-0.5}$
J05175+487	0.932	0.910	0.804	0.983	0.752	0.834	0.915	1.011	$+0.0^{+0.4}_{-0.4}$
J05187+464	1.309	0.469	0.329	1.153	1.711	0.403	0.648	0.950	$-11.6^{+0.8}_{-0.8}$
J05187–213	1.169	0.607	0.421	1.082	1.268	0.480	0.716	0.962	$-3.4^{+0.5}_{-0.7}$
J05195+649	1.163	0.593	0.388	1.100	1.266	0.465	0.710	0.991	$-2.0^{+0.2}_{-0.3}$
J05200–229	1.047	0.706	0.524	1.026	0.935	0.566	0.766	0.960	$+0.0^{+0.3}_{-0.3}$
J05223+305	1.165	0.648	0.441	1.059	1.243	0.516	0.759	1.034	$+0.0^{+0.3}_{-0.3}$
J05256–091 AB	1.162	0.596	0.420	1.071	1.185	0.464	0.701	0.928	$-7.3^{+0.4}_{-0.3}$
J05289+125	1.224	0.604	0.394	1.097	1.469	0.448	0.699	0.948	$-1.8^{+0.6}_{-0.3}$
J05294+155E	0.891	0.845	0.701	0.984	0.652	0.764	0.882	1.152	$+0.0^{+0.4}_{-0.4}$
J05295–113	1.187	0.618	0.411	1.090	1.363	0.493	0.755	1.048	$+0.0^{+0.2}_{-0.2}$
J05300+121E	0.934	0.861	0.738	0.990	0.762	0.787	0.884	1.081	$+0.0^{+0.4}_{-0.4}$
J05300+121W	0.862	0.951	0.901	0.971	0.611	1.012	0.973	1.058	$+0.6^{+0.2}_{-0.3}$
J05314–036	1.040	0.784	0.618	1.018	0.989	0.655	0.834	1.023	$+0.0^{+0.3}_{-0.3}$
J05320–030	1.040	0.729	0.569	1.040	0.918	0.632	0.803	1.039	$-4.0^{+0.3}_{-0.4}$
J05324–072	0.916	0.852	0.725	0.983	0.680	0.763	0.874	1.040	$+0.0^{+0.2}_{-0.2}$
J05328+338	1.144	0.642	0.431	1.067	1.320	0.467	0.703	0.916	$+0.0^{+0.2}_{-0.2}$
J05342+103N	1.145	0.647	0.446	1.056	1.139	0.531	0.771	1.065	$+0.0^{+0.2}_{-0.2}$
J05342+103S	1.382	0.587	0.383	1.116	1.870	0.456	0.722	1.003	$+0.0^{+0.2}_{-0.2}$
J05394+747	1.171	0.643	0.436	1.072	1.316	0.496	0.740	0.988	$+0.0^{+0.2}_{-0.2}$
J05415+534	0.995	0.825	0.677	0.998	0.867	0.697	0.846	0.972	$+0.0^{+0.2}_{-0.2}$
J05421+124	1.241	0.576	0.366	1.113	1.568	0.457	0.726	1.035	$-0.5^{+-0.5}_{-0.3}$
J05424+506	1.143	0.646	0.434	1.070	1.258	0.501	0.748	1.008	$-0.3^{+-0.3}_{-0.2}$
J05425+154	1.158	0.596	0.419	1.093	1.306	0.468	0.703	0.935	$-4.5^{+0.5}_{-0.2}$
J05427+026	1.161	0.647	0.440	1.067	1.259	0.520	0.775	1.065	$-0.3^{+0.1}_{-0.2}$
J05455–119	1.319	0.553	0.358	1.129	1.769	0.458	0.742	1.072	$-0.6^{+0.3}_{-0.5}$
J05456+111	0.895	0.886	0.788	0.980	0.678	0.850	0.910	1.128	$+0.4^{+0.1}_{-0.2}$

Table B.2: Seven representative spectral indices, ζ metallicity index, and Hα pseudo-equivalent width (cont.).

Karmn	PC1	TiO 2	TiO 5	VO-7912	Color-M	CaH 2	CaH 3	ζ	$pEW(\mathrm{H}\alpha)$ [Å]
J05456+729	1.132	0.675	0.476	1.057	1.228	0.527	0.763	0.991	$+0.0^{+0.2}_{-0.2}$
J05457–223	1.178	0.640	0.397	1.064	1.285	0.450	0.705	0.953	$+0.0^{+0.4}_{-0.4}$
J05458+729	1.092	0.685	0.486	1.044	1.011	0.549	0.776	1.026	$+0.0^{+0.3}_{-0.3}$
J05463+012	1.123	0.701	0.504	1.043	1.132	0.558	0.781	1.011	$+0.0^{+0.3}_{-0.3}$
J05501+051	1.015	0.781	0.646	1.022	0.896	0.692	0.833	1.023	$-3.4^{+0.4}_{-0.1}$
J05511+122	1.251	0.600	0.391	1.098	1.552	0.472	0.737	1.030	$-0.6^{+0.3}_{-0.2}$
J05566–103	1.194	0.589	0.411	1.091	1.390	0.451	0.685	0.910	$-3.4^{+0.6}_{-0.4}$
J05582–046	1.351	0.495	0.271	1.143	1.890	0.387	0.680	1.048	$-0.8^{+0.4}_{-0.2}$
J05588+213	1.380	0.456	0.284	1.167	2.246	0.393	0.685	1.040	$-1.5^{+0.5}_{-0.4}$
J05596+585	0.953	0.805	0.642	0.997	0.772	0.691	0.836	1.041	$+0.0^{+0.3}_{-0.3}$
J06024+663	1.349	0.529	0.332	1.143	1.872	0.443	0.723	1.071	$-0.7^{+0.3}_{-0.3}$
J06024+498	1.397	0.473	0.280	1.165	2.206	0.374	0.665	1.007	$-0.6^{+0.2}_{-0.3}$
J06035+168	1.229	0.547	0.381	1.109	1.518	0.421	0.650	0.893	$-5.0^{+0.3}_{-0.2}$
J06035+155	0.944	0.885	0.805	0.992	0.758	0.862	0.905	1.064	$+0.0^{+0.6}_{-0.6}$
J06054+608	1.301	0.488	0.355	1.158	1.769	0.457	0.710	1.033	$-9.3^{+0.6}_{-0.4}$
J06065+045	1.151	0.642	0.415	1.066	1.186	0.499	0.757	1.054	$+0.0^{+0.2}_{-0.2}$
J06066+465	1.153	0.658	0.464	1.062	1.286	0.518	0.763	0.998	$-0.5^{+0.1}_{-0.2}$
J06075+472	1.314	0.492	0.341	1.150	1.799	0.415	0.666	0.961	$-9.2^{+0.8}_{-0.9}$
J06102+225	1.277	0.512	0.372	1.126	1.421	0.451	0.672	0.958	$-7.9^{+0.6}_{-0.4}$
J06103+722	1.086	0.674	0.467	1.054	1.076	0.552	0.795	1.103	$+0.0^{+0.4}_{-0.4}$
J06145+025	1.143	0.626	0.428	1.071	1.172	0.515	0.760	1.058	$+0.0^{+0.4}_{-0.4}$
J06151–164	1.267	0.583	0.384	1.100	1.609	0.462	0.698	0.979	$+0.0^{+0.3}_{-0.3}$
J06171+051 AB	1.188	0.643	0.419	1.082	1.395	0.479	0.737	0.990	$+0.0^{+0.4}_{-0.4}$
J06185+250	1.244	0.576	0.387	1.110	1.505	0.486	0.757	1.084	$+0.0^{+0.4}_{-0.4}$
J06236–096 AB	1.160	0.624	0.437	1.075	1.302	0.477	0.710	0.924	$-2.2^{+0.5}_{-0.5}$
J06238+456	1.397	0.459	0.298	1.170	2.084	0.382	0.655	0.981	$-6.1^{+0.9}_{-0.6}$
J06246+234	1.214	0.559	0.342	1.103	1.489	0.412	0.669	0.959	$+0.0^{+0.4}_{-0.4}$
J06298–027 AB	1.250	0.502	0.352	1.123	1.487	0.457	0.724	1.056	$-5.7^{+0.5}_{-0.5}$
J06307+397	1.055	0.742	0.556	1.027	1.041	0.573	0.782	0.928	$+0.0^{+0.2}_{-0.2}$
J06313+006	1.022	0.806	0.631	1.014	0.931	0.657	0.838	1.000	$+0.0^{+0.2}_{-0.2}$
J06314–016	0.986	0.760	0.561	1.017	0.812	0.635	0.844	1.152	$+0.0^{+0.2}_{-0.2}$
J06323–097	1.290	0.543	0.349	1.127	1.743	0.437	0.704	1.012	$-0.9^{+0.3}_{-0.1}$
J06325+641	1.259	0.572	0.377	1.117	1.573	0.479	0.759	1.094	$-0.5^{+0.2}_{-0.1}$
J06332+054	1.070	0.734	0.551	1.030	1.037	0.608	0.815	1.058	$+0.0^{+0.3}_{-0.3}$
J06354–040 AB	1.467	0.418	0.283	1.183	2.351	0.364	0.647	0.980	$-7.1^{+0.7}_{-0.5}$
J06361+201	1.084	0.693	0.492	1.044	1.102	0.539	0.769	0.987	$+0.0^{+0.4}_{-0.4}$
J06367+378	1.219	0.568	0.396	1.110	1.336	0.475	0.718	1.000	$-6.8^{+0.4}_{-0.3}$
J06401–164	1.070	0.663	0.458	1.045	1.019	0.527	0.757	1.015	$+0.0^{+0.4}_{-0.4}$
J06435+166	1.288	0.538	0.340	1.130	1.730	0.445	0.723	1.060	$-0.7^{+0.2}_{-0.4}$
J06461+325	0.998	0.833	0.686	0.997	0.893	0.692	0.842	0.925	$+0.0^{+0.3}_{-0.3}$
J06474+054	1.266	0.587	0.382	1.109	1.567	0.486	0.758	1.094	$-0.3^{+0.1}_{-0.2}$
J06489+211	1.086	0.689	0.525	1.051	1.097	0.561	0.765	0.949	$-1.9^{+0.1}_{-0.3}$
J06509–091	1.187	0.632	0.429	1.068	1.330	0.498	0.748	1.013	$-0.3^{+0.1}_{-0.3}$
J06522+179	0.937	0.916	0.833	0.978	0.761	0.862	0.922	0.958	$+0.4^{+0.1}_{-0.2}$

Table B.2: Seven representative spectral indices, ζ metallicity index, and Hα pseudo-equivalent width (cont.).

Karmn	PC1	TiO 2	TiO 5	VO-7912	Color-M	CaH 2	CaH 3	ζ	pEW(Hα) [Å]
J06522+627	1.205	0.604	0.426	1.087	1.436	0.467	0.703	0.924	$-2.4^{+0.5}_{-0.3}$
J06523–051S AB	1.065	0.744	0.554	1.032	1.054	0.583	0.791	0.964	$+0.0^{+0.3}_{-0.3}$
J06523–051N	0.840	0.972	0.925	0.969	0.553	1.079	1.005	0.953	$+0.8^{+0.1}_{-0.4}$
J06548+332	1.156	0.662	0.458	1.061	1.277	0.514	0.753	0.990	$+0.0^{+0.3}_{-0.3}$
J06565+440	1.299	0.559	0.357	1.128	1.740	0.462	0.744	1.082	$-0.5^{+0.2}_{-0.5}$
J07001–190	1.388	0.476	0.327	1.170	1.941	0.435	0.713	1.054	$-8.6^{+0.7}_{-0.5}$
J07009–023	1.136	0.671	0.482	1.058	1.218	0.535	0.769	0.999	$+0.0^{+0.3}_{-0.3}$
J07031+836	1.170	0.621	0.417	1.066	1.273	0.468	0.711	0.948	$+0.0^{+0.3}_{-0.3}$
J07051–101	1.330	0.476	0.323	1.150	1.908	0.389	0.648	0.946	$-6.0^{+0.4}_{-0.7}$
J07105–087	1.203	0.613	0.423	1.088	1.421	0.480	0.727	0.972	$-1.7^{+0.5}_{-0.5}$
J07105+283	0.930	0.885	0.780	0.984	0.760	0.822	0.896	1.033	$+0.4^{+0.1}_{-0.2}$
J07111–035	0.979	0.871	0.748	0.992	0.848	0.762	0.879	0.960	$+0.0^{+0.3}_{-0.3}$
J07111+434 AB	1.577	0.350	0.181	1.229	2.971	0.289	0.597	1.019	$-1.4^{+0.4}_{-0.5}$
J07172–050	1.158	0.563	0.383	1.093	1.255	0.436	0.674	0.927	$-3.5^{+0.5}_{-0.5}$
J07182+137	1.211	0.608	0.421	1.088	1.439	0.499	0.755	1.038	$+0.0^{+0.4}_{-0.4}$
J07191+667	0.931	0.883	0.795	0.983	0.748	0.848	0.908	1.080	$+0.4^{+0.1}_{-0.2}$
J07195+328	0.932	0.873	0.773	0.980	0.749	0.813	0.900	1.051	$+0.0^{+0.4}_{-0.4}$
J07219–222	1.220	0.620	0.408	1.085	1.412	0.491	0.747	1.037	$-0.5^{+0.2}_{-0.2}$
J07274+052	1.176	0.612	0.408	1.091	1.393	0.481	0.740	1.015	$-0.5^{+0.2}_{-0.2}$
J07310+460	1.249	0.520	0.365	1.126	1.559	0.431	0.669	0.943	$-9.5^{+0.6}_{-0.5}$
J07319+362N	1.217	0.595	0.404	1.102	1.438	0.471	0.719	0.982	$-2.4^{+0.3}_{-0.2}$
J07319+362S AB	1.103	0.672	0.487	1.057	1.109	0.551	0.773	1.020	$-2.0^{+-2.0}_{-0.2}$
J07321–088	0.845	0.979	0.926	0.956	0.543	1.050	1.000	0.911	$+0.6^{+0.2}_{-0.2}$
J07324–130	0.900	0.880	0.759	0.980	0.686	0.812	0.892	1.090	$+0.0^{+0.4}_{-0.4}$
J07359+785	1.151	0.635	0.430	1.069	1.253	0.511	0.763	1.052	$+0.0^{+0.5}_{-0.5}$
J07361–031	0.979	0.833	0.704	1.004	0.875	0.724	0.851	0.960	$-1.0^{+0.3}_{-0.2}$
J07365–006	1.192	0.638	0.436	1.079	1.376	0.490	0.731	0.967	$-1.5^{+0.4}_{-0.3}$
J07366+440	1.175	0.654	0.453	1.071	1.315	0.525	0.766	1.035	$+0.0^{+0.4}_{-0.4}$
J07420+142	1.176	0.922	0.649	1.049	1.240	0.966	1.249	3.966	$+0.8^{+0.2}_{-0.4}$
J07429–107	1.104	0.677	0.493	1.061	1.150	0.547	0.766	0.993	$-2.0^{+0.4}_{-0.2}$
J07467+574	1.323	0.496	0.337	1.159	1.921	0.407	0.684	0.976	$-6.1^{+0.8}_{-0.6}$
J07470+760	1.219	0.598	0.397	1.096	1.479	0.467	0.728	1.001	$+0.0^{+0.3}_{-0.3}$
J07497–033	1.170	0.605	0.404	1.078	1.275	0.459	0.708	0.956	$-1.4^{+0.4}_{-0.4}$
J07498–032	1.153	0.553	0.387	1.094	1.192	0.447	0.677	0.936	$-7.5^{+0.4}_{-0.6}$
J07523+162	1.605	0.359	0.260	1.247	2.785	0.360	0.694	1.050	$-25.4^{+1.4}_{-1.0}$
J07545+085	1.103	0.699	0.502	1.044	1.166	0.532	0.755	0.938	$+0.0^{+0.3}_{-0.3}$
J07545–096	1.176	0.642	0.448	1.069	1.290	0.501	0.734	0.965	$-0.8^{+0.2}_{-0.5}$
J07558+833	1.451	0.572	0.404	1.129	2.212	0.409	0.661	0.860	$-5.2^{+0.6}_{-0.2}$
J07591+173	1.205	0.550	0.388	1.101	1.262	0.449	0.671	0.930	$-9.2^{+0.8}_{-0.5}$
J08025–130	1.122	0.676	0.489	1.057	1.176	0.535	0.762	0.976	$+0.0^{+0.4}_{-0.4}$
J08031+203 AB	1.165	0.586	0.425	1.089	1.232	0.467	0.687	0.907	$-7.2^{+0.5}_{-0.3}$
J08069+422	1.284	0.550	0.367	1.124	1.658	0.439	0.699	0.981	$-2.5^{+0.3}_{-0.4}$
J08082+211N	0.901	0.924	0.852	0.975	0.700	0.908	0.937	1.025	$+0.5^{+0.1}_{-0.2}$
J08082+211S AB	1.128	0.658	0.481	1.060	1.159	0.518	0.738	0.934	$-3.7^{+0.4}_{-0.5}$

Table B.2: Seven representative spectral indices, ζ metallicity index, and Hα pseudo-equivalent width (cont.).

Karmn	PC1	TiO 2	TiO 5	VO-7912	Color-M	CaH 2	CaH 3	ζ	$pEW(\mathrm{H}\alpha)$ [Å]
J08104–111	0.956	0.741	0.539	1.013	0.743	0.613	0.810	1.087	$+0.0^{+0.3}_{-0.3}$
J08105–138 AB	1.093	0.722	0.532	1.033	1.108	0.570	0.784	0.977	$+0.0^{+0.3}_{-0.3}$
J08117+531	1.109	0.646	0.446	1.060	1.137	0.535	0.788	1.101	$+0.0^{+0.3}_{-0.3}$
J08143+630	1.024	0.784	0.618	1.007	0.890	0.647	0.828	0.995	$+0.0^{+0.3}_{-0.3}$
J08161+013	1.056	0.752	0.561	1.025	1.023	0.598	0.804	0.997	$+0.0^{+0.3}_{-0.3}$
J08283+553	1.131	0.684	0.480	1.051	1.151	0.537	0.767	1.002	$+0.0^{+0.3}_{-0.3}$
J08286+660	1.228	0.557	0.386	1.113	1.414	0.438	0.682	0.934	$-7.7^{+0.3}_{-0.3}$
J08298+267	1.680	0.299	0.196	1.298	4.578	0.270	0.568	0.974	$-5.2^{+0.9}_{-1.1}$
J08353+141	1.277	0.522	0.341	1.133	1.608	0.440	0.715	1.041	$-3.5^{+0.5}_{-0.5}$
J08375+035	1.258	0.565	0.367	1.114	1.674	0.445	0.719	1.012	$+0.0^{+0.6}_{-0.6}$
J08386–028	0.815	0.952	0.930	0.961	0.506	1.054	0.999	0.858	$+0.4^{+0.1}_{-0.1}$
J08394–028	0.954	0.817	0.642	0.999	0.771	0.705	0.873	1.167	$+0.0^{+0.3}_{-0.3}$
J08423–048	1.132	0.678	0.476	1.058	1.234	0.532	0.773	1.012	$+0.0^{+0.4}_{-0.4}$
J08449–066 AB	1.164	0.631	0.421	1.075	1.331	0.466	0.699	0.926	$+0.0^{+0.3}_{-0.3}$
J08526+283	1.329	0.543	0.357	1.124	1.806	0.456	0.737	1.065	$-0.7^{+0.2}_{-0.3}$
J08531–202	1.135	0.654	0.457	1.065	1.213	0.512	0.752	0.987	$+0.0^{+0.4}_{-0.4}$
J08563–044	0.996	0.824	0.680	1.001	0.896	0.694	0.847	0.959	$+0.0^{+0.4}_{-0.4}$
J08572+194	1.183	0.636	0.425	1.073	1.294	0.500	0.746	1.020	$+0.0^{+0.4}_{-0.4}$
J08590+364	0.957	0.846	0.696	0.992	0.807	0.769	0.897	1.238	$+0.0^{+0.4}_{-0.4}$
J08595+537	1.195	0.586	0.412	1.092	1.368	0.444	0.669	0.886	$-5.0^{+0.4}_{-0.2}$
J08599+042	0.996	0.840	0.689	0.997	0.884	0.713	0.860	1.002	$+0.0^{+0.4}_{-0.4}$
J09003+218	1.737	0.307	0.201	1.269	4.123	0.293	0.598	0.998	$-10.0^{+0.8}_{-0.8}$
J09008+237	1.123	0.668	0.456	1.061	1.137	0.522	0.760	1.016	$+0.0^{+0.3}_{-0.3}$
J09023+177	1.210	0.588	0.393	1.092	1.458	0.470	0.736	1.021	$+0.0^{+0.6}_{-0.6}$
J09028+060	1.031	0.780	0.613	1.005	0.952	0.646	0.827	1.004	$+0.0^{+0.3}_{-0.3}$
J09040–159	1.077	0.709	0.536	1.039	1.052	0.563	0.768	0.934	$-2.9^{+0.2}_{-0.2}$
J09045+164 AB	0.844	0.970	0.923	0.972	0.568	1.076	1.003	0.974	$+0.7^{+0.1}_{-0.2}$
J09058+555	1.182	0.624	0.414	1.078	1.281	0.473	0.715	0.963	$+0.0^{+0.4}_{-0.4}$
J09091+227	1.314	0.527	0.332	1.139	1.932	0.416	0.688	0.997	$+0.0^{+0.2}_{-1.0}$
J09115+126	1.105	0.696	0.504	1.050	1.124	0.566	0.796	1.050	$+0.0^{+0.2}_{-0.2}$
J09143+526	0.941	0.902	0.805	0.981	0.750	0.839	0.909	1.001	$+0.0^{+0.3}_{-0.3}$
J09144+526	0.943	0.896	0.791	0.978	0.759	0.822	0.904	1.003	$+0.0^{+0.3}_{-0.3}$
J09151+233	0.938	0.879	0.767	0.979	0.750	0.803	0.896	1.040	$+0.0^{+0.3}_{-0.3}$
J09156–105 AB	1.369	0.431	0.280	1.174	1.981	0.351	0.609	0.943	$-3.9^{+0.5}_{-0.3}$
J09201+037	1.196	0.622	0.427	1.083	1.407	0.477	0.723	0.957	$-1.4^{+0.5}_{-0.6}$
J09206–169	0.922	0.908	0.811	0.981	0.735	0.855	0.917	1.042	$+0.0^{+0.4}_{-0.4}$
J09212+603	1.029	0.781	0.612	1.012	0.911	0.651	0.832	1.026	$+0.0^{+0.4}_{-0.4}$
J09218–023	1.051	0.723	0.531	1.033	1.065	0.537	0.751	0.883	$+0.0^{+0.3}_{-0.3}$
J09243+063	1.222	0.561	0.375	1.111	1.366	0.465	0.727	1.033	$-6.1^{+0.4}_{-0.3}$
J09248+306	1.162	0.595	0.435	1.085	1.316	0.476	0.696	0.912	$-7.2^{+0.5}_{-0.4}$
J09256+634	1.272	0.534	0.347	1.135	1.715	0.413	0.670	0.953	$-5.1^{+0.4}_{-0.7}$
J09301–009	0.947	0.864	0.732	0.993	0.789	0.810	0.910	1.267	$+0.4^{+0.1}_{-0.1}$
J09308+024	1.230	0.562	0.384	1.110	1.572	0.437	0.684	0.936	$-3.5^{+0.3}_{-0.3}$
J09328+269	1.479	0.415	0.257	1.216	2.454	0.356	0.660	1.019	$-7.2^{+0.6}_{-0.6}$

Table B.2: Seven representative spectral indices, ζ metallicity index, and Hα pseudo-equivalent width (cont.).

Karmn	PC1	TiO 2	TiO 5	VO-7912	Color-M	CaH 2	CaH 3	ζ	pEW(Hα) [Å]
J09351–103	0.804	0.940	0.870	0.949	0.467	1.018	0.971	1.392	$+0.6^{+0.1}_{-0.2}$
J09362+375	0.940	0.859	0.744	0.983	0.738	0.773	0.878	0.999	$-0.9^{+0.2}_{-0.3}$
J09394+146	1.151	0.631	0.442	1.073	1.310	0.478	0.705	0.912	$-1.8^{+0.6}_{-0.4}$
J09449–123	1.416	0.403	0.274	1.190	1.839	0.369	0.632	0.983	$-13.3^{+1.0}_{-1.0}$
J09488+156	1.094	0.673	0.479	1.060	1.197	0.491	0.712	0.872	$-2.9^{+0.4}_{-0.3}$
J09526–156	1.146	0.629	0.418	1.085	1.246	0.487	0.728	0.991	$+0.0^{+0.3}_{-0.3}$
J09538–073	0.966	0.899	0.754	0.989	0.748	0.765	0.868	0.922	$-1.3^{+0.2}_{-0.2}$
J09589+059	1.320	0.502	0.332	1.144	1.773	0.390	0.641	0.928	$-4.5^{+0.7}_{-0.6}$
J09597+721	1.185	0.636	0.431	1.082	1.374	0.485	0.734	0.974	$+0.0^{+0.3}_{-0.3}$
J10008+319	1.613	0.333	0.221	1.252	3.106	0.316	0.622	1.003	$-14.4^{+1.2}_{-1.8}$
J10020+697	1.263	0.557	0.356	1.121	1.671	0.437	0.698	0.995	$-0.8^{+0.2}_{-0.2}$
J10028+484	1.448	0.380	0.264	1.223	2.463	0.349	0.611	0.964	$-12.0^{+0.6}_{-0.6}$
J10063–064	1.415	0.521	0.312	1.099	1.704	0.456	0.724	1.120	$+0.0^{+0.4}_{-0.4}$
J10068–127	1.285	0.487	0.327	1.145	1.763	0.390	0.630	0.926	$-4.4^{+0.5}_{-0.6}$
J10098–007	0.862	0.943	0.889	0.984	0.604	1.023	0.973	1.209	$+0.6^{+0.1}_{-0.2}$
J10120–026 AB	1.087	0.726	0.532	1.041	1.140	0.560	0.777	0.950	$+0.0^{+0.3}_{-0.3}$
J10130+233	1.197	0.595	0.398	1.093	1.405	0.485	0.755	1.059	$+0.0^{+0.3}_{-0.3}$
J10148+213	1.276	0.500	0.329	1.144	1.696	0.395	0.643	0.938	$-5.9^{+0.5}_{-0.9}$
J10155–164	1.226	0.583	0.391	1.102	1.400	0.483	0.745	1.054	$-3.5^{+0.3}_{-0.5}$
J10196+198 AB	1.141	0.638	0.466	1.066	1.204	0.506	0.732	0.937	$-4.1^{+0.3}_{-0.4}$
J10200+289	1.111	0.678	0.479	1.056	1.216	0.514	0.742	0.938	$+0.0^{+0.4}_{-0.4}$
J10238+438	1.407	0.435	0.288	1.185	2.299	0.396	0.696	1.050	$-5.1^{+0.5}_{-0.5}$
J10240+366	1.184	0.623	0.423	1.095	1.382	0.487	0.735	0.991	$-1.9^{+0.2}_{-0.3}$
J10278+028	1.222	0.607	0.401	1.089	1.413	0.494	0.758	1.072	$+0.0^{+0.6}_{-0.6}$
J10304+559	0.891	0.942	0.883	0.971	0.663	0.931	0.947	0.902	$+0.5^{+0.1}_{-0.2}$
J10359+288	1.142	0.640	0.460	1.080	1.265	0.506	0.736	0.952	$-2.9^{+0.6}_{-0.4}$
J10368+509	1.271	0.510	0.347	1.138	1.747	0.413	0.665	0.948	$-4.5^{+0.3}_{-0.3}$
J10430–092 AB	1.471	0.439	0.259	1.190	2.546	0.363	0.677	1.038	$-1.7^{+0.4}_{-0.5}$
J10443+124	1.217	0.610	0.407	1.092	1.417	0.501	0.763	1.078	$+0.0^{+0.6}_{-0.6}$
J10482–113	1.787	0.266	0.149	1.307	4.604	0.237	0.534	0.999	$-3.7^{+0.6}_{-1.0}$
J10508+068	1.261	0.586	0.385	1.110	1.670	0.461	0.727	1.010	$+0.0^{+0.4}_{-0.4}$
J10546–073	1.256	0.609	0.380	1.106	1.540	0.466	0.752	1.061	$+0.0^{+0.4}_{-0.4}$
J10560+061	1.448	0.668	0.414	1.297	3.074	0.683	1.373	7.230	$+0.0^{+0.4}_{-0.4}$
J10563+042	1.102	0.699	0.510	1.046	1.137	0.551	0.772	0.973	$+0.0^{+0.4}_{-0.4}$
J10564+070	1.662	0.328	0.226	1.244	3.418	0.327	0.645	1.025	$-10.9^{+0.9}_{-0.2}$
J10584–107	1.324	0.445	0.312	1.156	1.933	0.387	0.635	0.948	$-6.1^{+0.4}_{-0.7}$
J11018–024	1.001	0.842	0.690	1.002	0.769	0.927	0.953	2.412	$+0.9^{+0.3}_{-0.1}$
J11030+037	1.112	0.698	0.501	1.052	1.165	0.540	0.770	0.972	$+0.0^{+0.3}_{-0.3}$
J11033+359	1.042	0.773	0.570	1.018	0.991	0.616	0.823	1.042	$+0.0^{+0.3}_{-0.3}$
J11046–042S AB	0.959	0.862	0.763	0.989	0.792	0.794	0.879	0.984	$-1.9^{+0.2}_{-0.1}$
J11054+435	0.978	0.829	0.678	0.995	0.853	0.687	0.845	0.947	$+0.0^{+0.3}_{-0.3}$
J11055+435	1.472	0.299	0.191	1.232	2.560	0.257	0.473	0.937	$-10.2^{+1.2}_{-1.9}$
J11075+437	1.135	0.651	0.468	1.068	1.256	0.488	0.713	0.891	$-2.9^{+0.4}_{-0.4}$
J11151+734N	1.097	0.707	0.517	1.043	1.120	0.555	0.774	0.968	$+0.0^{+0.3}_{-0.3}$

Table B.2: Seven representative spectral indices, ζ metallicity index, and Hα pseudo-equivalent width (cont.).

Karmn	PC1	TiO 2	TiO 5	VO-7912	Color-M	CaH 2	CaH 3	ζ	$pEW(\mathrm{H}\alpha)$ [Å]
J11151+734S	0.809	0.987	0.913	0.987	0.560	1.087	1.018	1.125	$+0.8^{+0.2}_{-0.2}$
J11201–104 AB	1.057	0.755	0.566	1.020	0.886	0.611	0.773	0.954	$-3.3^{+0.2}_{-0.2}$
J11201+301	1.001	0.802	0.646	0.999	0.795	0.897	0.948	2.449	$+0.9^{+0.2}_{-0.3}$
J11214–204N	0.902	0.938	0.870	0.973	0.676	0.934	0.943	0.998	$+0.0^{+0.3}_{-0.3}$
J11214–204S	1.124	0.697	0.535	1.053	1.211	0.552	0.757	0.904	$-3.3^{+0.2}_{-0.2}$
J11218+181	0.943	0.859	0.737	0.993	0.774	0.788	0.888	1.099	$+0.0^{+0.4}_{-0.4}$
J11240+381	1.259	0.510	0.352	1.136	1.693	0.405	0.649	0.921	$-6.9^{+0.4}_{-0.3}$
J11306–080	1.189	0.651	0.434	1.067	1.300	0.487	0.738	0.976	$+0.0^{+0.3}_{-0.3}$
J11312+631	0.907	0.934	0.855	0.974	0.696	0.912	0.941	1.029	$+0.3^{+0.2}_{-0.1}$
J11378+418	1.071	0.731	0.523	1.032	1.011	0.586	0.817	1.084	$+0.0^{+0.3}_{-0.3}$
J11403+095	1.006	0.804	0.628	1.015	0.881	0.647	0.824	0.961	$+0.0^{+0.3}_{-0.3}$
J11421+267	1.090	0.697	0.489	1.046	1.136	0.545	0.779	1.017	$+0.0^{+0.3}_{-0.3}$
J11451+183	1.246	0.576	0.389	1.107	1.492	0.488	0.759	1.086	$+0.0^{+0.3}_{-0.3}$
J11458+065	0.974	0.804	0.636	0.990	0.722	0.896	0.967	2.677	$+0.8^{+0.1}_{-0.2}$
J11472+770	0.893	0.902	0.807	0.970	0.650	0.888	0.927	1.212	$+0.4^{+0.1}_{-0.2}$
J11474+667	1.338	0.444	0.307	1.170	1.971	0.398	0.657	0.986	$-9.2^{+0.6}_{-0.6}$
J11485+076	1.171	0.570	0.408	1.100	1.369	0.440	0.663	0.883	$-6.2^{+0.5}_{-0.5}$
J11511+352	1.015	0.802	0.640	1.004	0.930	0.650	0.828	0.945	$+0.0^{+0.3}_{-0.3}$
J11522+100	1.297	0.571	0.374	1.112	1.635	0.470	0.739	1.057	$-0.8^{+0.4}_{-0.2}$
J11549–021	1.130	0.668	0.464	1.056	1.239	0.512	0.747	0.967	$+0.0^{+0.3}_{-0.3}$
J12025+084	1.011	0.769	0.589	1.012	0.949	0.590	0.790	0.898	$+0.0^{+0.3}_{-0.3}$
J12049+174	1.143	0.622	0.440	1.075	1.229	0.475	0.701	0.907	$-6.2^{+0.2}_{-0.2}$
J12069+058	0.874	0.956	0.901	0.966	0.624	0.999	0.971	1.011	$+0.5^{+0.1}_{-0.1}$
J12088+217	0.971	0.860	0.737	0.997	0.819	0.766	0.890	1.040	$+0.0^{+0.3}_{-0.3}$
J12093+210	1.131	0.661	0.472	1.066	1.230	0.527	0.758	0.989	$-0.7^{+0.3}_{-0.3}$
J12104–131	1.263	0.516	0.352	1.123	1.619	0.424	0.679	0.967	$-3.5^{+0.5}_{-0.5}$
J12124+121	1.053	0.746	0.560	1.022	1.027	0.599	0.798	0.989	$+0.0^{+0.3}_{-0.3}$
J12162+508	1.280	0.544	0.374	1.120	1.540	0.446	0.697	0.976	$-7.6^{+0.4}_{-0.4}$
J12228–040	1.288	0.488	0.335	1.152	1.709	0.402	0.651	0.943	$-6.5^{+0.5}_{-0.4}$
J12322+454	1.147	1.023	0.641	1.100	1.338	0.996	1.470	1.593	$+0.8^{+0.1}_{-0.2}$
J12349+322	1.157	0.649	0.439	1.078	1.330	0.497	0.741	0.985	$+0.0^{+0.3}_{-0.3}$
J12364+352	1.296	0.546	0.363	1.131	1.750	0.432	0.703	0.984	$-1.7^{+0.3}_{-0.3}$
J12368–019	1.226	0.603	0.400	1.103	1.444	0.490	0.758	1.067	$+0.0^{+0.3}_{-0.3}$
J12372+358	1.028	0.754	0.583	1.019	0.937	0.620	0.810	0.995	$+0.0^{+0.3}_{-0.3}$
J12417+567	1.155	0.604	0.433	1.083	1.327	0.469	0.694	0.905	$-5.0^{+0.3}_{-0.3}$
J12440–111	1.282	0.523	0.346	1.136	1.709	0.416	0.672	0.960	$-4.4^{+0.4}_{-0.3}$
J12456+271	1.211	0.872	0.542	1.114	1.521	0.859	1.346	5.309	$+0.7^{+0.2}_{-0.2}$
J12470+466	1.125	0.691	0.499	1.049	1.168	0.560	0.791	1.042	$+0.0^{+0.3}_{-0.3}$
J12488+120	1.303	0.539	0.331	1.119	1.718	0.424	0.710	1.032	$+0.0^{+0.3}_{-0.3}$
J12533–053	1.118	0.654	0.436	1.062	1.092	0.513	0.771	1.056	$+0.0^{+0.3}_{-0.3}$
J12533+466	1.145	0.913	0.601	1.098	1.630	0.945	1.329	3.775	$+0.7^{+0.2}_{-0.1}$
J12549–063	1.331	0.495	0.341	1.141	1.868	0.381	0.619	0.891	$-5.5^{+0.6}_{-0.4}$
J12593–001	1.241	0.603	0.398	1.091	1.443	0.483	0.757	1.059	$+0.0^{+0.3}_{-0.3}$
J13027+415	1.184	0.638	0.432	1.088	1.327	0.505	0.758	1.033	$+0.0^{+0.3}_{-0.3}$

Table B.2: Seven representative spectral indices, ζ metallicity index, and Hα pseudo-equivalent width (cont.).

Karmn	PC1	TiO 2	TiO 5	VO-7912	Color-M	CaH 2	CaH 3	ζ	pEW(Hα) [Å]
J13088–015	1.141	0.640	0.454	1.060	1.191	0.514	0.759	1.007	$+0.0^{+0.3}_{-0.3}$
J13102+477	1.348	0.478	0.306	1.165	1.921	0.390	0.655	0.978	$-5.9^{+0.5}_{-0.8}$
J13113+096	0.912	0.898	0.787	0.981	0.688	0.880	0.942	1.372	$+0.5^{+0.2}_{-0.2}$
J13143+133 AB	1.587	0.336	0.221	1.282	2.931	0.322	0.618	1.006	$-16.9^{+1.4}_{-1.1}$
J13167–123	1.195	0.617	0.415	1.084	1.374	0.469	0.712	0.953	$+0.0^{+0.4}_{-0.4}$
J13168+170	0.964	0.845	0.700	0.990	0.806	0.736	0.864	1.032	$+0.0^{+0.3}_{-0.3}$
J13179+362	0.986	0.806	0.632	1.005	0.861	0.703	0.870	1.186	$+0.0^{+0.3}_{-0.3}$
J13182+733	1.200	0.600	0.393	1.099	1.367	0.489	0.752	1.069	$+0.0^{+0.4}_{-0.4}$
J13247–050	1.260	0.571	0.377	1.112	1.643	0.457	0.721	1.014	$-1.2^{+0.5}_{-0.6}$
J13251–114	1.120	0.655	0.466	1.065	1.206	0.516	0.746	0.969	$-1.6^{+0.4}_{-0.2}$
J13253+426	0.887	0.959	0.900	0.965	0.648	0.982	0.970	0.970	$+0.5^{+0.1}_{-0.1}$
J13260+275	1.105	0.644	0.476	1.071	1.187	0.502	0.735	0.918	$-2.0^{+0.4}_{-0.4}$
J13294–143	1.181	0.583	0.426	1.092	1.251	0.473	0.688	0.913	$-6.1^{+0.4}_{-0.5}$
J13312+589	1.080	0.723	0.539	1.036	1.077	0.548	0.765	0.903	$+0.0^{+0.3}_{-0.3}$
J13314–079	0.928	0.879	0.754	0.978	0.709	0.812	0.906	1.157	$+0.4^{+0.2}_{-0.1}$
J13321–112	0.913	0.899	0.795	0.975	0.701	0.862	0.914	1.146	$+0.4^{+0.2}_{-0.1}$
J13326+309	1.266	0.508	0.346	1.135	1.630	0.415	0.664	0.952	$-5.3^{+0.3}_{-0.4}$
J13335+704	1.221	0.615	0.411	1.089	1.436	0.485	0.746	1.024	$+0.0^{+0.4}_{-0.4}$
J13386–115	1.263	0.499	0.348	1.133	1.565	0.411	0.648	0.930	$-6.4^{+0.5}_{-0.5}$
J13394+461 AB	1.024	0.780	0.606	1.011	0.928	0.671	0.854	1.139	$+0.0^{+0.3}_{-0.3}$
J13413–091	1.117	0.682	0.476	1.058	1.161	0.521	0.750	0.962	$+0.0^{+0.3}_{-0.3}$
J13414+489	1.169	0.667	0.451	1.069	1.327	0.498	0.742	0.965	$+0.0^{+0.3}_{-0.3}$
J13474+063	0.881	0.957	0.914	0.967	0.641	1.007	0.974	0.907	$+0.6^{+0.1}_{-0.1}$
J13503–216	1.212	0.612	0.400	1.085	1.442	0.479	0.735	1.019	$+0.0^{+0.3}_{-0.3}$
J13537+521 AB	1.160	0.600	0.422	1.081	1.271	0.507	0.746	1.036	$+0.0^{+0.6}_{-0.6}$
J13551–079	0.915	0.892	0.780	0.976	0.694	0.834	0.905	1.098	$+0.3^{+0.2}_{-0.1}$
J13555–073	1.132	0.673	0.477	1.039	1.166	0.530	0.761	0.991	$+0.0^{+0.3}_{-0.3}$
J13582–120	1.295	0.533	0.338	1.142	1.705	0.442	0.715	1.050	$+0.0^{+0.6}_{-0.6}$
J13583–132	1.243	0.565	0.377	1.110	1.574	0.440	0.697	0.965	$-1.9^{+0.4}_{-0.3}$
J13587+465	1.085	0.732	0.558	1.012	0.927	0.827	0.941	2.414	$+1.0^{+0.1}_{-0.1}$
J14019+432	1.087	0.686	0.487	1.042	1.052	0.541	0.767	0.995	$+0.0^{+0.3}_{-0.3}$
J14102–180	1.125	0.690	0.498	1.049	1.160	0.571	0.801	1.081	$+0.0^{+0.3}_{-0.3}$
J14159–110	1.032	0.757	0.602	1.012	0.892	0.625	0.794	0.931	$-2.0^{+0.2}_{-0.3}$
J14171+088	1.273	0.524	0.326	1.122	1.627	0.427	0.703	1.036	$-1.0^{+0.3}_{-0.4}$
J14175+025	1.121	0.669	0.483	1.059	1.192	0.512	0.731	0.915	$-2.5^{+0.5}_{-0.3}$
J14194+029	1.372	0.471	0.309	1.166	1.942	0.394	0.671	0.992	$-7.4^{+0.5}_{-0.7}$
J14195–051	1.217	0.576	0.370	1.107	1.494	0.446	0.687	0.972	$+0.0^{+0.3}_{-0.3}$
J14215–079	1.240	0.609	0.401	1.094	1.504	0.480	0.755	1.046	$+0.0^{+0.3}_{-0.3}$
J14227+164	1.342	0.476	0.326	1.147	1.857	0.399	0.652	0.954	$-6.4^{+0.4}_{-0.6}$
J14244+602	1.073	0.751	0.569	1.020	0.989	0.610	0.807	1.004	$+0.0^{+0.3}_{-0.3}$
J14251+518	1.083	0.707	0.511	1.034	1.063	0.558	0.780	0.995	$+0.0^{+0.3}_{-0.3}$
J14255–118	1.239	0.585	0.400	1.100	1.491	0.475	0.734	1.012	$-2.0^{+0.4}_{-0.4}$
J14312+754	1.194	0.548	0.377	1.100	1.436	0.406	0.630	0.870	$-4.7^{+0.5}_{-0.6}$
J14336+093	1.167	0.649	0.432	1.071	1.286	0.501	0.750	1.015	$+0.0^{+0.3}_{-0.3}$

Table B.2: Seven representative spectral indices, ζ metallicity index, and Hα pseudo-equivalent width (cont.).

Karmn	PC1	TiO 2	TiO 5	VO-7912	Color-M	CaH 2	CaH 3	ζ	$pEW(\mathrm{H}\alpha)$ [Å]
J14415+136	1.008	0.810	0.658	1.004	0.868	0.693	0.839	1.006	$+0.0^{+0.3}_{-0.3}$
J14446–222	1.315	0.540	0.350	1.116	1.654	0.468	0.755	1.119	$+0.0^{+0.3}_{-0.3}$
J14472+570	1.192	0.547	0.386	1.103	1.353	0.436	0.659	0.908	$-6.7^{+0.5}_{-0.3}$
J14480+384	0.880	0.937	0.858	0.972	0.639	0.932	0.945	1.092	$+0.4^{+0.1}_{-0.1}$
J14485+101	1.209	0.618	0.426	1.079	1.361	0.505	0.759	1.045	$+0.0^{+0.3}_{-0.3}$
J14492+498	1.020	0.779	0.611	1.021	0.920	0.648	0.821	1.000	$+0.0^{+0.3}_{-0.3}$
J14501+323	1.188	0.633	0.429	1.074	1.305	0.516	0.774	1.080	$+0.0^{+0.3}_{-0.3}$
J14544+161 ABC	0.981	0.748	0.570	1.006	0.802	0.619	0.798	1.002	$-1.4^{+0.3}_{-0.2}$
J14595+454	0.887	0.946	0.885	0.960	0.641	0.956	0.954	0.985	$+0.5^{+0.1}_{-0.1}$
J15079+762	1.268	0.469	0.322	1.149	1.556	0.412	0.667	0.986	$-9.0^{+0.5}_{-0.3}$
J15081+623	1.229	0.623	0.416	1.098	1.462	0.477	0.728	0.980	$+0.0^{+0.3}_{-0.3}$
J15118+395	1.107	0.701	0.504	1.045	1.130	0.537	0.759	0.946	$+0.0^{+0.3}_{-0.3}$
J15131+181	1.052	0.751	0.571	1.027	0.981	0.602	0.800	0.973	$+0.0^{+0.3}_{-0.3}$
J15142–099	1.226	0.538	0.355	1.109	1.414	0.428	0.674	0.960	$-3.8^{+0.6}_{-0.4}$
J15147+645	1.156	0.626	0.414	1.066	1.354	0.433	0.668	0.872	$-0.5^{+0.2}_{-0.1}$
J15151+333	1.064	0.734	0.529	1.023	1.039	0.562	0.774	0.957	$+0.0^{+0.3}_{-0.3}$
J15157–074	1.207	0.566	0.384	1.103	1.390	0.440	0.690	0.946	$-3.3^{+0.4}_{-0.2}$
J15164+167	0.880	0.936	0.868	0.965	0.645	0.963	0.969	1.203	$+0.6^{+0.1}_{-0.1}$
J15197+046	1.238	0.588	0.400	1.099	1.585	0.444	0.692	0.927	$-1.8^{+0.3}_{-0.3}$
J15204+001	0.899	0.921	0.829	0.972	0.673	0.872	0.927	1.026	$+0.4^{+0.2}_{-0.1}$
J15210+255	0.888	0.937	0.860	0.975	0.647	0.939	0.947	1.110	$+0.4^{+0.2}_{-0.1}$
J15238+584	1.197	0.549	0.381	1.105	1.345	0.432	0.660	0.913	$-8.2^{+0.3}_{-0.3}$
J15277–090	1.345	0.513	0.331	1.146	1.901	0.427	0.713	1.038	$+0.0^{+0.4}_{-0.4}$
J15290+467 AB	1.308	0.490	0.323	1.141	1.808	0.389	0.640	0.939	$-4.8^{+0.5}_{-0.4}$
J15291+574	0.981	0.838	0.708	0.991	0.840	0.729	0.867	0.995	$+0.0^{+0.3}_{-0.3}$
J15305+094	1.482	0.380	0.244	1.216	2.570	0.319	0.586	0.953	$-7.4^{+0.8}_{-0.8}$
J15340+513	1.337	0.551	0.348	1.119	1.848	0.446	0.730	1.057	$-0.9^{+0.4}_{-0.3}$
J15386+371	1.184	0.640	0.425	1.081	1.336	0.493	0.751	1.017	$+0.0^{+0.4}_{-0.4}$
J15430–130	1.015	0.788	0.617	1.018	0.922	0.644	0.818	0.973	$+0.0^{+0.3}_{-0.3}$
J15474+451	1.232	0.564	0.366	1.100	1.485	0.441	0.708	0.996	$-4.1^{+0.7}_{-0.5}$
J15476+226	1.276	0.504	0.338	1.134	1.630	0.417	0.672	0.973	$-4.7^{+0.4}_{-0.2}$
J15480+043	1.122	0.668	0.499	1.047	1.137	0.526	0.745	0.922	$-4.7^{+0.3}_{-0.2}$
J15481+015	1.132	0.682	0.495	1.052	1.241	0.533	0.751	0.946	$+0.0^{+0.4}_{-0.4}$
J15499+796	1.375	0.462	0.302	1.171	1.969	0.379	0.635	0.956	$-6.7^{+0.6}_{-0.9}$
J15552–101	1.107	0.672	0.466	1.045	1.029	0.544	0.785	1.072	$+0.0^{+0.3}_{-0.3}$
J15557–103	1.178	0.584	0.412	1.092	1.272	0.464	0.689	0.927	$-4.9^{+0.5}_{-0.4}$
J15558–118	1.157	0.671	0.454	1.060	1.163	0.515	0.765	1.018	$+0.0^{+0.3}_{-0.3}$
J15569+376	1.083	0.654	0.489	1.058	1.043	0.541	0.744	0.957	$-5.2^{+0.3}_{-0.3}$
J15578+090	1.280	0.581	0.373	1.106	1.629	0.463	0.740	1.051	$+0.0^{+0.3}_{-0.3}$
J16023+036	1.022	0.778	0.637	1.023	0.911	0.670	0.812	0.960	$-3.7^{+0.3}_{-0.3}$
J16042+235	1.398	0.455	0.302	1.165	2.058	0.380	0.645	0.966	$-6.8^{+0.8}_{-0.8}$
J16048+391	1.210	0.590	0.361	1.099	1.460	0.408	0.661	0.921	$-1.7^{+0.3}_{-0.5}$
J16120+033N	1.195	0.573	0.376	1.098	1.365	0.454	0.705	0.991	$-1.8^{+0.6}_{-1.0}$
J16139+337 AB	1.113	0.700	0.510	1.043	1.128	0.548	0.769	0.963	$+0.0^{+0.3}_{-0.3}$

Table B.2: Seven representative spectral indices, ζ metallicity index, and Hα pseudo-equivalent width (cont.).

Karmn	PC1	TiO 2	TiO 5	VO-7912	Color-M	CaH 2	CaH 3	ζ	pEW(Hα) [Å]
J16148+606 AB	1.109	0.655	0.454	1.057	1.151	0.481	0.708	0.899	$-1.1^{+0.3}_{-0.6}$
J16157+586	1.360	0.464	0.309	1.154	1.871	0.401	0.655	0.983	$-7.0^{+0.9}_{-0.6}$
J16167+672S	0.931	0.877	0.762	0.982	0.738	0.813	0.899	1.099	$+0.0^{+0.4}_{-0.4}$
J16183+757	1.266	0.561	0.368	1.113	1.604	0.440	0.700	0.982	$-1.0^{+0.5}_{-0.6}$
J16243+199	1.121	0.610	0.456	1.066	1.052	0.482	0.697	0.885	$-6.3^{+0.6}_{-0.4}$
J16254+543	1.014	0.768	0.591	1.016	0.920	0.592	0.777	0.878	$+0.0^{+0.3}_{-0.3}$
J16269+149	1.259	0.507	0.354	1.123	1.342	0.423	0.643	0.927	$-8.8^{+0.7}_{-0.9}$
J16276–035 AB	0.856	0.964	0.919	0.962	0.578	1.043	0.989	0.961	$+0.0^{+0.5}_{-0.5}$
J16299+048	1.144	0.646	0.450	1.071	1.239	0.503	0.738	0.969	$+0.0^{+0.3}_{-0.3}$
J16314+471	1.175	0.564	0.389	1.094	1.273	0.445	0.689	0.942	$-3.9^{+0.3}_{-0.4}$
J16330+031	1.172	0.648	0.440	1.064	1.265	0.511	0.756	1.022	$+0.0^{+0.3}_{-0.3}$
J16354–039	0.925	0.958	0.895	0.977	0.722	0.889	0.926	0.664	$+0.0^{+0.4}_{-0.4}$
J16365+287	1.214	0.602	0.407	1.088	1.353	0.500	0.757	1.069	$+0.0^{+0.3}_{-0.3}$
J16459+609	1.171	0.627	0.416	1.085	1.288	0.480	0.736	0.994	$+0.0^{+0.4}_{-0.4}$
J16465+345	1.658	0.354	0.189	1.238	3.594	0.300	0.634	1.042	$-1.7^{+0.7}_{-0.7}$
J16480+453	1.239	0.521	0.365	1.121	1.360	0.435	0.667	0.947	$-7.8^{+0.3}_{-0.4}$
J16528+610	1.333	0.526	0.327	1.138	1.828	0.431	0.713	1.050	$+0.0^{+0.5}_{-0.5}$
J16536+560	1.172	0.583	0.377	1.085	1.271	0.476	0.737	1.059	$+0.0^{+0.3}_{-0.3}$
J16543+256	1.138	0.645	0.433	1.066	1.187	0.521	0.769	1.070	$+0.0^{+0.3}_{-0.3}$
J16555–083	1.864	0.239	0.156	1.318	4.955	0.242	0.519	0.987	$-6.0^{+1.0}_{-1.1}$
J17011+555	1.098	0.721	0.512	1.038	1.109	0.536	0.757	0.926	$+0.0^{+0.3}_{-0.3}$
J17017+741	1.163	0.612	0.404	1.075	1.290	0.467	0.713	0.970	$+0.0^{+0.3}_{-0.3}$
J17052–050	1.028	0.747	0.559	1.019	0.928	0.631	0.828	1.113	$+0.0^{+0.3}_{-0.3}$
J17062+646	1.107	0.673	0.474	1.047	1.154	0.504	0.741	0.930	$+0.0^{+0.3}_{-0.3}$
J17094+391	1.103	0.663	0.448	1.051	1.121	0.499	0.728	0.954	$+0.0^{+0.3}_{-0.3}$
J17126–099	1.321	0.610	0.450	1.050	1.476	0.673	0.904	1.788	$+0.8^{+0.1}_{-0.1}$
J17140+176	1.104	0.693	0.486	1.046	1.110	0.547	0.784	1.033	$+0.0^{+0.3}_{-0.3}$
J17154+308	1.098	0.708	0.518	1.045	1.108	0.560	0.772	0.973	$+0.0^{+0.3}_{-0.3}$
J17163–053	1.282	0.552	0.317	1.112	1.506	0.427	0.668	1.009	$-3.1^{+0.4}_{-0.2}$
J17167+115	1.269	0.566	0.364	1.110	1.528	0.468	0.736	1.067	$+0.0^{+0.3}_{-0.3}$
J17176+524	1.197	0.616	0.404	1.091	1.387	0.467	0.708	0.965	$+0.0^{+0.6}_{-0.6}$
J17198+265	1.303	0.462	0.321	1.159	1.572	0.414	0.659	0.982	$-8.2^{+0.8}_{-0.7}$
J17199+242	1.273	0.521	0.362	1.136	1.518	0.431	0.673	0.953	$-9.1^{+0.5}_{-0.8}$
J17199+265	1.191	0.612	0.423	1.087	1.307	0.495	0.736	1.003	$-2.4^{+0.2}_{-0.2}$
J17216–171	1.150	1.101	0.724	1.084	1.384	1.062	1.502	0.840	$+0.6^{+0.2}_{-0.2}$
J17239+136	1.227	0.579	0.395	1.100	1.457	0.449	0.690	0.939	$-3.2^{+0.4}_{-0.3}$
J17246+617	1.160	0.610	0.441	1.062	1.163	0.499	0.721	0.957	$-2.8^{+0.6}_{-0.3}$
J17265–227	1.072	0.676	0.477	1.046	1.026	0.534	0.750	0.980	$+0.0^{+0.4}_{-0.4}$
J17267–050	1.087	0.698	0.520	1.036	1.057	0.577	0.790	1.026	$+0.0^{+0.4}_{-0.4}$
J17270+422	0.858	0.962	0.915	0.967	0.593	1.048	0.988	1.012	$+0.6^{+0.1}_{-0.2}$
J17281–017	1.259	0.546	0.365	1.120	1.572	0.439	0.688	0.973	$-2.6^{+0.5}_{-0.6}$
J17299–209	1.151	0.646	0.431	1.078	1.199	0.525	0.787	1.112	$+0.0^{+0.4}_{-0.4}$
J17301+546	1.205	0.628	0.414	1.089	1.333	0.503	0.755	1.056	$+0.0^{+0.4}_{-0.4}$
J17304+337	1.139	0.607	0.432	1.076	1.192	0.487	0.719	0.955	$-2.4^{+0.4}_{-0.4}$

Table B.2: Seven representative spectral indices, ζ metallicity index, and Hα pseudo-equivalent width (cont.).

Karmn	PC1	TiO 2	TiO 5	VO-7912	Color-M	CaH 2	CaH 3	ζ	pEW(Hα) [Å]
J17364+683	1.141	0.652	0.439	1.063	1.209	0.520	0.770	1.061	$+0.0^{+0.4}_{-0.4}$
J17412+724	1.230	0.566	0.367	1.113	1.516	0.430	0.680	0.951	$-2.8^{+0.6}_{-0.4}$
J17426+756	1.275	0.544	0.344	1.132	1.634	0.422	0.703	1.002	$-1.6^{+0.4}_{-0.4}$
J17428+167	1.027	0.768	0.602	1.014	0.943	0.624	0.818	0.973	$+0.0^{+0.4}_{-0.4}$
J17464+277 AB	1.190	0.640	0.431	1.076	1.302	0.514	0.762	1.053	$+0.0^{+0.4}_{-0.4}$
J17477+277	1.020	0.778	0.608	1.005	0.936	0.645	0.833	1.029	$+0.0^{+0.4}_{-0.4}$
J17520+566	1.219	0.577	0.427	1.089	1.273	0.477	0.705	0.936	$-7.3^{+0.6}_{-0.7}$
J17559+294	1.188	0.590	0.399	1.093	1.331	0.468	0.715	0.983	$+0.0^{+0.4}_{-0.4}$
J17578+046	1.168	0.596	0.382	1.088	1.384	0.426	0.666	0.912	$+0.0^{+0.3}_{-0.3}$
J17578+465	1.135	0.679	0.464	1.064	1.205	0.523	0.766	1.011	$+0.0^{+0.4}_{-0.4}$
J18006+685	0.927	0.903	0.834	0.963	0.696	0.871	0.916	0.959	$+0.0^{+0.4}_{-0.4}$
J18007+295	1.067	0.734	0.557	1.033	1.069	0.584	0.792	0.959	$+0.0^{+0.4}_{-0.4}$
J18019+001	1.191	0.596	0.402	1.092	1.393	0.438	0.673	0.900	$-2.5^{+0.6}_{-0.5}$
J18022+642	1.344	0.447	0.309	1.166	1.865	0.376	0.612	0.926	$-5.2^{+0.7}_{-0.6}$
J18028–030	1.215	0.612	0.396	1.098	1.412	0.498	0.770	1.105	$-0.7^{+0.4}_{-0.3}$
J18036–189	1.354	0.459	0.308	1.159	1.894	0.381	0.636	0.950	$-8.2^{+0.7}_{-0.6}$
J18041+838	1.233	0.622	0.420	1.093	1.431	0.490	0.744	1.012	$+0.0^{+0.4}_{-0.4}$
J18046+139	1.085	0.695	0.503	1.055	1.131	0.518	0.736	0.892	$+0.0^{+0.4}_{-0.4}$
J18054+015	1.183	0.632	0.426	1.075	1.322	0.503	0.751	1.030	$+0.0^{+0.4}_{-0.4}$
J18057–143	1.463	0.378	0.235	1.207	2.391	0.320	0.577	0.959	$-5.9^{+0.9}_{-0.5}$
J18068+177	1.215	0.589	0.382	1.094	1.452	0.446	0.681	0.946	$+0.0^{+0.4}_{-0.4}$
J18090+241	1.008	0.805	0.645	1.005	0.895	0.679	0.843	1.021	$+0.0^{+0.4}_{-0.4}$
J18112–010	1.182	0.593	0.406	1.103	1.280	0.457	0.691	0.932	$-5.6^{+0.7}_{-0.5}$
J18130+414	1.187	0.601	0.398	1.083	1.390	0.447	0.694	0.935	$-2.0^{+0.5}_{-0.5}$
J18131+260 AB	1.242	0.526	0.368	1.109	1.373	0.432	0.656	0.929	$-7.8^{+1.2}_{-0.7}$
J18135+055	1.250	0.611	0.410	1.076	1.487	0.492	0.740	1.027	$+0.0^{+0.4}_{-0.4}$
J18149+196	1.036	0.738	0.550	1.024	0.957	0.556	0.757	0.879	$+0.0^{+0.4}_{-0.4}$
J18162+686	1.009	0.755	0.616	1.011	0.878	0.633	0.817	0.954	$+0.0^{+0.4}_{-0.4}$
J18224+620	1.295	0.553	0.379	1.120	1.791	0.477	0.711	1.022	$-0.5^{+0.2}_{-0.3}$
J18253+186	1.184	0.621	0.420	1.072	1.289	0.486	0.724	0.981	$+0.0^{+0.4}_{-0.4}$
J18306–039	1.382	0.530	0.333	1.130	1.951	0.396	0.678	0.965	$-2.4^{+0.5}_{-0.4}$
J18313+649	1.144	0.574	0.416	1.081	1.235	0.455	0.684	0.906	$-3.2^{+0.5}_{-0.4}$
J18338+194	1.149	0.697	0.502	1.056	1.199	0.545	0.758	0.960	$-0.6^{+0.1}_{-0.2}$
J18353+457	0.938	0.855	0.717	0.986	0.744	0.780	0.889	1.163	$+0.0^{+0.4}_{-0.4}$
J18354+457	1.139	0.651	0.464	1.069	1.246	0.561	0.765	1.072	$+0.0^{+0.4}_{-0.4}$
J18400+726	1.726	0.275	0.188	1.317	4.112	0.279	0.562	0.985	$-6.2^{+2.1}_{-1.8}$
J18409+315	0.999	0.816	0.665	0.997	0.880	0.668	0.832	0.921	$+0.0^{+0.4}_{-0.4}$
J18423–013	1.200	0.894	0.837	1.015	1.354	0.908	0.960	1.215	$+0.9^{+0.3}_{-0.2}$
J18427+596N	1.117	0.682	0.473	1.054	1.200	0.526	0.769	1.003	$+0.0^{+0.4}_{-0.4}$
J18427+596S	1.149	0.640	0.431	1.071	1.330	0.484	0.736	0.974	$+0.0^{+0.4}_{-0.4}$
J18453+188	1.229	0.553	0.384	1.110	1.457	0.433	0.668	0.916	$-6.8^{+0.5}_{-0.4}$
J18467+007	1.211	0.524	0.368	1.112	1.398	0.428	0.652	0.920	$-6.3^{+0.7}_{-0.7}$
J18482+076	1.426	0.433	0..276	1.173	2.280	0.377	0.666	1.018	$-4.9^{+0.7}_{-0.6}$
J18491–032	1.311	0.536	0.338	1.125	1.693	0.444	0.714	1.050	$-0.6^{+0.3}_{-0.3}$

Table B.2: Seven representative spectral indices, ζ metallicity index, and Hα pseudo-equivalent width (cont.).

Karmn	PC1	TiO 2	TiO 5	VO-7912	Color-M	CaH 2	CaH 3	ζ	pEW(Hα) [Å]
J18499+186	1.293	0.537	0.349	1.141	1.756	0.423	0.696	0.989	$-1.4^{+0.6}_{-0.4}$
J18542+109	1.256	0.569	0.367	1.104	1.499	0.471	0.743	1.075	$+0.0^{+0.4}_{-0.4}$
J18550+429	1.215	0.528	0.361	1.122	1.366	0.426	0.657	0.934	$-6.4^{+0.5}_{-0.4}$
J18570+473	1.091	0.690	0.476	1.047	1.060	0.534	0.761	0.998	$+0.0^{+0.4}_{-0.4}$
J19052+387	1.216	0.621	0.401	1.089	1.433	0.461	0.708	0.961	$+0.0^{+0.6}_{-0.6}$
J19060–074	1.105	0.704	0.509	1.038	1.094	0.570	0.798	1.051	$+0.0^{+0.4}_{-0.4}$
J19070+208	1.035	0.764	0.577	1.016	0.978	0.588	0.784	0.909	$+0.0^{+0.4}_{-0.4}$
J19072+442	1.308	0.529	0.334	1.132	1.782	0.430	0.713	1.038	$-0.9^{+0.6}_{-0.3}$
J19105–075	1.165	0.636	0.430	1.074	1.260	0.512	0.766	1.058	$-0.5^{+0.2}_{-0.2}$
J19164+842	1.379	0.486	0.300	1.153	1.959	0.396	0.681	1.017	$-1.2^{+0.5}_{-0.4}$
J19168+003	1.186	0.575	0.412	1.083	1.259	0.460	0.675	0.908	$-6.9^{+0.5}_{-0.3}$
J19169+051N	1.093	0.704	0.512	1.042	1.082	0.574	0.791	1.038	$+0.0^{+0.4}_{-0.4}$
J19169+051S	1.983	0.344	0.261	1.292	6.103	0.334	0.641	0.979	$-9.5^{+1.1}_{-1.0}$
J19243+426	1.237	0.597	0.403	1.093	1.447	0.487	0.743	1.036	$+0.0^{+0.4}_{-0.4}$
J19260+244	1.305	0.517	0.353	1.146	1.671	0.433	0.692	0.988	$-6.3^{+0.6}_{-0.5}$
J19271+770	1.054	0.682	0.463	1.043	0.991	0.517	0.737	0.964	$+0.0^{+0.4}_{-0.4}$
J19282–001	1.450	0.452	0.280	1.188	2.061	0.399	0.711	1.082	$-11.0^{+1.0}_{-0.9}$
J19312+361	1.300	0.498	0.322	1.154	1.571	0.423	0.695	1.028	$-8.5^{+0.8}_{-0.5}$
J19316–069	1.107	0.686	0.485	1.050	1.087	0.547	0.774	1.018	$+0.0^{+0.4}_{-0.4}$
J19327–068	1.209	0.596	0.395	1.093	1.344	0.493	0.754	1.075	$+0.0^{+0.4}_{-0.4}$
J19346+045	1.024	0.949	0.876	0.978	0.908	0.883	0.930	0.775	$+0.0^{+0.4}_{-0.4}$
J19390+338	1.253	0.590	0.392	1.093	1.447	0.487	0.753	1.070	$+0.0^{+0.4}_{-0.4}$
J19393+148	1.141	0.656	0.468	1.059	1.180	0.532	0.766	1.017	$+0.0^{+0.4}_{-0.4}$
J19421+656	1.160	0.642	0.442	1.061	1.249	0.491	0.719	0.943	$+0.0^{+0.4}_{-0.4}$
J19430+102	1.066	0.721	0.545	1.035	0.999	0.583	0.787	0.977	$+0.0^{+0.5}_{-0.5}$
J19439–057	1.196	0.558	0.391	1.108	1.305	0.462	0.680	0.948	$-6.2^{+0.3}_{-0.2}$
J19452+407	0.957	0.877	0.757	0.988	0.802	0.786	0.884	1.002	$+0.0^{+0.4}_{-0.4}$
J19519+141	0.971	0.833	0.705	0.991	0.828	0.735	0.866	1.017	$+0.0^{+0.4}_{-0.4}$
J19524+603	1.148	0.669	0.452	1.069	1.260	0.503	0.730	0.955	$+0.0^{+0.4}_{-0.4}$
J19539+444W AB	1.438	0.388	0.253	1.214	2.548	0.332	0.594	0.954	$-5.1^{+1.0}_{-0.9}$
J19539+444E	1.489	0.372	0.232	1.230	2.677	0.315	0.592	0.969	$-4.4^{+1.0}_{-1.0}$
J19547+844	1.249	0.543	0.369	1.128	1.373	0.439	0.680	0.958	$-11.0^{+1.2}_{-0.8}$
J19564+591	1.172	0.640	0.427	1.075	1.245	0.504	0.760	1.043	$+0.0^{+0.4}_{-0.4}$
J19565+591	0.910	0.890	0.809	0.984	0.692	0.914	0.937	1.352	$+0.5^{+0.1}_{-0.1}$
J19578–108	1.284	0.531	0.354	1.132	1.582	0.423	0.678	0.961	$-5.9^{+0.7}_{-0.6}$
J20021+130	1.186	0.628	0.436	1.079	1.322	0.504	0.758	1.024	$+0.0^{+0.4}_{-0.4}$
J20033+672	1.129	0.665	0.466	1.037	1.158	0.530	0.753	1.000	$+0.0^{+0.4}_{-0.4}$
J20034+298	1.325	0.511	0.325	1.149	1.951	0.433	0.723	1.067	$-1.1^{+0.4}_{-0.3}$
J20047+512	1.154	0.653	0.433	1.080	1.270	0.520	0.763	1.061	$+0.0^{+0.4}_{-0.4}$
J20065+159	1.061	0.741	0.549	1.023	1.024	0.565	0.775	0.921	$+0.0^{+0.4}_{-0.4}$
J20077+189	1.219	0.586	0.380	1.107	1.406	0.486	0.746	1.080	$+0.0^{+0.4}_{-0.4}$
J20093–012	1.375	0.432	0.282	1.179	1.944	0.363	0.616	0.955	$-8.6^{+1.2}_{-0.7}$
J20108+772	0.884	0.916	0.848	0.974	0.636	0.934	0.935	1.136	$+0.5^{+0.3}_{-0.2}$
J20112+161	1.235	0.575	0.380	1.118	1.563	0.461	0.741	1.036	$-0.9^{+0.5}_{-0.5}$

Table B.2: Seven representative spectral indices, ζ metallicity index, and Hα pseudo-equivalent width (cont.).

Karmn	PC1	TiO 2	TiO 5	VO-7912	Color-M	CaH 2	CaH 3	ζ	$pEW(\mathrm{H}\alpha)$ [Å]
J20123–126	0.823	1.031	0.989	0.980	0.533	1.188	1.081	0.103	$+2.0^{+0.2}_{-0.5}$
J20177+059	1.133	0.668	0.465	1.048	1.143	0.533	0.766	1.025	$+0.0^{+0.4}_{-0.4}$
J20182–202	1.130	0.658	0.463	1.046	1.116	0.544	0.771	1.054	$+0.0^{+0.4}_{-0.4}$
J20216–199	1.041	0.764	0.584	1.009	0.964	0.613	0.803	0.969	$+0.0^{+0.4}_{-0.4}$
J20254–198	1.403	0.452	0.290	1.185	1.748	0.426	0.706	1.092	$-12.1^{+0.8}_{-1.0}$
J20283+617	1.106	0.688	0.493	1.050	1.157	0.528	0.763	0.960	$+0.0^{+0.4}_{-0.4}$
J20300+003 AB	1.231	0.504	0.329	1.118	1.558	0.384	0.621	0.912	$-2.8^{+0.8}_{-0.6}$
J20332+283	1.287	0.574	0.363	1.117	1.637	0.465	0.739	1.069	$-0.8^{+0.3}_{-0.4}$
J20336+365	1.205	0.602	0.393	1.094	1.409	0.459	0.708	0.973	$-0.4^{+0.2}_{-0.4}$
J20382+231	1.061	0.722	0.558	1.031	0.981	0.573	0.759	0.892	$-2.6^{+0.4}_{-0.4}$
J20405+154	1.335	0.513	0.331	1.136	1.817	0.428	0.706	1.032	$-0.9^{+0.4}_{-0.5}$
J20407+199 AB	1.082	0.698	0.498	1.042	1.093	0.540	0.758	0.961	$+0.0^{+0.4}_{-0.4}$
J20439+231	1.181	0.623	0.434	1.075	1.263	0.515	0.753	1.036	$+0.0^{+0.4}_{-0.4}$
J20467–118	1.220	0.518	0.371	1.117	1.426	0.437	0.667	0.939	$-7.8^{+0.7}_{-1.0}$
J20510+399	1.152	0.655	0.458	1.062	1.222	0.541	0.788	1.087	$+0.0^{+0.4}_{-0.4}$
J20540+603	1.102	0.690	0.506	1.037	1.086	0.545	0.760	0.955	$-1.7^{+0.3}_{-0.3}$
J20581+401 AB	0.911	0.915	0.832	0.975	0.698	0.896	0.929	1.091	$+0.4^{+0.1}_{-0.2}$
J20583+425	1.128	0.669	0.468	1.058	1.172	0.530	0.759	1.003	$+0.0^{+0.4}_{-0.4}$
J20593+530 AB	1.198	0.569	0.397	1.111	1.413	0.457	0.693	0.948	$-3.3^{+0.4}_{-0.4}$
J21009+510	1.088	0.646	0.467	1.051	1.054	0.519	0.743	0.967	$-3.3^{+0.7}_{-0.7}$
J21019–063	1.106	0.696	0.493	1.045	1.094	0.561	0.784	1.044	$+0.0^{+0.4}_{-0.4}$
J21027+349	1.273	0.474	0.313	1.146	1.570	0.424	0.695	1.043	$-4.5^{+0.6}_{-0.7}$
J21053+208	1.110	0.675	0.482	1.050	1.158	0.514	0.737	0.925	$+0.0^{+0.4}_{-0.4}$
J21057+502E	1.230	0.593	0.395	1.098	1.401	0.499	0.762	1.097	$+0.0^{+0.4}_{-0.4}$
J21057+502W	1.255	0.553	0.364	1.116	1.502	0.478	0.748	1.097	$+0.0^{+0.4}_{-0.4}$
J21068+387	0.848	0.964	0.920	0.963	0.572	1.044	0.991	0.947	$+0.7^{+0.1}_{-0.2}$
J21069+387	0.960	0.944	0.871	0.977	0.790	0.904	0.942	0.895	$+0.5^{+0.2}_{-0.2}$
J21074+198	0.960	0.751	0.566	1.008	0.783	0.631	0.813	1.063	$+0.0^{+0.4}_{-0.4}$
J21074+468	1.085	0.703	0.519	1.040	1.040	0.584	0.795	1.048	$+0.0^{+0.4}_{-0.4}$
J21109+469	1.168	0.623	0.428	1.076	1.256	0.518	0.760	1.062	$+0.0^{+0.4}_{-0.4}$
J21114+658	1.057	0.739	0.541	1.039	1.039	0.554	0.757	0.895	$+0.0^{+0.4}_{-0.4}$
J21127–073	1.202	0.617	0.407	1.078	1.237	0.501	0.757	1.069	$+0.0^{+0.4}_{-0.4}$
J21147+160	1.219	0.591	0.407	1.092	1.407	0.492	0.753	1.050	$+0.0^{+0.4}_{-0.4}$
J21245+400	1.538	0.429	0.263	1.192	2.820	0.375	0.701	1.069	$-1.1^{+0.6}_{-0.5}$
J21376+016	1.301	0.502	0.344	1.146	1.504	0.434	0.688	0.998	$-11.9^{+1.3}_{-0.8}$
J21414+207	1.146	0.608	0.442	1.072	1.203	0.491	0.706	0.928	$-5.0^{+0.7}_{-0.4}$
J21466+668	1.253	0.582	0.380	1.103	1.547	0.471	0.739	1.049	$+0.0^{+0.4}_{-0.4}$
J21467–212	1.229	0.563	0.389	1.108	1.408	0.438	0.671	0.918	$-5.1^{+1.0}_{-0.5}$
J21472–047	1.277	0.530	0.316	1.134	1.618	0.415	0.683	1.015	$+0.0^{+0.4}_{-0.4}$
J21554+596 AB	1.203	0.553	0.389	1.100	1.349	0.438	0.665	0.911	$-8.3^{+0.8}_{-0.5}$
J22021+014	0.958	0.858	0.731	0.990	0.798	0.758	0.871	0.998	$+0.0^{+0.4}_{-0.4}$
J22035+036 AB	1.245	0.520	0.352	1.123	1.529	0.412	0.645	0.922	$-5.6^{+0.8}_{-0.8}$
J22088+117	1.357	0.484	0.327	1.145	1.875	0.413	0.682	0.996	$-6.5^{+0.5}_{-0.5}$
J22089–177	1.104	0.696	0.489	1.047	1.104	0.497	0.705	0.856	$+0.0^{+0.4}_{-0.4}$

Table B.2: Seven representative spectral indices, ζ metallicity index, and Hα pseudo-equivalent width (cont.).

Karmn	PC1	TiO 2	TiO 5	VO-7912	Color-M	CaH 2	CaH 3	ζ	pEW(Hα) [Å]
J22095+118	1.136	0.681	0.483	1.057	1.180	0.543	0.780	1.028	$+0.0^{+0.4}_{-0.4}$
J22114+409	1.468	0.399	0.264	1.192	2.486	0.375	0.685	1.051	$-5.0^{+0.9}_{-0.5}$
J22160+546	1.236	0.578	0.390	1.109	1.511	0.446	0.701	0.955	$-2.1^{+0.5}_{-0.5}$
J22202+067	1.100	0.694	0.485	1.043	1.142	0.512	0.736	0.916	$+0.0^{+0.4}_{-0.4}$
J22234+324 AB	1.130	0.657	0.470	1.062	1.115	0.516	0.727	0.936	$-5.3^{+0.6}_{-0.3}$
J22264+583	1.160	0.666	0.462	1.066	1.265	0.512	0.757	0.986	$+0.0^{+0.4}_{-0.4}$
J22300+488 AB	1.322	0.543	0.396	1.113	1.841	0.412	0.655	0.868	$-6.1^{+0.9}_{-0.7}$
J22386+567	1.390	0.960	0.598	1.136	2.184	0.884	1.446	3.081	$+0.0^{+0.4}_{-0.4}$
J22387+252	1.192	0.648	0.450	1.072	1.351	0.509	0.755	1.002	$+0.0^{+0.4}_{-0.4}$
J22396–125	1.157	0.634	0.439	1.058	1.264	0.489	0.721	0.948	$-0.7^{+0.2}_{-0.2}$
J22415+260	1.161	0.635	0.451	1.083	1.264	0.489	0.720	0.928	$-4.0^{+0.5}_{-0.4}$
J22437+192	1.111	0.676	0.483	1.056	1.113	0.536	0.758	0.984	$-2.5^{+0.5}_{-0.4}$
J22476+184	1.101	0.658	0.453	1.065	1.109	0.525	0.764	1.033	$+0.0^{+0.4}_{-0.4}$
J22489+183	1.273	0.523	0.362	1.128	1.595	0.413	0.650	0.914	$-5.3^{+0.9}_{-0.6}$
J22509+499	1.243	0.491	0.343	1.138	1.403	0.428	0.683	0.990	$-8.9^{+0.8}_{-0.6}$
J22524+099 AB	1.116	0.669	0.468	1.051	1.195	0.493	0.723	0.907	$+0.0^{+0.4}_{-0.4}$
J22526+750	1.354	0.528	0.335	1.134	1.879	0.451	0.742	1.100	$-0.8^{+0.4}_{-0.3}$
J22582–110	1.133	0.606	0.434	1.074	1.144	0.490	0.706	0.939	$-2.9^{+0.4}_{-0.4}$
J22588+690	1.146	0.639	0.436	1.070	1.213	0.512	0.746	1.017	$+0.0^{+0.4}_{-0.4}$
J23006+036	1.148	0.663	0.462	1.063	1.204	0.516	0.753	0.985	$+0.0^{+0.4}_{-0.4}$
J23028+436	1.263	0.521	0.354	1.133	1.588	0.404	0.643	0.912	$-5.8^{+0.8}_{-0.9}$
J23036–072	1.152	0.657	0.464	1.065	1.195	0.535	0.767	1.030	$+0.0^{+0.4}_{-0.4}$
J23036+097	1.173	0.633	0.441	1.080	1.304	0.519	0.786	1.080	$+0.0^{+0.4}_{-0.4}$
J23051+519	1.184	0.621	0.432	1.091	1.296	0.519	0.771	1.074	$+0.0^{+0.4}_{-0.4}$
J23051+452	1.181	0.582	0.424	1.092	1.304	0.490	0.719	0.972	$-6.6^{+0.6}_{-0.4}$
J23070+094	1.272	0.813	0.663	1.029	1.444	0.813	0.919	1.653	$+0.8^{+0.2}_{-0.2}$
J23177+490	1.160	0.698	0.501	1.026	1.005	0.772	0.930	2.244	$+1.0^{+0.6}_{-0.3}$
J23182+795	1.116	0.644	0.444	1.067	1.124	0.526	0.765	1.052	$+0.0^{+0.4}_{-0.4}$
J23194+790	1.212	0.560	0.403	1.097	1.331	0.474	0.697	0.961	$-7.5^{+1.0}_{-0.8}$
J23209–017 AB	1.221	0.548	0.397	1.106	1.300	0.459	0.685	0.941	$-10.2^{+1.0}_{-0.7}$
J23220+569	1.157	0.633	0.434	1.066	1.230	0.522	0.783	1.093	$+0.0^{+0.4}_{-0.4}$
J23228+787	1.302	0.347	0.206	1.224	1.634	0.350	0.641	1.066	$-11.2^{+1.6}_{-1.2}$
J23235+457	0.852	0.955	0.913	0.969	0.564	1.061	0.986	1.062	$+0.8^{+0.2}_{-0.2}$
J23261+170 AB	1.257	0.549	0.369	1.119	1.532	0.428	0.676	0.943	$-3.1^{+0.8}_{-0.8}$
J23266+453	1.263	0.852	0.543	1.116	1.496	0.851	1.262	5.896	$+0.0^{+0.4}_{-0.4}$
J23306+466	1.048	0.745	0.573	1.022	0.996	0.603	0.805	0.980	$+0.0^{+0.4}_{-0.4}$
J23317–064	1.362	0.539	0.355	1.139	1.846	0.472	0.763	1.127	$-0.9^{+0.6}_{-0.6}$
J23376+163	1.459	0.386	0.250	1.210	2.384	0.330	0.602	0.963	$-6.2^{+0.7}_{-1.0}$
J23416–065	1.330	0.534	0.332	1.124	1.761	0.437	0.709	1.044	$+0.0^{+0.4}_{-0.4}$
J23417–059 AB	1.165	0.605	0.416	1.072	1.297	0.473	0.719	0.965	$+0.0^{+0.4}_{-0.4}$
J23419+441	1.386	0.467	0.293	1.170	2.372	0.409	0.710	1.072	$-1.0^{+0.4}_{-0.3}$
J23423+349	1.215	0.591	0.383	1.094	1.447	0.467	0.732	1.029	$-0.6^{+0.2}_{-0.4}$
J23425+392	0.928	0.904	0.823	0.982	0.739	0.875	0.921	1.054	$-1.6^{+0.4}_{-0.3}$
J23438+610	1.110	0.641	0.434	1.059	1.176	0.492	0.731	0.974	$+0.0^{+0.4}_{-0.4}$

Table B.2: Seven representative spectral indices, ζ metallicity index, and Hα pseudo-equivalent width (cont.).

Karmn	PC1	TiO 2	TiO 5	VO-7912	Color-M	CaH 2	CaH 3	ζ	$pEW(\mathrm{H}\alpha)$ [Å]
J23490–086	1.054	0.737	0.534	1.029	0.999	0.563	0.775	0.947	$+0.0^{+0.4}_{-0.4}$
J23559–133	1.184	0.568	0.405	1.094	1.331	0.472	0.700	0.959	$-4.2^{+0.5}_{-0.4}$
J23560+150	1.102	0.709	0.517	1.040	1.110	0.560	0.783	0.990	$+0.0^{+0.4}_{-0.4}$
J23569+230	1.012	0.801	0.640	1.007	0.914	0.680	0.848	1.045	$+0.0^{+0.4}_{-0.4}$
J23585+242	0.898	0.921	0.836	0.977	0.677	0.905	0.931	1.105	$+0.5^{+0.3}_{-0.2}$
J23590+208	1.111	0.668	0.469	1.059	1.097	0.561	0.785	1.095	$+0.0^{+0.4}_{-0.4}$

Table B.3: Spectral types of observed stars.

Karmn	Sp. type biblio.	Ref.[a]	Sp. type Best-fit	χ^2	Sp. type TiO2	TiO5	PC1	VO-7912	Color-M	Sp. type adopted
J00066–070 AB	M3.5 V+m4.5:	Reid07, Jan12	4.5	4.5	4.5	4.5	4.0	4.5	4.5	M4.5 V
J00077+603 AB	M4.5 V	Lep13	4.0	4.0	4.5	4.0	3.5	4.0	3.5	M4.0 V
J00115+591	M5.5 V	Lep03	6.0	6.0	5.5	6.0	5.5	5.5	5.5	M5.5 V
J00118+229	M3.5 V	Reid04	3.5	3.5	3.5	3.5	4.0	4.0	3.5	M3.5 V
J00119+330	M3.5 V	Giz97	3.5	3.0	3.5	3.5	3.5	3.5	3.5	M3.5 V
J00122+304	M5.0 V	Abe14	4.5	4.5	4.5	4.0	4.5	5.0	4.5	M4.5 V
J00133+275	M4.5 V	Abe14	4.5	4.5	4.5	4.5	4.5	4.5	4.5	M4.5 V
J00136+806	M1.5 V	PMSU	1.5	1.5	1.5	1.5	1.5	1.5	1.5	M1.5 V
J00146+202	M2 III	Gar89, Kir91	...	...	...	...	...	...	...	M III
J00152+530	M2.2 V	Mann13	2.5	2.0	2.5	2.0	2.5	2.0	2.5	M2.5 V
J00162+198E	M4.0 V	PMSU	4.0	4.0	4.0	4.0	4.5	4.5	4.0	M4.0 V
J00162+198W	M4.0 V	PMSU	4.0	4.0	4.0	4.0	4.0	4.5	4.0	M4.0 V
J00183+440	M1.0 V	PMSU	1.0	1.5	1.0	1.5	1.0	1.0	1.5	M1.0 V
J00228–164	...	...	4.0	4.0	4.0	4.0	4.0	4.0	4.0	M4.0 V
J00240+264	M4.0 V	Abe14	4.0	4.5	4.0	4.0	4.0	4.5	4.5	M4.0 V
J00253+235	...	...	1.5	1.5	1.0	1.0	1.0	1.5	1.5	M1.5 V
J00297+012	...	...	1.0	1.0	1.0	1.0	1.0	1.0	1.0	M1.0 V
J00313+336	K5 V	Ste86	0.0	0.0	0.0	0.0	0.0	0.5	0.5	M0.0 V
J00313+001	m:	Simbad	3.0	3.0	3.0	3.0	3.0	3.0	3.0	M3.0 V
J00322+544	k:	Simbad	4.5	4.5	4.0	4.0	4.5	4.5	4.5	M4.5 V
J00328–045 AB	M3.5 V	Reid07	4.5	4.5	4.0	4.0	4.5	4.5	4.5	M4.5 V
J00358+526	M3.5 V	Giz97	2.5	2.0	2.5	2.5	2.5	2.0	2.5	M2.5 V
J00367+444	K5 III	Gar89, Kir91	...	...	...	...	...	...	...	K III
J00380+169	...	...	3.0	2.5	3.0	3.0	3.0	3.0	3.0	M3.0 V
J00389+306	M2.5 V	PMSU	2.5	2.0	2.5	2.5	2.5	2.5	2.5	M2.5 V
J00395+149N	...	...	4.5	4.5	4.5	4.5	4.5	5.0	4.5	M4.5 V
J00395+149S	...	...	4.0	4.0	4.0	3.5	4.0	4.0	4.0	M4.0 V
J00452+002 AB	M3.8 V	Mann13	3.5	3.5	4.0	4.0	4.0	4.0	3.5	M4.0 V
J00464+506	M3.5 V	Reid04	4.0	4.0	4.0	4.0	4.0	4.5	4.0	M4.0 V
J00467–044	m:	Simbad	4.0	4.0	4.0	4.0	4.5	4.0	4.0	M4.0 V
J00484+753	...	...	3.0	2.5	3.0	3.0	3.0	3.0	2.5	M3.0 V
J00490+657	...	...	2.5	2.5	2.5	2.5	2.5	2.5	2.5	M2.5 V
J00490+578	K7 V	Hen94	–1.0	–1.0	–1.0	–1.0	–0.5	–0.5	–0.5	K7 V
J00502+601	K7 III	Jac84, Kir91	...	...	...	...	...	...	...	K III
J00502+086	...	...	4.5	4.5	4.5	4.5	4.5	4.5	4.0	M4.5 V
J00540+691	M2 V:	Bid85	2.5	2.5	2.0	2.0	2.0	2.0	2.5	M2.0 V

Table B.3: Spectral types of observed stars (cont.).

Karmn	Sp. type biblio.	Ref.[a]	Sp. type Best-fit	χ^2	Sp. type TiO2	TiO5	PC1	VO-7912	Color-M	Sp. type adopted
J00548+275	M4.6 V	Shk09	4.5	4.5	4.5	4.0	4.5	4.5	4.5	M4.5 V
J00580+393	M4.5 V	Abe14	4.5	4.5	4.5	4.0	4.5	4.5	4.5	M4.5 V
J01009–044	M3.5 V	PMSU	4.0	4.0	3.5	4.0	4.0	4.0	4.0	M4.0 V
J01012+571	...	...	...	...	...	...	...	...	...	M III
J01014–010	...	...	3.5	3.5	3.5	3.5	4.0	4.0	3.5	M3.5 V
J01014+188	...	...	2.0	2.0	2.5	2.5	2.0	2.0	2.0	M2.0 V
J01026+623	M1.5 V	PMSU	1.5	1.5	1.5	1.5	2.0	1.5	1.5	M1.5 V
J01028+189	M4 V	Riaz06	4.0	4.0	4.5	4.0	4.0	4.5	3.5	M4.0 V
J01028+470	m5:	LG11	1.5	1.0	2.0	2.0	1.0	1.5	1.0	M1.5 V
J01032+712	M3.5 V	Giz97	4.0	4.5	4.0	3.5	4.5	4.0	4.5	M4.0 V
J01033+623	M5.0 V	PMSU	5.0	5.0	5.0	5.0	5.0	5.0	4.5	M5.0 V
J01055+153	K7.4 V	Mann13	–1.0	–1.0	–1.0	–1.0	–1.5	–1.0	–2.0	K7 V
J01069+804	...	...	4.5	5.0	4.5	4.5	4.5	5.0	4.5	M4.5 V
J01074–025	...	...	≤–2.0	≤–2.0	...	...	...	...	...	K5 V
J01076+229E	M3.0 V	PMSU	3.5	3.0	4.0	3.5	3.5	4.0	3.5	M3.5 V
J01097+356	M0 III	Gar89	...	...	...	...	...	...	...	M III
J01186–008	K7 V	PMSU	–1.0	–1.0	–0.5	–0.5	–0.5	–0.5	–1.0	K7 V
J01214+313	M1 V:	Bid85	3.5	3.0	3.5	3.5	3.5	3.5	3.0	M3.5 V
J01226+127	K7.8 V	Mann13	–1.0	–1.0	–0.5	–0.5	–1.0	–0.5	–1.5	K7 V
J01342–015	m:	Simbad	1.0	1.0	1.5	1.5	1.0	1.0	1.0	M1.0 V
J01356–200 AB	m:	Simbad	2.5	2.0	2.5	2.5	2.5	2.5	2.0	M2.5 V
J01390–179 AB	M5.5 V+M6.0	Kirk91	5.0	5.0	5.0	4.5	4.5	5.5	5.0	M5.0 V
J01406–081	...	...	≤–2.0	≤–2.0	...	...	...	...	...	K5 V
J01431+210	M4.0 V	Fri13	3.5	4.0	4.5	4.0	4.0	4.5	3.5	M4.0 V
J01541–156	M4.0 V	Reid04	4.0	4.5	4.0	4.0	4.0	4.5	4.0	M4.0 V
J01551–162	...	...	–1.0	–1.0	–1.0	–1.0	–1.0	0.0	–1.0	K7 V
J01562+001	...	...	3.0	3.0	3.5	3.0	3.0	3.0	2.5	M3.0 V
J01567+305	M5.0 V	Abe14	4.5	4.5	5.0	4.5	4.5	5.0	4.5	M4.5 V
J01571–102	K7 V	PMSU	0.0	0.0	0.0	0.0	0.0	0.0	0.0	M0.0 V
J02000+135 AB	m:	Reid04	3.5	3.0	3.5	3.5	3.5	3.5	3.0	M3.5 V
J02002+130	M4.5 V	PMSU	3.5	3.5	3.0	3.0	3.0	4.5	4.0	M3.5: V
J02019+342	...	...	0.5	0.5	0.5	0.5	0.5	0.5	0.5	M0.5 V
J02022+103	M6.0 V	PMSU	5.5	5.5	5.5	6.0	5.5	5.5	5.5	M5.5 V
J02023+012	...	...	2.5	2.5	2.0	2.0	2.5	2.0	2.5	M2.5 V
J02100–088	M3.5 V	Giz97	3.0	3.0	4.0	3.5	3.0	3.5	2.5	M3.0 V
J02133+368 AB	M4.5 V	Riaz06	4.5	4.5	5.0	4.5	4.5	4.5	4.5	M4.5 V
J02142–039	M5.5 V	CrRe02	5.5	5.5	6.0	5.5	5.5	6.0	5.5	M5.5 V

Table B.3: Spectral types of observed stars (cont.).

Karmn	Sp. type	Ref.[a]	Sp. type		Sp. type					Sp. type
	biblio.		Best-fit	χ^2	TiO2	TiO5	PC1	VO-7912	Color-M	adopted
J02159–094 ABC	M2.5 V	Riaz06	2.5	2.5	3.0	2.5	2.5	3.0	2.0	M2.5 V
J02274+031	...	...	4.0	4.0	4.0	4.0	3.5	4.0	3.5	M4.0 V
J02285–200	M2.9 V	Mann13	2.5	2.5	2.5	2.5	2.0	2.5	2.5	M2.5 V
J02291+228	K5.9 V	Mann13	–1.0	–1.0	–1.0	–1.0	–1.0	–0.5	–0.5	K7 V
J02362+068	M4.0 V	PMSU	3.5	4.0	3.5	4.0	3.5	4.0	4.0	M4.0 V
J02367+226	M5.0 V	Reid04	5.0	5.0	5.0	5.0	5.0	5.0	5.0	M5.0 V
J02412–045	M4.0 V	CrRe02	4.5	4.5	4.5	4.0	4.5	4.5	4.5	M4.5 V
J02441+492	M1.5 V	PMSU	1.5	1.5	1.5	1.5	1.5	1.5	1.5	M1.5 V
J02456+449	M0.0 V	PMSU	0.5	0.5	0.0	0.5	0.5	0.5	1.0	M0.5 V
J02479–124	M5 III	SB06	...	...	...	...	...	...	...	M III
J02502+628	...	...	2.5	2.5	3.0	2.5	3.0	2.5	3.0	M2.5 V
J02530+168	M6.5 V	Tee03	7.0	6.5	7.0	7.0	7.0	6.5	7.0	M7.0 V
J02555+268	M4.0 V	PMSU	4.0	4.0	4.0	4.0	4.5	4.0	4.0	M4.0 V
J02558+183	M6 III	Gar89, SB06	...	...	...	...	...	...	...	M III
J02562+239	M4.5 V	Reid07	5.0	5.0	5.0	4.5	5.0	5.0	4.5	M5.0 V
J03026–181	M2.0 V	PMSU	2.5	2.0	2.5	2.5	2.5	2.5	2.5	M2.5 V
J03033–080	M3.0 V	Reid07	2.5	2.5	3.5	3.0	3.0	3.5	3.0	M3.0 V
J03047+617	M3.0 V	PMSU	2.5	2.5	3.0	3.0	3.0	3.0	3.0	M3.0 V
J03110–046	M2.5 V	Sch05	2.5	2.5	3.0	3.0	3.0	3.0	3.0	M3.0 V
J03147+114	M1 V	Li00	2.0	1.5	2.5	2.0	1.5	2.5	2.0	M2.0 V
J03154+578	m:	Cab09	3.5	3.5	3.5	3.5	3.0	3.0	3.0	M3.5 V
J03162+581N	M2.0 V	PMSU	2.0	2.0	2.0	2.0	2.0	2.0	2.0	M2.0 V
J03162+581S	M2.0 V	Bid85	2.0	2.0	2.0	2.0	2.0	2.0	2.0	M2.0 V
J03167+389	...	...	3.5	3.5	3.5	3.5	3.5	3.5	3.5	M3.5 V
J03174–011	k:	Simbad	0.5	0.5	1.0	1.0	0.5	0.5	0.0	M0.5 V
J03179–010	m:	Simbad	2.0	2.0	2.0	2.5	2.0	1.5	1.5	M2.0 V
J03181+426	M4.0 V	Reid04	3.5	3.5	3.5	3.5	4.0	4.0	3.5	M3.5 V
J03194+619	M4.1 V	Shk09	4.0	4.0	4.5	4.0	4.0	4.5	4.0	M4.0 V
J03236+056	...	...	4.5	4.5	4.5	4.5	5.0	5.0	4.5	M4.5 V
J03236+476	...	...	0.5	0.5	0.5	0.5	0.5	0.5	1.0	M0.5 V
J03263+171	...	...	4.0	4.0	3.5	4.0	4.0	4.0	4.0	M4.0 V
J03275+222	M4.0 V	Abe14	4.5	4.5	4.5	4.5	4.5	4.5	4.0	M4.5 V
J03294+117	...	...	2.5	2.0	3.0	3.0	2.0	3.0	2.0	M2.5 V
J03303+346	...	...	4.0	4.0	4.0	4.0	4.0	4.5	3.5	M4.0 V
J03309+706	m5:	LG11	3.5	3.5	3.5	3.5	3.0	3.5	3.5	M3.5 V
J03319+492	m3:	LG11	...	...	...	...	...	...	...	K III
J03320+436	K7.3 V	Mann13	–1.0	–1.0	–0.5	–0.5	–0.5	–0.5	–0.5	K7 V

Table B.3: Spectral types of observed stars (cont.).

Karmn	Sp. type	Ref.[a]	Sp. type		Sp. type					Sp. type
	biblio.		Best-fit	χ^2	TiO2	TiO5	PC1	VO-7912	Color-M	adopted
J03325+287 ABC	M4.0 V	Riaz06	4.5	4.5	4.5	4.5	4.5	4.5	4.0	M4.5 V
J03332+462	M0.0 V	Lep13	–1.0	–1.0	0.0	0.0	–0.5	0.5	–0.5	M0.0 V
J03354+428	M0.4 V	Mann13	0.5	0.5	0.0	0.0	0.5	0.5	0.5	M0.5 V
J03356–084	m:	Simbad	5.5	5.5	5.0	5.5	5.0	5.0	5.5	M5.5 V
J03361+313	M4.5 V	Riaz06	4.5	5.0	5.0	4.5	4.5	5.0	4.5	M4.5 V
J03375+288	...	...	0.0	0.0	0.0	0.0	0.0	0.0	0.5	M0.0 V
J03375+178N AB	M2.0 V+M3.6	PMSU, Shk10	2.5	2.0	2.5	2.0	2.5	2.5	2.5	M2.5 V
J03375+178S AB	M3.0 V+M4.3	PMSU, Shk10	3.5	3.5	3.0	3.0	3.0	4.0	3.5	M3.5 V
J03392+565 AB	m6:	LG11	2.5	2.5	3.0	3.0	3.0	3.0	3.0	M2.5 V
J03430+459	m5:	LG11	4.0	4.0	4.0	4.0	3.5	4.0	4.0	M4.0 V
J03466+243 AB	K3 V	Simbad	$\leq$–2.0	$\leq$–2.0	...	...	...	...	...	K5 V
J03473–019	M2.8 V	Shk09	3.0	3.0	3.0	2.5	3.0	2.5	2.5	M3.0 V
J03480+405	M2.0 V	New14	1.5	1.5	1.5	1.5	1.5	2.0	1.5	M1.5 V
J03510+142	...	...	4.5	4.5	4.5	4.0	4.5	4.5	4.0	M4.5 V
J03519+397	M0.0 V	Lep13	0.0	0.0	–0.5	–0.5	0.0	–0.5	0.0	M0.0 V
J03548+163 AB	...	...	4.0	4.0	4.0	4.0	4.0	4.5	4.0	M4.0 V
J03556+522	M2.7 V	Mann13	2.5	2.0	2.5	2.5	2.5	2.0	2.5	M2.5 V
J03565+319	M3.0 V	Reid07	4.0	3.5	4.0	3.5	3.5	4.0	3.5	M3.5 V
J03566+507	...	...	–2.0	–2.0	–1.5	–1.5	–1.0	–0.5	–1.0	K7 V
J03574–011 AB	M2.0 V	PMSU	2.5	2.0	2.5	2.0	2.5	2.5	2.5	M2.5 V
J03588+125	...	...	4.0	4.0	4.0	4.0	4.5	4.5	4.5	M4.0 V
J04041+307	M1.5 V	Giz97	1.5	1.5	1.5	2.0	1.5	1.5	2.0	M1.5 V
J04061–055	M3.5 V	Reid07	3.5	4.0	3.5	3.5	3.5	3.5	3.5	M3.5 V
J04079+142	...	...	2.5	2.5	3.0	3.0	3.0	3.0	3.0	M2.5 V
J04081+743	M3.5 V	Giz97	3.5	3.5	3.5	3.5	3.5	3.5	3.5	M3.5 V
J04083+691	m4.5:	Law08	4.5	4.5	4.5	4.5	4.5	4.5	4.5	M4.5 V
J04123+162 AB	M1	BS08	4.0	3.5	4.0	3.5	4.0	4.0	3.5	M4.0 V
J04153–076	M4.5 V	PMSU	4.5	4.5	5.0	4.5	4.5	4.5	4.0	M4.5 V
J04177+410	...	...	3.5	3.5	3.5	3.0	3.5	3.5	3.0	M3.5 V
J04177+136 AB	M1 V	Simbad	1.5	1.5	1.5	1.0	2.0	1.5	2.0	M1.5 V
J04191–074	M4.0 V	Sch05	3.5	3.5	4.0	4.0	4.0	4.0	3.5	M3.5 V
J04191+097	...	...	3.5	3.0	3.0	3.0	3.0	3.0	3.5	M3.0 V
J04205+815	...	...	3.0	3.0	2.5	2.5	3.0	2.5	3.0	M3.0 V
J04206+272	M3–4 IV	Sce08	4.5	4.5	4.5	4.5	5.0	5.0	4.0	M4.5 V
J04206–168	M3III	KMc89, Gar89	...	...	...	...	...	...	...	M III
J04207+152 AB	m5:	LG11	4.0	4.0	4.0	4.0	4.0	4.0	4.0	M4.0 V
J04224+036	...	...	3.5	3.0	4.0	3.5	3.5	4.0	3.0	M3.5 V

Table B.3: Spectral types of observed stars (cont.).

Karmn	Sp. type	Ref.[a]	Sp. type		Sp. type					Sp. type
	biblio.		Best-fit	χ^2	TiO2	TiO5	PC1	VO-7912	Color-M	adopted
J04227+205	...	...	4.0	4.0	4.0	4.0	4.0	4.5	4.0	M4.0 V
J04229+259	M4.0 V	Reid04	4.0	4.5	4.0	4.0	4.5	4.5	4.5	M4.5 V
J04234+809	...	...	4.0	4.0	4.0	3.5	4.0	4.0	3.5	M4.0 V
J04238+149 AB	M3 V	Simbad	3.5	3.0	3.5	3.0	3.5	3.5	3.0	M3.5 V
J04238+092 AB	M3 V	Simbad	3.0	3.0	3.0	2.5	3.5	3.0	3.0	M3.0 V
J04247–067 ABC	M4.5+M5.5+M5.7	Shk10	4.0	4.0	4.0	4.0	4.0	4.0	3.5	M4.0 V
J04252+172 ABC	M3 V+M3+M4:	Cut00	3.5	3.5	4.0	3.5	3.5	4.0	3.0	M3.5 V
J04290+186	...	...	2.5	2.5	2.5	2.5	2.5	3.0	2.5	M2.5 V
J04308–088	M4.0 V	Reid04	4.0	4.5	4.0	4.0	4.0	4.0	4.0	M4.0 V
J04310+367	...	...	3.0	3.0	3.5	3.0	3.0	3.0	3.0	M3.0 V
J04313+241 AB	M5.5 V	Mar94	4.5	5.0	4.5	4.5	5.0	5.0	4.5	M4.5:
J04329+001S	M0.5 V	Reid04	0.5	0.5	1.0	1.0	0.5	0.5	0.0	M0.5 V
J04347–004	m:	Simbad	4.0	4.0	4.0	4.0	4.0	4.0	4.0	M4.0 V
J04360+188	M3.5 V	Simbad	2.5	2.5	3.0	3.0	2.5	3.0	2.5	M2.5 V
J04366+186	...	...	2.0	2.0	2.5	2.0	2.5	2.0	2.0	M2.0 V
J04373+193	...	...	4.0	4.5	4.5	4.0	4.0	4.5	4.0	M4.0 V
J04386–115	M3.0 V	Sch05	3.0	3.5	3.0	3.5	3.5	3.5	3.0	M3.5 V
J04388+217	M3.5 V	Reid04	3.5	3.0	3.5	3.5	3.5	3.5	3.5	M3.5 V
J04393+335	M2.5 V	Simbad	4.0	4.0	4.0	4.0	4.0	4.5	3.5	M4.0 V
J04398+251	M3.0 V	Reid07	3.5	3.5	3.5	3.5	3.5	3.5	3.5	M3.5 V
J04413+327	...	...	4.0	4.0	3.5	3.5	4.0	4.0	4.0	M4.0 V
J04425+204 AB	...	...	3.0	3.0	3.5	3.0	3.0	3.5	3.0	M3.0 V
J04430+187 AB	K8 V	Vys56	≤–2.0	≤–2.0	...	...	...	...	...	K5 V
J04458–144	M4.0 V	Reid07	4.0	4.0	4.0	4.0	4.0	4.0	4.0	M4.0 V
J04468–112 AB	M4.9 V	Shk09	3.0	3.0	3.5	3.5	3.0	3.5	2.5	M3.0 V
J04472+206	M4.5 V	Reid07	5.0	5.0	5.0	5.0	5.0	5.0	4.5	M5.0 V
J04494+484 AB	M4.0 V	Shk09	4.0	4.0	4.0	4.0	4.0	4.0	4.0	M4.0 V
J04496–153	...	...	–2.0	–2.0	...	...	...	...	...	K5 V
J04499+711	...	...	4.0	3.5	3.5	3.5	4.0	3.5	4.0	M3.5 V
J04536+623	...	...	3.5	3.5	3.5	3.5	3.5	3.5	3.5	M3.5 V
J04538+158	M2.5 V	Reid07	2.5	2.5	2.5	2.5	2.5	2.5	3.0	M2.5 V
J04544+650	...	...	4.0	4.0	4.0	4.0	4.0	4.5	4.0	M4.0 V
J04559+046	M3 V	New14	2.0	2.0	2.0	2.0	2.0	2.0	2.0	M2.0 V
J04560+432	...	...	4.0	4.0	3.5	4.0	4.0	4.0	4.0	M4.0 V
J05003+251 AB	...	...	1.5	1.5	1.5	1.0	1.0	1.0	1.0	M1.0 V
J05019+011	M4.5 V	Lep13	4.0	4.0	4.0	4.0	4.0	4.5	3.5	M4.0 V
J05030+213 AB	m4.5:+m5.0:	Law08	5.0	5.0	5.0	4.5	5.0	5.0	5.0	M5.0 V

Table B.3: Spectral types of observed stars (cont.).

Karmn	Sp. type	Ref.[a]	Sp. type		Sp. type					Sp. type
	biblio.		Best-fit	χ^2	TiO2	TiO5	PC1	VO-7912	Color-M	adopted
J05032+213	M1.5 V	Reid04	1.5	1.5	2.0	2.0	1.5	2.0	1.5	M1.5 V
J05050+442	...	...	5.0	5.0	4.5	5.0	5.0	5.0	5.0	M5.0 V
J05062+046	M4.0 V	Lep13	4.5	4.0	4.5	4.0	4.0	4.5	3.5	M4.0 V
J05068+516	k:	Kri93	–2.0	–2.0	...	...	...	...	...	K5 V
J05072+375	M5.0 V	Abe14	5.0	5.0	5.0	5.0	4.5	5.0	4.5	M5.0 V
J05083+756	M5.0 V	Sch05	4.5	4.5	4.5	4.5	4.5	4.5	4.5	M4.5 V
J05151–073	M0.5 V	PMSU	1.0	1.0	1.0	1.0	1.0	1.0	1.0	M1.0 V
J05152+236	M4.5 V	Abe14	5.0	5.0	5.0	4.5	5.0	5.0	4.5	M5.0 V
J05173+321	M3.5 V	Reid04	3.5	3.0	3.5	3.5	3.5	3.5	3.5	M3.5 V
J05175+487	...	...	0.0	0.0	–0.5	–0.5	0.0	0.0	0.0	M0.0 V
J05187+464	...	...	4.5	4.5	5.0	4.5	4.5	5.0	4.5	M4.5 V
J05187–213	...	...	3.5	3.5	3.5	3.5	3.5	3.5	3.0	M3.5 V
J05195+649	M4.0 V	Lep13	3.5	3.0	3.5	4.0	3.5	4.0	3.0	M3.5 V
J05200–229	...	...	2.0	2.0	2.5	2.5	2.0	2.0	1.5	M2.0 V
J05223+305	...	...	3.5	3.0	3.0	3.0	3.5	3.0	3.0	M3.0 V
J05256–091 AB	M3.5 V+M5.0	Reid04, Shk09	3.5	3.5	3.5	3.5	3.5	3.5	3.0	M3.5 V
J05289+125	M4.0 V	PMSU	4.0	4.0	3.5	3.5	4.0	4.0	4.0	M4.0 V
J05294+155E	M0.0 V:	PMSU	–1.0	–1.0	0.5	0.5	–1.0	0.0	–1.0	M0.0: V
J05295–113	...	...	3.5	3.5	3.5	3.5	3.5	4.0	3.5	M3.5 V
J05300+121E	...	...	0.0	0.5	0.5	0.5	0.0	0.5	0.0	M0.5 V
J05300+121W	...	...	–2.0	–2.0	...	...	...	...	...	K5 V
J05314–036	M1.5 V	PMSU	1.5	1.5	1.5	1.5	2.0	1.5	2.0	M1.5 V
J05320–030 AB	M2.0 V	Riaz06	1.5	1.5	2.5	2.0	2.0	2.5	1.5	M2.0 V
J05324–072	M0–1 V	Ste86	0.5	0.5	0.5	0.5	–0.5	0.0	–0.5	M0.5 V
J05328+338	M3.5 V	Reid04	3.5	3.5	3.5	3.5	3.0	3.0	3.5	M3.5 V
J05342+103N	M3.5 V	PMSU	3.0	3.0	3.0	3.0	3.0	3.0	2.5	M3.0 V
J05342+103S	M3.0 V	PMSU	4.5	4.5	4.0	4.0	5.0	4.0	4.5	M4.5 V
J05394+747	...	...	3.5	3.5	3.0	3.5	3.5	3.5	3.5	M3.5 V
J05415+534	M0.5 V	PMSU	1.0	1.0	1.0	1.0	1.0	1.0	1.0	M1.0 V
J05421+124	M4.0 V	PMSU	4.0	4.0	4.0	4.0	4.0	4.0	4.0	M4.0 V
J05424+506	m:	Simbad	3.0	3.0	3.0	3.5	3.0	3.5	3.0	M3.0 V
J05425+154	M5.0 V	LC08	3.5	3.5	3.5	3.5	3.5	4.0	3.5	M3.5 V
J05427+026	m:	Simbad	3.5	3.0	3.0	3.0	3.5	3.0	3.0	M3.0 V
J05455–119	...	...	4.5	4.5	4.0	4.0	4.5	4.5	4.5	M4.5 V
J05456+111	...	...	–1.0	–1.0	0.0	0.0	–1.0	0.0	–0.5	M0.0 V
J05456+729	...	...	3.0	3.0	3.0	3.0	3.0	3.0	3.0	M3.0 V
J05457–223	m6:	Simbad	3.5	3.5	3.5	3.5	3.5	3.0	3.0	M3.5 V

Table B.3: Spectral types of observed stars (cont.).

Karmn	Sp. type biblio.	Ref.[a]	Sp. type Best-fit	χ^2	Sp. type TiO2	TiO5	PC1	VO-7912	Color-M	Sp. type adopted
J05458+729	...	...	2.5	2.5	3.0	3.0	2.5	2.5	2.0	M2.5 V
J05463+012	M1 V	New14	2.5	2.5	2.5	2.5	3.0	2.5	2.5	M2.5 V
J05501+051	...	...	1.5	1.0	1.5	1.0	1.5	2.0	1.5	M1.5 V
J05511+122	...	...	4.0	4.0	3.5	4.0	4.0	4.0	4.0	M4.0 V
J05566–103	M3.5 V	Riaz06	3.5	3.5	4.0	3.5	3.5	4.0	3.5	M3.5 V
J05582–046	M5.0 V	RA12	4.5	5.0	4.5	5.0	5.0	4.5	4.5	M4.5 V
J05588+213	M4.5 V	Reid04	5.0	5.0	5.0	5.0	5.0	5.0	5.0	M5.0 V
J05596+585	M0.5 V	PMSU	0.0	0.0	1.0	1.0	0.5	0.5	0.5	M0.5 V
J06024+663	M4.5 V	Giz97	4.5	4.5	4.5	4.5	5.0	4.5	4.5	M4.5 V
J06024+498	M5.0 V	PMSU	5.0	5.0	5.0	5.0	5.0	5.0	5.0	M5.0 V
J06035+168	...	...	4.0	4.0	4.0	4.0	4.0	4.0	4.0	M4.0 V
J06035+155	M0.0 V	Lep13	0.5	0.0	0.0	–0.5	0.0	0.5	0.0	M0.0 V
J06054+608	M4.5 V	Giz97	4.5	4.5	4.5	4.0	4.5	5.0	4.5	M4.5 V
J06065+045	m:	Simbad	3.0	3.0	3.5	3.5	3.0	3.0	3.0	M3.0 V
J06066+465	...	...	3.0	3.0	3.0	3.0	3.0	3.0	3.0	M3.0 V
J06075+472	M3.5 V	Reid07	4.5	4.5	4.5	4.5	4.5	5.0	4.5	M4.5 V
J06102+225	...	...	4.0	4.0	4.5	4.0	4.5	4.5	3.5	M4.0 V
J06103+722	...	...	2.5	2.0	3.0	3.0	2.5	3.0	2.5	M2.5 V
J06145+025	M3.0 V	Sch05	2.5	2.5	3.5	3.5	3.0	3.5	3.0	M3.0 V
J06151–164	...	...	4.0	4.0	4.0	4.0	4.0	4.0	4.0	M4.0 V
J06171+051 AB	M3.5 V	PMSU	3.5	3.5	3.0	3.5	3.5	3.5	3.5	M3.5 V
J06185+250	M4.0 V	Reid04	4.0	3.5	4.0	4.0	4.0	4.0	4.0	M4.0 V
J06236–096 AB	M3.5 V	Reid04	3.5	3.5	3.5	3.5	3.5	3.5	3.5	M3.5 V
J06238+456	M5.0 V	Sch05	5.0	5.0	5.0	5.0	5.0	5.0	5.0	M5.0 V
J06246+234	M4.5 V	PMSU	4.0	4.0	4.0	4.5	4.0	4.0	4.0	M4.0 V
J06298–027 AB	M3.5 V+M6.3	Reid04, Shk10	4.0	4.0	4.5	4.0	4.0	4.5	4.0	M4.0 V
J06307+397	...	...	2.0	2.0	2.0	2.0	2.0	2.0	2.0	M2.0 V
J06313+006	...	...	1.5	1.5	1.0	1.5	1.5	1.5	1.5	M1.5 V
J06314–016	m:	Simbad	1.5	1.0	2.0	2.0	1.0	1.5	0.5	M1.5 V
J06323–097	...	...	4.0	4.5	4.0	4.0	4.5	4.5	4.5	M4.5 V
J06325+641	M4.0 V	Giz97	4.0	4.0	4.0	4.0	4.0	4.5	4.0	M4.0 V
J06332+054	M1.0 V	New14	2.0	2.0	2.0	2.0	2.0	2.0	2.0	M2.0 V
J06354–040 AB	...	...	5.5	5.5	5.5	5.0	5.5	5.0	5.0	M5.5 V
J06361+201	M2.5 V	Reid04	2.5	2.5	2.5	2.5	2.5	2.5	2.5	M2.5 V
J06367+378	...	...	3.5	3.5	4.0	3.5	4.0	4.0	3.5	M3.5 V
J06401–164	...	...	2.5	2.5	3.0	3.0	2.0	2.5	2.0	M2.5 V
J06435+166	M4.5 V	Reid04	4.0	4.5	4.0	4.5	4.5	4.5	4.5	M4.5 V

Table B.3: Spectral types of observed stars (cont.).

Karmn	Sp. type	Ref.[a]	Sp. type		Sp. type					Sp. type
	biblio.		Best-fit	χ^2	TiO2	TiO5	PC1	VO-7912	Color-M	adopted
J06461+325	M0.5 V	PMSU	1.0	1.0	1.0	1.0	1.0	0.5	1.5	M1.0 V
J06474+054	...	...	4.0	4.0	4.0	4.0	4.0	4.0	4.0	M4.0 V
J06489+211	...	...	2.5	2.5	2.5	2.5	2.5	3.0	2.5	M2.5 V
J06509–091	k:	Simbad	3.5	3.5	3.5	3.5	3.5	3.0	3.5	M3.5 V
J06522+179	m:	Simbad	0.0	0.0	–0.5	–0.5	0.0	0.0	0.0	M0.0 V
J06522+627	...	...	3.5	4.0	3.5	3.5	3.5	3.5	3.5	M3.5 V
J06523–051S AB	M2.0 V	PMSU	2.0	2.0	2.0	2.0	2.0	2.0	2.5	M2.0 V
J06523–051N	K3 V	Simbad	–4.0	<–3.0	...	...	...	...	...	<K5 V
J06548+332	M3.0 V	PMSU	3.0	3.0	3.0	3.0	3.0	3.0	3.0	M3.0 V
J06565+440	m:	Simbad	4.5	4.5	4.0	4.0	4.5	4.5	4.5	M4.5 V
J07001–190	...	...	5.0	5.0	5.0	4.5	5.0	5.0	4.5	M5.0 V
J07009–023	...	...	3.0	3.0	3.0	3.0	3.0	3.0	3.0	M3.0 V
J07031+836	...	...	3.0	3.5	3.5	3.5	3.5	3.0	3.0	M3.5 V
J07051–101	...	...	5.0	5.0	5.0	4.5	4.5	4.5	4.5	M5.0 V
J07105–087	...	...	3.5	3.5	3.5	3.5	3.5	3.5	3.5	M3.5 V
J07105+283	K7 V	Ste86	0.0	0.0	0.0	0.0	0.0	0.0	0.0	M0.0 V
J07111–035	...	...	1.0	0.5	0.0	0.0	1.0	0.5	1.0	M0.5 V
J07111+434 AB	M6.0 V+M7.5	Sch05, Mon06	5.5	5.5	6.0	6.5	6.0	5.5	6.0	M5.5 V
J07172–050	M4.0 V	Riaz06	3.5	3.5	4.0	4.0	3.5	4.0	3.0	M3.5 V
J07182+137	...	...	3.5	3.5	3.5	3.5	4.0	3.5	3.5	M3.5 V
J07191+667	...	...	0.0	0.0	0.0	–0.5	0.0	0.0	0.0	M0.0 V
J07195+328	K7 V	PMSU	0.0	0.0	0.0	0.0	0.0	0.0	0.0	M0.0 V
J07219–222	...	...	3.5	3.5	3.5	3.5	4.0	3.5	3.5	M3.5 V
J07274+052	M3.5 V	PMSU	3.5	3.5	3.5	3.5	3.5	4.0	3.5	M3.5 V
J07310+460	M4.0 V	Riaz06	4.0	4.0	4.5	4.0	4.0	4.5	4.0	M4.0 V
J07319+362N	M3.5 V	PMSU	4.0	3.5	3.5	3.5	4.0	4.0	3.5	M3.5 V
J07319+362S AB	M2.5 V	PMSU	2.5	2.5	3.0	3.0	2.5	3.0	2.5	M2.5 V
J07321–088	...	...	–2.0	–2.0	...	...	...	...	...	K5 V
J07324–130	...	...	0.0	0.0	0.0	0.0	–0.5	0.0	–0.5	M0.0 V
J07359+785	M3.5 V	Reid04	3.0	3.0	3.5	3.5	3.0	3.5	3.0	M3.0 V
J07361–031	m:	Simbad	1.0	1.0	1.0	0.5	1.0	1.0	1.0	M1.0 V
J07365–006	...	...	3.5	3.5	3.5	3.5	3.5	3.5	3.5	M3.5 V
J07366+440	...	...	3.5	3.0	3.0	3.0	3.5	3.5	3.5	M3.5 V
J07420+142	M3 S	KMc89, SB06	...	...	...	...	...	...	...	M III
J07429–107	...	...	2.5	2.5	3.0	2.5	2.5	3.0	2.5	M2.5 V
J07467+574	...	...	5.0	5.0	4.5	4.5	4.5	5.0	4.5	M4.5 V
J07470+760	M4.0 V	Reid04	4.0	4.0	3.5	3.5	4.0	4.0	4.0	M4.0 V

Table B.3: Spectral types of observed stars (cont.).

Karmn	Sp. type	Ref.[a]	Sp. type		Sp. type					Sp. type
	biblio.		Best-fit	χ^2	TiO2	TiO5	PC1	VO-7912	Color-M	adopted
J07497–033	M4.0 V	Reid07	3.5	3.5	3.5	3.5	3.5	3.5	3.0	M3.5 V
J07498–032	...	...	3.5	3.5	4.0	4.0	3.0	4.0	3.0	M3.5 V
J07523+162	M7.0 V	Reid03	6.0	6.0	6.0	5.5	6.0	6.0	5.5	M6.0 V
J07545+085	...	...	2.5	2.5	2.5	2.5	2.5	2.5	3.0	M2.5 V
J07545–096	...	...	3.5	3.0	3.5	3.0	3.5	3.5	3.5	M3.5 V
J07558+833	M3.5 V	PMSU	5.0	5.0	4.0	3.5	5.5	4.5	5.0	M4.5: V
J07591+173	...	...	3.5	4.0	4.0	4.0	3.5	4.0	3.0	M4.0 V
J08025–130	...	...	2.5	2.5	3.0	2.5	3.0	3.0	3.0	M2.5 V
J08031+203 AB	M3.3 V	Riaz06	3.5	3.5	4.0	3.5	3.5	3.5	3.0	M3.5 V
J08069+422	M4.5 V	Reid04	4.0	4.5	4.0	4.0	4.5	4.5	4.0	M4.0 V
J08082+211N	K5 V	PMSU	–1.0	–1.0	–1.0	–1.0	–0.5	–0.5	–0.5	K7 V
J08082+211S AB	M2.5 V+M3.1	PMSU, Shk10	3.0	3.0	3.0	3.0	3.0	3.0	3.0	M3.0 V
J08104–111	...	...	0.5	1.0	2.0	2.0	0.5	1.5	0.0	M1.0 V
J08105–138 AB	M2.0 V	PMSU	2.5	2.5	2.5	2.5	2.5	2.0	2.5	M2.5 V
J08117+531	...	...	2.5	2.5	3.0	3.0	2.5	3.0	2.5	M2.5 V
J08143+630	...	...	1.5	1.5	1.5	1.5	1.5	1.0	1.5	M1.5 V
J08161+013	M2.0 V	PMSU	2.0	2.0	2.0	2.0	2.0	2.0	2.0	M2.0 V
J08283+553	...	...	2.5	2.5	3.0	3.0	3.0	3.0	2.5	M2.5 V
J08286+660	M0 Ve	App98	4.0	4.0	4.0	4.0	4.0	4.0	3.5	M4.0 V
J08298+267	M6.0 V	PMSU	6.5	6.5	6.5	6.0	6.0	6.5	7.0	M6.5 V
J08353+141	M4.5 V	Reid07	4.5	4.5	4.5	4.5	4.5	4.5	4.0	M4.5 V
J08375+035	...	...	4.0	4.5	4.0	4.0	4.0	4.0	4.0	M4.0 V
J08386–028	...	...	–2.0	–2.0	...	...	...	...	...	K5 V
J08394–028	...	...	0.5	0.5	1.0	1.0	0.5	1.0	0.5	M0.5 V
J08423–048	M2.5 V	Sch05	3.0	3.0	3.0	3.0	3.0	3.0	3.0	M3.0 V
J08449–066 AB	M3.0 V	Reid07	3.5	3.5	3.5	3.5	3.5	3.5	3.5	M3.5 V
J08526+283	M4.0 V	PMSU	4.5	4.5	4.0	4.0	4.5	4.5	4.5	M4.5 V
J08531–202	...	...	3.0	3.0	3.0	3.0	3.0	3.0	3.0	M3.0 V
J08563–044	k:	Simbad	1.0	1.0	1.0	1.0	1.0	1.0	1.5	M1.0 V
J08572+194	M4.0 V	Sch05	3.5	3.5	3.5	3.5	3.5	3.5	3.5	M3.5 V
J08590+364	k:	Simbad	0.5	0.5	0.5	0.5	0.5	0.5	0.5	M0.5 V
J08595+537	...	...	3.5	4.0	4.0	3.5	3.5	4.0	3.5	M3.5 V
J08599+042	...	...	1.0	1.0	0.5	1.0	1.0	0.5	1.0	M1.0 V
J09003+218	M6.5 V	Reid03	6.5	6.5	6.5	6.0	6.5	6.0	6.5	M6.5 V
J09008+237	...	...	2.5	2.5	3.0	3.0	3.0	3.0	2.5	M2.5 V
J09023+177	M3.5 V	Reid07	4.0	3.5	4.0	4.0	4.0	4.0	4.0	M4.0 V
J09028+060	...	...	1.5	1.5	1.5	1.5	1.5	1.0	1.5	M1.5 V

Table B.3: Spectral types of observed stars (cont.).

Karmn	Sp. type	Ref.[a]	Sp. type		Sp. type					Sp. type
	biblio.		Best-fit	χ^2	TiO2	TiO5	PC1	VO-7912	Color-M	adopted
J09040–159	M2.5 V	Riaz06	2.5	2.5	2.5	2.5	2.5	2.5	2.5	M2.5 V
J09045+164 AB	K5 V	Simbad	–4.0	<–3.0	...	...	...	...	...	<K5 V
J09058+555	...	...	3.5	3.5	3.5	3.5	3.5	3.5	3.0	M3.5 V
J09091+227	M3.0 V	Abe14	4.5	4.5	4.5	4.5	4.5	4.5	4.5	M4.5 V
J09115+126	...	...	2.5	2.5	2.5	2.5	2.5	2.5	2.5	M2.5 V
J09143+526	K7 V	Kir91	0.0	0.0	–0.5	–0.5	0.0	0.0	0.0	M0.0 V
J09144+526	M0 V	Kir91	0.0	0.0	–0.5	–0.5	0.0	0.0	0.0	M0.0 V
J09151+233	...	...	0.0	0.0	0.0	0.0	0.0	0.0	0.0	M0.0 V
J09156–105 AB	M5 V+M5	Sch05, Mon06	5.0	5.0	5.0	5.0	5.0	5.0	5.0	M5.0 V
J09201+037	...	...	3.5	3.5	3.5	3.5	3.5	3.5	3.5	M3.5 V
J09206–169	...	...	0.0	0.0	–0.5	–0.5	–0.5	0.0	0.0	M0.0 V
J09212+603	...	...	1.5	1.5	1.5	1.5	1.5	1.5	1.5	M1.5 V
J09218–023	...	...	2.5	2.0	2.5	2.5	2.0	2.0	2.5	M2.5 V
J09243+063	...	...	4.0	4.0	4.0	4.0	4.0	4.0	3.5	M4.0 V
J09248+306	...	...	3.5	3.5	3.5	3.5	3.5	3.5	3.5	M3.5 V
J09256+634 AB	...	...	4.0	4.5	4.5	4.5	4.5	4.5	4.5	M4.5 V
J09301–009	k:	Simbad	0.0	0.5	0.5	0.5	0.0	0.5	0.5	M0.5 V
J09308+024	...	...	4.0	4.0	4.0	4.0	4.0	4.0	4.0	M4.0 V
J09328+269	M5.5 V	PMSU	5.5	5.5	5.5	5.5	5.5	5.5	5.5	M5.5 V
J09351–103	m:	Simbad	–2.0	–2.0	...	...	...	...	...	K5 V
J09362+375	M0.5 V	Lep13	0.0	0.0	0.5	0.0	0.0	0.0	0.0	M0.0 V
J09394+146	...	...	3.5	3.5	3.5	3.0	3.0	3.5	3.5	M3.5 V
J09449–123	M5.0 V	Sch05	5.0	5.0	5.5	5.0	5.0	5.0	4.5	M5.0 V
J09488+156	M2.0 V	Shk09	3.0	3.0	3.0	3.0	2.5	3.0	3.0	M3.0 V
J09526–156	M4.0 V	Sch05	3.5	3.0	3.5	3.5	3.0	3.5	3.0	M3.5 V
J09538–073	M1Ve	Ste86	0.5	1.0	–0.5	0.0	0.5	0.5	0.0	M0.5 V
J09589+059	m4.5:	Law08	4.5	5.0	4.5	4.5	4.5	4.5	4.5	M4.5 V
J09597+721	...	...	3.5	3.5	3.5	3.5	3.5	3.5	3.5	M3.5 V
J10008+319	M6.5 V	Giz00	6.0	6.0	6.0	6.0	6.0	6.0	6.0	M6.0 V
J10020+697	M4.5 V	Reid04	4.0	4.5	4.0	4.0	4.0	4.5	4.0	M4.0 V
J10028+484	M5.0 V	Boc05	5.5	5.5	5.5	5.5	5.5	5.5	5.5	M5.5 V
J10063–064	...	...	4.0	4.5	4.5	4.5	5.0	4.0	4.5	M4.5 V
J10068–127	M4.5 V	Reid07	4.5	4.5	4.5	4.5	4.5	4.5	4.5	M4.5 V
J10098–007	K4 V	Ste86	–2.0	–2.0	...	...	...	...	...	K5 V
J10120–026 AB	M2.5 V	PMSU	2.5	2.5	2.5	2.5	2.5	2.5	2.5	M2.5 V
J10130+233	M4.0 V	Sch05	3.5	3.5	3.5	3.5	3.5	4.0	3.5	M3.5 V
J10148+213	M4.5 V	Sch05	4.5	4.5	4.5	4.5	4.5	4.5	4.5	M4.5 V

Table B.3: Spectral types of observed stars (cont.).

Karmn	Sp. type	Ref.[a]	Sp. type		Sp. type					Sp. type
	biblio.		Best-fit	χ^2	TiO2	TiO5	PC1	VO-7912	Color-M	adopted
J10155–164	...	...	4.0	3.5	4.0	4.0	4.0	4.0	3.5	M4.0 V
J10196+198 AB	M3.0 V	PMSU	3.0	3.0	3.5	3.0	3.0	3.0	3.0	M3.0 V
J10200+289	M3.0 V	Sch05	3.0	2.5	3.0	3.0	2.5	3.0	3.0	M3.0 V
J10238+438	M4.5 V	Reid04	5.0	5.0	5.0	5.0	5.0	5.0	5.0	M5.0 V
J10240+366	M3.0 V	Reid07	3.5	3.5	3.5	3.5	3.5	4.0	3.5	M3.5 V
J10278+028	k:	Simbad	3.5	3.5	3.5	3.5	4.0	3.5	3.5	M3.5 V
J10304+559	K7 V	Simbad	–1.0	–1.0	–1.5	–1.5	–1.0	–0.5	–1.0	K7 V
J10359+288	M2.5 V	Reid07	3.0	3.0	3.5	3.0	3.0	3.5	3.0	M3.0 V
J10368+509	M3.5 V	Reid04	4.5	4.5	4.5	4.5	4.5	4.5	4.5	M4.5 V
J10430–092 AB	M5–6 V	Gig98	5.5	5.5	5.0	5.5	5.5	5.0	5.5	M5.5 V
J10443+124	M4.0 V	Sch05	3.5	3.5	3.5	3.5	4.0	4.0	3.5	M3.5 V
J10482–113	M6.5 V	PMSU	6.5	6.5	7.0	7.0	6.5	7.0	7.0	M6.5 V
J10508+068	M4.0 V	PMSU	4.0	4.5	4.0	4.0	4.0	4.0	4.0	M4.0 V
J10546–073	M4.0 V	Sch05	4.0	4.0	3.5	4.0	4.0	4.0	4.0	M4.0 V
J10560+061	M5.5 III	KMc89, Gar89	...	...	...	...	...	...	...	M III
J10563+042	...	...	2.5	2.5	2.5	2.5	2.5	2.5	2.5	M2.5 V
J10564+070	M5.5 V	PMSU	6.0	6.0	6.0	6.0	6.0	6.0	6.0	M6.0 V
J10584–107	M5.0 V	Sch05	5.0	5.0	5.0	4.5	4.5	5.0	4.5	M5.0 V
J11018–024	M0 III	Gar89, SB06	...	...	...	...	...	...	...	M III
J11030+037	...	...	2.5	2.5	2.5	2.5	2.5	3.0	3.0	M2.5 V
J11033+359	M2.0 V	PMSU	1.5	1.5	1.5	2.0	2.0	1.5	2.0	M1.5 V
J11046–042S AB	M0 Vke	Gray03	0.0	0.5	0.5	0.0	0.5	0.5	0.5	M0.5 V
J11054+435	M0.5 V	PMSU	1.0	1.0	1.0	1.0	1.0	0.5	1.0	M1.0 V
J11055+435	M6.0 V	PMSU	6.0	6.0	6.5	6.5	5.5	5.5	5.5	M5.5 V
J11075+437	...	...	3.0	3.0	3.0	3.0	3.0	3.0	3.0	M3.0 V
J11151+734N	M2 V	Bid85	2.5	2.5	2.5	2.5	2.5	2.5	2.5	M2.5 V
J11151+734S	K3 V	Bid85	...	<–3.0	...	...	...	...	–2.5	<K5 V
J11201–104 AB	M2.0 V	Riaz06	2.0	2.0	2.0	2.0	2.0	1.5	1.0	M2.0 V
J11201+301	M0 III	MP50, JE12	...	...	...	...	...	...	...	M III
J11214–204S	M1.0 V	PMSU	2.5	2.5	2.5	2.5	3.0	3.0	3.0	M2.5 V
J11214–204N	K6 V	Gray06	–1.0	–1.0	–1.0	–1.0	–0.5	–0.5	–1.0	K7 V
J11218+181	K6.5 V	Simbad	0.0	0.0	0.5	0.5	0.0	0.5	0.5	M0.0 V
J11240+381	M4.5 V	Reid07	4.5	4.5	4.5	4.0	4.0	4.5	4.5	M4.5 V
J11306–080	M3 V	Gray06	3.0	3.5	3.0	3.5	3.5	3.0	3.5	M3.5 V
J11312+631	K5 V	PMSU	–1.0	–1.0	–1.0	–1.0	–0.5	–0.5	–0.5	K7 V
J11378+418	...	...	2.0	2.0	2.0	2.5	2.0	2.0	2.0	M2.0 V
J11403+095	...	...	1.5	1.5	1.5	1.5	1.0	1.5	1.0	M1.5 V

Table B.3: Spectral types of observed stars (cont.).

Karmn	Sp. type	Ref.[a]	Sp. type		Sp. type					Sp. type
	biblio.		Best-fit	χ^2	TiO2	TiO5	PC1	VO-7912	Color-M	adopted
J11421+267	M2.5 V	PMSU	2.5	2.5	2.5	2.5	2.5	2.5	2.5	M2.5 V
J11451+183	M4.0 V	Sch05	4.0	3.5	4.0	4.0	4.0	4.0	4.0	M4.0 V
J11458+065	M1 III	KMc89, Gar89	...	...	...	...	...	...	...	M III
J11472+770	...	...	0.0	–1.0	–0.5	–0.5	–1.0	–0.5	–1.0	K7 V
J11474+667	M4.0 V	Reid07	5.0	5.0	5.0	4.5	4.5	5.0	5.0	M5.0 V
J11485+076	M3.5 V	Shk09	3.5	4.0	4.0	3.5	3.5	4.0	3.5	M3.5 V
J11511+352	M1.0 V	PMSU	1.5	1.5	1.5	1.5	1.5	1.0	1.5	M1.5 V
J11522+100	M4.0 V	PMSU	4.0	4.0	4.0	4.0	4.5	4.0	4.0	M4.0 V
J11549–021	...	...	3.0	3.0	3.0	3.0	3.0	3.0	3.0	M3.0 V
J12025+084	sdM2.0	Giz97	1.5	1.5	1.5	2.0	1.5	1.5	1.5	M1.5 V
J12049+174	M2.5 V	Riaz06	3.5	3.5	3.5	3.0	3.0	3.5	3.0	M3.5 V
J12069+058	...	...	–2.0	–2.0	...	...	...	...	...	K5 V
J12088+217	M3.0 V	New14	0.5	0.5	0.5	0.5	0.5	0.5	0.5	M0.5 V
J12093+210	M8 V:e	Ste86	2.5	2.5	3.0	3.0	3.0	3.0	3.0	M2.5 V
J12104–131	M4.5 V	Riaz06	4.5	4.5	4.5	4.0	4.0	4.5	4.0	M4.5 V
J12124+121	...	...	2.0	2.0	2.0	2.0	2.0	2.0	2.0	M2.0 V
J12162+508	...	...	4.0	4.0	4.0	4.0	4.5	4.5	4.0	M4.0 V
J12228–040	M4.5 V	Sch05	4.5	4.5	4.5	4.5	4.5	5.0	4.5	M4.5 V
J12322+454	M1 III	JE12	...	...	...	...	...	...	...	M III
J12349+322	...	...	3.5	3.0	3.0	3.5	3.0	3.5	3.5	M3.5 V
J12364+352	M3.5 V	Reid04	4.5	4.5	4.0	4.0	4.5	4.5	4.5	M4.5 V
J12368–019	...	...	3.5	3.5	3.5	3.5	4.0	4.0	3.5	M3.5 V
J12372+358	...	...	1.5	1.5	2.0	2.0	1.5	1.5	1.5	M1.5 V
J12417+567	M3.0 V	Riaz06	3.5	3.5	3.5	3.5	3.0	3.5	3.5	M3.5 V
J12440–111	M4.5 V	Sch05	4.5	4.5	4.5	4.5	4.5	4.5	4.5	M4.5 V
J12456+271	M4 III	Jac84, Kir91	...	...	...	...	...	...	...	M III
J12470+466	M2.5 V	PMSU	2.5	2.5	2.5	2.5	3.0	2.5	3.0	M2.5 V
J12488+120	M4.0 V	Reid06	4.5	4.5	4.0	4.5	4.5	4.5	4.5	M4.5 V
J12533–053	M3.0 V	Sch05	2.5	3.0	3.0	3.5	3.0	3.0	2.5	M3.0 V
J12533+466	M3 III	JE12	...	...	...	...	...	...	...	M III
J12549–063	M4.0 V	PMSU	5.0	5.0	4.5	4.5	4.5	4.5	4.5	M4.5 V
J12593–001	M4.0 V	Sch05	4.0	4.0	3.5	3.5	4.0	4.0	3.5	M4.0 V
J13027+415	k:	Simbad	3.5	3.0	3.5	3.5	3.5	3.5	3.5	M3.5 V
J13088–015	M3.0 V	Sch05	3.0	3.0	3.5	3.0	3.0	3.0	3.0	M3.0 V
J13102+477	M4.5 V	Riaz06	5.0	5.0	5.0	5.0	5.0	5.0	4.5	M5.0 V
J13113+096	M0.0 V	New14	–1.0	–1.0	–0.5	0.0	–0.5	0.0	–0.5	M0.0 V
J13143+133 AB	M6–8 V	Sch14	6.0	6.0	6.0	6.0	6.0	6.5	6.0	M6.0 V

Table B.3: Spectral types of observed stars (cont.).

Karmn	Sp. type biblio.	Ref.[a]	Sp. type Best-fit	χ^2	Sp. type TiO2	TiO5	PC1	VO-7912	Color-M	Sp. type adopted
J13167–123	M3.0 V	Sch05	3.5	3.5	3.5	3.5	3.5	3.5	3.5	M3.5 V
J13168+170	M0.5 V	PMSU	0.5	0.5	0.5	0.5	0.5	0.5	0.5	M0.5 V
J13179+362	M1.0 V	PMSU	1.0	1.0	1.0	1.5	1.0	1.0	1.0	M1.0 V
J13182+733	...	...	3.5	3.5	3.5	4.0	3.5	4.0	3.5	M3.5 V
J13247–050	M4.0 V	Sch05	4.0	4.0	4.0	4.0	4.0	4.0	4.0	M4.0 V
J13251–114	...	...	3.0	2.5	3.0	3.0	3.0	3.0	3.0	M3.0 V
J13253+426	K5 V	Ste86	–1.0	–1.0	–1.5	–1.5	–1.0	–1.0	–1.0	K7 V
J13260+275	...	...	3.0	3.0	3.0	3.0	2.5	3.5	3.0	M3.0 V
J13294–143	M3.0 V	Reid07	3.5	3.5	4.0	3.5	3.5	4.0	3.0	M3.5 V
J13312+589	...	...	2.5	2.5	2.5	2.0	2.5	2.5	2.5	M2.5 V
J13314–079	K7 V	Bid85	0.0	0.0	0.0	0.0	0.0	0.0	–0.5	M0.0 V
J13321–112	...	...	0.0	0.0	–0.5	–0.5	–0.5	–0.5	–0.5	M0.0 V
J13326+309	M4.5 V	Sch05	4.5	4.5	4.5	4.5	4.0	4.5	4.0	M4.5 V
J13335+704	M2.5 V	Reid07	3.5	3.5	3.5	3.5	4.0	3.5	3.5	M3.5 V
J13386–115	...	...	4.5	4.5	4.5	4.5	4.0	4.5	4.0	M4.5 V
J13394+461 AB	M1.0 V	PMSU	1.0	1.5	1.5	1.5	1.5	1.5	1.5	M1.5 V
J13413–091	...	...	2.5	2.5	3.0	3.0	3.0	3.0	3.0	M2.5 V
J13414+489	M3.5 V	Lep13	3.5	3.5	3.0	3.0	3.5	3.5	3.5	M3.5 V
J13474+063	M0 V	Bid85	–1.0	–1.0	–1.5	–1.5	–1.0	–1.0	–1.0	K7 V
J13503–216	M3 V:	Bid85	4.0	3.5	3.5	3.5	4.0	3.5	3.5	M3.5 V
J13537+521 AB	M3.5 V	Reid07	3.5	3.0	3.5	3.5	3.5	3.5	3.0	M3.5 V
J13551–079	M0 V	Ste86	0.0	0.0	0.0	0.0	–0.5	–0.5	–0.5	M0.0 V
J13555–073	k:	Simbad	3.0	3.0	3.0	3.0	3.0	2.5	3.0	M3.0 V
J13582–120	M4.0 V	Sch05	4.5	4.5	4.5	4.5	4.5	4.5	4.5	M4.5 V
J13583–132	M4 V	Sch05	4.0	4.0	4.0	4.0	4.0	4.0	4.0	M4.0 V
J13587+465	M2 III	MP50, JE12	...	...	...	...	...	...	...	M III
J14019+432	...	...	2.5	2.0	3.0	3.0	2.5	2.5	2.5	M2.5 V
J14102–180	...	...	2.5	2.5	2.5	2.5	3.0	2.5	3.0	M2.5 V
J14159–110	...	...	1.5	1.5	2.0	1.5	1.5	1.5	1.5	M1.5 V
J14171+088	...	...	4.5	4.5	4.5	4.5	4.5	4.5	4.0	M4.5 V
J14175+025	...	...	3.0	3.0	3.0	3.0	3.0	3.0	3.0	M3.0 V
J14194+029	m4.5:	Law08	5.0	5.0	5.0	4.5	5.0	5.0	4.5	M5.0 V
J14195–051	M5 V	New14	4.0	4.0	4.0	4.0	4.0	4.0	4.0	M4.0 V
J14215–079	...	...	4.0	4.0	3.5	3.5	4.0	4.0	4.0	M4.0 V
J14227+164	...	...	5.0	5.0	5.0	4.5	4.5	4.5	4.5	M5.0 V
J14244+602	...	...	2.0	2.0	2.0	2.0	2.0	1.5	2.0	M2.0 V
J14251+518	M2.5 V	PMSU	2.5	2.0	2.5	2.5	2.5	2.0	2.5	M2.5 V

Table B.3: Spectral types of observed stars (cont.).

Karmn	Sp. type	Ref.[a]	Sp. type		Sp. type					Sp. type
	biblio.		Best-fit	χ^2	TiO2	TiO5	PC1	VO-7912	Color-M	adopted
J14255–118	...	...	4.0	4.0	4.0	3.5	4.0	4.0	4.0	M4.0 V
J14312+754	M4.0 V	Reid07	4.0	4.0	4.0	4.0	3.5	4.0	3.5	M4.0 V
J14336+093	M3 V:	Bid85	3.5	3.0	3.0	3.5	3.5	3.5	3.0	M3.5 V
J14415+136	M3 V:	Bid85	1.0	1.0	1.0	1.0	1.5	1.0	1.0	M1.0 V
J14446–222	M4.5 V	Reid04	4.5	4.5	4.0	4.0	4.5	4.5	4.0	M4.5 V
J14472+570	...	...	3.5	4.0	4.0	4.0	3.5	4.0	3.5	M4.0 V
J14480+384	K5 V	PMSU	–1.0	–1.0	–1.0	–1.0	–1.0	–0.5	–1.0	K7 V
J14485+101	...	...	3.5	3.5	3.5	3.5	4.0	3.5	3.5	M3.5 V
J14492+498	...	...	1.5	1.5	1.5	1.5	1.5	2.0	1.5	M1.5 V
J14501+323	M3.0 V	Reid04	3.5	3.0	3.5	3.5	3.5	3.5	3.5	M3.5 V
J14544+161 ABC	M2.0 V+M8.5+M9.0	PMSU, Simbad	0.5	1.0	2.0	2.0	1.0	1.0	0.5	M1.0: V
J14595+454	M0 V	Bid85	–1.0	–1.0	–1.5	–1.5	–1.0	–1.0	–1.0	K7 V
J15079+762	...	...	4.5	4.5	5.0	4.5	4.0	4.5	4.0	M4.5 V
J15081+623	...	...	4.0	4.0	3.5	3.5	4.0	4.0	4.0	M4.0 V
J15118+395	...	...	2.5	2.5	2.5	2.5	2.5	2.5	2.5	M2.5 V
J15131+181	...	...	2.0	1.5	2.0	2.0	2.0	2.0	2.0	M2.0 V
J15142–099	...	...	4.0	4.0	4.0	4.0	4.0	4.0	3.5	M4.0 V
J15147+645	m:	Simbad	3.5	3.5	3.5	3.5	3.0	3.0	3.5	M3.5 V
J15151+333	M2.5 V	Reid04	2.0	2.0	2.0	2.5	2.0	2.0	2.0	M2.0 V
J15157–074	M2–3 V	Gig98	4.0	4.0	4.0	4.0	3.5	4.0	3.5	M4.0 V
J15164+167	...	...	–2.0	–2.0	...	...	...	...	...	K5 V
J15197+046	...	...	4.0	4.0	4.0	3.5	4.0	4.0	4.0	M4.0 V
J15204+001	K5 V	Bid85	0.0	0.0	–1.0	–0.5	–1.0	–0.5	–1.0	M0.0 V
J15210+255	K8 V	Ste86	–1.0	–1.0	–1.0	–1.0	–1.0	–0.5	–1.0	K7 V
J15238+584	M3.5 V	Sch05	4.0	4.0	4.0	4.0	3.5	4.0	3.5	M4.0 V
J15277–090	M4.5 V	PMSU	4.5	4.5	4.5	4.5	4.5	4.5	4.5	M4.5 V
J15290+467 AB	M4.5 V+m5.0:	Reid07, Jan12	4.5	4.5	4.5	4.5	4.5	4.5	4.5	M4.5 V
J15291+574	...	...	1.0	1.0	0.5	0.5	1.0	0.5	1.0	M1.0 V
J15305+094	...	...	5.5	5.5	5.5	5.5	5.5	5.5	5.5	M5.5 V
J15340+513	...	...	4.5	4.5	4.0	4.5	4.5	4.5	4.5	M4.5 V
J15386+371	M:	SP88	3.5	3.5	3.5	3.5	3.5	3.5	3.5	M3.5 V
J15430–130	...	...	1.5	1.5	1.5	1.5	1.5	1.5	1.5	M1.5 V
J15474+451	M4.0 V	Sch05	4.0	4.0	4.0	4.0	4.0	4.0	4.0	M4.0 V
J15476+226	M3.5 V	Abe14	4.5	4.5	4.5	4.5	4.5	4.5	4.0	M4.5 V
J15480+043	...	...	2.5	2.5	3.0	2.5	3.0	2.5	2.5	M2.5 V
J15481+015	M3.0 V	Eis07	2.5	2.5	3.0	2.5	3.0	3.0	3.0	M2.5 V
J15499+796	m4.5:	Law08	5.0	5.0	5.0	5.0	5.0	5.0	4.5	M5.0 V

Table B.3: Spectral types of observed stars (cont.).

Karmn	Sp. type	Ref.[a]	Sp. type		Sp. type					Sp. type
	biblio.		Best-fit	χ^2	TiO2	TiO5	PC1	VO-7912	Color-M	adopted
J15552–101	...	...	2.5	2.5	3.0	3.0	2.5	2.5	2.0	M2.5 V
J15557–103	M3.5 V	Riaz06	3.5	3.5	4.0	3.5	3.5	4.0	3.0	M3.5 V
J15558–118	M3.0 V	Sch05	3.0	3.0	3.0	3.0	3.0	3.0	3.0	M3.0 V
J15569+376	M2.5 V	Riaz06	2.5	2.0	3.0	2.5	2.5	3.0	2.0	M2.5 V
J15578+090	...	...	4.0	4.0	4.0	4.0	4.5	4.0	4.0	M4.0 V
J16023+036	...	...	1.5	1.5	1.5	1.5	1.5	2.0	1.5	M1.5 V
J16042+235	...	...	5.0	5.0	5.0	5.0	5.0	5.0	5.0	M5.0 V
J16048+391	M4.0 V	PMSU	4.0	4.0	4.0	4.0	4.0	4.0	4.0	M4.0 V
J16120+033N	...	...	3.5	3.5	4.0	4.0	3.5	4.0	3.5	M3.5 V
J16139+337 AB	M2.5 V	PMSU	2.5	2.5	2.5	2.5	2.5	2.5	2.5	M2.5 V
J16148+606 AB	M3.5 V	Reid04	3.0	3.0	3.0	3.0	2.5	3.0	2.5	M3.0 V
J16157+586	M5.0 V	Sch05	5.0	5.0	5.0	4.5	5.0	5.0	4.5	M5.0 V
J16167+672S	M1.0 V	PMSU	0.0	0.0	0.0	0.0	0.0	0.0	0.0	M0.0 V
J16183+757	M4.0 V	PMSU	4.0	4.0	4.0	4.0	4.0	4.0	4.0	M4.0 V
J16243+199	...	...	3.0	3.0	3.5	3.0	3.0	3.0	2.5	M3.0 V
J16254+543	M2.0 V	PMSU	1.5	1.5	2.0	1.5	1.5	1.5	1.5	M1.5 V
J16269+149	...	...	4.0	4.0	4.5	4.0	4.0	4.5	3.5	M4.0 V
J16276–035 AB	K4 V	Ste86	–2.0	–2.0	...	...	...	...	...	K5 V
J16299+048	...	...	3.0	3.0	3.0	3.0	3.0	3.5	3.0	M3.0 V
J16314+471	...	...	3.5	3.5	4.0	4.0	3.5	4.0	3.0	M3.5 V
J16330+031	...	...	3.0	3.0	3.0	3.0	3.5	3.0	3.0	M3.0 V
J16354–039	m:	Simbad	0.0	0.0	–1.5	–1.5	0.0	–0.5	0.0	sdM0:
J16365+287	...	...	3.5	3.5	3.5	3.5	4.0	3.5	3.5	M3.5 V
J16459+609	...	...	3.5	3.5	3.5	3.5	3.5	3.5	3.0	M3.5 V
J16465+345	M6.5 V	Reid03	6.0	6.0	6.0	6.5	6.0	6.0	6.0	M6.0 V
J16480+453	M4.0 V	Riaz06	4.0	4.0	4.5	4.0	4.0	4.5	3.5	M4.0 V
J16528+610	M6 V	Simbad	4.5	4.5	4.5	4.5	4.5	4.5	4.5	M4.5 V
J16536+560	...	...	3.5	3.0	4.0	4.0	3.5	3.5	3.0	M3.5 V
J16543+256	...	...	2.5	2.5	3.0	3.5	3.0	3.0	3.0	M3.0 V
J16555–083	M7.0 V	PMSU	7.0	6.5	7.0	7.0	7.0	7.0	7.0	M7.0 V
J17011+555	...	...	2.5	2.5	2.5	2.5	2.5	2.5	2.5	M2.5 V
J17017+741	...	...	3.5	3.5	3.5	3.5	3.5	3.5	3.5	M3.5 V
J17052–050	M2.0 V	PMSU	1.5	1.5	2.0	2.0	1.5	1.5	1.5	M1.5 V
J17062+646	M2.5 V	GR97	3.0	3.0	3.0	3.0	2.5	2.5	2.5	M3.0 V
J17094+391	m:	Simbad	3.0	3.0	3.0	3.0	2.5	3.0	2.5	M3.0 V
J17126–099	M2: III	JE12	...	...	...	...	...	...	...	M III
J17140+176	...	...	2.5	2.5	2.5	3.0	2.5	2.5	2.5	M2.5 V

Table B.3: Spectral types of observed stars (cont.).

Karmn	Sp. type biblio.	Ref.[a]	Sp. type Best-fit	χ^2	Sp. type TiO2	TiO5	PC1	VO-7912	Color-M	Sp. type adopted
J17154+308	M2.5 V	Reid04	2.5	2.5	2.5	2.5	2.5	2.5	2.5	M2.5 V
J17163–053	...	...	4.0	4.5	4.0	4.5	4.5	4.0	4.0	M4.0 V
J17167+115	...	...	4.0	4.0	4.0	4.0	4.0	4.0	4.0	M4.0 V
J17176+524	M4.0 V	Sch05	3.5	3.5	3.5	3.5	3.5	4.0	3.5	M3.5 V
J17198+265	M4.5 V	PMSU	4.5	4.5	5.0	4.5	4.5	5.0	4.0	M4.5 V
J17199+265	M3.5 V	PMSU	3.5	3.5	3.5	3.5	3.5	3.5	3.5	M3.5 V
J17199+242	...	...	4.0	4.5	4.5	4.0	4.5	4.5	4.0	M4.5 V
J17216–171	M2 III	JE12	...	...	...	...	...	...	...	M III
J17239+136	M3.5 V	Reid07	4.0	4.0	4.0	3.5	4.0	4.0	3.5	M4.0 V
J17246+617	...	...	3.0	3.0	3.5	3.0	3.5	3.0	3.0	M3.0 V
J17265–227	...	...	2.5	2.5	3.0	3.0	2.0	2.5	2.0	M2.5 V
J17267–050	...	...	2.5	2.0	2.5	2.5	2.5	2.5	2.5	M2.5 V
J17270+422	...	...	–2.0	–2.0	...	...	...	...	...	K5 V
J17281–017	...	...	4.0	4.0	4.0	4.0	4.0	4.5	4.0	M4.0 V
J17299–209	M3.5 V	Reid04	3.5	3.0	3.0	3.5	3.0	3.5	3.0	M3.0 V
J17301+546	...	...	3.5	3.5	3.5	3.5	3.5	3.5	3.5	M3.5 V
J17304+337	M3.0 V	Reid07	3.5	3.0	3.5	3.5	3.0	3.5	3.0	M3.5 V
J17364+683	M3.0 V	PMSU	3.0	3.5	3.0	3.5	3.0	3.0	3.0	M3.0 V
J17412+724	...	...	4.0	4.0	4.0	4.0	4.0	4.0	4.0	M4.0 V
J17426+756	M4.5 V	GR97	4.5	4.5	4.0	4.5	4.5	4.5	4.0	M4.5 V
J17428+167	...	...	1.5	1.5	2.0	1.5	1.5	1.5	1.5	M1.5 V
J17464+277 AB	M3.5 V	PMSU	3.5	3.5	3.5	3.5	3.5	3.5	3.5	M3.5 V
J17477+277	...	...	1.5	1.5	1.5	1.5	1.5	1.0	1.5	M1.5 V
J17520+566	M3.5 V	Riaz06	3.5	3.5	4.0	3.5	4.0	3.5	3.0	M3.5 V
J17559+294	...	...	3.5	3.5	4.0	3.5	3.5	4.0	3.5	M3.5 V
J17578+046	M4.0 V	PMSU	3.5	3.5	3.5	4.0	3.5	3.5	3.5	M3.5 V
J17578+465	M3.0 V	PMSU	2.5	2.5	3.0	3.0	3.0	3.0	3.0	M2.5 V
J18006+685	...	...	–1.0	0.0	–1.0	–1.0	–0.5	0.0	–0.5	K7 V
J18007+295	M2.0 V	Jah08	2.5	2.5	2.0	2.0	2.0	2.0	2.5	M2.0 V
J18019+001	...	...	3.5	4.0	3.5	3.5	3.5	4.0	3.5	M3.5 V
J18022+642	M5.0 V	Riaz06	5.0	5.0	5.0	4.5	4.5	5.0	4.5	M5.0 V
J18028–030	M3.0 V	RS14	3.5	3.5	3.5	3.5	4.0	4.0	3.5	M3.5 V
J18036–189	m:	Simbad	5.0	5.0	5.0	4.5	5.0	5.0	4.5	M5.0 V
J18041+838	M4.5 V	RS14	3.5	4.0	3.5	3.5	4.0	4.0	3.5	M3.5 V
J18046+139	M2.5 V	Reid07	2.5	2.5	2.5	2.5	2.5	3.0	2.5	M2.5 V
J18054+015	M7.0 V	RS14	3.5	3.0	3.5	3.5	3.5	3.5	3.5	M3.5 V
J18057–143	...	...	5.5	5.5	5.5	5.5	5.5	5.5	5.5	M5.5 V

Table B.3: Spectral types of observed stars (cont.).

Karmn	Sp. type	Ref.[a]	Sp. type		Sp. type					Sp. type
	biblio.		Best-fit	χ^2	TiO2	TiO5	PC1	VO-7912	Color-M	adopted
J18068+177	M4.0 V	Reid04	4.0	4.0	4.0	4.0	4.0	4.0	3.5	M4.0 V
J18090+241	...	...	1.0	1.0	1.0	1.0	1.5	1.0	1.5	M1.0 V
J18112–010	M3.5 V	Riaz06	3.5	3.5	3.5	3.5	3.5	4.0	3.0	M3.5 V
J18130+414	...	...	3.5	3.5	3.5	3.5	3.5	3.5	3.5	M3.5 V
J18131+260 AB	M4.0 V+M3.8:	PMSU, Shk09	4.0	4.0	4.5	4.0	4.0	4.0	3.5	M4.0 V
J18135+055	...	...	4.0	4.0	3.5	3.5	4.0	3.5	4.0	M4.0 V
J18149+196	M4.0 V	RS14	2.0	2.0	2.0	2.0	1.5	2.0	1.5	M2.0 V
J18162+686	m:	Simbad	1.5	1.5	2.0	1.5	1.5	1.5	1.0	M1.5 V
J18224+620	M4.5 V	PMSU	4.0	4.0	4.0	4.0	4.5	4.5	4.5	M4.0 V
J18253+186	...	...	3.5	3.5	3.5	3.5	3.5	3.5	3.0	M3.5 V
J18306–039	...	...	4.5	5.0	4.5	4.5	5.0	4.5	4.5	M4.5 V
J18313+649	M4.5 V	RS14	3.5	3.5	4.0	3.5	3.0	3.5	3.0	M3.5 V
J18338+194	M3.0 V	RS14	3.0	3.0	2.5	2.5	3.0	3.0	3.0	M3.0 V
J18353+457	M0.0 V	PMSU	0.5	0.5	0.5	0.5	0.0	0.0	0.0	M0.5 V
J18354+457	M3.5 V	PMSU	2.5	2.5	3.0	3.0	3.0	3.5	3.0	M2.5 V
J18400+726	M6.5 V	Reid04	7.0	6.0	6.5	6.5	6.5	7.0	6.5	M6.5 V
J18409+315	M1.5 V	Lep13	1.0	1.0	1.0	1.0	1.0	0.5	1.0	M1.0 V
J18423–013	M2 III:wk	JE12	...	...	...	...	...	...	...	M III
J18427+596N	M3.0 V	PMSU	3.0	3.0	3.0	3.0	3.0	3.0	3.0	M3.0 V
J18427+596S	M3.5 V	PMSU	3.5	3.5	3.5	3.5	3.0	3.5	3.5	M3.5 V
J18453+188	...	...	4.0	4.0	4.0	4.0	4.0	4.0	3.5	M4.0 V
J18467+007	...	...	4.0	4.0	4.5	4.0	4.0	4.0	3.5	M4.0 V
J18482+076	M5.0 V	Lep13	5.0	5.5	5.0	5.0	5.0	5.0	5.0	M5.0 V
J18491–032	...	...	4.5	4.5	4.5	4.5	4.5	4.5	4.5	M4.5 V
J18499+186	M4.5 V	Reid04	4.5	4.5	4.0	4.0	4.5	4.5	4.5	M4.5 V
J18542+109	...	...	4.0	4.0	4.0	4.0	4.0	4.0	4.0	M4.0 V
J18550+429	M4.0 V	Riaz06	4.0	4.0	4.5	4.0	4.0	4.5	3.5	M4.0 V
J18570+473	M2.5 V	RS14	2.5	2.5	2.5	3.0	2.5	2.5	2.5	M2.5 V
J19052+387	M3.5 V	Reid07	3.5	3.5	3.5	3.5	4.0	3.5	3.5	M3.5 V
J19060–074	M5.5 V	RS14	2.5	2.5	2.5	2.5	2.5	2.5	2.5	M2.5 V
J19070+208	M2.0 V	PMSU	2.0	2.0	2.0	2.0	1.5	1.5	2.0	M2.0 V
J19072+442	M4.5 V	Reid04	4.5	4.5	4.5	4.5	4.5	4.5	4.5	M4.5 V
J19105–075	...	...	3.5	3.0	3.5	3.5	3.5	3.5	3.0	M3.5 V
J19164+842	...	...	5.0	5.0	4.5	5.0	5.0	5.0	4.5	M5.0 V
J19168+003	...	...	3.5	3.5	4.0	3.5	3.5	3.5	3.0	M3.5 V
J19169+051N	M2.5 V	PMSU	2.5	2.0	2.5	2.5	2.5	2.5	2.5	M2.5 V
J19169+051S	M8.0 V	PMSU	8.0	>6.0	...	...	8.0	...	7.5	M8.0 V

Table B.3: Spectral types of observed stars (cont.).

Karmn	Sp. type	Ref.[a]	Sp. type		Sp. type					Sp. type
	biblio.		Best-fit	χ^2	TiO2	TiO5	PC1	VO-7912	Color-M	adopted
J19243+426	M3.0 V	RS14	3.5	4.0	3.5	3.5	4.0	4.0	3.5	M3.5 V
J19260+244	M4.5 V	Reid04	4.5	4.5	4.5	4.0	4.5	4.5	4.0	M4.5 V
J19271+770	M4.0 V	RS14	2.5	2.5	3.0	3.0	2.0	2.5	2.0	M2.5 V
J19282–001	...	...	5.0	5.0	5.0	5.0	5.5	5.0	5.0	M5.0 V
J19312+361	M4.5 V	Cab10	4.5	4.5	4.5	4.5	4.5	5.0	4.0	M4.5 V
J19316–069	...	...	2.5	2.5	3.0	3.0	2.5	3.0	2.5	M2.5 V
J19327–068	...	...	3.5	3.5	3.5	3.5	4.0	4.0	3.5	M3.5 V
J19346+045	K5 V	PMSU	1.5	1.5	–1.5	–1.0	1.5	0.0	1.5	sdM1:
J19390+338	...	...	3.5	3.5	4.0	4.0	4.0	4.0	3.5	M3.5 V
J19393+148	...	...	3.0	3.0	3.0	3.0	3.0	3.0	3.0	M3.0 V
J19421+656	M4.0 V	RS14	3.0	3.0	3.5	3.0	3.5	3.0	3.0	M3.0 V
J19430+102	M3.0 V	RS14	2.0	2.0	2.5	2.0	2.0	2.5	2.0	M2.0 V
J19439–057	M4.0 V	Riaz06	3.5	3.5	4.0	4.0	3.5	4.0	3.5	M3.5 V
J19452+407	...	...	0.5	0.5	0.0	0.0	0.5	0.5	0.5	M0.5 V
J19519+141	M1.0 V	RS14	0.5	0.5	1.0	0.5	0.5	0.5	1.0	M0.5 V
J19524+603	...	...	3.0	3.0	3.0	3.0	3.0	3.5	3.0	M3.0 V
J19539+444W AB	M5.5 V	PMSU	5.5	5.5	5.5	5.5	5.0	5.5	5.5	M5.5 V
J19539+444E	M5.5 V	PMSU	5.5	5.5	5.5	5.5	5.5	5.5	5.5	M5.5 V
J19547+844	...	...	4.0	4.0	4.0	4.0	4.0	4.5	3.5	M4.0 V
J19564+591	M3.5 V	PMSU	3.5	3.0	3.5	3.5	3.5	3.5	3.0	M3.5 V
J19565+591	M0:p V	PMSU	–1.0	–1.0	0.0	–0.5	–0.5	0.0	–0.5	K7 V
J19578–108	M4.0 V	Riaz06	4.5	4.5	4.5	4.0	4.5	4.5	4.0	M4.5 V
J20021+130 AB	...	...	3.5	3.5	3.5	3.5	3.5	3.5	3.5	M3.5 V
J20033+672	M3.0 V	RS14	3.0	2.5	3.0	3.0	3.0	2.5	3.0	M3.0 V
J20034+298	M4.5 V	PMSU	4.5	4.5	4.5	4.5	4.5	4.5	4.5	M4.5 V
J20047+512	M3.5 V	Bid85	3.5	3.0	3.0	3.5	3.0	3.5	3.0	M3.0 V
J20065+159	...	...	2.0	2.0	2.0	2.0	2.0	2.0	2.0	M2.0 V
J20077+189	M3: V	Bid85	3.5	3.5	4.0	4.0	4.0	4.0	3.5	M3.5 V
J20093–012	M5.0 V	Riaz06	5.0	5.0	5.0	5.0	5.0	5.0	4.5	M5.0 V
J20108+772	K5 V	PMSU	–1.0	–1.0	–0.5	–1.0	–1.0	–0.5	–1.5	K7 V
J20112+161	M4.0 V	PMSU	4.0	4.0	4.0	4.0	4.0	4.5	4.0	M4.0 V
J20123–126	...	...	–4.0	<–3.0	...	...	...	...	...	<K5 V
J20177+059	M3.0 V	RS14	2.5	2.5	3.0	3.0	3.0	2.5	2.5	M2.5 V
J20182–202	M2.5 V	Reid07	2.5	2.5	3.0	3.0	3.0	2.5	2.5	M2.5 V
J20216–199	...	...	2.0	1.5	2.0	2.0	2.0	1.5	2.0	M2.0 V
J20254–198	...	...	4.5	5.0	5.0	5.0	5.0	5.0	4.5	M5.0 V
J20283+617	...	...	2.5	2.5	3.0	2.5	2.5	2.5	2.5	M2.5 V

Table B.3: Spectral types of observed stars (cont.).

Karmn	Sp. type biblio.	Ref.[a]	Sp. type Best-fit	χ^2	Sp. type TiO2	TiO5	PC1	VO-7912	Color-M	Sp. type adopted
J20300+003 AB	...	...	4.0	4.5	4.5	4.5	4.0	4.5	4.0	M4.5 V
J20332+283	...	...	4.0	4.0	4.0	4.0	4.5	4.5	4.0	M4.0 V
J20336+365	M3.5 V	Reid04	3.5	4.0	3.5	3.5	3.5	4.0	3.5	M3.5 V
J20382+231	M4.5 V	RS14	2.0	2.0	2.5	2.0	2.0	2.0	2.0	M2.0 V
J20405+154	M4.5 V	PMSU	4.5	4.5	4.5	4.5	4.5	4.5	4.5	M4.5 V
J20407+199 AB	M2.5 V	PMSU	2.5	2.5	2.5	2.5	2.5	2.5	2.5	M2.5 V
J20439+231	M3.5 V	RS14	3.5	3.0	3.5	3.5	3.5	3.5	3.0	M3.5 V
J20467–118	M4.0 V	Sch05	4.0	4.0	4.5	4.0	4.0	4.5	3.5	M4.0 V
J20510+399	M3.0 V	RS14	3.0	3.0	3.0	3.0	3.0	3.0	3.0	M3.0 V
J20540+603	...	...	2.5	2.5	2.5	2.5	2.5	2.5	2.5	M2.5 V
J20581+401 AB	M1 V	Lee84	–1.0	–1.0	–0.5	–0.5	–0.5	–0.5	–0.5	K7 V
J20583+425	M3.0 V	RS14	2.5	2.5	3.0	3.0	3.0	3.0	3.0	M2.5 V
J20593+530 AB	M3.5 Ve	Mot97	3.5	4.0	4.0	3.5	3.5	4.0	3.5	M3.5 V
J21009+510	M2.0 Ve	Mot97	2.5	2.5	3.0	3.0	2.5	3.0	2.5	M2.5 V
J21019–063	M3.0 V	PMSU	2.5	2.5	2.5	2.5	2.5	2.5	2.5	M2.5 V
J21027+349	M4.5 V	Reid04	4.5	4.5	5.0	4.5	4.5	4.5	4.0	M4.5 V
J21053+208	M2.5 V	RS14	2.5	2.5	3.0	3.0	2.5	2.5	3.0	M2.5 V
J21057+502E	...	...	3.5	3.5	3.5	3.5	4.0	4.0	3.5	M3.5 V
J21057+502W	...	...	4.0	3.5	4.0	4.0	4.0	4.0	4.0	M4.0 V
J21068+387	K5 V	Hen94	–2.0	–2.0	...	...	...	...	...	K5 V
J21069+387	K7 V	Hen94	0.5	0.5	–1.5	–1.0	0.5	–0.5	0.5	M0.5: V
J21074+198	...	...	0.5	1.0	2.0	2.0	0.5	1.0	0.5	M1.0 V
J21074+468	...	...	2.0	2.0	2.5	2.5	2.5	2.5	2.0	M2.0 V
J21109+469	M2.5 V	Reid04	3.5	3.0	3.5	3.5	3.5	3.5	3.0	M3.5 V
J21114+658	M3.0 V	RS14	2.0	2.0	2.0	2.0	2.0	2.5	2.0	M2.0 V
J21127–073	...	...	3.0	3.5	3.5	3.5	3.5	3.5	3.0	M3.5 V
J21147+160	M3.5 V	RS14	3.5	3.5	4.0	3.5	4.0	4.0	3.5	M3.5 V
J21245+400	M6.5 V	Lep03	5.5	5.5	5.0	5.5	5.5	5.0	5.5	M5.5 V
J21376+016	M4.5 V	Lep13	4.5	4.5	4.5	4.5	4.5	4.5	4.0	M4.5 V
J21414+207	M4.5 V	RS14	3.0	3.0	3.5	3.0	3.0	3.5	3.0	M3.0 V
J21466+668	M4.0 V	Lep13	4.0	4.0	4.0	4.0	4.0	4.0	4.0	M4.0 V
J21467–212	...	...	4.0	4.0	4.0	4.0	4.0	4.0	3.5	M4.0 V
J21472–047	M3.0 V	Lam14	4.0	4.0	4.5	4.5	4.5	4.5	4.0	M4.5 V
J21554+596 AB	M4.0 Ve	Mot98	3.5	4.0	4.0	4.0	3.5	4.0	3.5	M4.0 V
J22021+014	M0.0 V	PMSU	0.5	0.5	0.5	0.5	0.5	0.5	0.5	M0.5 V
J22035+036 AB	...	...	4.0	4.5	4.5	4.0	4.0	4.5	4.0	M4.0 V
J22088+117	...	...	5.0	5.0	4.5	4.5	5.0	4.5	4.5	M4.5 V

Table B.3: Spectral types of observed stars (cont.).

Karmn	Sp. type	Ref.[a]	Sp. type		Sp. type					Sp. type
	biblio.		Best-fit	χ^2	TiO2	TiO5	PC1	VO-7912	Color-M	adopted
J22089–177	M2.5 V	Boc05	2.5	2.5	2.5	2.5	2.5	2.5	2.5	M2.5 V
J22095+118	...	...	3.0	3.0	3.0	3.0	3.0	3.0	3.0	M3.0 V
J22114+409	M5.5 V	Abe14	5.5	5.5	5.5	5.5	5.5	5.0	5.5	M5.5 V
J22160+546	M4.0 V	PMSU	4.0	4.0	4.0	4.0	4.0	4.0	4.0	M4.0 V
J22202+067	M3 V:	Bid85	3.0	3.0	2.5	3.0	2.5	2.5	2.5	M2.5 V
J22234+324 AB	M3.0 V	PMSU	3.0	2.5	3.0	3.0	3.0	3.0	2.5	M3.0 V
J22264+583	...	...	3.0	3.5	3.0	3.0	3.5	3.0	3.0	M3.0 V
J22300+488 AB	...	...	5.0	5.0	4.0	3.5	4.5	4.0	4.5	M4.5 V
J22386+567	M4 III	Gar89, Kir91	...	...	...	...	...	...	...	M III
J22387+252	M3.5 V	Reid04	3.5	3.5	3.0	3.0	3.5	3.5	3.5	M3.5 V
J22396–125	M3.0 V	PMSU	3.0	3.0	3.5	3.5	3.0	3.0	3.0	M3.0 V
J22415+260	M3.0 V	Riaz06	3.5	3.5	3.5	3.0	3.5	3.5	3.0	M3.5 V
J22437+192	M3.0 V	Reid07	3.0	2.5	3.0	3.0	2.5	3.0	2.5	M3.0 V
J22476+184	M3.5 V	Reid04	2.5	2.5	3.0	3.0	2.5	3.0	2.5	M2.5 V
J22489+183	M4.0 V	Abe14	4.0	4.5	4.5	4.0	4.5	4.5	4.0	M4.5 V
J22509+499	...	...	4.0	4.0	4.5	4.5	4.0	4.5	3.5	M4.0 V
J22524+099 AB	M3.0 V	PMSU	3.0	3.0	3.0	3.0	3.0	3.0	3.0	M3.0 V
J22526+750	...	...	4.5	4.5	4.5	4.5	5.0	4.5	4.5	M4.5 V
J22582–110	M2.5 V	Reid07	2.5	2.5	3.5	3.5	3.0	3.5	2.5	M2.5 V
J22588+690	m:	Simbad	3.0	3.0	3.5	3.5	3.0	3.5	3.0	M3.0 V
J23006+036	...	...	3.0	3.0	3.0	3.0	3.0	3.0	3.0	M3.0 V
J23028+436	M4.0 V	Reid07	4.0	4.5	4.5	4.0	4.0	4.5	4.0	M4.0 V
J23036–072	k:	Simbad	2.5	2.5	3.0	3.0	3.0	3.0	3.0	M2.5 V
J23036+097	...	...	3.5	3.0	3.5	3.0	3.5	3.5	3.5	M3.5 V
J23051+519	...	...	3.5	3.0	3.5	3.5	3.5	4.0	3.5	M3.5 V
J23051+452	...	...	3.5	3.5	4.0	3.5	3.5	4.0	3.5	M3.5 V
J23070+094	M1 III	JM53, Kir91	...	...	...	...	...	...	...	M III
J23177+490	M2 III	Gar89, SB06	...	...	...	...	...	...	...	M III
J23182+795	m:	Simbad	3.0	3.0	3.0	3.0	3.0	3.0	2.5	M3.0 V
J23194+790	M4.0 V	Lep13	3.5	3.5	4.0	3.5	4.0	4.0	3.5	M3.5 V
J23209–017 AB	M4.0 V+m4.0:	Riaz06, Dae07	4.0	4.0	4.0	3.5	4.0	4.0	3.5	M4.0 V
J23220+569	...	...	2.5	3.0	3.5	3.5	3.0	3.0	3.0	M3.0 V
J23228+787	m5.0	Law08	4.5	4.5	6.0	6.0	4.5	5.5	4.0	M5.0: V
J23235+457	K8 V	Simbad	–4.0	<–3.0	...	...	...	...	...	<K5 V
J23261+170 AB	M4.5	Reid07	4.0	4.5	4.0	4.0	4.0	4.5	4.0	M4.0 V
J23266+453	M3.5 III	Bid85	...	...	...	...	...	...	...	M III
J23306+466	M3 V	Bid85	1.5	1.5	2.0	2.0	2.0	2.0	2.0	M2.0 V

Table B.3: Spectral types of observed stars (cont.).

Karmn	Sp. type	Ref.[a]	Sp. type		Sp. type					Sp. type
	biblio.		Best-fit	χ^2	TiO2	TiO5	PC1	VO-7912	Color-M	adopted
J23317–064	M4.5 V	Reid07	4.5	4.5	4.0	4.0	5.0	4.5	4.5	M4.5 V
J23376+163	M5.5 V	Sch05	5.5	5.5	5.5	5.5	5.5	5.5	5.5	M5.5 V
J23416–065	...	...	4.5	4.5	4.5	4.5	4.5	4.5	4.5	M4.5 V
J23417–059 AB	M3.0 V	New14	3.5	3.5	3.5	3.5	3.5	3.5	3.5	M3.5 V
J23419+441	M5.0 V	PMSU	5.0	5.0	5.0	5.0	5.0	5.0	5.0	M5.0 V
J23423+349	...	...	4.0	4.0	4.0	4.0	4.0	4.0	3.5	M4.0 V
J23425+392	...	...	0.0	0.0	–0.5	–0.5	0.0	0.0	0.0	M0.0 V
J23438+610	k:	Simbad	3.0	3.0	3.5	3.5	2.5	3.0	3.0	M3.0 V
J23490–086	M2.5 V	Reid04	2.0	2.0	2.0	2.5	2.0	2.0	2.0	M2.0 V
J23559–133	M3.0 V	Sch05	3.5	3.5	4.0	3.5	3.5	4.0	3.5	M3.5 V
J23560+150	...	...	2.5	2.5	2.5	2.5	2.5	2.5	2.5	M2.5 V
J23569+230	K7 V	Ste86	1.5	1.0	1.5	1.5	1.5	1.0	1.5	M1.5 V
J23585+242	K7 V	Lee84	–1.0	–1.0	–1.0	–1.0	–1.0	–0.5	–0.5	K7 V
J23590+208	...	...	2.5	2.0	3.0	3.0	2.5	3.0	2.5	M2.5 V

C

Long tables of Chapter 3

This is the on-line material of the paper included in Chapter 3, that will be available at VizieR.

- Table C.1: corresponds to Table A.1 of the article. Compilation of β Pictoris members and member candidates. Col. 1 discovery or most common name; Col. 2-3 coordinates (J2000.0); Col. 4 distance from the bibliography; Col. 5 reference for distance from the bibliography; Col. 6 membership flag 1 for incontrovertible members, 2 for candidates without definitive confirmation, 3 for dubious moving group candidates.

- Table C.2: corresponds to Table A.2 of the article. Unresolved or unidentified systems (generally their small angular separation or brightness difference of bright prevent their separate study). Col. 1 component name; Col. 2 discovery name used by the WDS or reference; Col. 3 status of the pair, Physical for truly bound systems, SB for spectroscopic binaries, Visual for none related pairs; Col. 4 angular separation of the system; Col. 5 position angle measured by us; Col. 6 identifier provided by the WDS.

- Table C.3: corresponds to Table A.3 of the article. Catalogue of astrometry measurements. Col. 1 object name; Col. 2-3 coordinates (J2000.0); Col. 4-5 proper motions provided from PPMXL catalogue; Col. 6-7 adopted proper motions from *Hipparcos*, Tycho or our measurements; Col. 8 temporal interval between the first and the last epoch used for the astrometry measurements; Col. 9 number of epochs used for the astrometry measurements; Col. 10 origin of the adopted proper motions; Col. 11 status of the companion after the astrometric study.

- Table C.4: corresponds to Table A.4 of the article. Photometric values of the objects that passed the astrometric filtering. Col. 1 object name; Col. 2-3 coordinates (J2000.0); Col. 4-7 photometry on different bands from blue to near-infrared, the sources are described in the text; Col. 8 distance used for determining the absolute magnitudes; Col. 9 status of the companion after the photometric study, the object of the system that were known to belong the moving group are named in parenthesis.

- Table C.5: corresponds to Table A.5 of the article. Common proper-motion companion candidates obtained. Col. 1 WDS identifier, those presented italic font are systems not included jet in the WDS catalogue; Col. 2 discovery name of the system; Col. 3 name of the objects; Col. 4-5 coordinates (J2000.0); Col. 6 adopted distance for the system; Col. 7 absolute magnitude

in the J-band; Col. 8 spectral type from the literature, the lower-case letters indicate photometric spectral types; Col. 9 angular separation of the system measured by us at the 2MASS epoch; Col. 10 angular position of the companion measured by us at the 2MASS epoch; Col. 11 projected physical separation computed by us; Col. 12 masses obtained from the literature o computed by us; Col. 13 binding energy of the system considering their masses and projected physical separation; Col. 14 comments provided for the most remarkable systems, such as those ones that are suspected to belong to other moving groups or new member candidates.

Table C.1: Investigated β Pictoris members and member candidates.

Simbad name	α (J2000)	δ (J2000)	d [pc]	Reference for distance	Memb. flag
HD 203	00:06:50.08	–23:06:27.2	39.39 ± 0.59	van Leeuwen 2007	1
RBS 38	00:17:23.54	–66:45:12.5	39.0 ± 2.6	Riedel et al. 2014	2
RX J0019.7+1951	00:19:43.04	+19:51:11.7	59.4 ± 7.9	Schlieder et al. 2012a	2
FK Psc	00:23:34.68	+20:14:28.3	53 ± 4	Malo et al. 2014b	2
1RXS J002700.0+663025	00:27:02.83	+66:30:39.0	56.9 ± 8.3	Schlieder et al. 2012a	3
GJ 2006 A	00:27:50.23	–32:33:06.4	33.2 ± 2.8	Riedel et al. 2014	1
GJ 2006 B	00:27:50.35	–32:33:23.9	31.5 ± 2.4	Riedel et al. 2014	1
LP 525–39 AB	00:32:34.81	+07:29:27.1	41.1 ± 4.4	Schlieder et al. 2012b	2
EROS–MP J0032–4405	00:32:55.84	–44:05:05.8	26.1 ± 2.0	Gagné et al. 2014	2
2MASS J00464841+0715177	00:46:48.41	+07:15:17.7	$33.8\ ^{+2.8}_{-3.2}$	Gagné et al. 2015	2
TYC 2288–758–1	00:48:28.65	+36:32:34.5	61.4 ± 8.4	Schlieder et al. 2012a	2
RX J0102.8+1857	01:02:50.99	+18:56:54.2	40.9 ± 4.4	Schlieder et al. 2012a	2
TYC 5853–1318–1 AB	01:07:11.93	–19:35:36.2	54	McCarthy & White 2012	2
LP 467–16 AB	01:11:25.42	+15:26:21.5	21.8 ± 0.8	Riedel et al. 2014	1
2E 327 AB	01:13:28.17	–38:21:02.5	29 ± 2	Malo et al. 2014a	2
2MASS J01294256–0823580	01:29:42.56	–08:23:58.0	32.5 ± 3.2	Gagné et al. 2015	2
1RXS J013514.2-071254	01:35:13.93	–07:12:51.8	37.9 ± 2.4	Shkolnik et al. 2012	2
LP 648–20 (EX Cet B)	01:36:55.17	–06:47:37.9	24.0 ± 0.4	Malo et al. 2014b	3
BD+17 232AB	01:37:39.39	+18:35:32.7	52.6	McCarthy & White 2012	3
1RXS J015255.9–632939	01:52:55.34	–63:29:30.1	23.7 ± 2.4	Gagné et al. 2014	2
RBS 253 AB	01:53:50.77	–14:59:50.3	28 ± 2	Malo et al. 2014a	2
[SLS2012] PYC J02017+0117N	02:01:46.77	+01:17:16.2	63.7 ± 9.0	Schlieder et al. 2012a	2
[SLS2012] PYC J02017+0117S	02:01:46.93	+01:17:06.0	63.7 ± 9.0	Schlieder et al. 2012a	2
HD 14082 B	02:17:24.73	+28:44:30.5	27.34 ± 4.26	van Leeuwen 2007	1
HD 14082 A	02:17:25.27	+28:44:42.3	34.52 ± 3.43	van Leeuwen 2007	1
RX J0217.9+1225	02:17:56.01	+12:25:26.6	67.9 ± 6.1	Binks & Jeffries 2013	2
[SLS2012] PYC J02226+3055	02:22:40.83	+30:55:16.0	46.8 ± 5.1	Schlieder et al. 2012a	2
LP 353–51	02:23:26.63	+22:44:06.9	28.7 ± 2.3	van Leeuwen 2007	1
HD 15115	02:26:16.25	+06:17:33.1	45.23 ± 1.31	van Leeuwen 2007	1
AG Tri B	02:27:28.05	+30:58:40.5	39.95 ± 3.59	van Leeuwen 2007	1
AG Tri A	02:27:29.25	+30:58:24.7	39.95 ± 3.59	van Leeuwen 2007	1
CD–44 753 Aa,Ab	02:30:32.41	–43:42:23.3	35.7	McCarthy & White 2012	3
EXO 0235.2–5216	02:36:51.71	–52:03:03.7	28.7	Elliott et al. 2014	3
BD+05 378 AB	02:41:25.89	+05:59:18.2	42.03 ± 2.65	van Leeuwen 2007	1
TVLM 831–154910	02:50:11.67	–01:51:29.5	33.1 ± 4.9	Gagné et al. 2015	2
DENIS J025344.4–795913	02:53:44.49	–79:59:13.3	$28.9^{+2.8}_{-3.2}$	Gagné et al. 2015	2
TYC 1231–151–1	03:10:32.74	+21:31:44.3	63.6 ± 8.7	Schlieder et al. 2012a	2
1RXS J031052.7+183855	03:10:53.57	+18:38:38.5	67.5 ± 9.9	Schlieder et al. 2012a	2
RX J0332.6+2843 ABC	03:32:35.79	+28:43:55.5	55 ± 4	Malo et al. 2014b	2
2MASS J03350208+2342356	03:35:02.09	+23:42:35.6	42.4 ± 2.3	Shkolnik et al. 2012	1
1RXS J033936.7+453126	03:39:37.01	+45:31:16.0	59.6 ± 7.3	Schlieder et al. 2012a	2
2MASS J03445673–1145126	03:44:56.73	–11:45:12.6	$31.3^{+4.0}_{-4.4}$	Gagné et al. 2015	2
HD 232862 AB	03:57:19.99	+50:51:18.6	51.7 ± 5.7	Schlieder et al. 2012a	2
1RXS J041137.6+250413	04:11:36.38	+25:04:41.8	64.2 ± 9.0	Schlieder et al. 2012a	2
c Eri A	04:37:36.13	–02:28:24.8	29.43 ± 0.29	van Leeuwen 2007	1
c Eri Ca,Cb	04:37:37.47	–02:29:28.4	29.43 ± 0.29	van Leeuwen 2007	1
2MUCD 10320	04:43:37.61	+00:02:05.2	$25.7^{+3.2}_{-2.4}$	Gagné et al. 2014	2
V962 Per	04:43:56.87	+37:23:03.3	59 ± 5	Malo et al. 2014b	2
LDS 5606 A	04:48:00.86	+14:39:58.1	65 ± 6	Rodríguez et al. 2014	2
LDS 5606 B	04:48:02.58	+14:39:51.6	65 ± 6	Rodríguez et al. 2014	2
V1005 Ori	04:59:34.83	+01:47:00.7	25.9 ± 1.7	van Leeuwen 2007	1
CD–57 1054	05:00:47.15	–57:15:25.6	26.78 ± 0.81	van Leeuwen 2007	1
V1841 Ori	05:00:49.29	+15:27:00.7	53.8 ± 7.5	Schlieder et al. 2012a	2

Table C.1: Investigated β Pictoris members and member candidates (cont.).

Simbad name	α (J2000)	δ (J2000)	d [pc]	Reference for distance	Memb. flag
1RXS J050156.7+010845	05:01:56.66	+01:08:42.9	27.0 ± 3.2	Schlieder et al. 2012b	2
LP 476–207 ABC	05:01:58.81	+09:58:58.8	24.6 ± 1.3	Riedel et al. 2014	1
TYC 693–948–1	05:02:47.84	+12:22:56.4	66.8 ± 11.9	Schlieder et al. 2012a	2
RX J0506.2+0439	05:06:12.93	+04:39:27.2	41.8 ± 6.0	Schlieder et al. 2012a	2
BD–21 1074Ba,Bb	05:06:49.47	–21:35:03.8	19.2 ± 0.5	Riedel et al. 2014	1
BD–21 1074A	05:06:49.92	–21:35:09.2	18.3 ± 0.7	Riedel et al. 2014	1
1RXS J050712.4+143024	05:07:11.37	+14:30:01.4	51.2 ± 7.0	Schlieder et al. 2012a	2
1RXS J050827.3-210130	05:08:27.29	–21:01:44.4	25 ± 5	Malo et al. 2014b	2
1RXS J051954.1+315944	05:19:53.18	+31:59:33.9	48.4 ± 5.2	Schlieder et al. 2012a	2
TYC 112–917–1	05:20:00.29	+06:13:03.6	68.5	Elliott et al. 2014	2
2E 1249 AB	05:20:31.83	+06:16:11.5	69.7	Elliott et al. 2014	2
CD–39 1935	05:22:45.69	–39:17:06.1	33 ± 6	Malo et al. 2013	2
1RXS J052419.1–160117 AB	05:24:19.14	–16:01:15.3	20 ± 5	Malo et al. 2014b	2
AF Lep AB	05:27:04.77	–11:54:03.3	27.04 ± 0.35	van Leeuwen 2007	1
2E 1287	05:29:44.68	–32:39:14.2	26.18 ± 1.10	Riedel et al. 2014	2
V1311 Ori AB	05:32:04.50	–03:05:29.2	42 ± 6	Malo et al. 2013	1
RBS 661	05:33:28.03	–42:57:20.5	16 ± 4	Malo et al. 2013	2
RX J0534.0–0221	05:33:59.81	–02:21:32.5	42 ± 5	Malo et al. 2014b	2
1RXS J054223.7–275803	05:42:23.87	–27:58:03.1	44 ± 9	Malo et al. 2013	2
β Pic	05:47:17.08	–51:03:59.5	19.44 ± 0.04	van Leeuwen 2007	1
2MASS J06085283–2753583	06:08:52.83	–27:53:58.3	31.269± 3.55	Faherty et al. 2012	2
1RXS J061313.2–274205 AB	06:13:13.30	–27:42:05.4	29.4 ± 0.9	Riedel et al. 2014	1
TYC 6513–1245–1	06:13:57.75	–27:23:55.3	51 ± 8	Malo et al. 2013	2
1RXS J061610.6–132046 AB	06:16:10.33	–13:20:42.3	47 ± 7	Malo et al. 2013	2
AO Men	06:18:28.24	–72:02:41.6	38.55 ± 0.13	van Leeuwen 2007	1
1RXS J065940.5+054541	06:59:41.57	+05:45:40.0	44.3 ± 6.5	Schlieder et al. 2012a	2
LP 58–170	07:23:29.41	+66:46:44.3	139.28 ± 42.48	van Leeuwen 2007	2
1RXS J072643.1+185026	07:26:41.54	+18:50:34.7	57.7 ± 8.1	Schlieder et al. 2012a	2
1RXS J072931.4+355607 AB	07:29:31.09	+35:56:00.4	42.2 ± 4.0	Schlieder et al. 2012b	2
YZ CMi AB	07:44:40.17	+03:33:08.8	5.96 ± 0.08	van Leeuwen 2007	2
2MASS J08025781–830076	08:02:57.81	–83:30:07.6	$20.5^{+2.4}_{-2.0}$	Gagné et al. 2015	2
EUVE J0817–82.7 AB	08:17:39.44	–82:43:29.8	27 ± 2	Malo et al. 2014a	2
L 186–67 Aa,Ab	08:22:47.45	–57:26:53.0	11.1 ± 3.3	Lépine & Gaidos 2011	3
2MASS J08224748+0757171	08:22:47.49	+07:57:17.2	62.4 ± 9.8	Schlieder et al. 2012b	2
[SLS2012] PYC J08290+1125	08:29:04.12	+11:25:05.4	58.8 ± 8.5	Schlieder et al. 2012a	2
HD 73018 AB	08:37:39.24	+41:48:02.3	51.9 ± 5.7	Schlieder et al. 2012a	2
[SLS2012] PYC J09226+7122S	09:22:37.64	+71:22:07.3	65.9 ± 9.6	Schlieder et al. 2012a	2
HD 82939 Ba,Bb	09:36:15.91	+37:31:45.5	33.75 ± 2.61	van Leeuwen 2007	3
RX J1002.0+6651	10:01:59.95	+66:51:27.7	38.7 ± 4.0	Schlieder et al. 2012b	3
DK Leo AB	10:14:19.18	+21:04:29.5	23.08 ± 0.96	van Leeuwen 2007	2
TWA 22 Aa,Ab	10:17:26.89	–53:54:26.5	17.5 ± 0.2	Malo et al. 2014b	1
[SLS2012] PYCJ10175+5542	10:17:31.43	+55:42:29.4	63.0 ± 8.3	Schlieder et al. 2012a	2
RX J1035.9+2853	10:35:57.25	+28:53:31.7	37.8 ± 3.9	Schlieder et al. 2012b	2
HD 95174 A	10:59:38.31	+25:26:15.5	22.6 ± 2.0	Schlieder et al. 2012b	2
HD 95174 B	10:59:38.68	+25:26:13.7	22.6 ± 2.0	Schlieder et al. 2012b	2
[SLS2012] PYC J11167+3814	11:16:46.09	+38:14:13.6	67.6 ± 9.6	Schlieder et al. 2012a	2
RBS 1043 Aa,Ab,B	11:51:56.81	+07:31:26.3	33.2 ± 2.7	Schlieder et al. 2012a	2
2E 2613	12:11:53.09	+12:49:13.5	62.7 ± 8.2	Schlieder et al. 2012a	2
1RXS J135452.3–712157	13:54:53.90	–71:21:47.7	21 ± 1	Malo et al. 2014a	3
TYC 4634–1184–1	14:12:49.93	+84:01:31.2	57.9 ± 9.7	Schlieder et al. 2012a	2
MV Vir Aa,Ab,B	14:14:21.36	–15:21:21.7	30.2 ± 4.5	van Leeuwen 2007	2
SCR J1425–4113 AB	14:25:29.13	–41:13:32.4	66.9 ± 4.3	Riedel et al. 2014	3
StKM 1–1155	14:25:55.93	+14:12:10.1	51.8 ± 7.3	Schlieder et al. 2012a	2

Table C.1: Investigated β Pictoris members and member candidates (cont.).

Simbad name	α (J2000)	δ (J2000)	d [pc]	Reference for distance	Memb. flag
α Cir AB	14:42:30.42	–64:58:30.5	16.57 ± 0.03	van Leeuwen 2007	3
V343 Nor B	15:38:56.79	–57:42:19.0	38.54 ± 1.69	van Leeuwen 2007	1
V343 Nor A	15:38:57.57	–57:42:27.3	38.54 ± 1.69	van Leeuwen 2007	1
TYC 4571–1414–1	16:17:11.48	+77:33:47.8	65.0 ± 13.5	Schlieder et al. 2012a	3
d Sco	16:18:17.90	–28:36:50.5	41.29 ± 0.38	van Leeuwen 2007	1
1RXS J164302.3–175418	16:43:01.28	–17:54:27.4	59.2 ± 2.8	Binks & Jeffries 2013	2
1RXS J165719.9–534328	16:57:20.30	–53:43:31.7	51 ± 3	Malo et al. 2014a	2
1RXS J171502.4–333344	17:15:02.20	–33:33:39.8	23 ± 1	Malo et al. 2014a	2
CD–27 11535 Aa,Ab,B	17:15:03.61	–27:49:39.7	84.1	Elliott et al. 2014	2
V824 Ara Aa,Ab	17:17:25.51	–66:57:03.9	31.45 ± 4.94	van Leeuwen 2007	1
V824 Ara B	17:17:31.29	–66:57:05.6	31.45 ± 4.94	van Leeuwen 2007	1
1RXS J172919.1–501454 AB	17:29:20.67	–50:14:52.9	64 ± 5	Malo et al. 2014a	1
CD–54 7336	17:29:55.07	–54:15:48.8	66	McCarthy & White 2012	1
HD 160305	17:41:49.03	–50:43:27.9	72.46 ± 4.57	van Leeuwen 2007	1
HD 161460 AB	17:48:33.74	–53:06:43.3	69.8	Elliott et al. 2014	1
HD 164249 AB	18:03:03.41	–51:38:56.4	48.15 ± 1.30	van Leeuwen 2007	1
HD 165189 AB	18:06:49.90	–43:25:30.8	41.84 ± 1.16	van Leeuwen 2007	1
V4046 Sgr AB	18:14:10.48	–32:47:34.4	73 ± 18	Kastner et al. 2011	1
V4046 Sgr C	18:14:22.07	–32:46:10.1	73 ± 18	Kastner et al. 2011	1
1RXS J181514.7–492755	18:15:15.64	–49:27:47.2	61 ± 4	Malo et al. 2014a	2
HD 168210	18:19:52.21	–29:16:32.8	72.57 ± 5.37	van Leeuwen 2007	1
FK Ser AB	18:20:22.75	–10:11:13.6	75.93 ± 22.00	van Leeuwen 2007	3
1RXS J184206.5–555426	18:42:06.95	–55:54:25.5	54 ± 4	Malo et al. 2014a	2
HD 172555 A	18:45:26.91	–64:52:16.5	28.55 ± 0.16	van Leeuwen 2007	1
HD 172555 Ba,Bb	18:45:37.05	–64:51:46.1	29.24 ± 0.60	van Leeuwen 2007	1
Smethells 20 (HD 173167 B)	18:46:52.56	–62:10:36.7	54 ± 3	Malo et al. 2014a	1
HD 173167 A	18:48:06.36	–62:13:47.0	52	Holmberg et al 2009	2
1RXS J184956.1-013402	18:49:55.44	–01:34:08.7	23 ± 6	Malo et al. 2014b	3
CD–31 16041	18:50:44.48	–31:47:47.2	53 ± 3	Malo et al. 2014a	1
PZ Tel Aa,Ab	18:53:05.87	–50:10:50.0	51.49 ± 2.60	van Leeuwen 2007	1
TYC 6872–1011–1	18:58:04.15	–29:53:04.6	76 ± 5	Malo et al. 2014b	1
2MASS J18580464–2953320	18:58:04.66	–29:53:32.2	76 ± 5	Malo et al. 2014b	1
1RXS J191028.6-231934	19:10:28.20	–23:19:48.6	67 ± 5	Malo et al. 2014b	2
CD–26 13904 AB	19:11:44.68	–26:04:08.5	80	McCarthy & White 2012	1
η Tel AB	19:22:51.22	–54:25:26.3	48.22 ± 0.49	van Leeuwen 2007	1
η Tel C	19:22:58.95	–54:32:17.1	51.81 ± 1.74	van Leeuwen 2007	1
1RXS J192338.2–460631	19:23:38.20	–46:06:31.6	70 ± 4	Malo et al. 2014b	2
RX J1924.5-3442	19:24:34.95	–34:42:39.3	54 ± 3	Malo et al. 2014a	2
2MASS J19395435–5216468	19:39:54.35	–52:16:46.8	$28.9^{+2.8}_{-2.4}$	Gagné et al. 2015	2
HDE 331149 A	19:43:37.90	+32:25:12.5	37.6 ± 8.3	Schlieder et al. 2012a	2
2MASS J19444417–4359015	19:44:44.17	–43:59:01.5	28.1 ± 2.4	Gagné et al. 2015	2
1RXS J195602.8–320720 AB	19:56:02.94	–32:07:18.7	55 ± 4	Malo et al. 2014a	1
TYC 7443–1102–1	19:56:04.38	–32:07:37.6	55 ± 3	Malo et al. 2014a	1
2MASS J20004841–7523070	20:00:48.42	–75:23:07.0	$33.3^{+3.2}_{-2.8}$	Gagné et al. 2014	2
1RXS J200136.9–331307	20:01:37.18	–33:13:14.0	61 ± 4	Malo et al. 2014a	2
HD 191089	20:09:05.22	–26:13:26.5	52.22 ± 1.23	van Leeuwen 2007	1
1RXS J201001.0–280139 AB	20:10:00.02	–28:01:41.0	48.0 ± 3.1	Riedel et al. 2014	1
SCR J2033-4903	20:33:01.86	–49:03:10.5	16.3 ± 5.0	Gagné et al. 2015	2
1RXS J203336.9-255654	20:33:37.59	–25:56:52.1	48.3 ± 3.3	Riedel et al. 2014	1
2MASS J20334670–3733443	20:33:46.70	–37:33:44.3	33.8 ± 2.8	Gagné et al. 2015	2
AU Mic BC (AT Mic AB)	20:41:51.12	–32:26:07.3	10.70 ± 0.42	van Leeuwen 2007	1
StHA 182 AB	20:43:41.14	–24:33:53.4	28.1 ± 3.9	Shkolnik et al. 2012	2
AU Mic	20:45:09.49	–31:20:26.7	9.91 ± 0.10	van Leeuwen 2007	1

Table C.1: Investigated β Pictoris members and member candidates (cont.).

Simbad name	α (J2000)	δ (J2000)	d [pc]	Reference for distance	Memb. flag
2MASS J20513567+1924020	20:51:35.68	+19:24:02.0	51.0 ± 8.0	Schlieder et al. 2012a	2
HD 199143 AB	20:55:47.68	–17:06:51.0	45.66 ± 1.60	van Leeuwen 2007	1
HD 199143 CD (AZ Cap AB)	20:56:02.75	–17:10:53.9	45.66 ± 1.60	van Leeuwen 2007	1
1RXS J210736.5–130500	21:07:36.79	–13:04:58.2	36 ± 2	Malo et al. 2013	3
EUVE J2110–19.3	21:10:05.36	–19:19:57.4	32 ± 2	Malo et al. 2014b	2
2MASS J21103096–2710513	21:10:30.96	–27:10:51.3	40 ± 2	Malo et al. 2013	2
2MASS J21103147–2710578	21:10:31.48	–27:10:57.8	41 ± 3	Malo et al. 2014b	2
2MASS J21140802–2251358	21:14:08.03	–22:51:35.8	22.1 ± 1.6	Gagné et al. 2014	2
StKM 1–1877	21:18:33.76	+30:14:34.6	50.5 ± 8.0	Schlieder et al. 2012b	2
V390 Pav A	21:21:24.49	–66:54:57.4	30.2 ± 1.3	van Leeuwen 2007	3
V390 Pav B	21:21:28.72	–66:55:06.3	30.2 ± 1.3	van Leeuwen 2007	3
2E 4498 AB	21:37:40.19	+01:37:13.7	39.2 ± 4.0	Schlieder et al. 2012b	2
1RXS J214127.5+204302	21:41:26.62	+20:43:10.7	57.2 ± 8.5	Schlieder et al. 2012a	2
1RXS J215518.2–004603	21:55:17.41	–00:45:47.8	47 ± 4	Malo et al. 2013	2
RX J2155.3+5938 AB	21:55:24.36	+59:38:37.1	29.9 ± 4.1	Schlieder et al. 2012a	2
RX J2200.7+2715	22:00:41.58	+27:15:13.5	44 ± 4	Malo et al. 2013	1
LSPM J2240+0532	22:40:01.45	+05:32:16.3	23.6 ± 2.7	Gagné et al. 2015	2
CPD–72 2713	22:42:48.96	–71:42:21.1	37 ± 2	Malo et al. 2014a	1
WW PsA A	22:44:57.94	–33:15:01.6	23.34 ± 1.97	van Leeuwen 2007	1
WW PsA B (TX PsA)	22:45:00.05	–33:15:25.8	23.34 ± 1.97	van Leeuwen 2007	1
1RXS J225710.4+363950	22:57:11.31	+36:39:45.2	68.7 ± 11.4	Schlieder et al. 2012b	2
LP 462–19 AB	23:17:28.07	+19:36:46.9	12 ± 1	Malo et al. 2013	2
AF Psc	23:31:44.93	–02:44:39.6	29.15 ± 2.64	van Altena et al. 1995	3
BD–13 6424	23:32:30.85	–12:15:51.3	28 ± 1	Malo et al. 2014a	1
2E 4766	23:50:06.39	+26:59:51.9	24 ± 2	Malo et al. 2014a	3
G 68–46	23:51:22.28	+23:44:20.8	16 ± 1	Malo et al. 2014a	3

Table C.2: Unresolved or unidentified systems.

Simbad name	Discovery name or reference	Status	ρ [arcsec]	θ [deg]	WDS identifier
LP 525–39 AB	MCT 1	Physical	0.7	334	00326+0729
RBS 153 AB	BRG 3	Physical	0.4	168	01072–1936
LP 467–16 AB	BEU 2	Physical	0.3	241	01114+1526
2E 327 AB	BRG 4	Physical	1.4	28	01135–3821
LP 648–20 BC	BRG 5	Visual	5.4	184	01376–0645
LP 648–20 BD	BWL 7	Visual	6.7	23	
BD+17 232AB	COU 254	Physical	1.6	24	01377+1836
RBS 253 AB	BRG 7	Physical	2.8	292	01538–1500
HD 15115 AB	VIG 2	Visual	12.6	195	02263+0618
BD+05 378AB	Song et al. 2003	SB1	...	...	...
CD–44 753 Aa,Ab	Elliott et al. 2015	Physical	0.13	295	02305–4305
RX J0332.6+2843 AB	JNN 24	Physical	0.1	282	03326+2844
RX J0332.6+2843 AC	JNN 24	Physical	0.5	106	
HD 232862 AB	COU 2357	Physical	0.7	93	03573+5051
c Eri Ab	Macintosh et al. 2015	Physical	0.4	170	04376–0228
c Eri Ca,Cb	KAS 1	Physical	0.3	18	
V1005 Ori AB	LAF 33	Visual	5.2	220	04596+0147
V1005 Ori AC	LAF 33	Visual	7.4	234	
V1005 Ori Aa,Ab	Elliott et al. 2014	SB1?	...	...	
LP 476–207 Aa,Ab	Delfosse et al. 1999	SB2	...	...	05020+0959
LP 476–207 Aa,Ab,B	HDS 654	Physical	1.3	151	
BD–21 1074Ba,Bb	DON 93	Physical	0.8	321	05069–2135
2E 1249 AB	Elliott et al. 2015	Physical	0.42	235	...
1RXS J052419.1–160117 AB	BRG 21	Physical	0.6	68	05243–1601
AF Lep AB	Nordström et al. 2004	SB2	...	...	...
V1311 Ori AB	JNN 39	Physical	0.2	56	05321–0305
1RXS J061313.2-274205 AB	TSN 2	Physical	0.1	215	06132–2742
1RXS J061610.6-132046 AB	BRG 22	Physical	0.2	167	06162–1232
1RXS J072931.4+355607 AB	JNN 57	Physical	0.2	253	07295+3556
YZ CMi AB	LAF 36	Visual	8.8	114	07447+0333
EUVE J0817–82.7 AB	CVN 22	Physical	0.6	353	08177–8243
L 186–67 Aa,Ab	BRG27	Physical	0.8	150	08228–5727
HD 73018 AB	STF 1244	Physical	3.9	0	08377+4148
HD 82939 Ba,Bb	Schlieder et al. 2012b	SB2	...	...	...
DK Leo AB	Shkolnik et al. 2012	SB1	...	...	...
TWA 22 Aa,Ab	CVN 16	Physical	0.1	15	10174–5354
TWA 22 Aa,Ab–Zd	CVN 16	Visual	3.5–16.8	...	
RBS 1043 Aa,Ab	Bowler et al. 2015	SB2	...	...	...
RBS 1043 Aa,Ab,B	Bowler et al. 2015	Physical	0.5	110	
MV Vir Aa,Ab	CVN 25	Physical	0.3	257	14144–1521

Table C.2: Unresolved or unidentified systems (cont.).

Simbad name	Discovery name or reference	Status	ρ [arcsec]	θ [deg]	WDS identifier
MV Vir Aa,Ab,B	RST 3869	Physical	1.1	62	
SCR J1425–4113 AB	Riedel et al. 2014	Physical	0.6	282	...
α Cir AB	DUN 166	Physical	15.4	226	14425–6459
V343 Nor AB	SKF1501	Physical	10.2	325	15390–5742
V343 Nor A–Zd	VGT 4	Visual	2.2–7.5	...	
V343 Nor B–T	CVN 52	Visual	1.4–7.9	...	
CD–27 11535 Aa,Ab	Elliott et al. 2015	SB1	...	...	...
CD–27 11535 Aa,Ab,B	Elliott et al. 2015	Physical	0.08	278	
V824 Ara AC	CVN55	Visual	7.9	120	17174–6657
V824 Ara Aa,Ab	Strassmeier & Rice 2000	SB2	...	...	...
1RXS J172919.1–501454 AB	Elliott et al. 2015	Physical	0.73	20	...
HD 161460 AB	CVN 29	Physical	0.1	233	17486–5307
HD 164249 AB	SKF 1420	Physical	6.7	89	18031–5139
HD 164249 A–J	CVN57	Visual	7.4–14.8	...	
HD 165189 AB	HJ 5014	Physical	1.8	4	18068–4325
V4046 Sgr AB	Torres et al. 2008	SB2	...	...	...
FK Ser AB	HER 2	Physical	1.0	17	18204–1011
HD 172555 AC	CVN 59	Visual	7.4	319	18454–6452
HD 172555 Ba,Bb	BIL 4	Physical	0.2	95	
CD–31 16041 A–J	CVN 60	Visual	1.9–6.9	...	18507–3148
PZ Tel Aa,Ab	MUG 10	Physical	0.4	60	18531–5011
PZ Tel Aa,Ab–E	CVN 61	Visual	4.0–10.7	...	
CD–26 13904 AB	RST 2094	Physical	1.1	49	19117–2604
η Tel AB	LWR 3	Physical	4.2	170	19229–5425
η Tel CD	CVN 63	Visual	4.8	251	19230–5432
η Tel CE	CVN 63	Visual	5.8	275	
1RXS J195602.8–320720 AB	Elliott et al. 2014	SB2	...	...	...
HD 191089 A–C	MET 88	Visual	10.4–10.8	...	20091–2613
HD 191089 A–H	VIG 19	Visual	4.8–12.3	...	
1RXS J201001.0–280139 AB	BRG 30	Physical	0.7	283	20100-2802
StHA 182 AB	Shkolnik et al. 2012	Physical	1.5	217	...
AU Mic BC (AT Mic AB)	LDS 720	Physical	2.3	153	20452-3120
HD 199143 AB	JAY 1	Physical	1.1	324	20558–1707
HD 199143 CD (AZ Cap AB)	JAY 2	Physical	2.2	140	
2E 4498 AB	JNN 291	Physical	0.4	341	21376+0137
RX J2155.3+5938 AB	JNN 292	Phsyical	0.2	102	21554+5938
LP 462–19 AB	BEU 23	Physical	0.1	220	23175+1937

Table C.3: Astrometry measurements.

Simbad name	α (J2000)	δ (J2000)	$\mu_\alpha \cos\delta$ [mas a^{-1}]	μ_δ [mas a^{-1}]	$\mu_\alpha \cos\delta$ [mas a^{-1}]	μ_δ [mas a^{-1}]	Δt [a]	Number of detections	Origin of adopted proper motions	Astrometric status
			PPMXL		Adopted					
RX J0019.7+1951	00:19:43.04	+19:51:11.7	+69.8 ± 5.1	−49.8 ± 5.1	+72.6 ± 0.2	−43.9 ± 0.3	56.586	6	*This work*	
2MASS J00193931+1951050	00:19:39.31	+19:51:05.1	+70.3 ± 4.1	−48.9 ± 4.1	+74.7 ± 0.4	−40.9 ± 0.1	56.586	6	*This work*	Physical (in WDS)
GJ 2006 A	00:27:50.23	−32:33:06.0	+96.3 ± 22.0	−101.9 ± 22.0	+108.5 ± 0.4	−47.8 ± 0.8	27.188	5	*This work*	
GJ 2006 B	00:27:50.35	−32:33:23.8	+117.1 ± 20.7	−45.7 ± 20.7	+101.8 ± 0.3	−42.2 ± 1.0	27.188	4	*This work*	Physical (in WDS)
LP 648–20 (EX Cet B)	01:36:55.17	−06:47:37.9	+180.3 ± 4.1	−105.4 ± 4.1	+166.8 ± 0.3	−99.9 ± 0.3	11.682	5	*This work*	
EX Cet	01:37:35.47	−06:45:37.5	+171.2 ± 0.8	−97.7 ± 0.6	+171.3 ± 0.7	−98.5 ± 0.5	...	...	HIP2	Phot. follow-up
BD+17 232 AB	01:37:39.39	+18:35:32.7	+69.9 ± 1.5	−47.5 ± 1.5	+69.9 ± 1.5	−47.5 ± 1.5	...	...	TYC	
2MASS J01372935+1805559	01:37:29.35	+18:05:55.9	+73.4 ± 4.1	−45.1 ± 4.1	+73.4 ± 0.1	−46.2 ± 0.1	55.603	5	*This work*	Phot. follow-up
[SLS2012] PYC J02017+0117N	02:01:46.78	+01:17:16.2	+20.6 ± 6.3	−16.8 ± 6.3	+77.5 ± 0.3	−46.5 ± 1.0	55.969	8	*This work*	
[SLS2012] PYC J02017+0117S	02:01:46.93	+01 17 06.0	+81.2 ± 12.5	−60.7 ± 12.1	+67.8 ± 0.7	−50.6 ± 0.6	56.724	8	*This work*	Phot. follow-up
HD 14082 A	02:17:25.27	+28:44:42.3	+84.4 ± 1.5	−76.8 ± 1.4	+87.6 ± 2.2	−72.4 ± 2.5	...	...	HIP2	
HD 14082 B	02:17:24.73	+28:44:30.5	+88.5 ± 1.7	−73.0 ± 1.7	+80.2 ± 4.4	−78.4 ± 4.9	...	...	HIP2	Physical (in WDS)
2MASS J02195655+2806230	02:19:56.55	+28:06:23.0	+90.1 ± 4.2	−78.8 ± 4.2	+91.0 ± 0.6	−79.1 ± 0.2	55.738	6	*This work*	Phot. follow-up
[SLS2012] PYC J02226+3055	02:22:40.83	+30:55:16.0	+68.4 ± 5.4	−66.4 ± 5.4	+69.7 ± 0.1	−67.1 ± 0.5	55.738	6	*This work*	
2MASS J02221455+3056377	02:22:14.55	+30:56:37.7	+74.0 ± 4.2	−66.5 ± 4.2	+76.5 ± 0.5	−65.6 ± 0.4	55.738	6	*This work*	Phot. follow-up
HD 15115	02:26:16.24	+06:17:33.2	+87.1 ± 0.8	−50.7 ± 0.6	+86.3 ± 0.7	−50.0 ± 0.5	...	...	HIP2	
TYC 45–1241–1	02:27:05.45	+06:31:16.3	+85.4 ± 1.9	−51.5 ± 1.9	+88.2 ± 2.4	−51.7 ± 2.4	...	...	TYC	Phot. follow-up
AG Tri A	02:27:29.25	+30:58:24.7	+79.3 ± 1.5	−71.7 ± 1.6	+79.8 ± 2.6	−70.0 ± 1.7	...	...	HIP2	
AG Tri B	02:27:28.05	+30:58:40.5	+78.9 ± 5.4	−75.2 ± 5.4	+77.5 ± 0.3	−72.1 ± 0.1	55.738	5	*This work*	Physical (in WDS)
CD–44 753 Aa,Ab	02:30:32.41	−43:42:23.3	+78.9 ± 2.1	−11.6 ± 2.1	+80.5 ± 1.6	−14.9 ± 1.6	...	...	TYC	
CD–44 753 B	02:30:46.23	−43:43:49.3	+82.2 ± 3.1	−18.3 ± 3.1	+79.8 ± 1.5	−18.2 ± 0.8	107.623	6	*This work*	Physical (in WDS)
CD–43 759	02:29:55.59	−43:19:07.8	+73.3 ± 2.0	−11.1 ± 2.0	+69.1 ± 2.1	−12.6 ± 1.9	...	...	TYC	Phot. follow-up
2MASS J02292952–4321108	02:29:29.52	−43:21:10.8	+71.7 ± 8.5	−12.8 ± 8.5	+78.2 ± 0.1	−20.7 ± 0.3	32.601	4	*This work*	Phot. follow-up
DENIS J025344.4–795913	02:53:44.48	−79:59:13.3	+74.6 ± 9.2	+103.9 ± 9.2	+83.3 ± 0.4	+84.5 ± 0.6	20.608	4	*This work*	
2MASS J02441357–7919202	02:44:13.57	−79:19:20.2	+74.8 ± 9.7	+97.0 ± 9.7	+85.9 ± 0.2	+83.5 ± 0.5	20.608	4	*This work*	Phot. follow-up
HD 232862 AB	03:57:19.99	+50:51:18.6	+45.8 ± 1.8	−71.8 ± 1.8	+45.8 ± 1.8	−71.8 ± 1.8	...	...	TYC	
2MASS J03545988+5044350	03:54:59.88	+50:44:35.0	+44.8 ± 5.4	−75.2 ± 5.4	−10.6 ± 0.8	+7.6 ± 0.9	51.083	6	*This work*	Visual
c Eri A	04:37:36.13	−02:28:24.8	+42.2 ± 1.5	−63.3 ± 1.5	+44.2 ± 0.3	−64.4 ± 0.3	...	...	HIP2	
c Eri Ca,Cb	04:37:37.47	−02:29:28.4	+44.6 ± 2.1	−62.9 ± 2.1	+43.5 ± 0.9	−65.5 ± 3.3	113.731	7	*This work*	Physical (in WDS)
c Eri "B" (2MASS J04373798-0228164)	04:37:37.99	−02:28:16.4	+0.5 ± 2.1	+20.5 ± 2.5	+1.0 ± 3.2	+23.5 ± 2.8	105.034	4	*This work*	Visual (in WDS)
V962 Per	04:43:56.87	+37:23:03.3	+27.3 ± 5.1	−64.4 ± 5.1	+14.0 ± 0.2	−63.5 ± 0.4	54.367	5	*This work*	
2MASS J04450683+3704056	04:45:06.83	+37:04:05.6	+28.2 ± 4.2	−58.7 ± 4.2	+30.7 ± 0.5	−58.6 ± 0.2	54.637	6	*This work*	Phot. follow-up
LDS 5606 A	04:48:00.86	+14:39:58.1	+19.0 ± 4.3	−40.0 ± 4.3	+19.7 ± 0.2	−39.7 ± 0.7	54.536	5	*This work*	
LDS 5606 B	04:48:02.58	+14:39:51.6	+18.7 ± 4.3	−43.4 ± 4.3	+20.7 ± 0.2	−42.5 ± 0.4	54.536	5	*This work*	Physical (in WDS)
V1005 Ori	04:59:34.83	+01:47:00.7	+39.7 ± 1.8	−95.1 ± 1.9	34.6 ± 2.3	−94.3 ± 1.4	...	...	HIP2	
StKM 1–526	04:55:48.00	+02:02:07.5	+39.8 ± 1.9	−89.5 ± 1.9	37.0 ± 1.9	−88.8 ± 1.9	...	...	TYC	Phot. follow-up
CD–57 1054	05:00:47.15	−57:15:25.6	+35.8 ± 1.0	+72.8 ± 0.9	+36.3 ± 1.4	+70.2 ± 1.3	...	...	HIP2	
2MASS J05052576–5719046	05:05:25.76	−57:19:04.6	+39.5 ± 10.8	+70.9 ± 10.8	+37.8 ± 0.6	+81.0 ± 1.1	25.993	7	*This work*	Phot. follow-up
BD–21 1074	05:06:49.92	−21:35:09.2	+48.1 ± 3.2	−22.7 ± 3.4	+48.1 ± 3.2	−22.7 ± 3.4	...	4	TYC	
BD–21 1074Ba,Bb	05:06:49.47	−21:35:03.8	+37.0 ± 3.5	−38.1 ± 3.5	+37.0 ± 3.5	−38.1 ± 3.6	...	4	TYC	Physical (in WDS)
2MASS J05113065–2155189	05:11:30.65	−21:55:18.9	+40.4 ± 10.1	−37.3 ± 12.5	−5.7 ± 0.1	+19.3 ± 0.1	11.575	3	*This work*	Visual
2MASS J05071096–2156441	05:07:10.96	−21:56:44.1	+40.2 ± 5.3	−41.6 ± 5.3	+44.8 ± 1.1	−28.6 ± 1.7	29.559	7	*This work*	Phot. follow-up
2MASS J05050338–2200480	05:05:03.38	−22:00:48.0	+39.6 ± 5.3	−37.9 ± 5.3	+55.1 ± 0.9	−42.4 ± 0.6	27.544	4	*This work*	Visual
1RXS J050712.4+143024	05:07:11.37	+14:30:01.3	+16.4 ± 5.0	−76.1 ± 5.0	+14.0 ± 0.3	−74.7 ± 0.4	55.655	5	*This work*	
2MASS J05080140+1403539	05:08:01.40	+14:03:53.9	+16.5 ± 4.0	−69.7 ± 4.0	+13.5 ± 0.2	−67.1 ± 0.2	55.655	4	*This work*	Phot. follow-up
TYC 112–917–1	05:20:00.29	+06:13:03.6	+6.9 ± 2.8	−35.5 ± 2.9	+5.5 ± 4.1	−37.8 ± 4.0	...	...	TYC	
2E 1249 AB	05:20:31.83	+06:16:11.5	+9.4 ± 1.9	−37.3 ± 1.9	+12.4 ± 2.6	−38.8 ± 2.5	...	...	TYC	Phot. follow-up
AF Lep AB	05:27:04.77	−11:54:03.3	+17.7 ± 0.5	−49.5 ± 0.5	+17.6 ± 0.4	−50.2 ± 0.4	...	...	HIP2	
2MASS J05244065–1233402	05:24:40.65	−12:33:40.2	+18.5 ± 4.1	−49.8 ± 4.1	+12.0 ± 0.3	−49.2 ± 0.5	54.544	4	*This work*	Phot. follow-up
1RXS J065940.5+054541	06:59:41.57	+05:45:40.0	−27.2 ± 5.5	−73.4 ± 5.5	−23.1 ± 0.3	−68.3 ± 0.2	56.504	5	*This work*	
2MASS J07010444+0533517	07:01:04.44	+05:33:51.7	−25.8 ± 5.3	−78.7 ± 5.4	−5.2 ± 0.3	−27.6 ± 1.1	55.090	5	*This work*	Visual

Table C.3: Astrometry measurements (cont.).

Simbad name	α (J2000)	δ (J2000)	$\mu_\alpha \cos\delta$ [mas a^{-1}]	μ_δ [mas a^{-1}]	$\mu_\alpha \cos\delta$ [mas a^{-1}]	μ_δ [mas a^{-1}]	Δt [a]	Number of detections	Origin of adopted proper motions	Astrometric status
			PPMXL		Adopted					
1RXS J072643.1+185026	07:26:41.54	+18:50:34.7	−20.0 ± 4.9	−61.3 ± 4.9	−17.9 ± 0.2	−61.4 ± 0.4	57.473	5	*This work*	
2MASS J07280694+1838117	07:28:06.94	+18:38:11.7	−18.4 ± 5.3	−60.1 ± 5.3	−45.0 ± 0.6	−64.25 ± 0.9	57.472	5	*This work*	Visual
1RXS J072931.4+355607 AB	07:29:31.09	+35:56:00.4	−31.2 ± 2.3	−101.7 ± 2.3	−31.7 ± 0.2	−102.4 ± 0.7	81.247	6	*This work*	
2MASS J07293670+3554531	07:29:36.70	+35:54:53.1	−27.2 ± 5.0	−103.9 ± 5.0	−29.7 ± 0.5	−104.4 ± 0.2	55.379	6	*This work*	Physical (in WDS)
L 186–67 Aa,Ab	08:22:47.45	−57:26:53.0	−334.7 ± 18.2	+572.0 ± 18.2	−404.9 ± 0.4	+473.9 ± 0.7	30.528	4	*This work*	
L 186–67 B	08:22:47.99	−57:26:48.1	...	...	−359.5 ± 0.7	+463.9 ± 0.8	30.528	4	*This work*	Physical (in WDS)
[SLS2012] PYC J08290+1125	08:29:04.12	+11:25:05.4	−45.6 ± 5.3	−64.2 ± 5.3	−46.9 ± 0.3	−62.6 ± 0.3	58.511	7	*This work*	
2MASS J08274412+1122029	08:27:44.12	+11:22:02.9	−49.9 ± 1.5	−60.9 ± 1.5	−52.2 ± 0.4	−58.0 ± 0.1	58.511	7	*This work*	Phot. follow-up
HD 82939 Ba,Bb	09:36:15.91	+37:31:45.5	−101.9 ± 1.9	−89.4 ± 1.3	−99.4 ± 2.5	−89.5 ± 1.4	...	...	HIP2	
HD 82939 A	09:36:04.28	+37:33:10.4	−99.9 ± 0.9	−89.4 ± 0.6	−99.1 ± 1.1	−89.4 ± 0.6	...	...	HIP2	Physical (in WDS)
2MASS J09372954+3749458	09:37:29.54	+37:49:45.8	−100.4 ± 4.6	−92.8 ± 4.6	−101.3 ± 1.2	−90.9 ± 0.5	56.556	6	*This work*	Phot. follow-up
2MASS J09365772+3758354	09:36:57.72	+37:58:35.4	−100.4 ± 4.0	−87.5 ± 4.0	−99.5 ± 1.0	−86.2 ± 0.8	56.556	5	*This work*	Phot. follow-up
[SLS2012] PYC J10175+5542	10:17:31.43	+55:42:29.4	−59.8 ± 3.0	−49.3 ± 3.0	−61.0 ± 1.8	−50.1 ± 1.4	98.221	6	*This work*	
[SLS2012] PYC J10175+5542 "B"	10:17:26.66	+55:41:45.4	−74.6 ± 4.0	−34.0 ± 4.0	−71.7 ± 0.1	−31.9 ± 0.1	55.420	4	*This work*	Visual (in WDS)
HD 95174 A	10:59:38.31	+25:26:15.5	−184.0 ± 1.7	−49.9 ± 1.6	−184.0 ± 1.7	−49.9 ± 1.6	...	...	TYC	
HD 95174 B	10:59:38.68	+25:26:13.7	−177.5 ± 1.7	−81.5 ± 1.6	−177.5 ± 1.7	−81.5 ± 1.6	...	...	TYC	Physical (in WDS)
BD+26 2148	10:56:04.06	+25:41:17.2	−182.6 ± 1.1	−79.5 ± 0.8	−185.3 ± 1.3	−79.3 ± 0.8	...	...	HIP2	Phot. follow-up
2E 2613	12:11:53.09	+12:49:13.5	−70.1 ± 1.2	−60.1 ± 1.4	−73.8 ± 0.2	−57.5 ± 0.4	55.215	6	*This work*	
2MASS J12120849+1248050	12:12:08.49	+12:48:05.0	−70.2 ± 1.3	−59.3 ± 1.3	−74.5 ± 0.2	−61.6 ± 0.7	55.215	6	*This work*	Phot. follow-up
1RXS J135452.3–712157	13:54:53.90	−71:21:47.7	−142.6 ± 17.4	−112.5 ± 17.4	−143.7 ± 0.8	−130.1 ± 0.5	34.243	8	*This work*	
2MASS J13585056–7223161	13:58:50.56	−72:23:16.1	−145.2 ± 7.4	−103.2 ± 7.3	+27.3 ± 0.3	+5.0 ± 1.2	34.243	6	*This work*	Visual
2MASS J14100900–7107256	14:10:09.00	−71:07:25.6	−142.7 ± 8.1	−107.0 ± 8.1	−11.0 ± 0.3	−9.5 ± 0.4	34.243	6	*This work*	Visual
TYC 4634–1184–1	14:12:49.93	+84:01:31.2	−49.9 ± 1.9	36.1 ± 1.9	−50.0 ± 3.0	+36.9 ± 2.9			TYC	
2MASS J14192861+8426534	14:19:28.61	+84:26:53.4	−50.0 ± 5.5	36.6 ± 5.5	−59.1 ± 0.3	+28.6 ± 0.6	55.272	4	*This work*	Phot. follow-up
2MASS J14040157+8405075	14:04:01.57	+84:05:07.5	−52.7 ± 4.0	38.6 ± 4.0	−51.2 ± 0.1	+43.8 ± 0.6	55.272	4	*This work*	Phot. follow-up
MV Vir Aa,Ab,B	14:14:21.36	−15:21:21.7	−143.0 ± 1.9	−196.3 ± 2.0	−140.5 ± 1.9	−200.4 ± 2.0	...	...	TYC	
MV Vir C	14:14:17.00	−15:21:12.7	−128.0 ± 5.3	−192.3 ± 5.3	−118.5 ± 0.5	−197.4 ± 0.2	52.130	6	*This work*	Physical (in WDS)
SCR J1425-4113 AB	14:25:29.13	−41:13:32.4	−60.5 ± 14.3	−55.2 ± 14.3	−44.3 ± 0.5	−45.6 ± 0.5	28.701	4	*This work*	
2MASS J14241480–4124200	14:24:14.80	−41:24:20.0	−55.9 ± 10.8	−54.8 ± 10.8	−25.1 ± 0.7	−6.5 ± 0.4	28.701	4	*This work*	Visual
α Cir AB	14:42:30.39	−64:58:30.5	−187.4 ± 0.8	−231.5 ± 0.8	−192.53 ± 0.1	−233.5 ± 0.1	...	...	HIP2	
α Cir "C" (2MASS J14421982-6458362)	14:42:19.82	−64:58:36.2	−3.3 ± 2.8	−1.7 ± 2.8	−1.7 ± 1.1	1.1 ± 1.5	105.774	4	*This work*	Visual (in WDS)
TYC 4571–1414–1	16:17:11.35	+77:33:47.8	−32.7 ± 1.8	+39.7 ± 1.8	−33.3 ± 1.7	+39.9 ± 0.8	114.893	8	*This work*	
2MASS J16170673+7734028	16:17:06.73	+77:34:02.8	−35.7 ± 4.1	+42.4 ± 4.1	−38.2 ± 0.6	+39.7 ± 0.9	55.116	5	*This work*	Phot. follow-up
1RXS J164302.3–175418	16:43:01.28	−17:54:27.4	−27.4 ± 3.8	−51.3 ± 4.2	−30.7 ± 0.6	−51.9 ± 1.4	94.248	7	*This work*	
2MASS J16425150–1814492	16:42:51.50	−18:14:49.2	−30.1 ± 4.0	−47.3 ± 4.0	−25.2 ± 0.8	−48.8 ± 0.7	56.000	6	*This work*	Phot. follow-up
1RXS J165719.9–534328	16:57:20.30	−53:43:31.7	5.5 ± 24.1	−83.8 ± 24.1	−20.61 ± 0.6	−78.48 ± 0.9	31.078	5	*This work*	
2MASS J16545062–5347082	16:54:50.62	−53:47:08.2	5.2 ± 7.5	−87. ± 7.5	−7.5 ± 1.0	+6.6 ± 1.2	22.889	6	*This work*	Visual
2MASS J16574619–5400523	16:57:46.19	−54:00:52.3	5.0 ± 10.3	−84.3 ± 10.4	−4.1 ± 0.8	−9.2 ± 1.3	22.037	5	*This work*	Visual
2MASS J16552211–5348436	16:55:22.11	−53:48:43.6	5.8 ± 7.9	−77.1 ± 7.9	+3.2 ± 1.2	+5.0 ± 1.1	22.889	6	*This work*	Visual
1RXS J171502.4–333344	17:15:02.20	−33:33:39.8	5.7 ± 3.0	−179.3 ± 3.0	+6.5 ± 0.1	−177.8 ± 0.2	97.087	4	*This work*	
2MASS J17123508–3229368	17:12:35.08	−32:29:36.8	6.2 ± 9.7	−185.6 ± 9.7	+34.4 ± 3.2	+46.8 ± 1.3	13.247	4	*This work*	Visual
V824 Ara Aa,Ab	17:17:25.50	−66:57:03.7	−18.5 ± 1.5	−137.4 ± 1.6	−21.8 ± 0.4	−136.9 ± 0.4	...	...	HIP2	
V824 Ara B	17:17:31.29	−66:57:05.6	−400.2 ± 14.5	−291.2 ± 14.5	−7.1 ± 0.6	−154.4 ± 1.7	34.977	6	*This work*	Physical (in WDS)
1RXS J172919.1–501454 AB	17:29:20.67	−50:14:52.9	−8.7 ± 3.2	−59.9 ± 3.2	−5.4 ± 0.4	−54.8 ± 0.2	105.931	4	*This work*	
2MASS J17294889–4956417	17:29:48.89	−49:56:41.7	−8.5 ± 9.6	−54.5 ± 9.8	−9.8 ± 0.4	−0.9 ± 0.5	30.005	4	*This work*	Visual
2MASS J17270839–5023572	17:27:08.39	−50:23:57.2	−9.5 ± 7.4	−62.5 ± 7.4	−22.38 ± 0.5	−45.9 ± 1.1	20.102	5	*This work*	Phot. follow-up
2MASS J17265404–5010448	17:26:54.04	−50:10:44.8	−9.4 ± 7.8	−59.6 ± 7.8	−7.5 ± 0.9	−40.2 ± 1.5	30.005	4	*This work*	Visual
2MASS J17300841–5014154	17:30:08.41	−50:14:15.4	−9.6 ± 7.4	−65.0 ± 7.4	−9.4 ± 1.3	−2.1 ± 1.4	24.833	6	*This work*	Visual
HD 160305	17:41:49.03	−50:43:27.9	−2.5 ± 1.0	−67.0 ± 1.9	−3.7 ± 1.1	−65.7 ± 0.9	...	...	HIP2	
2MASS J17410520–5055268	17:41:05.20	−50:55:26.8	−2.4 ± 7.8	−66.7 ± 7.8	−1.0 ± 0.1	−4.0 ± 0.9	23.961	5	*This work*	Visual
HD 164249 AB	18:03:03.41	−51:38:56.4	+3.3 ± 0.7	−86.5 ± 0.5	+4.02 ± 0.60	−86.46 ± 0.36	...	...	HIP2	
2MASS J18043865–5118456	18:04:38.65	−51:18:45.6	+3.5 ± 8.8	−87.6 ± 8.8	−0.3 ± 0.6	−33.3 ± 1.1	29.125	4	*This work*	Visual

Table C.3: Astrometry measurements (cont.).

Simbad name	α (J2000)	δ (J2000)	$\mu_\alpha \cos\delta$ [mas a^{-1}]	μ_δ [mas a^{-1}]	$\mu_\alpha \cos\delta$ [mas a^{-1}]	μ_δ [mas a^{-1}]	Δt [a]	Number of detections	Origin of adopted proper motions	Astrometric status
			PPMXL		Adopted					
HD 165189 AB	18:06:49.90	–43:25:30.8	+13.8 ± 2.4	–105.3 ± 2.2	+13.8 ± 2.4	–105.3 ± 2.2	...	...	TYC	
2MASS J18041814–4316406	18:04:18.14	–43:16:40.6	+14.7 ± 9.0	–114.4 ± 9.6	–6.9 ± 1.3	+26.4 ± 1.4	24.941	7	*This work*	Visual
2MASS J18091082–4300490	18:09:10.82	–43:00:49.0	+14.7 ± 9.0	–111.4 ± 9.0	+0.28 ± 0.05	–0.6 ± 1.5	24.763	5	*This work*	Visual
V4046 Sgr AB	18:14:10.48	–32:47:34.4	+2.4 ± 2.7	–56.2 ± 2.8	+2.1 ± 2.3	–54.5 ± 2.1			TYC	
V4046 Sgr C	18:14:22.07	–32:46:10.1	+13.5 ± 36.7	–38.4 ± 36.7	+7.14 ± 0.04	–51.7 ± 0.2	11.994	4	*This work*	Physical (not in WDS)
1RXS J181514.7–492755	18:15:15.64	–49:27:47.2	+8.9 ± 3.2	–73.2 ± 3.2	+8.7 ± 0.2	–72.6 ± 1.5	105.112	5	*This work*	
2MASS J18174204–4915591	18:17:42.04	–49:15:59.1	+8.1 ± 8.9	–74.2 ± 8.9	+0.16 ± 0.8	–12.28 ± 0.4	32.061	7	*This work*	Visual
1RXS J184206.5–555426	18:42:06.95	–55:54:25.5	+1.3 ± 14.0	–72.5 ± 14.0	+12.8 ± 0.6	–74.7 ± 1.2	31.925	7	*This work*	
2MASS J18420483–5554126	18:42:04.83	–55:54:12.6	+4.2 ± 14.0	–76.7 ± 14.0	+13.8 ± 0.3	–78.2 ± 0.9	31.925	6	*This work*	Physical (in WDS)
2MASS J18445576–5547120	18:44:55.76	–55:47:12.0	+1.4 ± 10.3	–66.9 ± 10.3	+0.2 ± 0.7	–25.5 ± 0.8	31.925	6	*This work*	Visual
HD 172555 A	18:45:26.91	–64:52:16.5	+32.6 ± 0.4	–148.8 ± 0.4	+32.4 ± 0.2	–149.5 ± 0.2	...	...	HIP2	
HD 172555 Ba,Bb	18:45:37.05	–64:51:46.1	...	...	+32.5 ± 0.5	–155.4 ± 0.7	99.462	4	*This work*	Physical (in WDS)
HD 173167 B	18:46:52.56	–62:10:36.7	+15.2 ± 3.3	–80.7 ± 3.3	+18.1 ± 4.7	–76.6 ± 4.2	...	...	TYC	
HD 173167 A	18:48:06.36	–62:13:47.0	+16.1 ± 1.7	–82.4 ± 1.7	+16.1 ± 1.4	–80.3 ± 1.3	...	...	TYC	Phot. follow-up
2MASS J18452867–6236003	18:45:28.67	–62:36:00.3	+14.9 ± 8.4	–79.1 ± 8.4	+16.8 ± 0.42	–74.5 ± 1.0	34.158	6	*This work*	Phot. follow-up
PZ Tel Aa,Ab	18:53:05.87	–50:10:50.0	+16.1 ± 0.9	–83.8 ± 0.7	+17.6 ± 1.1	–83.6 ± 0.8	...	...	HIP2	
CD–50 12186	18:52:49.76	–50:14:37.0	+14.6 ± 2.1	–85.2 ± 2.2	+8.3 ± 1.6	–78.1 ± 1.6	...	...	TYC	Phot. follow-up
TYC 6872–1011–1	18:58:04.15	–29:53:04.6	+11.1 ± 3.5	–47.9 ± 3.6	+16.1 ± 4.7	–47.2 ± 4.2	...	...	TYC	
2MASS J18580464–2953320	18:58:04.66	–29:53:32.2	+7.0 ± 5.4	–56.7 ± 5.4	+9.0 ± 0.3	–50.5 ± 0.3	32.020	5	*This work*	Physical (in WDS)
η Tel AB	19:22:51.22	–54:25:26.3	+25.5 ± 0.7	–83.0 ± 0.5	+25.6 ± 0.2	–82.7 ± 0.1	...		HIP2	
η Tel C	19:22:58.95	–54:32:17.1	+23.8 ± 0.8	–82.1 ± 0.6	+24.9 ± 0.7	–81.8 ± 0.4	...		HIP2	Physical (in WDS)
2MASS J19233074–5450090	19:23:30.74	–54:50:09.0	+25.9 ± 9.2	–90.5 ± 9.2	+29.2 ± 0.1	–92.5 ± 0.1	29.605	4	*This work*	Phot. follow-up
1RXS J192338.2–460631	19:23:38.20	–46:06:31.6	+20.5 ± 3.2	–58.3 ± 3.2	+20.5 ± 0.3	–58.4 ± 0.7	105.019	5	*This work*	
2MASS J19251419–4553480	19:25:14.19	–45:53:48.0	+21.3 ± 3.2	–54.4 ± 3.2	+21.8 ± 0.6	–55.0 ± 0.4	105.010	6	*This work*	Phot. follow-up
2MASS J19230177–4603243	19:23:01.77	–46:03:24.3	+20.1 ± 10.1	–60.6 ± 10.1	+31.2 ± 0.8	–56.3 ± 0.4	31.919	6	*This work*	Phot. follow-up
2MASS J19224371–4554186	19:22:43.71	–45:54:18.6	+21.2 ± 10.2	–55.3 ± 10.2	+6.9 ± 0.4	–27.2 ± 0.9	27.942	4	*This work*	Visual
RX J1924.5–3442	19:24:34.94	–34:42:39.2	+20.8 ± 14.3	–65.8 ± 14.3	+20.5 ± 0.2	–69.8 ± 0.2	28.525	5	*This work*	
2MASS J19245811–3445450	19:24:58.11	–34:45:45.0	+21.2 ± 9.6	–61.0 ± 9.6	+9.2 ± 0.5	–31.2 ± 1.5	28.525	5	*This work*	Visual
2MASS J19253773–3449583	19:25:37.73	–34:49:58.3	+21.6 ± 10.2	–65.7 ± 10.2	+33.1 ± 0.9	+19.5 ± 2.6	16.593	5	*This work*	Visual
HDE 331149 A	19:43:37.90	+32:25:12.5	+44.0 ± 1.8	–8.9 ± 1.8	+46.3 ± 2.4	–11.4 ± 2.3	...	...	TYC	
HDE 331149 B	19:43:36.74	+32:25:20.8	+43.5 ± 2.5	–6.7 ± 2.5	+44.9 ± 0.3	–8.0 ± 0.3	76.693	4	*This work*	Physical (in WDS)
2MASS J19541276–5711271	19:54:12.76	–57:11:27.1	+61.8 ± 9.2	–73.7 ± 9.2	+63.3 ± 0.6	–92.1 ± 1.0	33.997	6	*This work*	
2MASS J19490300–5653427	19:49:03.00	–56:53:42.7	+58.1 ± 10.5	–74.9 ± 10.5	+59.9 ± 0.7	–81.8 ± 0.9	33.997	6	*This work*	Phot. follow-up
2MASS J19572208–5632342	19:57:22.08	–56:32:34.2	+67.2 ± 8.8	–69.5 ± 8.8	+75.8 ± 1.2	–56.1 ± 1.5	15.195	4	*This work*	Visual
2MASS J19540626–5635297	19:54:06.26	–56:35:29.7	+60.7 ± 9.2	–70.9 ± 9.2	+57.1 ± 0.4	–67.3 ± 0.7	29.554	4	*This work*	Visual
TYC 7443–1102–1	19:56:04.38	–32:07:37.6	+32.8 ± 2.9	–62.7 ± 2.9	+31.2 ± 3.1	–65.0 ± 3.2	...	...	TYC	
1RXS J195602.8–320720 AB	19:56:02.94	–32:07:18.7	+41.6 ± 11.3	–71.6 ± 11.3	+34.4 ± 0.5	–59.6 ± 0.4	27.957	5	*This work*	Physical (in WDS)
2MASS J19535525–3220023	19:53:55.25	–32:20:02.3	+32.7 ± 10.1	–63.5 ± 10.1	+4.499 ± 0.5	+2.2 ± 0.6	27.957	5	*This work*	Visual
2MASS J19552077–3144521	19:55:20.77	–31:44:52.1	+36.2 ± 9.9	–65.0 ± 10.5	+7.777 ± 0.4	+5.5 ± 0.5	27.957	5	*This work*	Visual
1RXS J200136.9–331307	20:01:37.18	–33:13:14.0	+39.5 ± 13.8	–63.3 ± 13.8	+30.3 ± 0.7	–67.6 ± 0.2	27.459	5	*This work*	
2MASS J19592933–3313078	19:59:29.33	–33:13:07.8	+37.9 ± 9.4	–63.6 ± 9.4	–1.9 ± 1.5	–46.8 ± 1.1	33.929	7	*This work*	Visual
HD 191089	20:09:05.22	–26:13:26.5	+38.3 ± 0.7	–68.2 ± 0.5	+39.2 ± 0.5	–68.3 ± 0.4	...	...	HIP2	
2MASS J20100328–2637403	20:10:03.28	–26:37:40.3	+41.8 ± 19.4	–69.2 ± 19.4	–2.5 ± 1.0	+2.3 ± 1.5	32.946	8	*This work*	Visual
1RXS J201001.0–280139 AB	20:10:00.02	–28:01:41.0	+38.5 ± 5.2	–64.6 ± 5.2	+35.8 ± 0.3	–69.9 ± 0.8	26.939	5	*This work*	
2MASS J20085122–2740536	20:08:51.22	–27:40:53.6	+40.4 ± 4.0	–61.7 ± 4.0	+40.3 ± 0.4	–68.6 ± 1.0	27.957	5	*This work*	Phot. follow-up
AU Mic	20:45:09.49	–31:20:26.7	+279.7 ± 1.2	–360.3 ± 0.8	+280.0 ± 1.3	–360.6 ± 0.7	...	...	HIP2	
AU Mic BC (AT Mic AB)	20:41:51.12	–32:26:07.3	+261.3 ± 3.6	–344.8 ± 3.9	+270.5 ± 4.6	–365.6 ± 3.5	...	...	HIP2	Physical (in WDS)
2MASS J20521133–2912398	20:52:11.33	–29:12:39.8	+294.5 ± 10.0	–370.1 ± 10.0	–3.8 ± 1.1	–5.0 ± 1.0	24.116	6	*This work*	Visual
EM* StHA 182 AB	20:43:41.14	–24:33:53.4	+61.9 ± 5.0	–73.7 ± 5.0	+46.8 ± 0.2	–73.5 ± 0.6	18.073	5	*This work*	
CD–24 16238 A	20:44:23.39	–23:38:58.4	+58.5 ± 1.6	–72.3 ± 1.5	+61.4 ± 1.9	–71.9 ± 1.6	...	...	TYC	Visual
CD–24 16238 BC (CPD–24 7061 AB)	20:44:23.90	–23:38:22.0	+2.2 ± 2.2	–8.8 ± 2.2	+2.7 ± 2.0	–10.5 ± 1.7	...	...	TYC	Visual (in WDS)
2MASS J20513567+1924020	20:51:35.68	+19:24:02.0	+46.6 ± 4.8	–41.8 ± 4.8	+42.3 ± 0.3	–39.7 ± 0.1	56.748	5	*This work*	
2MASS J20511685+1858123	20:51:16.85	+18:58:12.3	+44.3 ± 5.4	–42.8 ± 5.4	-0.9 ± 0.6	–4.8 ± 0.1	56.748	5	*This work*	Visual

Table C.3: Astrometry measurements (cont.).

Simbad name	α (J2000)	δ (J2000)	$\mu_\alpha \cos\delta$ [mas a^{-1}]	μ_δ [mas a^{-1}]	$\mu_\alpha \cos\delta$ [mas a^{-1}]	μ_δ [mas a^{-1}]	Δt [a]	Number of detections	Origin of adopted proper motions	Astrometric status
			PPMXL		Adopted					
HD 199143 AB	20:55:47.68	–17:06:51.0	+59.9 ± 1.0	–62.3 ± 0.8	+58.81 ± 0.8	–35.0 ± 0.7	...	...	HIP2	
HD 199143 CD (AZ Cap AB)	20:56:02.75	–17:10:53.9	+59.0 ± 2.9	–64.2 ± 3.0	+59.3 ± 3.2	–63.0 ± 3.0	...	..	TYC	Physical (in WDS)
EUVE J2110–19.3	21:10:05.36	–19:19:57.4	+93.0 ± 3.9	–87.4 ± 3.9	+91.7 ± 1.3	–89.0 ± 1.4	90.696	6	*This work*	
BPS CS 22898–0066	21:10:04.60	–19:20:30.3	+83.8 ± 5.1	–91.2 ± 5.1	+82.8 ± 1.0	–99.7 ± 0.8	55.918	6	*This work*	Physical (in WDS)
2MASS J21103147–2710578	21:10:31.47	–27:10:57.8	+43.0 ± 7.0	–58.5 ± 6.2	+73.8 ± 0.1	–71.3 ± 0.4	23.344	5	*This work*	
2MASS J21103096–2710513	21:10:30.96	–27:10:51.3	+64.6 ± 4.0	–69.3 ± 4.0	+77.9 ± 0.4	–71.3 ± 0.3	23.344	5	*This work*	Physical (in WDS)
2MASS J21094649–2728291	21:09:46.49	–27:28:29.1	+60.3 ± 4.0	–63.6 ± 4.0	+70.8 ± 0.6	–74.6 ± 0.5	28.477	6	*This work*	Phot. follow-up
2MASS J21085656–2650119	21:08:56.56	–26:50:11.9	+47.1 ± 3.9	–57.7 ± 3.9	+47.8 ± 0.4	–54.2 ± 0.6	25.735	6	*This work*	Visual
2MASS J21123604-2726172	21:12:36.04	–27:26:17.2	+47.5 ± 4.0	–63.5 ± 4.0	+44.5 ± 0.6	–66.4 ± 0.2	28.477	4	*This work*	Visual
V390 Pav A	21:21:24.49	–66:54:57.4	+95.6 ± 1.4	–98.9 ± 1.6	+95.5 ± 0.7	–102.7 ± 1.0	...	...	TYC	
V390 Pav B	21:21:28.72	–66:55:06.3	+98.4 ± 2.1	–95.8 ± 2.0	+96.9 ± 2.8	–96.6 ± 2.6	...	...	TYC	Physical (in WDS)
1RXS J215518.2–004603	21:55:17.41	–00:45:47.8	+64.5 ± 4.1	–53.7 ± 4.1	+63.6 ± 0.5	–60.2 ± 0.5	55.927	5	*This work*	
2MASS J21551738–0046231	21:55:17.38	–00:46:23.1	+64.0 ± 4.1	–52.3 ± 4.1	+64.7 ± 0.3	–58.1 ± 0.3	55.927	5	*This work*	Physical (in WDS)
RX J2155.3+5938 AB	21:55:24.36	+59:38:37.1	+117.2 ± 4.7	15.7 ± 4.7	+112.1 ± 0.1	+14.5 ± 0.1	57.788	4	*This work*	
2MASS J21543570+6008558	21:54:35.70	+60:08:55.8	+112.9 ± 5.1	15.6 ± 5.2	+18.17 ± 0.45	–15.1 ± 0.1	47.029	4	*This work*	Visual
LSPM J2240+0532	22:40:01.45	+05:32:16.3	+113.1 ± 3.9	–126.7 ± 3.9	+107.5 ± 1.0	–128.7 ± 0.6	55.918	6	*This work*	
HD 214786	22:40:27.22	+04:34:30.1	+106.4 ± 0.9	–124.1 ± 0.7	+105.2 ± 0.8	–124.4 ± 0.2	...	...	HIP2	Phot. follow-up
CPD–72 2713	22:42:48.96	–71:42:21.1	+95.2 ± 1.6	–55.1 ± 1.6	+94.1 ± 1.8	–54.4 ± 1.7	...	...	TYC	
2MASS J22353683–7149426	22:35:36.83	–71:49:42.6	+91.2 ± 9.4	–54.2 ± 9.4	+84.3 ± 0.4	–46.7 ± 0.8	28.803	4	*This work*	Phot. follow-up
2MASS J22372184–7118216	22:37:21.84	–71:18:21.6	+92.1 ± 9.4	–52.9 ± 9.4	+88.2 ± 0.6	–41.2 ± 0.4	28.803	4	*This work*	Phot. follow-up
2MASS J22401265–7123467	22:40:12.65	–71:23:46.7	+90.6 ± 14.9	–57.7 ± 14.9	+81.7 ± 1.2	–31.4 ± 0.8	28.803	4	*This work*	Visual
WW PsA A	22:44:57.94	–33:15:01.6	+184.7 ± 29.4	–112.8 ± 29.4	+184.8 ± 2.6	–119.8 ± 2.3	...	...	HIP2	
WW PsA B(TX PsA)	22:45:00.05	–33:15:25.8	+173.2 ± 24.7	–125.3 ± 24.7	+169.5 ± 0.4	–119.7 ± 0.3	26.297	5	*This work*	Physical (in WDS)
AF Psc	23:31:44.93	–02:44:39.6	+95.1 ± 4.7	–73.3 ± 4.7	+94.5 ± 0.6	–73.5 ± 0.4	55.927	7	*This work*	
AF Psc "B" (2MASS J23314589–0244273)	23:31:45.89	–02:44:27.3	+8.9 ± 5.0	–6.6 ± 5.0	–3.5 ± 2.5	+0.2 ± 1.1	55.141	6	*This work*	Visual (in WDS)
2MASS J23301129–0237227	23:30:11.30	–02:37:22.7	+101.7 ± 4.6	–77.3 ± 4.6	+102.1 ± 0.4	–72.6 ± 0.6	58.903	6	*This work*	Phot. follow-up
BD–13 6424	23:32:30.85	–12:15:51.3	+136.3 ± 2.0	–81.4 ± 2.0	+139.2 ± 1.70	–83.4 ± 1.6	...	...	TYC	
2MASS J23322017–1150414	23:32:20.17	–11:50:41.4	+133.1 ± 16.0	–77.4 ± 16.0	+46.1 ± 1.3	–76.1 ± 0.3	56.879	6	*This work*	Visual

Table C.4: Photometry measurements.

Simbad name	α (J2000)	δ (J2000)	B [mag]	V [mag]	r' [mag]	K_s [mag]	d [pc]	Photometric status
RX J0019.7+1951	00:19:43.04	+19:51:11.7	17.075 ± 0.700	...	14.694 ± 0.064	9.864 ± 0.018	59.40 ± 7.90	
2MASS J00193931+1951050	00:19:39.31	+19:51:05.1	17.079 ± 0.010	15.540 ± 0.010	14.913 ± 0.040	10.078 ± 0.018		Physical (A in β Pic)
GJ 2006 A	00:27:50.23	−32:33:06.0	14.333 ± 0.050	12.869 ± 0.100	12.312 ± 0.100	8.012 ± 0.033	33.2 ± 2.80	
GJ 2006 B	00:27:50.35	−32:33:23.8	14.659 ± 0.080	13.165 ± 0.030	12.605	8.116 ± 0.027		Physical (A and B in β Pic)
LP 648–20 (Ex Cet B)	01:36:55.17	−06:47:37.9	15.725 ± 0.050	13.996 ± 0.110	13.385 ± 0.080	8.862 ± 0.021	23.95 ± 0.42	
EX Cet	01:37:35.47	−06:45:37.5	8.661 ± 0.990	7.750 ± 0.990	7.635 ± 0.001	5.752 ± 0.018		Physical candidate (B in β Pic)
BD+17 232AB	01:37:39.39	+18:35:32.7	11.062 ± 0.060	9.890 ± 0.020	9.600 ± 0.010	6.716 ± 0.018	52.59	
2MASS J01372935+1805559	01:37:29.35	+18:05:55.9	16.826 ± 0.200	15.454 ± 0.340	14.621 ± 0.030	10.734 ± 0.022		Visual
[SLS2012] PYC J02017+0117N	02:01:46.78	+01:17:16.2	14.246 ± 0.100	12.785 ± 0.140	12.345	8.265 ± 0.016	63.70 ± 9.00	
[SLS2012] PYC J02017+0117S	02:01:46.93	+01 17 06.0	14.299 ± 0.180	12.719 ± 0.140	12.024 ± 0.120	8.258 ± 0.029		Physical candidate (A and B in β Pic)
HD 14082 A	02:17:25.27	+28:44:42.3	7.626 ± 0.990	7.048 ± 0.990	7.612 ± 0.001	5.787 ± 0.027	34.52 ± 3.43	
HD 14082 B	02:17:24.73	+28:44:30.5	8.493 ± 0.990	7.804 ± 0.990	11.984 ± 0.006	6.262 ± 0.017	27.34 ± 4.26	Physical (A and B in β Pic)
2MASS J02195655+2806230	02:19:56.55	+28:06:23.0	18.555 ± 0.700	...	17.235 ± 0.203	13.626 ± 0.037		Visual
[SLS2012] PYC J02226+3055	02:22:40.83	+30:55:16.0	15.685 ± 0.060	14.151 ± 0.050	13.517 ± 0.060	9.062 ± 0.017	46.79 ± 5.09	
2MASS J02221455+3056377	02:22:14.55	+30:56:37.7	16.986 ± 0.100	15.468 ± 0.040	14.876 ± 0.060	10.984 ± 0.019		Visual
HD 15115	02:26:16.24	+06:17:33.2	8.788 ± 0.010	8.595 ± 0.010	9.333 ± 0.001	5.822 ± 0.021	45.22 ± 1.30	
TYC45–1241–1	02:27:05.45	+06:31:16.3	12.053 ± 0.040	11.347 ± 0.010	11.142 ± 0.020	9.678 ± 0.021		Visual
AG Tri A	02:27:29.25	+30:58:24.7	11.491 ± 0.050	10.300 ± 0.100	9.793 ± 0.040	7.079 ± 0.026	39.95 ± 3.58	
AG Tri B	02:27:28.05	+30:58:40.5	13.425 ± 0.700	...	11.855	7.921 ± 0.031		Physical (A and B in β Pic)
CD–44 753 Aa,Ab	02:30:32.41	−43:42:23.3	11.380 ± 0.050	10.309 ± 0.040	9.876 ± 0.050	7.230 ± 0.027	35.70	
CD–44 753 B	02:30:46.23	−43:43:49.3	13.244 ± 0.030	11.918 ± 0.010	11.326 ± 0.010	8.267 ± 0.034		Physical (Aa,Ab in β Pic)
CD–43 759	02:29:55.59	−43:19:07.8	11.267 ± 0.020	10.576	10.371	8.862 ± 0.023		Visual
2MASS J02292952–4321108	02:29:29.52	−43:21:10.8	16.941 ± 0.110	15.543 ± 0.030	14.953 ± 0.020	11.480 ± 0.021		Visual
DENIS J025344.4–795913	02:53:44.48	−79:59:13.3	17.989 ± 0.700	...	...	10.378 ± 0.021	28.89 ± 3.20	
2MASS J02441357–7919202	02:44:13.57	−79:19:20.2	17.360 ± 0.110	15.960 ± 0.120	15.309 ± 0.060	12.031 ± 0.023		Visual
c Eri A	04:37:36.13	−02:28:24.8	5.559 ± 0.990	5.250 ± 0.990	...	4.537 ± 0.024	29.43 ± 0.29	
c Eri Ca,Cb	04:37:37.47	−02:29:28.4	11.942 ± 0.010	10.534	10.069 ± 0.040	6.413 ± 0.018		Physical (A and Ca,Cb in β Pic)
V962 Per	04:43:56.87	+37:23:03.3	14.791 ± 0.090	13.317 ± 0.090	12.678 ± 0.060	8.800 ± 0.018	59.00 ± 5.00	
2MASS J04450683+3704056	04:45:06.83	+37:04:05.6	16.767 ± 0.090	15.621 ± 0.070	15.156 ± 0.030	12.390 ± 0.023		Visual
LDS 5606 A	04:48:00.86	+14:39:58.1	17.650 ± 0.010	16.654 ± 0.010	15.725 ± 0.010	10.730 ± 0.018	65.00 ± 6.00	
LDS 5606 B	04:48:02.58	+14:39:51.6	18.210 ± 0.160	...	16.096 ± 0.114	10.683 ± 0.018		Physical (A and B in β Pic)
V1005 Ori	04:59:34.83	+01:47:00.7	11.453 ± 0.040	10.060 ± 0.040	9.507 ± 0.080	6.261 ± 0.017	25.89 ± 1.70	
StKM 1–526	04:55:48.00	+02:02:07.5	12.753 ± 0.020	11.633 ± 0.030	11.156 ± 0.030	8.829 ± 0.021		Visual
CD–57 1054	05:00:47.15	−57:15:25.6	11.267 ± 0.010	10.210 ± 0.010	9.977 ± 0.010	6.244 ± 0.024	26.78 ± 0.81	
2MASS J05052576–5719046	05:05:25.76	−57:19:04.6	19.700 ± 0.700	...	...	14.135 ± 0.067		Visual
BD–21 1074A	05:06:49.92	−21:35:09.2	11.569 ± 0.040	10.092 ± 0.030	9.609 ± 0.080	6.117 ± 0.017	18.3 ± 0.70	
BD–21 1074Ba,Bb	05:06:49.47	−21:35:03.8	13.713 ± 0.990	11.706 ± 0.990	10.387 ± 0.042	6.113 ± 0.021		Physical (A and Ba,Bb in β Pic)
2MASS J05071096–2156441	05:07:10.96	−21:56:44.1	20.314 ± 0.700	...	...	13.423 ± 0.039	18.3 ± 0.70	Visual
1RXS J050712.4+143024	05:07:11.37	+14:30:01.3	17.454 ± 0.130	15.727 ± 0.010	15.090 ± 0.020	9.663 ± 0.023	51.20 ± 7.00	
2MASS J05080140+1403539	05:08:01.40	+14:03:53.9	20.215 ± 0.700	...	18.055 ± 0.007	13.451 ± 0.030		Visual
TYC 112–917–1	05:20:00.29	+06:13:03.6	12.802 ± 0.040	11.659 ± 0.030	11.201 ± 0.060	8.573 ± 0.020	68.50	
2E 1249 AB	05:20:31.83	+06:16:11.5	13.015 ± 0.040	11.869 ± 0.020	11.413 ± 0.030	8.567 ± 0.019	69.69	Physical candidate (A and BC in β Pic)
AF Lep AB	05:27:04.77	−11:54:03.3	6.954 ± 0.990	6.362 ± 0.990	...	4.926 ± 0.021	27.04 ± 0.35	
2MASS J05244065–1233402	05:24:40.65	−12:33:40.2	19.755 ± 0.700	...	...	13.451 ± 0.033		Visual
1RXS J072931.4+355607 AB	07:29:31.09	+35:56:00.4	13.345 ± 0.010	11.876 ± 0.030	11.276 ± 0.020	7.796 ± 0.024	42.20 ± 4.00	
2MASS J07293670+3554531	07:29:36.70	+35:54:53.1	15.585 ± 0.020	14.112 ± 0.050	13.515 ± 0.040	9.560 ± 0.018		Physical (AB in β Pic)
[SLS2012] PYC J08290+1125	08:29:04.12	+11:25:05.4	13.600 ± 0.040	12.244 ± 0.020	11.694 ± 0.040	8.758 ± 0.025	58.79 ± 8.50	
2MASS J08274412+1122029	08:27:44.12	+11:22:02.9	14.885 ± 0.040	13.467 ± 0.020	12.906 ± 0.020	9.864 ± 0.019		Physical candidate (A in β Pic)
HD 82939 Ba,Bb	09:36:15.91	+37:31:45.5	12.453 ± 0.010	11.015 ± 0.010	10.416 ± 0.010	7.235 ± 0.018	33.75 ± 2.60	
HD 82939 A	09:36:04.28	+37:33:10.4	9.184 ± 0.990	8.324 ± 0.990	8.052 ± 0.001	6.511 ± 0.027	38.65 ± 1.45	Physical (Ba,Bb in β Pic)
2MASS J09372954+3749458	09:37:29.54	+37:49:45.8	14.029 ± 0.020	12.757 ± 0.140	12.191 ± 0.040	9.656 ± 0.017		Visual

Table C.4: Photometry measurements (cont.).

Simbad name	α (J2000)	δ (J2000)	B [mag]	V [mag]	r' [mag]	K_s [mag]	d [pc]	Photometric status
2MASS J09365772+3758354	09:36:57.72	+37:58:35.4	19.869 ± 0.700	...	18.254 ± 0.007	13.670 ± 0.040		Visual
HD 95174 A	10:59:38.31	+25:26:15.5	9.171 ± 0.030	8.465 ± 0.100	14.295 ± 0.011	5.840 ± 0.053	22.60 ± 2.00	
HD 95174 B	10:59:38.68	+25:26:13.7	10.564	9.218	7.598 ± 0.001	5.978 ± 0.021		Physical (A and B in β Pic)
BD+26 2148	10:56:04.06	+25:41:17.2	10.090 ± 0.010	9.369 ± 0.050	9.100 ± 0.020	7.547 ± 0.018		Visual
2E 2613	12:11:53.09	+12:49:13.5	14.020 ± 0.100	12.546 ± 0.040	11.930 ± 0.030	8.663 ± 0.024	62.70 ± 8.19	
2MASS J12120849+1248050	12:12:08.49	+12:48:05.0	13.923 ± 0.100	12.538 ± 0.060	11.937 ± 0.060	8.916 ± 0.020		Physical candidate (A in β Pic)
TYC 4634–1184–1	14:12:49.93	+84:01:31.2	13.279 ± 0.090	11.994 ± 0.030	11.515 ± 0.060	8.774 ± 0.022	57.90 ± 9.69	
2MASS J14192861+8426534	14:19:28.61	+84:26:53.4	20.194 ± 0.700	...	...	13.001 ± 0.036		Visual
2MASS J14040157+8405075	14:04:01.57	+84:05:07.5	19.534 ± 0.700	...	...	13.902 ± 0.066		Visual
MV Vir Aa,Ab,B	14:14:21.36	–15:21:21.7	11.482 ± 0.040	10.222 ± 0.060	9.939 ± 0.030	6.600 ± 0.023	30.20 ± 4.50	
MV Vir C	14:14:17.00	–15:21:12.7	15.586 ± 0.060	13.937 ± 0.050	13.342 ± 0.020	8.824 ± 0.019		Physical (Aa,Ab,B in β Pic)
TYC 4571–1414–1	16:17:11.35	+77:33:47.8	13.556 ± 0.030	12.129 ± 0.010	11.816 ± 0.010	8.653 ± 0.016	65.00 ± 13.50	
2MASS J16170673+7734028	16:17:06.73	+77:34:02.8	20.450 ± 0.700	...	...	12.228 ± 0.019		Physical candidate (A in β Pic)
1RXS J164302.3–175418	16:43:01.28	–17:54:27.4	14.225 ± 0.700	...	11.948 ± 0.020	8.548 ± 0.025	59.20 ± 2.80	
2MASS J16425150–1814492	16:42:51.50	–18:14:49.2	16.504 ± 0.700	...	14.628	11.729 ± 0.026		Visual
V824 Ara Aa,Ab	17:17:25.51	–66:57:03.9	7.876 ± 0.990	6.960 ± 0.990	...	4.702 ± 0.016	31.45 ± 4.94	
V824 Ara B	17:17:31.29	–66:57:05.6	14.36* ± 0.700	12.82	...	7.629 ± 0.018		Physical (Aa,Ab and B in β Pic)
1RXS J172919.1–501454 AB	17:29:20.67	–50:14:52.9	14.319 ± 0.010	12.810 ± 0.010	12.237 ± 0.010	7.994 ± 0.027	64.00 ± 5.00	
2MASS J17270839–5023572	17:27:08.39	–50:23:57.2	15.000 ± 0.700	...	...	12.930 ± 0.044		Visual
V4046 Sgr AB	18:14:10.48	–32:47:34.4	11.662 ± 0.990	10.769 ± 0.990	9.966 ± 0.031	7.249 ± 0.020	73 ± 18	
V4046 Sgr C	18:14:22.07	–32:46:10.1	14.020 ± 0.700	...	12.193 ± 0.038	8.539 ± 0.023		Physical (AB and C in β Pic)
1RXS J184206.5–555426	18:42:06.95	–55:54:25.5	15.161 ± 0.220	13.602 ± 0.190	13.024 ± 0.150	8.583 ± 0.020	54.00 ± 5.00	
2MASS J18420483–5554126	18:42:04.83	–55:54:12.6	16.826 ± 0.190	15.411 ± 0.100	...	9.852 ± 0.021		Physical (A in β Pic)
HD 172555 A	18:45:26.91	–64:52:16.5	5.024 ± 0.990	4.798 ± 0.990	...	4.297 ± 0.031	28.54 ± 0.16	
HD 172555 Ba,Bb	18:45:37.05	–64:51:46.1	10.517 ± 0.140	9.432 ± 0.050	9.154 ± 0.020	6.096 ± 0.027	29.23 ± 0.60	Physical (A and Ba,Bb in β Pic)
Smethells 20 (HD 173167 B)	18:46:52.56	–62:10:36.7	13.300 ± 0.040	11.831 ± 0.020	11.204 ± 0.020	7.854 ± 0.024	54.00 ± 3.00	
HD 173167 A	18:48:06.36	–62:13:47.0	7.836 ± 0.990	7.337 ± 0.990	...	6.136 ± 0.023		Physical candidate (B in β Pic)
2MASS J18452867–6236003	18:45:28.67	–62:36:00.3	17.722 ± 0.170	16.066 ± 0.010	15.474 ± 0.020	12.005 ± 0.023		Visual
PZ Tel Aa,Ab	18:53:05.87	–50:10:50.0	9.402 ± 0.990	8.503 ± 0.990	...	6.366 ± 0.024	51.49 ± 2.59	
CD–50 12186	18:52:49.76	–50:14:37.0	11.248	10.586 ± 0.030	10.411 ± 0.010	9.059 ± 0.023		Visual
TYC 6872–1011–1	18:58:04.15	–29:53:04.6	13.069 ± 0.040	11.800 ± 0.020	11.267 ± 0.020	8.017 ± 0.021	76.00 ± 5.00	
2MASS J18580464–2953320	18:58:04.66	–29:53:32.2	15.104 ± 0.700	...	13.097 ± 0.050	8.758 ± 0.023		Physical (A and B in β Pic)
η Tel AB	19:22:51.22	–54:25:26.3	5.053 ± 0.990	5.032 ± 0.990	...	5.007 ± 0.033	48.22 ± 0.49	
η Tel C	19:22:58.95	–54:32:17.1	8.946 ± 0.100	8.760 ± 0.070	8.451 ± 0.010	5.909 ± 0.029	51.81 ± 1.74	Physical (AB and C in β Pic)
2MASS J19233074–5450090	19:23:30.74	–54:50:09.0	17.649 ± 0.700	...	...	12.064 ± 0.026		Visual
1RXS J192338.2–460631	19:23:38.20	–46:06:31.6	13.189 ± 0.020	11.876 ± 0.020	11.298 ± 0.010	8.272 ± 0.027	70.00 ± 4.00	
2MASS J19251419–4553480	19:25:14.19	–45:53:48.0	13.590 ± 0.010	12.810 ± 0.010	12.579 ± 0.010	10.941 ±		Visual
2MASS J19230177–4603243	19:23:01.77	–46:03:24.3	18.829 ± 0.700	...	...	12.920 ± 0.037		Visual
HDE 331149 A	19:43:37.90	+32:25:12.5	12.215 ± 0.990	10.897 ± 0.990	10.020 ± 0.015	7.178 ± 0.017	37.59 ± 8.30	
HDE 331149 B	19:43:36.74	+32:25:20.8	11.880 ± 0.700	...	10.678 ± 0.056	8.081 ± 0.018		Physical (A in β Pic)
2MASS J19541276–5711271	19:54:12.76	–57:11:27.1	18.020 ± 0.700	...	...	10.925 ± 0.025	35.40 ± 3.20	
2MASS J19490300–5653427	19:49:03.00	–56:53:42.7	17.729 ± 0.700	...	...	12.840 ± 0.029		Visual
TYC 7443–1102–1	19:56:04.38	–32:07:37.6	13.008 ± 0.020	11.588 ± 0.020	10.982 ± 0.020	7.846 ± 0.021	55.00 ± 3.00	
1RXS J195602.8–320720 AB	19:56:02.94	–32:07:18.7	14.786 ± 0.030	13.229 ± 0.040	12.619 ± 0.030	8.114 ± 0.027		Physical (A and BC in β Pic)
1RXS J201001.0–280139 AB	20:10:00.02	–28:01:41.0	14.486 ± 0.010	12.987 ± 0.020	12.352 ± 0.020	7.732 ± 0.027	48.00 ± 3.09	
2MASS J20085122–2740536	20:08:51.22	–27:40:53.6	17.959 ± 0.700	...	15.755 ± 0.201	11.779 ± 0.023		Visual
AU Mic	20:45:09.49	–31:20:26.7	10.062 ± 0.020	8.887 ± 0.180	8.635 ± 0.090	4.528 ± 0.020	9.90 ± 0.10	
AU Mic BC (AT Mic AB)	20:41:51.12	–32:26:07.3	11.790 ± 0.090	10.333 ± 0.030	9.727 ± 0.010	4.943 ± 0.042	10.69 ± 0.42	Physical (A and BC in β Pic)
HD 199143 AB	20:55:47.68	–17:06:51.0	7.949 ± 0.990	7.392 ± 0.990	...	5.810 ± 0.020	45.59 ± 1.60	
HD 199143 CD (AZ Cap AB)	20:56:02.75	–17:10:53.9	11.859 ± 0.990	10.732 ± 0.990	9.873	7.039 ± 0.020		Physical (AB and CD in β Pic)
EUVE J2110–19.3	21:10:05.36	–19:19:57.4	13.173 ± 0.040	11.750 ± 0.040	11.152 ± 0.050	7.196 ± 0.017	32.00 ± 2.00	
BPS CS 22898–0066	21:10:04.60	–19:20:30.3	14.673 ± 0.020	13.142 ± 0.040	12.545 ± 0.010	7.552 ± 0.017		Physical (A in β Pic)

Table C.4: Photometry measurements (cont.).

Simbad name	α (J2000)	δ (J2000)	B [mag]	V [mag]	r' [mag]	K_s [mag]	d [pc]	Photometric status
2MASS J21103147–2710578	21:10:31.47	−27:10:57.8	16.840 ± 0.080	15.145 ± 0.010	14.569 ± 0.010	9.411 ± 0.021	41.00 ± 3.00	
2MASS J21103096–2710513	21:10:30.96	−27:10:51.3	16.840 ± 0.080	15.145 ± 0.010	14.569 ± 0.010	10.236 ± 0.026	40.00 ± 2.00	Physical (A and B in β Pic)
2MASS J21094649–2728291	21:09:46.49	−27:28:29.1	15.574 ± 0.030	14.314 ± 0.010	13.704 ± 0.010	10.883 ± 0.023		Visual
V390 Pav A	21:21:24.49	−66:54:57.4	10.225 ± 0.990	9.038 ± 0.990	...	6.400 ± 0.017		
V390 Pav B	21:21:28.72	−66:55:06.3	11.961 ± 0.010	10.595 ± 0.010	...	7.008 ± 0.023	30.20 ± 1.30	Physical (A and B in β Pic)
1RXS J215518.2–004603	21:55:17.41	−00:45:47.8	17.340 ± 0.100	15.739 ± 0.010	15.128 ± 0.010	10.196 ± 0.021	47.00 ± 4.00	
2MASS J21551738–0046231	21:55:17.38	−00:46:23.1	17.278 ± 0.100	15.673 ± 0.010	15.038 ± 0.010	10.090 ± 0.021		Physical (B in β Pic)
LSPM J2240+0532	22:40:01.45	+05:32:16.3	19.134 ± 0.700	...	17.180	10.748 ± 0.021	23.60 ± 2.70	
HD 214786	22:40:27.22	+04:34:30.1	8.177 ± 0.990	6.947 ± 0.990	10.670 ± 0.008	4.275 ± 0.029		Visual
CPD–72 2713	22:42:48.96	−71:42:21.1	11.718 ± 0.030	10.423	...	6.894 ± 0.018	37.00 ± 2.00	
2MASS J22353683–7149426	22:35:36.83	−71:49:42.6	18.56* ± 0.32	17.87*	...	12.524 ± 0.021		Visual
2MASS J22372184–7118216	22:37:21.84	−71:18:21.6	17.85* ± 0.29	17.70*	...	12.793 ± 0.034		Visual
WW PsA A	22:44:57.94	−33:15:01.6	13.618 ± 0.030	12.099 ± 0.010	11.493 ± 0.020	6.932 ± 0.029	23.34 ± 1.97	
WW PsA B (TX PsA)	22:45:00.05	−33:15:25.8	14.989 ± 0.040	13.371 ± 0.020	12.777 ± 0.010	7.793 ± 0.026		Physical (A and B in β Pic)
AF Psc	23:31:44.93	−02:44:39.6	16.062 ± 0.070	14.562 ± 0.010	13.923 ± 0.010	8.666 ± 0.019	29.14 ± 2.64	
2MASS J23301129–0237227	23:30:11.30	−02:37:22.7	17.204 ± 0.700	...	15.090 ± 0.056	9.767 ± 0.019		Physical candidate (A in β Pic)

Table C.5: Common proper-motion companion candidates.

WDS identifier	Discovery name[a]	Simbad name	α (J2000)	δ (J2000)	d [pc]	M_J [mag]	Sp. type	ρ [arcsec]	θ [deg]	s [10^3 au]	$\mathcal{M}$ [$M_\odot$]	$-U_g^*$ [10^{33} J]	Comments
Our common proper-motion candidates													
01376–0645		EX Cet	01:37:35.47	–06:45:37.5	23.95 ± 0.42	4.32 ± 0.04	G5 V				0.92		
	CAB 3	LP 648–20 (EX Cet B)	01:36:55.17	–06:47:37.9		7.81 ± 0.04	M3.5 V	612.1	259	15	0.12	13	In AF11, 1 new star, Her-Lyr?
02017+0117		[SLS2012] PYC J02017+0117N	02:01:46.78	+01:17:16.2	63.7 ± 9.0	5.1 ± 0.3	...				0.73		
	New	[SLS2012] PYC J02017+0117S	02:01:46.93	+01:17:06.0		5.1 ± 0.3	...	10.48	167	0.67	0.71	1400	...
05200+0613		TYC 112–917–1	05 20 00.29	+06 13 03.6	68.5	5.15 ± 0.03	K3				0.70		
	New	2E 1249 AB	05 20 31.83	+06 16 11.5		5.07 ± 0.02	K3	506.2	248	35	0.66+0.15	28	...
08290+1125		[SLS2012] PYC J08290+1125	08:29:04.12	+11:25:05.4	58.8 ± 8.5	5.7 ± 0.3	...				0.50		
	New	2MASS J08274412+1122029	08:27:44.12	+11:22:02.9		6.9 ± 0.3	...	1190	261	70	0.21	2.7	1 new star, co-moving?
12118+1249		2E 2613	12:11:53.09	+12:49:13.5	62.7 ± 8.2	5.5 ± 0.3	m1:				0.59		
	New	2MASS J12120849+1248050	12:12:08.49	+12:48:05.0		5.7 ± 0.3	m0:	235.5	107	15	0.50	35	1 new star
16172+7734		TYC 4571–1414–1	16:17:11.48	+77:33:47.8	65.0 ± 13.5	5.4 ± 0.4	m0:				0.60		
	New	2MASS J16170673+7734028	16:17:06.73	+77:34:02.8		9.0 ± 0.4	...	21.22	315	1.4	0.05	36	1 new star, AB Dor?
18481–6214		HD 173167 A	18:48:06.36	–62:13:47.0		2.75 ± 0.12	F5 V				1.32		
	CAB 8	Smethells 20 (HD 173167 B)	18:46:52.56	–62:10:36.7	54 ± 3	5.08 ± 0.12	M1 Ve	550.4	290	30	0.72	57	In AF11, 1 new star
23317–0245		AF Psc	23:31:44.93	–02:44:39.6	29.2 ± 2.6	7.18 ± 0.19	M4.5				0.18		
	New	2MASS J23301129–0237227	23:30:11.30	–02:37:22.7		8.32 ± 0.19	M6.0	1469	287	43	0.08	0.57	1 new star, co-moving?
Previously known systems													
00197+1951		RX J0019.7+1951	00:19:43.04	+19:51:11.7	59.4 ± 7.9	6.8 ± 0.3	M4				0.22		
	GWP 40	2MASS J00193931+1951050	00:19:39.31	+19:51:05.1		7.0 ± 0.3	M4	52.95	263	3.2	0.19	24	1 new star
00279–3235		GJ 2006 A	00:27:50.23	–32:33:06.0	33.2 ± 2.8	6.28 ± 0.19	M4.0				0.34		
	LDS 18	GJ 2006 B	00:27:50.35	–32:33:23.8		6.37 ± 0.18	M3.5	17.83	175	0.59	0.31	310	...
02174+2845		HD 14082 A	02:17:25.27	+28:44:42.3	34.5 ± 3.4	3.4 ± 0.2	F5 V				1.11		
	STF 239	HD 14082 B	02:17:24.73	+28:44:30.5		3.9 ± 0.2	G2 V	13.80	211	0.48	0.91	3800	...
02274+3059		AG Tri A	02:27:29.25	+30:58:24.7	40.0 ± 3.6	4.9 ± 0.2	K7 V				0.79		
	INN 1	AG Tri B	02:27:28.05	+30:58:40.5		5.8 ± 0.2	M0	22.11	316	0.88	0.47	75	...
02305–4342		CD–44 753 Aa,Ab	02:30:32.41	–43:42:23.3	35.7	5.26 ± 0.03	K5 V(e)				0.49+0.37		
	SKF 1427	CD–44 753 B	02:30:46.23	–43:43:49.3		6.38 ± 0.02	...	172.9	120	6.2	0.31	76	1 new star, Columba?
04376–0228		*c* Eri A	04:37:36.13	–02:28:24.8	29.43 ± 0.29	2.40 ± 0.04	F0 IV				1.57		
	WAL 32	*c* Eri Ca,Cb	04:37:37.47	–02:29:28.4		4.96 ± 0.03	m0.0+m3.0	66.48	163	2.0	0.67+0.44	1600	...
04481+1441		LDS 5606 A	04:48:00.86	+14:39:58.1	65.0 ± 6	7.6 ± 0.2	M5.0e				0.14		
	LDS 5606	LDS 5606 B	04:48:02.58	+14:39:51.6		7.6 ± 0.2	M5.0e	25.86	105	1.7	0.14	19	...
05069–2135		BD–21 1074A	05:06:49.92	–21:35:09.2	18.3 ± 0.7	5.73 ± 0.09	M1.5 V				0.52		
	DON 93	BD–21 1074Ba,Bb	05:06:49.47	–21:35:03.8		5.69 ± 0.09	M2.5+M5:	8.218	311	0.15	0.31+0.21	3200	...
07295+3556		1RXS J072931.4+355607 AB	07:29:31.09	+35:56:00.4	42.2 ± 4.0	5.5 ± 0.2	m1 V+m3 V				0.54+0.29		
	UC 1586	2MASS J07293670+3554531	07:29:36.70	+35:54:53.1		7.2 ± 0.2	m3:	95.83	135	4.0	0.17	62	1 new star
08228–5727		L 186–67 Aa,Ab	08:22:47.45	–57:26:53.0	11.1 ± 3.3	8.4 ± 0.6	m4.5 V+m5.5 V				0.18+0.14		
	LDS 217	L 186–67 B	08:22:47.99	–57:26:48.1		10.0 ± 0.6	m:	8.589	23	0.10	0.02	110	1 new star, field?
09361+3733		HD 82939 A	09:36:04.28	+37:33:10.4	38.7 ± 1.4	3.94 ± 0.08	G5 V				1.01		
	SKF 254	HD 82939 Ba,Bb	09:36:15.91	+37:31:45.5		5.15 ± 0.08	M2 V+M2 V	162.3	121	6.3	0.38+0.38	220	1 new star, young field?
10596+2527		HD 95174 A	10:59:38.31	+25:26:15.5	22.6 ± 2.0	4.7 ± 0.19	K2				0.84		
	AG 342	HD 95174 B	10:59:38.68	+25:26:13.7		4.8 ± 0.2	K5	5.282	108	0.12	0.79	9800	...
14144–1521		MV Vir Aa,Ab,B	14:14:21.36	–15:21:21.7	30.2 ± 4.5	5.0 ± 0.3	K5.5 Vke				0.52+0.31+0.39		
	LDS 483	MV Vir C	14:14:17.00	–15:21:12.7		7.3 ± 0.3	M3.5	64.33	278	1.9	0.17	190	1 new star
17174–6657		V824 Ara Aa,Ab	17:17:25.50	–66:57:03.7	31.4 ± 4.9	2.8 ± 0.3	G5 IV+K0 IV–V				1.10+1.00		
	CVN 55	V824 Ara B	17:17:31.29	–66:57:05.6		6.0 ± 0.3	M3 Ve	33.96	93	1.1	0.40	1400	...
18141–3248		V4046 Sgr AB	18:14:10.48	–32:47:34.4	73 ± 18	3.8 ± 0.5	K5+K7				0.91+0.88		
	...	V4046 Sgr C	18:14:22.07	–32:46:10.1		5.1 ± 0.5	M1 Ve	168.8	60	12	0.71	182	Not in WDS
18421–5554		1RXS J184206.5–555426	18:42:06.95	–55:54:25.5	54.0 ± 5.0	5.8 ± 0.2	M3.5				0.47		

Table C.5: Common proper-motion companion candidates (cont.).

WDS identifier	Discovery name[a]	Simbad name	α (J2000)	δ (J2000)	d [pc]	M_J [mag]	Sp. type	ρ [arcsec]	θ [deg]	s [10^3 au]	$\mathcal{M}$ [$M_\odot$]	$-U^*_g$ [10^{33} J]	Comments
	UC 3646	2MASS J18420483–5554126	18:42:04.83	–55:54:12.6		7.0 ± 0.2	M4.5	21.92	306	1.2	0.20	140	1 new star
18454–6452		HD 172555 A	18:45:26.91	–64:52:16.5	28.55 ± 0.16	2.1 ± 0.3	A7 V				1.75		
	SKF 105	HD 172555 Ba,Bb	18:45:37.05	–64:51:46.1		4.63 ± 0.02	K5 Ve	71.38	65	2.0	0.83+0.21	1600	...
18581–2953		TYC 6872–1011–1	18:58:04.15	–29:53:04.6	76 ± 5	4.46 ± 0.14	M0 Ve				0.90		
	SKF 1507	2MASS J18580464–2953320	18:58:04.66	–29:53:32.2		5.22 ± 0.14	...	28.18	167	2.1	0.72	530	...
19229–5425		η Tel AB	19:22:51.22	–54:25:26.3	48.2 ± 0.5	1.68 ± 0.04	A0 V+M7–8 V				2.40+0.05		
	TOK 331	η Tel C	19:22:58.95	–54:32:17.1		2.78 ± 0.03	F6 V	416.3	171	20	1.40	300	...
19437+3225		HDE 331149 A	19:43:37.90	+32:25:12.5	37.6 ± 8.3	5.1 ± 0.5	K0				0.72		
	HJ 1433	HDE 331149 B	19:43:36.74	+32:25:20.8		6.0 ± 0.5	...	16.82	299	0.63	0.43	860	1 new star
19561–3208		TYC 7443–1102–1	19:56:04.38	–32:07:37.6	55 ± 3	5.01 ± 0.12	K9 IVe				0.74		
	UC 4054	1RXS J195602.8–320720 AB	19:56:02.94	–32:07:18.7		5.26 ± 0.12	M4	26.30	316	1.4	0.50+0.38	790	...
20452–3120		AU Mic	20:45:09.49	–31:20:26.7	9.91 ± 0.10	5.46 ± 0.03	M1 Ve				0.45		
	LDS 720	AU Mic BC (AT Mic AB)	20:41:51.12	–32 26 07.3		5.83 ± 0.03	M4 Ve	4681	212	46	0.52	8.9	...
20558–1707		HD 199143 AB	20:55:47.68	–17:06:51.0	45.7 ± 1.6	2.91 ± 0.08	F7V+M2				1.25+0.60		
	TOK 343	HD 199143 CD (AZ Cap AB)	20:56:02.75	–17:10:53.9		4.55 ± 0.08	K7	325.1	138	15	0.90+0.55	320	...
21100–1920		EUVE J2110–19.3	21:10:05.36	–19:19:57.4	32 ± 2	5.59 ± 0.14	M2				0.55		
	LDS 734	BPS CS 22898–0066	21:10:04.60	–19:20:30.3		5.90 ± 0.14	...	34.44	198	1.1	0.44	390	1 new star
21105–2711		2MASS J21103147–2710578	21:10:31.47	–27:10:57.8	41 ± 3	7.23 ± 0.16	M4.5				0.17		
	BRG 32	2MASS J21103096–2710513	21:10:30.96	–27:10:51.3		8.14 ± 0.16	M5	9.474	313	0.39	0.08	67	...
21214–6655		V390 Pav A	21:21:24.49	–66:54:57.4	33.1 ± 1.5	4.43 ± 0.10	K2 V				0.85		
	HJ 5255	V390 Pav B	21:21:28.72	–66:55:06.3		5.28 ± 0.10	K7 V	26.63	110	0.80	0.59	1100	Tuc-Hor?
21553–0046		2MASS J21551738–0046231	21:55:17.38	–00:46:23.1	47 ± 4	7.62 ± 0.19	m5e				0.14		
	CBL 536	1RXS J215518.2–004603	21:55:17.41	–00:45:47.8		7.73 ± 0.19	M4.5	35.34	0	1.7	0.12	18	1 new star
22450–3314		WW PsA A	22:44:57.94	–33:15:01.6	23.3 ± 2.0	5.95 ± 0.19	M4 IVe				0.43		
	LDS 793	WW PsA B (TX PsA)	22:45:00.05	–33:15:25.8		6.84 ± 0.19	M5 IVe	35.91	132	0.84	0.22	200	...